

Doctoral Thesis



Static and Fatigue Characteristics of Composite Joint Repair in Aircraft Structures

**NABIL MUNTASER
CHOWDHURY**

B. Eng. (Aerospace) Hons & B.Sc
(Applied Mathematics)

A thesis submitted for the degree of
Doctor of Philosophy at Monash
University, Department of Mechanical
and Aerospace Engineering

2016

© 2016

Nabil Muntaser Chowdhury

ALL RIGHTS RESERVED

Under the Copyright Act 1968, this thesis may not be reproduced in any form without the written permission of the author. I certify that I have made all reasonable efforts to secure copyright permissions for third-party content included in this thesis and have not knowingly added copyright content to my work without the owner's permission.

Abstract

Composite materials are seeing increasing use in the engineering industry, in particular the aerospace sector. The move towards light weight high stiffness structures that have good durability and corrosion resistance has led to the move from metal structures to composite structures. With this brings the added concern of certifying new components as they must meet the same structural integrity, safety and durability requirements as those in metals and hence this is where the challenge now lies.

When a metallic structure is damaged at some point during its life, there is a possibility it will be repaired however if the damage is significant then the component(s) will be replaced. With composite materials on the other hand, the flexibility in design and fabrication has led to larger single component pieces and thus repairing these structures is more economical than replacement. This puts further emphasis in creating new and efficient repair methods that can be certified whilst still withstanding the various stresses and loads inflicted on the aircraft during its remaining service life.

In this study, a comparison is made between three fundamental joint structures - mechanically fastened joints, bonded joints and hybrid joints. The work is targeted towards the repair of aircrafts made from fibre reinforced polymer matrix composites known for their high strength, high stiffness, long fatigue life and low density.

Stage 1 of the investigation focused on testing thin double lap joint repairs and Stage 2 focused on testing thick step lap joint repairs containing a total of five steps. The aim was to compare the static strength and fatigue resistance of a hybrid joint configuration consisting of both bonding and fastening, a purely fastened joint and a purely bonded joint. Rivets and countersunk bolts were selected as the fasteners for thin and thick joint repairs respectively. The effect of changing various parameters such as the mechanical fastener array, clamping pressure, bond strength, initial defects and curing conditions were also investigated. The experimental results for both Stage 1 and Stage 2 found there was no significant difference between the static strength of a bonded joint compared to a hybrid joint. However, the fatigue resistance of a hybrid joint was superior to a bonded joint configuration particularly where bondline defects such as initial cracks or a semi-cured adhesive was present.

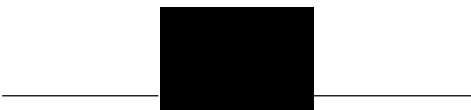
Finite element analysis (FEA) was also performed to verify the static and fatigue strength of the various configurations. Nonlinear adhesive material properties, fastener surface contacts and frictional forces were all included in the three-dimensional (3D) finite element (FE) models. The Multicontinuum Theory (MCT) is used to simulate the progressive failure process and determine the stress states in the various specimen configurations. The strain energy release rate (SERR) as a function of crack length for the bonded and hybrid specimens were also compared. Results found that it was vital to position fasteners closer towards the ends of the bondline to suppress rapid crack growth. As soon as a crack enters the fasteners' clamping zone, there is a significant drop in the SERR which reduces the crack growth rate, leading to an improvement in fatigue resistance. The key advantage in this case, is being able to detect damage before catastrophic failure.

A final extension to the investigation looked into optimising the individual step length, step heights and the number of steps for the thick joint repair cases. The previous step lap joint containing five steps with a 90mm long overlap was able to achieve only a 52% load recovery at best compared to a pristine undamaged parent structure. Through the parametric studies conducted using Abaqus CAE, two new step lap joint designs were numerically analysed and experimentally tested. One of the optimised step lap joint designs contained seven steps (with thin outer step heights and thicker inner step heights) and the second contained six steps (with an outer overlap). Overall, the static and fatigue resistance was improved in both of the new step lap joint designs. A bonded step lap joint with seven steps was now able to achieve a 70% load recovery with a 95% increase in fatigue resistance.

Overall the work discussed as part of this dissertation provides detailed methods in optimising composite joint repair whilst providing benchmark comparisons between thin and thick fastened, bonded and hybrid joint cases. This is an area of research which has seen limited attention in the past but is crucial for the continual growth of composite material usage in both commercial and military sectors. Achieving composite joint repair certification is a stringent and costly process, through this research various methods have been presented to not only improve repair durability but to assist damage detection and prevent final catastrophic failure, all of which will greatly assist composite repair certification.

Declaration

This thesis contains no material which has been accepted for the award of any other degree or diploma at any university or equivalent institution and that, to the best of my knowledge and belief, this thesis contains no material previously published or written by another person, except where due reference is made in the text of the thesis.



Candidate: Nabil Muntaser Chowdhury

May 2016

Publications

Nabil. Chowdhury, W.K. Chiu, J. Wang, P. Chang, “Static and fatigue testing thin riveted, bonded and hybrid carbon fibre double lap joints used in aircraft structures”, *Composite Structures*, 2015. Vol 121, pp. 315-323

Nabil. Chowdhury, J. Wang, W.K. Chiu, P. Chang, “Experimental and finite element studies of thin bonded and hybrid carbon fibre double lap joints used in aircraft structures”, *Composites Part B: Engineering*, 2016. Vol 85, pp. 233-242

Nabil. Chowdhury, J. Wang, W.K. Chiu, P. Chang, “Static and fatigue testing bolted, bonded and hybrid step lap joints of thick carbon fibre/epoxy laminates used on aircraft structures”, *Composite Structures*, 2016. Vol 142, pp. 96-106

Nabil. Chowdhury, W.K. Chiu, J. Wang, P. Chang, “Experimental and finite element studies of bolted, bonded and hybrid step lap joints of thick carbon fibre/epoxy panels used in aircraft structures”, *Composites Part B: Engineering*, 2016. Vol 100, pp. 68-77

Nabil. Chowdhury, W. K. Chiu, J. Wang, “Review on the fatigue of composite hybrid joints used in aircraft structures”, *Advanced Materials Research*, 2015. Vol 891-892, pp. 1591-1596

Nabil. Chowdhury, W. K. Chiu, J. Wang, “A review of damage tolerant design, certification and repair in metals compared to composite materials”, *Advanced Materials Research*, 2015. Vol 891-892, pp. 1597-1602

Leslie. Wong, Nabil. Chowdhury, J. Wang, W.K. Chiu, J. Kodikara, “Fatigue damage monitoring of a composite step lap joint using distributed optical fibre sensors”, *Materials*, 2016, Vol 9, pp. 374

Nabil. Chowdhury, W.K. Chiu, J. Wang, P. Chang, “Optimisation of bonded and hybrid step lap joints of thick carbon fibre/epoxy panels used in aircraft structures”, *Composites Part B: Engineering*, Under Review

Nabil. Chowdhury, W.K. Chiu, J. Wang, P. Chang, “Fatigue resistance of mechanically fastened, bonded and hybrid joints used in composite structures”, 8th Australian Congress on Applied Mechanics, 23-26th Nov 2014, Melbourne, Australia

Nabil. Chowdhury, W.K. Chiu, J. Wang, P. Chang, “Comparison of static and fatigue characteristics of hybrid and standard joints for thick composite structures”, 18th International Conference on Composite Structures, 15-18th June 2015, Lisbon, Portugal

Acknowledgements

I would like to express my sincerest gratitude and appreciation to my supervisors, Professor Wing Kong Chiu and Dr John Wang from the Defence Science and Technology Group, for the guidance and support provided throughout the entire duration of my candidature. Their knowledge and expertise provided in this research field was invaluable to the success of this project.

I would also like to extend my appreciation to Dr Paul Chang for your valuable feedback and assistance in specimen design and fabrication, Dr Nik Rajic for use of the MiTE Thermal Imaging software and to Ivan Stoyanovski for support and training in composite material layup, fabrication, bonding and assembly. I would also like to extend my appreciation to Alan Coram for access to the servo-hydraulic machines located in the Institute of Railway and Technology High Bay area and to the Mechanical and Aerospace Engineering Workshop Staff for assistance in specimen machining.

I would like to acknowledge the Cooperative Research Centre for Advanced Composite Structures (CRC-ACS), established and supported under the Australian Government's Cooperative Research Centres Program and to the Australian Defence Materiel Organisation for partial financial support provided throughout the project.

This thesis would not have been made possible without the support of my family. Thank you to my parents for the love, encouragement and support provided over the many years. Finally, special thanks to all of my friends at Monash University for the engaging discussions and activities shared throughout this period, your company has made this a very pleasurable experience.

Contents

1	Introduction	1
1.1	Background.....	1
1.2	Research Objective	3
1.3	Thesis Structure	5
2	Literature Review	8
2.1	Introduction.....	8
2.2	Composite Failure Mechanisms.....	12
2.3	Composite Joint Methods	13
2.3.1	Mechanically Fastened Joints	13
2.3.2	Bonded Joints.....	16
2.3.3	Hybrid Joints.....	19
2.4	Types of Composite Structural Joints.....	21
2.4.1	Single and Double Lap Joints	21
2.4.2	Tapered Lap Joints.....	23
2.4.3	Scarf and Step Lap Joints.....	25
2.5	Experimental testing.....	27
2.5.1	Static Testing	28
2.5.2	Fatigue Testing.....	30
2.6	Composite Damage Detection	34
2.7	Finite Element Analysis.....	37
2.7.1	Multicontinuum Theory.....	38
2.7.2	Strain Energy Release Rate	41
2.8	Scope of Further Research	44
2.9	Chapter Summary	45
3	Materials and Manufacture	47
3.1	Introduction.....	47

3.2 Material Properties	48
3.3 Joint Configurations	51
3.3.1 Double Lap Joint	52
3.3.2 Step Lap Joint	54
3.4 Machining of Laminates.....	57
3.4.1 Bolt Hole Clearance	58
3.5 Specimen Assembly.....	61
3.5.1 Surface Preparation	62
3.5.2 Adhesive Thickness Determination	64
3.5.3 Bolt Clamping Pressure	65
3.5.4 Non-Destructive Inspection.....	66
3.6 Initial Bondline Defects	69
3.6.1 Semi-Cured Adhesive.....	69
3.6.2 Initial Bondline Crack.....	71
3.7 Chapter Summary	72
4 Stage 1-Experimental Testing.....	73
4.1 Introduction.....	73
4.2 Experimental Setup	74
4.3 Testing Procedure.....	75
4.4 Experimental Results.....	77
4.4.1 Static Test Results.....	77
4.4.2 Fatigue Test Results.....	80
4.5 Discussion and Observation	82
4.5.1 Failure Modes in Pristine Specimen Configurations 1.1-1.4	83
4.5.2 Failure Modes in Defective Specimen Configurations 1.5-1.8	85
4.5.3 Double Lap Joint Comparison	87
4.6 Chapter Summary	89
5 Stage 1-Finite Element Analysis.....	90
5.1 Introduction.....	90

5.2 Finite Element Analysis Setup.....	91
5.2.1 Load-Displacement Correction.....	93
5.2.2 Fibre and Matrix Degradation.....	94
5.3 Experimental Comparison with Finite Element	97
5.3.1 Pristine Specimens (Configuration 1.1 - 1.4).....	97
5.3.1.1 Configuration 1.1	99
5.3.1.2 Configuration 1.2	100
5.3.1.3 Configuration 1.3	101
5.3.1.4 Configuration 1.4	103
5.3.2 Defective Specimens (Configuration 1.5 - 1.8).....	104
5.3.2.1 Configuration 1.5	105
5.3.2.2 Configuration 1.6	106
5.3.2.3 Configuration 1.7 & 1.8.....	107
5.3.3 Joint Configuration Summary.....	108
5.4 Numerical Analysis on the Fatigue of Bonded and Hybrid Joints.....	109
5.4.1 SERR Model Setup.....	110
5.4.2 Comparison of Bonded and Hybrid Specimens Containing Two Rows of Rivets.....	111
5.4.3 Hybrid A - Effect on Strain Energy Release Rate by Removing the First Row of Rivets	112
5.4.4 Hybrid B - Effect on Strain Energy Release Rate by Removing the First Row of Fasteners Holes and Rivets	115
5.5 Chapter Summary	117
6 Stage 2-Experimental Testing.....	118
6.1 Introduction.....	118
6.2 Experimental Setup	120
6.3 Testing Procedure.....	125
6.4 Results and Observation.....	126
6.4.1 Static Test Results.....	126
6.4.2 Fatigue Test Results.....	130
6.4.3 Damage Detection for Specimen Configuration 2.9.....	132

6.4.4 Damage Detection for Specimen Configuration 2.5	136
6.4.5 Suppressing Out of Plane Bending.....	138
6.5 Discussion on Failure Patterns	141
6.6 Chapter Summary	144
7 Stage 2-Finite Element Analysis.....	146
7.1 Introduction.....	146
7.2 Finite Element Analysis Setup.....	148
7.3 Finite Element Analysis Compared to Experimental Results.....	150
7.3.1 Load-Displacement Behaviour for Pristine Specimens.....	151
7.3.2 Bolt Load Share and Stress Distribution for Pristine Specimens.....	153
7.3.3 Load-Displacement Behaviour for 2mm Initial Crack Specimens	155
7.3.4 Bolt Load Share and Stress Distribution for 2mm Initial Crack Specimens	156
7.3.5 Defective Semi-Cured Adhesive Specimens	159
7.4 Fatigue of Bonded and Hybrid Joints.....	160
7.4.1 Model Setup.....	161
7.4.2 Fatigue Performance Comparison	162
7.5 Chapter Summary	165
8 Step Lap Joint Optimisation	167
8.1 Introduction.....	167
8.2 Step Lap Joint Configurations	169
8.3 Parametric Study - New Step Lap Joint Designs.....	170
8.3.1 Double and Single Strap Specimen Configurations	171
8.3.2 Flush Step Lap Joint Configurations	173
8.3.3 Overlap Step Lap Joint Configurations.....	175
8.4 Computational Results	178
8.4.1 Fastened Step Lap Joint	178
8.4.2 Bonded Step Lap Joint	179
8.4.3 Hybrid Step Lap Joint	182
8.5 Experimental Validation.....	184

8.5.1 Specimen Manufacture and Methodology.....	185
8.5.2 Static Test Results.....	186
8.5.3 Fatigue Test Results.....	188
8.6 Discussion	189
8.7 Chapter Summary	191
9 Summary and Conclusions	193
9.1 Major Findings	194
9.1.1 Experimentally Testing Thin Double Lap Joint Repairs.....	194
9.1.2 Numerical Analysis of Thin Double Lap Joint Repairs	196
9.1.3 Experimentally Testing Thick Step Lap Joint Repairs	197
9.1.4 Numerical Analysis of Thick Step Lap Joint Repairs.....	199
9.1.5 Thick Step Lap Joint Optimisation	200
9.2 Recommendation for Future Work	201
<i>Bibliography</i>.....	203

List of Figures

Figure 2.1 The use of composite materials in commercial and military aircrafts.....	8
Figure 2.2 Ply stacking sequence based on a unidirectional fabric	9
Figure 2.3 Common woven fabric configurations; (a) plain weave; (b) twill weave; (c) basket weave; (d) satin weave.....	10
Figure 2.4 Vacuum bagging schematic containing a composite layup	11
Figure 2.5 Failure modes for bolted joints used with composite laminates	14
Figure 2.6 Failure modes in adhesive bonded joints; (a) cohesive failure; (b) adhesive failure; (c) mixed failure; (d) adherend failure	17
Figure 2.7 The relative strength of adherends and adhesives affected by bond flaws [25]	18
Figure 2.8 Bonded single lap joint	22
Figure 2.9 Bonded double lap joint.....	22
Figure 2.10 Specimen type and dimensions used in taper angle experiment; dimensions in mm [47]	24
Figure 2.11 Bonded scarf joint.....	25
Figure 2.12 Bonded step lap joint with three steps.....	26
Figure 2.13 Fracture modes	27
Figure 2.14 Test pyramid approach to achieve certification	28
Figure 2.15 Constant amplitude fatigue cycles	32
Figure 2.16 Variable amplitude fatigue cycles.....	33
Figure 2.17 Block amplitude fatigue cycles.....	33
Figure 2.18 Non-destructive testing using an Olympus Epoch XT ultrasonic A-scanner	35
Figure 2.19 Non-destructive inspection using a FLIR A615 thermal camera	36
Figure 2.20 Optical Distributed Sensor Interrogator.....	36
Figure 2.21 Extrapolating stresses at the crack tip.....	43

Figure 3.1 HexPly M18/1/G939 satin weave with 0° and 90° fibres	48
Figure 3.2 FM300-2K film adhesive with nominal uncured thickness of 0.41mm	49
Figure 3.3 Schematic of Cheri Maxibolt CR7621 rivet [123]	50
Figure 3.4 Schematic of Aviaquip NAS1581 countersunk bolt [124]	51
Figure 3.5 Double lap joint containing six fasteners in a square array; dimensions in mm	53
Figure 3.6 Double lap joint containing three fasteners in a staggered array; dimensions in mm ...	53
Figure 3.7 Step lap joint containing five bolts in a single column array; dimensions in mm	55
Figure 3.8 Step lap joint containing three bolts in a single column array; dimensions in mm	55
Figure 3.9 Long hybrid step lap joint containing seven steps (Configuration 3.2) with five bolts in a single column array; dimensions in mm	56
Figure 3.10 Overlap hybrid step lap joint containing six steps with five bolts (Configuration 4.2) in a single column array; dimensions in mm	56
Figure 3.11 Thin HexPly M18/1/G939 carbon fibre adherends cut from a panel using water jet .	58
Figure 3.12 Thick HexPly M18/1/G939 carbon fibre adherends machined using an NC machine	58
Figure 3.13 Solid carbide drill bit and reamer used for rivet holes in Stage 1	60
Figure 3.14 Solid carbide drill bit, reamer and countersink used for the countersunk bolt holes in Stage 2	60
Figure 3.15 Drilled and reamed fastener hole in carbon fibre adherend with no back-face plate (left) and with back-face plate (right)	60
Figure 3.16 Vacuum bagging hybrid double lap joint specimens to cure bondline in an autoclave	61
Figure 3.17 Grit blasting machine used to surface prep adherend surfaces for bonding	63
Figure 3.18 FM300-2K bondline thickness determination at different curing pressures (121°C for 90min)	64
Figure 3.19 Ultrasonic scanning positions for Hybrid Configuration 1.4	66
Figure 3.20 Spectrum envelope of a 10 and 5 ply thick adherend used in Stage 1	67
Figure 3.21 Spectrum envelope of Configuration 1.3 - Hybrid double lap joint with six rivets	67
Figure 3.22 Spectrum envelope of Configuration 1.4 - Hybrid double lap joint with three rivets..	68

Figure 3.23 Bondline defect in position 1 of Configuration 1.4	68
Figure 3.24 Peak strength of FM300-2K cured at different curing temperature and time; Specimen 1 - 121°C for 90min; Specimen 2 - 93°C for 60 min; Specimen 3 - 66°C for 60min; Specimen 4 - 85°C for 60min	70
Figure 3.25 Location of Teflon tape to simulate a 2mm long initial crack in a double lap joint (top) and step lap joint (bottom)	71
Figure 4.1 Fully assembled pristine double lap joint configurations ready for testing; Configuration 1.2, Configuration 1.3, Configuration 1.4 and Configuration 1.1 (left to right)	75
Figure 4.2 100kN Instron 1342 servo-hydraulic machine	76
Figure 4.3 Peak strength achieved by fastened, bonded and hybrid configurations; refer to Table 4.1 for the detailed description of the configurations	78
Figure 4.4 Region of disbond (indicated in red) after 400,000 cycles in the hybrid specimen with a staggered rivet array (Configuration 1.4) cured in an oven at 121°C for 90 minutes..	85
Figure 5.1 Three major geometry configurations (tabs used for clamping shown for representation only); (a) Configuration 1.1 – Bonded Double Lap Joint, (b) Configuration 1.4 – Hybrid Double Lap Joint with three rivets, (c) Configuration 1.3 – Hybrid Double Lap joint with six rivets; RR1 – Rivet Row One (closest fastener row to tapered edge); RR2 – Rivet Row Two (furthest fastener row from tapered edge)	92
Figure 5.2 Meshed assembly of a hybrid double lap joint (Configuration 1.3); quarter of full geometry	92
Figure 5.3 Determining calibration factor for specimens true displacement	94
Figure 5.4 Progressive damage states using the Multicontinuum Theory	95
Figure 5.5 Optimising the matrix degradation value for the HexPly M18/1/G939 carbon fibre prepreg; F - (fibre degradation value); M - (matrix degradation value)	95
Figure 5.6 Optimising the fibre degradation value for the HexPly M18/1/G939 carbon fibre prepreg; F - (fibre degradation value); M - (matrix degradation value)	96
Figure 5.7 Adhesive spew fillet located at the ends of the overlap	98
Figure 5.8 Load-displacement comparison between experimental and FEA for Configuration 1.1 - 1.4 with no spew; displacement represents the specimens total elongation for the given load	98
Figure 5.9 Load-displacement comparison between experimental and FEA for Configuration 1.1 - 1.4 with 1.5mm long spew; displacement represents the specimens total elongation for the given load	99

Figure 5.10 Adhesive stress distribution taken midway through the width of the specimen Configuration 1.1; σ_{33} – Normal Stress; σ_{13} – Shear Stress	100
Figure 5.11 Rivet load distribution in Configuration 1.2	101
Figure 5.12 Adhesive stress distribution taken midway through the width of the specimen Configuration 1.3; σ_{33} – Normal Stress; σ_{13} – Shear Stress	102
Figure 5.13 Rivet load carrying capability in Configuration 1.3	102
Figure 5.14 Adhesive stress distribution taken midway through the width of the specimen Configuration 1.4; σ_{33} – Normal Stress; σ_{13} – Shear Stress	103
Figure 5.15 Rivet load carrying capability in Configuration 1.4	104
Figure 5.16 Load-displacement comparison between experimental and FEA for Configuration 1.5 & 1.6; displacement represents the specimens total elongation for the given load	105
Figure 5.17 Adhesive stress distribution taken midway through the width of the specimen Configuration 1.5; σ_{33} – Normal Stress; σ_{13} – Shear Stress	106
Figure 5.18 Adhesive stress distribution taken midway through the width of the specimen Configuration 1.6; σ_{33} – Normal Stress; σ_{13} – Shear Stress	106
Figure 5.19 Load-displacement comparison between experimental and FEA for Configuration 1.8; a combination of Configuration 1.2 and 1.3 FEA results.....	108
Figure 5.20 Available average energy for crack growth at different crack lengths subjected to a 3000 μE displacement for a Bonded, Hybrid, Hybrid A (Fasteners in row 1 removed) and Hybrid B (Fasteners and Holes in row 1 removed) Configuration; *Applicable to hybrid joints only; (RR1 – Rivet Row One, RR2 – Rivet Row Two)	111
Figure 5.21 Separation of adherends with a 25mm long crack (5x deformation scale)	112
Figure 5.22 Schematic of ‘Hybrid A’ with the first row of rivets removed and all fastener holes still present	113
Figure 5.23 Schematic of ‘Hybrid B’ with the first row of rivets and fastener holes removed	113
Figure 5.24 Available energy for crack growth taken mid-width for different crack lengths subjected to a 3000 μE displacement for a Hybrid and a Hybrid A Configuration; *Applicable to hybrid joints only (RR1 – Rivet Row One, RR2 – Rivet Row Two).....	114
Figure 5.25 Available average energy for crack growth for different crack lengths subjected to a 3000 μE displacement for a Hybrid and a Hybrid A Configuration; *Applicable to hybrid joints only (RR1 – Rivet Row One, RR2 – Rivet Row Two)	114

Figure 5.26 Available energy for crack growth taken mid-width for different crack lengths subjected to a 3000 μE displacement for a Bonded and a Hybrid B Configuration; *Applicable to hybrid joints only (RR1 – Rivet Row One, RR2 – Rivet Row Two).....	116
Figure 5.27 Available average energy for crack growth for different crack lengths subjected to a 3000 μE displacement for a Bonded and a Hybrid B Configuration; *Applicable to hybrid joints only (RR1 – Rivet Row One, RR2 – Rivet Row Two)	116
Figure 6.1 Step lap joint geometries considered in parametric study; (a) symmetric outer step lap joint; (b) symmetric flush step lap joint; (c) asymmetric flush step lap joint.....	121
Figure 6.2 Configuration 2.1 - bonded step lap joint specimen	123
Figure 6.3 Configuration 2.2 - Bolted step lap joint configuration with five fasteners	123
Figure 6.4 Configuration 2.3 - hybrid step lap joint with five fasteners.....	124
Figure 6.5 Configuration 2.4 - hybrid step lap joint with three fasteners.....	124
Figure 6.6 Peak strength achieved by fastened, bonded and hybrid configurations; refer to Table 6.1 for the detailed description of the configurations	126
Figure 6.7 Damage detection using a FLIR A615 thermal camera for specimen Configuration 2.1 based on thermal data; (a) Frame 116 captured after 19.3sec; (b) Frame 323 captured after 53.8sec; (c) Frame 440 captured after 73.3sec; (d) Frame 476 captured 79.3sec after commencing the static test.....	128
Figure 6.8 Thermal image using a FLIR A615 camera of specimen Configuration 2.9 after 110,000 cycles, 2000 μE	134
Figure 6.9 Fibre optic cable bonded to one face of Configuration 2.5	136
Figure 6.10 Viewing live data from the Optical Distributed Sensor Interrogator.....	137
Figure 6.11 Fibre strain measurement at crack location in Configuration 2.5.....	137
Figure 6.12 Guide plate system used to suppress out of plane bending; (a) hybrid specimen; (b) bonded specimens containing guide without slot for bolts.....	139
Figure 6.13 Comparison of specimen configurations fatigue tested using the block loading regime; Standard – specimens tested with no guide plate; Guide Plate – specimen constrained using the guide plate system; refer to Table 6.1 for the detailed description of the configurations.....	140
Figure 7.1 Three major geometry configurations; (a) Configuration 2.1 – Bonded Step Lap Joint; (b) Configuration 2.2 – Bolted Step Lap Joint; (c) Configuration 2.3 – Hybrid Step Lap Joint with five Countersunk Bolts; B1-B5 = Bolt 1 – Bolt 5; bolts placed central of each step; OBJ – Outer butt joint where adhesive acts in tension	148

Figure 7.2 Meshed assembly of hybrid joint configuration containing five countersunk fasteners	149
Figure 7.3 Load-displacement comparison between experimental and FEA for Configuration 2.1 - 2.4; displacement represents the specimens total elongation for the given load	152
Figure 7.4 Comparison of load distribution between bolts in Configuration 2.2 (fastened step lap joint)	153
Figure 7.5 Comparison of load distributions in Configuration 2.3 and 2.4; C3 - Configuration 2.3; C4 - Configuration 2.4.....	153
Figure 7.6 Comparison of adhesive stress distribution taken about the middle line; (a) Configuration 2.1; (b) Configuration 2.3; (c) Configuration 2.4; σ_{33} – Normal Stress; σ_{13} – Shear Stress	154
Figure 7.7 Load-displacement comparison between experimental and FEA for Configurations 2.5- 2.7; displacement represents the specimens total elongation for the given load	156
Figure 7.8 Comparison of load distributions in Configuration 2.6 and 2.7; C6 - Configuration 2.6; C7 - Configuration 2.7.....	157
Figure 7.9 Comparison of adhesive stress distributions taken about the middle line; (a) Configuration 2.5; (b) Configuration 2.6; (c) Configuration 2.7; σ_{33} – Normal Stress; σ_{13} – Shear Stress	158
Figure 7.10 Load-displacement comparison between experimental and FEA for Configuration 2.9; a combination of Configuration 2.2 and 2.3 FEA results.....	159
Figure 7.11 Available average energy for crack growth subjected to a remote 1000 $\mu\epsilon$ displacement; Configuration 2.1 - Bonded; Configuration 2.4 - Hybrid with 3 bolts; vertical black dashed lines represent the start/end of each step in the joint	161
Figure 7.12 Available average energy for crack growth subjected to a remote 1000 $\mu\epsilon$ displacement; Configuration 2.1 - Bonded; Configuration 2.3 - Hybrid with 5 bolts; vertical black dashed lines represent the start/end of each step in the joint	162
Figure 7.13 Available average energy in Mode I for crack growth subjected to a remote 1000 $\mu\epsilon$ displacement; Configuration 2.1 - Bonded; Configuration 2.3 - Hybrid with 5 bolts; Configuration 2.4 - Hybrid with 3 bolts; vertical black dashed lines represent the start/end of each step in the joint.....	163
Figure 8.1 Peak strength achieved by an undamaged parent structure and fastened, bonded and hybrid step lap joint configurations; refer to Table 6.1 for the detailed description of the configurations.....	169
Figure 8.2 Outer butt joint regions (circled in red) result in early crack initiation in a bonded and hybrid step lap joint.....	171

Figure 8.3 Previous bonded step lap joint (Configuration 2.1) with double straps placed on both top and bottom surfaces	172
Figure 8.4 Previous bonded step lap joint (Configuration 2.1) with a single strap placed on the top surface.....	172
Figure 8.5 Bonded step lap joint specimens (not to scale); a) Configuration 5; b) Configuration 7; c) Configuration 9A; d) Configuration 9B; e) Configuration 11; refer to Table 8.1 for configuration description	174
Figure 8.6 Peak load carried by various bonded step lap joint configurations made from 24 plies of HexPly M18/1/G939.....	174
Figure 8.7 Two major geometry configurations; (a) Configuration 3.1 – seven step bonded lap joint; (b) Configuration 3.2 – seven step hybrid lap joint; B1-B5 = Bolt 1 – Bolt 5; bolts placed central of each step	175
Figure 8.8 Modification of previous step lap joint (Configuration 2) with a new top overlap adherend	176
Figure 8.9 Overlap step lap joint optimisation; dimensions in mm and filler adherend placed on bottom right hand end with a 0.3mm thick bondline	176
Figure 8.10 Optimising overlap length to improve the peak load carried by a bonded overlap step lap joint specimen	177
Figure 8.11 Two major geometry configurations; (a) Configuration 4.1 – six step bonded overlap lap joint; (b) Configuration 4.2 – six step hybrid overlap lap joint; B1-B5 = Bolt 1 – Bolt 5; bolts placed central of each step	177
Figure 8.12 Load-displacement comparison of numerically modelled fastened step lap joint configurations for residual strength comparison	179
Figure 8.13 Load-displacement comparison of numerically modelled bonded step lap joint configurations.....	180
Figure 8.14 Comparison of adhesive stress distribution taken midway through the width of the specimens; (a) Configuration 2.1; (b) Configuration 3.1; (c) Configuration 4.1; σ_{33} – Normal Stress; σ_{13} – Shear Stress.....	181
Figure 8.15 Load-displacement comparison of numerically modelled hybrid step lap joint configurations.....	182
Figure 8.16 Comparison of adhesive stress distribution taken midway through the width of the specimens; (a) Configuration 2.3; (b) Configuration 3.2; (c) Configuration 4.2; σ_{33} – Normal Stress; σ_{13} – Shear Stress.....	183

Figure 8.17 Bolt load share comparison between Configuration 3.2 and Configuration 4.2; Failure Load - the peak load carried by the configuration before final failure; Applied Load - total load carried by the configuration for a given point in time.....	184
Figure 8.18 Bonded step lap joint configurations cured in an autoclave at 121°C for 90min; Configuration 4.1 - top; Configuration 3.1 - bottom.....	185
Figure 8.19 Hybrid step lap joint configurations cured in an autoclave at 121°C for 90min; Configuration 3.2 - top; Configuration 4.2 - bottom.....	186
Figure 8.20 Comparison of static load-displacement results for four specimen Configurations 3.1, 3.2, 4.1 and 4.2 numerically analysed and tested experimentally	187

List of Tables

Table 2.1 Advantages and disadvantages of mechanically fastened joints	16
Table 2.2 Advantages and disadvantages of adhesive bonded joints	19
Table 2.3 Advantages and disadvantages of hybrid joints	21
Table 3.1 Properties of HexPly M18/1/G939 carbon fibre prepreg; [118]	48
Table 3.2 Properties of FM300-2K film adhesive; [121, 122]	49
Table 3.3 Cheri Maxibolt CR7621U-05-04 rivet specification [123]	50
Table 3.4 Aviaquip NAS1581C4T4 bolt specification [124]	51
Table 3.5 Overview of thin double lap joint configurations	52
Table 3.6 Overview of thick step lap joint configurations containing five steps	54
Table 3.7 Overview of the optimised thick step lap joint configurations	57
Table 4.1 Number of specimens static and fatigue tested in Stage 1	74
Table 4.2 Block loading regime #1 - strain amplitude increased every 10^5 cycles	77
Table 4.3 Summary of average peak load achieved by specimen Configuration 1.1-1.8	79
Table 4.4 Fatigue resistance of specimen Configuration 1.1-1.8 under block loading, r-ratio = 0.1 frequency = 5Hz	80
Table 4.5 Failure of the eight specimen configurations tested under fatigue loading at an r-ratio = 0.1 at 5Hz; both front and back images of failed gauge region shown	82
Table 4.6 Specimen Configuration 1.3 failing under a fatigue block loading regime and failing under static testing with a cross-head speed of 1mm/min	84
Table 6.1 Number of specimens static and fatigue tested in Stage 2	122
Table 6.2 Block loading regime – strain amplitude increased every 10^5 cycles starting at 1000µε	125
Table 6.3 Summary of average peak load achieved by specimen Configuration 2.1-2.10	127
Table 6.4 Fatigue resistance of specimen Configuration 2.1-2.10 under block loading, r-ratio = 0.1 frequency = 5Hz	130

Table 6.5 Monitoring and detecting crack growth rate in specimen Configuration 2.9	133
Table 6.6 Failure of the ten step lap joint configurations fatigue tested using a block loading regime; r-ratio=0.1	142
Table 8.1 The number of plies per step placed in a step lap joint made up of 24 plies with a fixed [(0/90)/(45/-45)/(45/-45)/(0/90)] ₆ orientation.....	173
Table 8.2 Block loading regime – strain amplitude increased every 10 ⁵ cycles; frequency=5Hz, r- ratio=0.1	188
Table 8.3 Fatigue resistance of four specimen configurations subjected to a block loading regime	189
Table 8.4 Failure of four step lap joint configurations fatigue tested using a block loading regime	190

Abbreviations

Abbreviation	Definition
<i>3D</i>	Three-Dimensional
<i>AFHR</i>	Adhesive to Fastener Hole Ratio
<i>ASTM</i>	American Society for Testing and Materials
<i>CAE</i>	Computer Aided Engineering
<i>CASA</i>	Civil Aviation Safety Authority
<i>CFRP</i>	Carbon Fibre Reinforced Polymers
<i>Configuration 1.1</i>	Pristine bonded double lap joint
<i>Configuration 1.2</i>	Pristine riveted double lap joint with six rivets (square array)
<i>Configuration 1.3</i>	Pristine hybrid double lap joint with six rivets (square array)
<i>Configuration 1.4</i>	Pristine hybrid double lap joint with three rivets (staggered array)
<i>Configuration 1.5</i>	Defective bonded double lap joint with 2mm long initial crack
<i>Configuration 1.6</i>	Defective hybrid double lap joint with six rivets and a 2mm long initial crack
<i>Configuration 1.7</i>	Defective bonded double lap joint with a semi-cured adhesive
<i>Configuration 1.8</i>	Defective hybrid double lap joint with six rivets and a semi-cured adhesive
<i>Configuration 2.1</i>	Pristine bonded step lap joint with five steps
<i>Configuration 2.2</i>	Pristine bolted step lap joint with five steps and five bolts
<i>Configuration 2.3</i>	Pristine hybrid step lap joint with five steps and five bolts
<i>Configuration 2.4</i>	Pristine hybrid step lap joint with five steps and three bolts
<i>Configuration 2.5</i>	Defective bonded step lap joint with five steps and a 2mm long initial crack
<i>Configuration 2.6</i>	Defective hybrid step lap joint with five steps, five bolts and a 2mm long initial crack
<i>Configuration 2.7</i>	Defective hybrid step lap joint with five steps, three bolts and a 2mm long initial crack
<i>Configuration 2.8</i>	Defective bonded step lap joint with five steps and a semi-cured adhesive
<i>Configuration 2.9</i>	Defective hybrid step lap joint with five steps, five bolts and a semi-cured adhesive
<i>Configuration 2.10</i>	Defective hybrid step lap joint with five steps, three bolts and a semi-cured adhesive
<i>Configuration 3.0</i>	Pristine bolted step lap joint with seven steps and five bolts

Abbreviation	Definition
<i>Configuration 3.1</i>	Pristine bonded step lap joint with seven steps
<i>Configuration 3.2</i>	Pristine hybrid step lap joint with seven steps and five bolts
<i>Configuration 4.0</i>	Pristine bolted step lap joint with six steps and five bolts with an outer overlap
<i>Configuration 4.1</i>	Pristine bonded step lap joint with six steps with an outer overlap
<i>Configuration 4.2</i>	Pristine hybrid step lap joint with six steps and five bolts with an outer overlap
<i>CSR</i>	Constant Strain Rate
<i>DAQ</i>	Data Acquisition
<i>DCB</i>	Double Cantilever Beam
<i>DOFS</i>	Distributed Optical Fibre Sensor
<i>EASA</i>	European Aviation Safety Authority
<i>ENF</i>	End Notch Flexure
<i>FAA</i>	Federal Aviation Authority
<i>FE</i>	Finite Element
<i>FEA</i>	Finite Element Analysis
<i>FLIR</i>	Forward-Looking Infrared Radiometer
<i>FRP</i>	Fibre Reinforced Plastic
<i>GFRP</i>	Glass Fibre Reinforced Polymers
<i>Hybrid A</i>	Hybrid double lap joint with the first row of rivets removed
<i>Hybrid B</i>	Hybrid double lap joint with the first row of rivets and holes removed
<i>KTF</i>	Kinetic Theory of Fracture
<i>MCT</i>	Multicontinuum Theory
<i>MEK</i>	Methyl-Ethyl-Ketone
<i>NC</i>	Numerical Control
<i>NDI</i>	Non-Destructive Inspection
<i>NDT</i>	Non-Destructive Testing
<i>OBJ</i>	Outer Butt Joint Region (step lap joint)
<i>PTFE</i>	Polytetrafluoroethylene
<i>RR1</i>	Rivet Row 1
<i>RR2</i>	Rivet Row 2

Abbreviation	Definition
<i>RTM</i>	Resin Transfer Moulding
<i>RVE</i>	Representative Volume Element
<i>SERR</i>	Strain Energy Release Rate
<i>SHM</i>	Structural Health Monitoring

Nomenclature

Symbol	Description
γ_e	Elastic shear strain
γ_p	Plastic shear strain
μ	Shear modulus
φ_f	Fibre volume fraction
φ_m	Matrix volume fraction
σ	Stress
σ_f	Fibre stress
σ_{ij}	Generalised stress
σ_{ij}^f	Generalised fibre stress
σ_m	Matrix stress
σ_{ij}^m	Generalised matrix stress
ν	Poisson's ratio
ν_{12}	In-plane Poisson's ratio
A_1^f	Fibre failure criteria coefficient
A_1^m	Matrix failure criteria coefficient
C	Materials stiffness matrix
$\frac{da}{dN}$	Crack growth rate
E	Young's modulus
E_{11}	In-plane Young's modulus in the 1-material direction
E_{22}	In-plane Young's modulus in the 2-material direction
E_{33}	In-plane Young's modulus in the 3-material direction
ε	Strain
ε_f	Fibre strain
ε_m	Matrix strain
F	Fibre degradation value
G	Strain energy release rate
G	Shear modulus
G_{12}	In-plane shear modulus

Symbol	Description
G_{13}	Interlaminar shear modulus in the 1-3 plane
G_{23}	Interlaminar shear modulus in the 2-3 plane
G_{IC}	Mode I fracture toughness
G_{IIC}	Mode II fracture toughness
I_i	Isotropic stress invariants
K_i	Stress intensity factor
M	Matrix degradation value
N	Total number of cycles
n	Number of cycles
R	Continuum point
$+S_{11}$	Tensile strength in the 1-material direction
$+S_{22}$	Tensile strength in the 2-material direction
$-S_{11}$	Compressive strength in the 1-material direction
$-S_{22}$	Compressive strength in the 2-material direction
S_{12}	In-plane shear strength
V	Volume

1

Introduction

1.1 Background

The use of composite materials as a replacement for commonly used metals such as aluminium and steel are ever increasing in the engineering industry, particularly in the aerospace sector. The need for safe, light and economical airplanes has always been an area of research even up to this day. In the early 20th century, the fabrication and use of metals became increasingly popular and began wide spread use in the manufacture of airplanes. At the time due to the lightness and strength of aluminium, this was the preferred material of choice by aircraft manufactures and became the norm in the fabrication of fuselages, wings and empennages.

Over the years, composite materials such as carbon fibre reinforced polymers (CFRP) and glass fibre reinforced polymers (GFRP) became more prominent in the industry. Advantages such as good fatigue durability, corrosion resistance and high strength to weight ratio have now led to the rapid move from metal structures to composite structures. This change allows for further flexibility in design and fabrication of various components and joints.

The earliest use of composite materials dates back to 1500 B.C. when the Egyptians and Mesopotamian settlers used a mixture of mud and straw to create strong and durable

buildings. The production and use of composite materials now is much of a form of art as it is science. Various manufacturing processes such as prepreg consolidation, dry or wet filament winding, hand layup or automatic robot-assisted layup followed by direct resin transfer moulding (RTM), or vacuum assisted resin transfer moulding (VARTM) are now utilised to achieve mass production of composite structures with high strength and durability [1].

A composite material is made up of two parts, the fibre and the matrix. Each of these have distinct material properties. The fibre is considered the reinforcement in the composite material and has very high strength whilst the matrix is responsible for keeping the fibres aligned and is isotropic; typically epoxy resin is used as a matrix. It is the orientation of the fibres which predominantly influence the composite material properties which are known to be anisotropic. Fibre reinforced composite materials are divided into two main categories which are short fibre reinforced materials and continuous fibre reinforced materials. Short fibre reinforced materials are typically used in compression moulded applications whilst continuous fibre reinforced composites are used in a number of applications in particular laminated structures.

With every new material used in the engineering industry, it is paramount to understand their strengths and weaknesses and the various factors which can influence its behaviour. The main damage mechanisms in metallic materials are due to corrosion and/or cracking; composite material on the other hand exhibit vastly different damage mechanisms which can range from fibre pull-out and cracking right through to inter-ply delamination. This results in the need for new damage growth predictions and failure models for composite materials which may be achieved through rigorous testing and analysis.

In the aerospace industry, the testing and analysis of materials play a large role in the certification of components. In the early 20th century aviation remained a dangerous business. It was soon realised that its full potential, in particular the commercial aspects could not be reached unless federal action was taken to improve and maintain safety standards. This was the introduction of licensing and certification. Various bodies such as the FAA (Federal Aviation Authorities), EASA (European Aviation Safety Authority) and CASA (Civil Aviation Safety Authority) are responsible for the legislation and regulation of aircrafts. One aspect of their work involves the certification of aircraft components which has led to the substantial amount of new research.

An aircraft consists of thousands of individual components that are joined together by mechanical fasteners such as rivets, screws and bolts. In order to ensure an aircraft is structurally sound depends heavily on how effectively the components are joined together and the method by which they are joined. For example, the wing of an Airbus 380 alone is composed of over 30,000 elements, with approximately 750,000 bolted joints. These joints are of key importance since they form a weak point that can contribute to the breakage of the element, as well as increase the weight of the aircraft if the design is inefficient. With the use of composite materials, it has become ever more important in understanding how to effectively join these materials together. Bolted joints are commonly found in joining metallic structures together as high stress concentration may be alleviated through localised plasticisation. These stress concentrations are much more severe and detrimental when used in composite adherends (also termed laminate). As these composite materials are now commonly being used to improve the performance of aircrafts it is vital to find new and effective joining/repairing methods. This will ensure its widespread use in the industry.

1.2 Research Objective

The intent of this research is to develop and compare three distinct joining/repairing methods for aerospace grade composite materials currently used in aircraft structures.

- 1) Mechanically fastened joints
- 2) Bonded joints
- 3) Hybrid joints

Comparing and understanding the behaviour of these three joints provides a vital piece of information to the industry as it qualitatively defines the advantages and disadvantages in its use. This is crucial in order to progress the more widespread use of new and efficient joining and repairing techniques in the Aerospace field. From the available literature, there is no work that has compared these various joint types for both thick and thin structures. This dissertation aims at fulfilling this requirement and assist in composite joint/repair certification.

From the three joint types defined, mechanical fasteners such as pins, rivets and bolts have been commonly used in the aerospace industry for many decades [2-4]. The ease of disassembling components and allowing for reliable inspection has been a great benefit.

The key problem that arises through the use of mechanical fasteners is the high stress concentrations around the fastener holes which are much more severe in composite laminates compared to metal plates under the same loading condition. This is primarily due to the materials properties where metals are ductile and can yield [5].

Adhesively bonded joints are structurally more efficient than mechanically fastened joints as they perform better in distributing loads and hence eliminate a majority of high stress concentration problems seen in bolted joints. When conducting bonded repairs on structures, it is important to consider that the strength of the bond should not fall below that of the surrounding structure or the design ultimate strength of the structure. As such in the Aerospace Industry, strong ductile adhesives are used so that the loading capacity of the bond is significantly higher than the adherends for properly designed joints between thin members. Since adhesively bonded joints are strong in shear but weak in peel, the joints are designed so that the majority of the load is transferred in shear [5]. The quality of adhesively bonded repairs critically relies on the process control during the repair application. Improper processes would result in a weak bond that is not generally possible to be detected by means of non-destructive inspection (NDI). The detrimental effect of some improper surface treatment may not even manifest in a significant reduction of the initial static strength of the bond but in an adverse impact on the durability of the adhesive bond at service temperature and moisture environment and/or under fatigue loading.

The combination of mechanical fastening and bonding (i.e. hybrid joints) has been employed to safeguard against defects within the adhesive layer which may cause premature or catastrophic failure [6]. In contrast to the mechanically fastened joints, the stress concentrations around the fastener holes are significantly reduced due to the presence of the adhesive layer which evenly distributes the load within the bond region. It is only after the bond has failed where the fasteners begin to carry the remaining load in the joint. It is this safety factor that has allowed the certification of these joints in some aircraft structures.

Two distinctly different joint types are considered in this dissertation one for thin adherends (<5mm thick) and the second for thick adherends (>5mm thick).

- 1) Double Lap Joint (thin joint type)
- 2) Step Lap Joint (thick and flush joint type)

Extensive experimental testing is conducted using a servo-hydraulic testing machine. These joint types are to be employed in aircraft structures and hence it is vital to not only understand their strength behaviour but more importantly their durability. Hence, static and fatigue tests are conducted on each joint configuration. Finite Element Analysis (FEA) using Abaqus CAE is used to gain further understanding of load distribution and failure mechanisms. A micromechanical analysis method called the Multicontinuum Theory (MCT) is adopted in the simulation to progressively degrade the fibre and matrix material which allows in analysing failure in the composite structure from start to finish [7, 8].

Overall through the comparisons made between thin and thick fastened, bonded and hybrid joints, a better understanding of their joint behaviour and durability is achieved and will serve as a vital tool for composite joint/repair certification.

1.3 Thesis Structure

A review of previously published work on composite materials and various failure mechanisms is presented in Chapter 2. The chapter outlines the common certification approach adopted by aircraft manufacturers particularly for composite joints. The limitations and advantages of composite materials over conventional metallic materials such as aluminium is also identified. Furthermore, the types of joint configurations commonly adopted in aircrafts are discussed. This area also touches on various joint types such as single lap joints, double lap joints, butt joints, step lap joints right through the scarf joints. In addition, types of fatigue tests such as constant amplitude and variable amplitude testing are also discussed.

Chapter 3 presents an overview of the materials used for testing and how they have been used in previous applications. The main focus of this chapter will be on specimen design, manufacture and assembly of double lap joint and step lap joint specimens. Emphasis on surface preparation techniques required for proper bonded and non-destructive inspection techniques such as using an Ultrasonic A-Scanning with a 5MHz probe is also mentioned here.

Static and fatigue test results for thin double lap joint configurations are discussed in Chapter 4 which is considered to be ‘Stage 1’ of the dissertation. Detailed discussion on failure types and trends will be a part of this chapter. An overall comparison between the

static test configurations and the fatigue test configurations are highlighted. A total of eight different configurations are tested which include (i) pristine specimens which contain a properly cured bondline, (ii) defective specimens which contain a 2mm long initial crack and (iii) defective specimens which contain a semi-cured bondline.

Finite Element Analysis on all eight of the double lap joint configurations is discussed in Chapter 5. Here the model setup and conditions are explained as well as the use of the progressive damage model based on the Multicontinuum Theory. This section will compare the static experimental results discussed in Chapter 4 with the numerically obtained load-displacement graphs using Abaqus CAE. Information on the shear and normal stress distribution within the joint regions is provided. Critical information as to why a hybrid joint has significantly greater fatigue resistance than a bonded joint is discussed by comparing the Strain Energy Release Rate (SERR) for different bonded and hybrid configurations.

Chapter 6 focuses on static and fatigue testing of thick step lap joint configurations; considered to be ‘Stage 2’ of the dissertation. Information on the parametric study conducted in Abaqus CAE will be mentioned here followed by the final joint design selection. Detailed experimental results will follow in addition to in-situ non-destructive test data gathered using an Ultrasonic A-Scanner and Thermal Camera. A total of ten different joint configurations is discussed in this chapter. Once again the configurations are broken up into three distinct categories: (i) pristine specimens which contain a properly cured bondline, (ii) defective specimens which contain a 2mm long initial crack and (iii) defective specimens which contain a semi-cured bondline.

Finite Element Analysis using Abaqus CAE and the Multicontinuum Theory for the thick step lap joints are presented in Chapter 7. A comparison between the static experimental and numerical results are discussed as well as the reasoning behind certain outcomes. This chapter also explains how and why the bolts in a hybrid joint configuration arrests crack propagation which aids durability. The Strain Energy Release Rates (SERR) are determined for the bonded and hybrid step lap joints to provide an indication of fatigue life. This is then compared with the experimental fatigue life.

An optimisation study is discussed in Chapter 8 which aims at improving the fatigue resistance of the previous step lap joint design containing uniform step heights with a total of five steps. This Chapter will provide useful information on how an existing step lap

joint design can be improved upon with minimal increase to the joint area. The chapter will contain experimental and numerical work.

The conclusions drawn from the work are highlighted in Chapter 9. This will identify the major findings gathered from the research and the contribution it will make within the aerospace field. Further recommendations and future scope of research are also presented in this chapter.

End of Chapter 1

2

Literature Review

2.1 Introduction

Fibre reinforced polymer matrix composites are being increasingly used in aircraft structures because of their superior structural performance, such as high strength, high stiffness, long fatigue life, and low density. Materials such as carbon fibre reinforced polymers (CFRP) and glass fibre reinforced polymers (GFRP) are now commonly found in many aircraft components such as fuselage skins, wing ribs, formers and stringers.

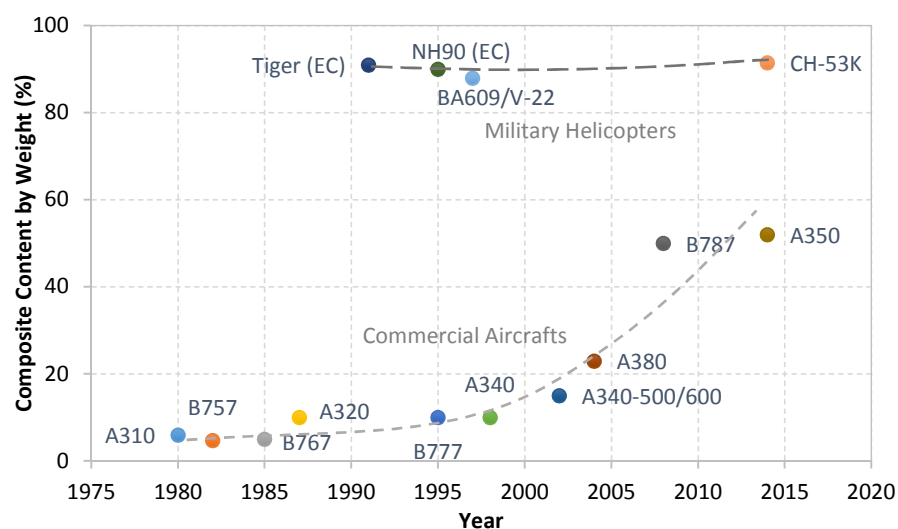


Figure 2.1 The use of composite materials in commercial and military aircrafts

Figure 2.1 shows the increasing use of composite materials in the construction of aircrafts over the last several decades. From the figure, it is clear that military air vehicles have advanced significantly earlier in terms of composite material usage than commercial air vehicles. However with the emergence of the Boeing 787 and Airbus 350 comprising of more than 50% composite material, it is clear that materials such as carbon and aramid fibres are soon to be the main construction material in commercial aircrafts as well. This puts further emphasis on the need to understand the long-term behaviour of these materials in order to create new and efficient air vehicles.

As previously mentioned, composite materials are made up of two parts - the matrix and the fibre. The fibres are considered to be the reinforcement in the composite material with very high strength and anisotropic whilst the matrix is responsible for keeping the fibres aligned and is isotropic. A unidirectional fabric is one of the most basic fabrics available. This fabric has the majority of its fibres running in one direction. This offers the ability to place fibres in a component exactly where it is required. Additionally, multiple layers of fabric can be stacked on top of each other to offer strength in multiple directions.

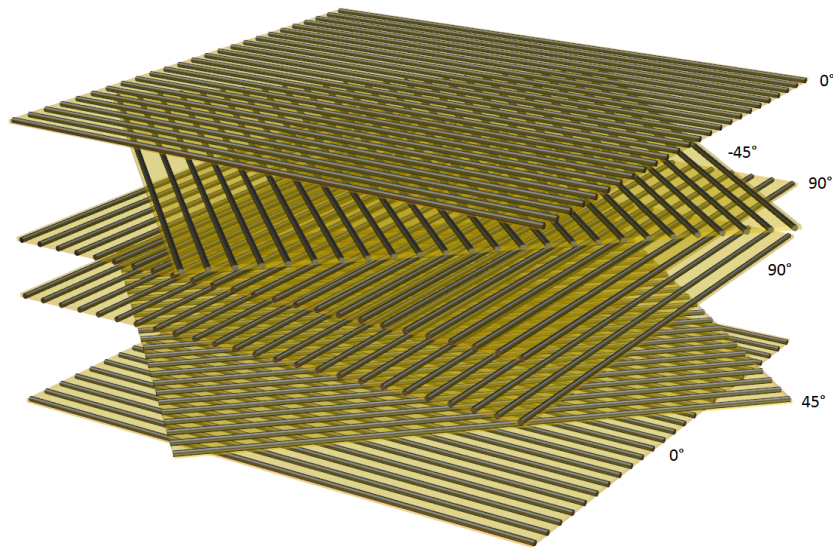


Figure 2.2 Ply stacking sequence based on a unidirectional fabric

Figure 2.2 shows a balanced layup using a unidirectional fabric. A stacking sequence of $[0/45/90/90/-45/0]$ has been used in this instance. In general, the stacking sequence is an important part of the design as it needs to provide the required engineering properties, in-plane stiffness and strength as well as bending stiffness.

A commonly used alternative to unidirectional fabrics is woven fabrics. These can be found in a number of weave configurations shown in Figure 2.3

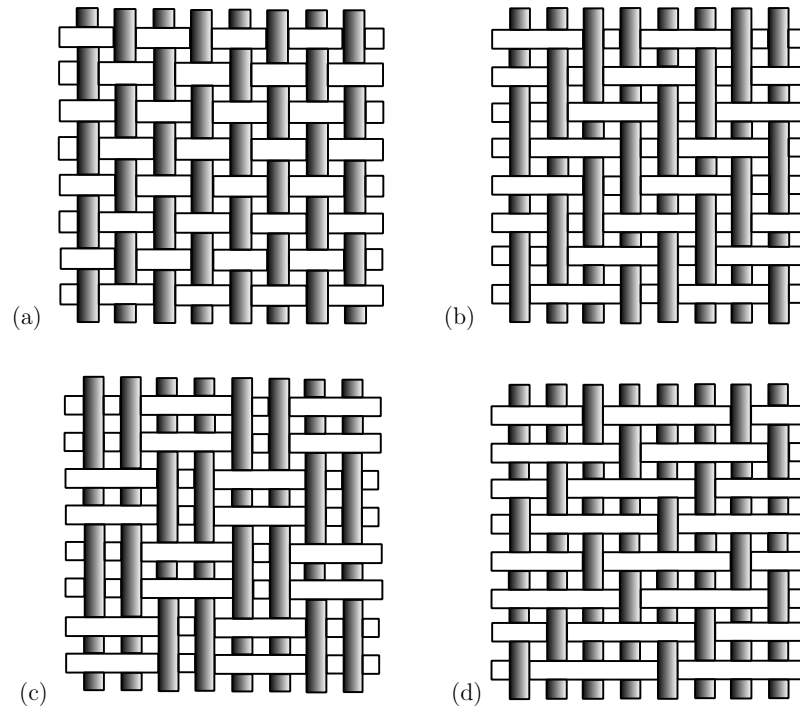


Figure 2.3 Common woven fabric configurations; (a) plain weave; (b) twill weave; (c) basket weave; (d) satin weave

The type of weave selected for use is dependent on cost, strength and surface coverage required. Woven fabrics have the advantage of better drapeability over complex shapes and due to the interlacement of fibres, they achieve good structural integrity compared to unidirectional fabrics.

Plain weave is the most common weave configuration. It is firm, stable and ideally suited to covering large flat surfaces. Twill weave is more pliable than plain weave and has a good draping capacity hence allowing better coverage over curved surfaces. Basket weave is a coarse weave configuration but with increased strength whilst satin weave can be found in 4, 5 and 8 shaft satin styles. This weave has excellent pliability over compound curves; allows for high fabric density and high strength in most surface directions. All of these fabrics can be found in a ‘dry’ form where no matrix is impregnated or it may be found in a ‘prepreg’ form where the matrix, such as epoxy is already present. Here the matrix is partially cured to allow for easier handling and eliminates resin rich and resin poor regions.

Each layer of fabric is still considered as a single ‘ply’ similar to a unidirectional fabric. By stacking multiple plies on top of each other using hand layup techniques (matrix added to dry fabric) or by using prepreg, the desired material strength and thickness can be achieved to form a ‘laminate’. Note that a vacuum bag is used to eliminate voids and air bubbles present during the layup stage, Figure 2.4. Depending on the matrix used, the composite structure may be cured at atmospheric conditions or under heat either in an oven or an autoclave.

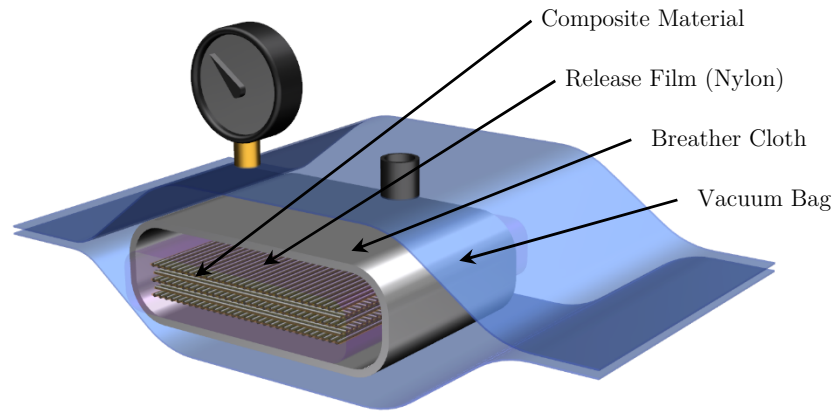


Figure 2.4 Vacuum bagging schematic containing a composite layup

The move towards light weight, high stiffness structures that have good fatigue durability and corrosion resistance has led to the rapid move from metal structures to composite structures [9]. With this brings the added concern of certifying new components as the damage mechanisms and failure modes in composites differ significantly than those of metals. At the same time, it must be noted that the certification philosophy for composites must meet the same structural integrity, safety and durability requirements as that of metals. Hence, this is where the challenge now lies. Due to the complexity in design and fabrication of aircraft structures, the need for joining components together plays an important role. When it comes to using composites although the in-plane strength is very good, the out of plane strength is usually very poor and needs to be accounted for when creating these structures. In order to design these, it is imperative that the structure is safe with optimal performance. The joining of these structures/components can be achieved through fastening (mechanical joining), bonding using adhesives or the combination of both bonding and fastening, also known as hybrid joints. Furthermore, composite materials

can provide wider applications in repairing damaged and degraded materials suffering from corrosion and fatigue.

2.2 Composite Failure Mechanisms

The use of composite materials in the aerospace industry requires a significant amount of numerical and experimental testing. These experimental tests include static testing components and more importantly fatigue testing. An aircraft undergoes thousands of repeated loading and unloading cycles due to take-off and landing throughout its service life. The constant loading and unloading can result in repeated strain on various aircraft components causing it to degrade over time. This degradation is termed ‘fatigue’. During the initial period of fatigue in composite materials, many non-interactive cracks occur in the matrix. When the matrix crack density reaches saturation, fibre failure, interfacial debonding and delamination occurs; all of these rapidly increase the damage in the material which causes a non-linear damage evolution.

One method in which composite fatigue is tested is through cyclic loading. This is done through a systematic repetitive loading sequence with regular reoccurring stresses on a part that can lead to fatigue fracture. There are several methods for predicting the behaviour of composites under cyclic loading; these include modulus degradation [10-12], the derivation of fatigue modulus [13], residual strength [14], the strength-life-equal-rank assumption [15, 16], cumulative damage [17] and the energy criteria [18].

The four basic failure types that occur in composites under cyclic loading include matrix cracking, interfacial debonding, delamination and fibre breakage. When a laminate is subjected to tension, cracks appear in the off-axis plies. Matrix cracking also appears in the longitudinal plies, due to the mismatch in the in-plane Poisson’s ratios of the longitudinal and transverse plies. Interfacial debonding occurs when there is a matrix crack which propagates, thus inducing forces on various fibres that no longer adhere to the cured resin. Delamination is caused by repeated cyclic stresses and impacts. These cause layers to separate and thus result in significant loss of mechanical toughness. Fibre pull-out and delamination is a result of weak bonding. Delamination is a dangerous mode of failure as it can develop inside of a material without being obvious on the surface thus making it difficult to find using non-destructive inspection (NDI) techniques. Finally, fibre breakage is a failure mechanism which can cause catastrophic failure of components and is thus vital

that regular inspections are carried out to monitor this behaviour and that suitable predictions are made based on when it is likely to occur. The sequence at which these failure mechanisms occur is not always the same. For instance in constant strain rate (CSR) applications and fatigue tests, delamination is typically observed first followed by transverse cracking. In creep tests, transverse cracking is usually first observed followed by delamination.

2.3 Composite Joint Methods

The joining and repairing of components in aircraft structures play a fundamental role in the operation and longevity of the vehicle. It is common practice to assume that all aircrafts contain minor defects in its structural components due to manufacturing; the continual loading and unloading of these components only add to the severity of further promoting these defects. If not continually monitored and regularly maintained these defects reach a critical level that can cause serious detriment to the aircraft and more importantly its occupants. It is for this reason when a flaw is detected, the repair carried out whether it is a patch repair or a component replacement; the joint configuration used in the repair needs to be thoroughly assessed and well understood. As previously discussed, typical methods of repair can be carried out by using fasteners or by using different bonding techniques.

2.3.1 Mechanically Fastened Joints

There are many types of fasteners used in joining materials together such as aluminium sheets as well as composite laminates. Typical fasteners include using pins, screws and rivets which are an effective and easy way of joining adherends together. Using bolts is another popular fastening method. Bolted joints are commonly used in the aviation industry as well as in repair [2, 3]. They are used to fasten components together and offer easy inspection as they are removable, they can be easily manufactured and hence cost effective and at the moment are seen as being more reliable methods of repair compared to bonded joints. In terms of static testing a composite material with a single fastener, variables that need to be considered include the following: hole size, laminate layup and thickness, environment factor (room temperature-dry, hot-wet, cold-dry), load type (tension, compression, different bypass ratios and pull through), geometry (width/

diameter, edge distance and diameter), fastener head type, joint type (single or double lap, step, scarf), joint material and clamping load provided by the fastener [19].

Accurate prediction of stresses in the bolted joints is essential for the reliable design of the entire structure. Out of all the various fasteners mentioned, bolted joints are found to be the most efficient form of mechanical fastening in composite materials [4]. There are four failure modes in composite joints with a fastener such as a bolt. These include, tension failure, shear out failure, cleavage tension failure and bearing failure.

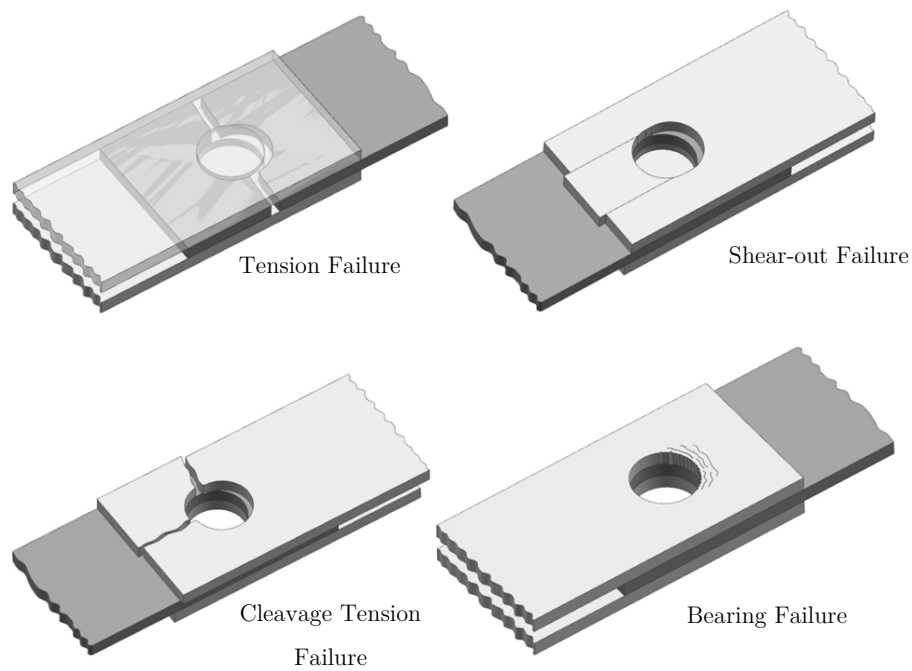


Figure 2.5 Failure modes for bolted joints used with composite laminates

As it can be seen from Figure 2.5, tension failure occurs from the fastener hole to the edge of the plate which is parallel to the loading direction. This typically occurs when the cross-sectional area of the sample is particularly small and has excessive tensile stress [20]. Shear-out failure occurs along the shear-out plane on the hole boundary and usually occurs when the distance between the edge of the fastener hole and the laminate hole is small [21]. Bearing failure occurs in the vicinity of the fastener. It is typically caused by the tilting of the fastener in the hole of the sample which causes compressive stress near the boundaries of the hole [21]. This mode of failure is somewhat desirable compared to the others modes of failure as it is relatively slow and provides some time for it to be detected before final

failure [22]. Cleavage failure is known as a mixed mode failure involving tension and bending. Alongside these failure modes, fastener failure may also take place such as a bolt pulling through the laminate or the bolt failing due to shear.

Riveting can be considered as another form of fastening materials together and are suitable for laminates up to 5mm thick. However, the closing pressure of a rivet is not always controllable, hence resulting in a wide variation of clamping pressure. It should also be noted that the riveting operation can potentially damage the laminates and in addition cause stress concentrations around the holes. When looking at metal structures, its ductility can reduce the high stress concentration around bolt holes. With composites however, there is no such relief from the elastic stress concentration if the holes or cut-outs are large enough. Local debonding between fibres and matrix resin and interplay splitting does however locally alleviate some of the most severe stress concentrations [5]. In other words, since composite materials have no yield point, if one fastener is tighter in its hole then that fastener will have the higher bearing stress; as a result, the higher load could cause ultimate failure of the material. It should be mentioned that Hart-Smith noted that slippage between resin and fibres provide some relief of stress concentration induced around bolt-holes and various cut-outs. The slippage between resin and fibres averages out local stress concentrations and results in more of the fibres being loaded before final failure [5].

It must also be noted that a combination of failure modes can take place to result in catastrophic failure of a composite bolted joint. The allowable stresses in each of these modes is a function of the following:

- 1) Joint geometry including laminate and hole size, laminate width and hole distance from the edge of the laminate.
- 2) The fibre orientation and ply stacking sequence
- 3) The moisture content and ambient air temperature
- 4) Clamping area and pressure applied to the fasteners
- 5) The nature of loading such as tension, compression, out of plane loads, sustained or cycled loads

Although only a single fastener hole has been considered thus far, the main principles hold for multiple fastener configurations. In practical applications, a single row of fasteners may

be sufficient to transfer loads effectively from one plate to the other. In highly loaded applications multi-row fasteners are used (e.g. wing of a plane). The configurations of these fasteners also play an important role in the efficiency of the joint. Table 2.1 summarises key advantages and disadvantages associated with mechanically fastened joints.

Table 2.1 Advantages and disadvantages of mechanically fastened joints

Advantages	Disadvantages
Easy to disassemble in certain cases	Large weight penalty
No surface preparation required	Susceptible to corrosion
Not environmentally sensitive	Sensitivity to clamping force
Simple inspection procedure	Substantial stress concentration
No residual stress problem	Sensitivity to hole size tolerance
Simple joint configuration	Relatively poor fatigue properties
No thickness limitations	Machining fastener holes can introduce damage

2.3.2 Bonded Joints

Adhesive joints also known as bonded joints are structurally more efficient than mechanically fastened joints as they perform better in distributing loads and hence eliminate a majority of the high stress concentration problems seen in bolted joints. When conducting bonded repairs on structures, it is important to consider that in no case should the strength of the bond fall below that of the surrounding structure. This is because the bonded joint will have no damage tolerance and will act as a weak link. As such in the Aerospace Industry, strong ductile adhesives are used so that the bond is stronger than the adherends for properly designed joints between thin members. Since adhesively bonded joints are strong in shear but weak in peel, it is good to design the joints so that the majority of the load is transferred in shear [5].

In terms of the environmental conditions, the performance of adhesives is highly affected by temperature and humidity, the stiffness and strength of an adhesive drops sharply beyond the glass transition temperature. The material is rubbery above the glass transition temperature and glass like below it. One variable that does in fact affect the strength of

bonded joints include moisture. Even very small amounts of moisture can be very harmful to bonded composites. The absorption of water plasticises adhesives and lowers their mechanical performance. Over time, moisture can degrade away the epoxy and this can lead to fibres being exposed. If metal is also used in the repair such as a bolted joint, this can cause an electro-potential between the two materials and thus begin corrosion on the more active material (anode) at an accelerated rate. Overall, absorbed water in cured laminates must be removed carefully through drying, if moisture is driven off too rapidly then it will delaminate the composite [5].

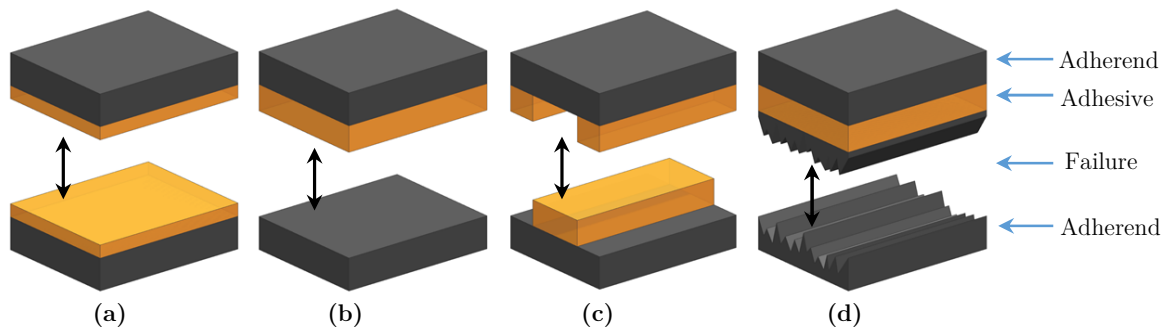


Figure 2.6 Failure modes in adhesive bonded joints; (a) cohesive failure; (b) adhesive failure; (c) mixed failure; (d) adherend failure

Figure 2.6 shows the four common modes of failure in adhesive bonded composite joints. In the adherend failure can be tensile, inter-laminar or transverse. The surface preparation of composite bonded joints is an important factor in its performance. A clean surface is a necessary condition for adhesion but it is not a sufficient condition for bond durability. Most structural adhesives work as a result of the formation of chemical bonds (mainly covalent, but some ionic and static attractive bonds may also be present) between the adherend surface atoms and the compounds constituting the adhesive [23]. These chemical links are the load transfer mechanism between the adherends. Most adhesive bond failures can be attributed to poor processes during fabrication, with the lack of quality surface preparation being the most significant deficiency [24]. Chapter 3 touches on the surface preparation techniques employed in this research to minimise and/or prevent adhesive failure.

Typically the bond strength must exceed the adherent strength by at least 50%. The analysis of adhesively bonded joints requires a nonlinear shear stress-strain curve because even brittle adhesives exhibit substantial nonlinear behaviour at temperatures approaching

their upper service limits [5]. The thickness of the adherends also plays an important role in the efficiency of the joints. For thin adherends (composite or metal), adhesive bonding is more suitable than mechanical fastening and more than likely the strength of the joint will exceed the strength of the members being joined. In the case of thicker more highly loaded structure, either mechanical fastening or more complex bonded stepped-lap joints are needed; adhesive bonds would only act as weak link fuses in the thick structures.

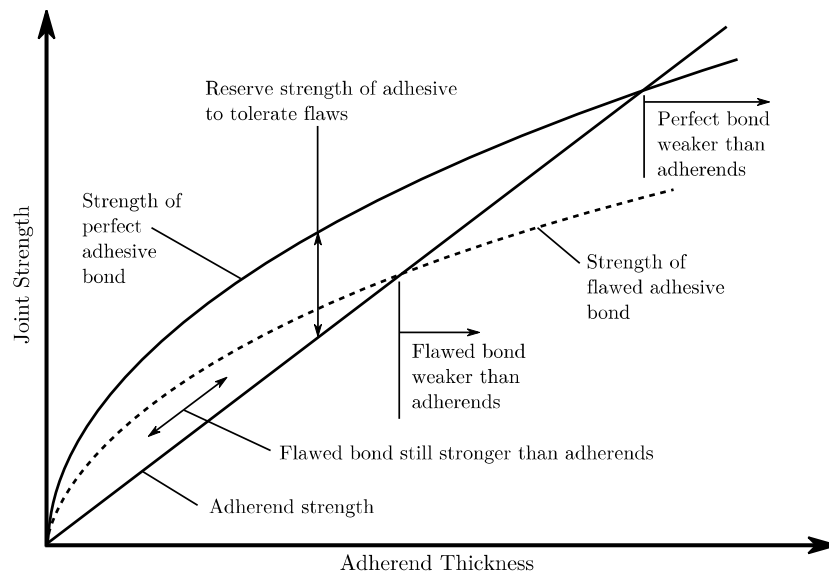


Figure 2.7 The relative strength of adherends and adhesives affected by bond flaws [25]

Figure 2.7, summarises the relationship between bond strength and adherend thickness. From it, it can be concluded that as adherend thickness increases, the relative strength of the bond compared to the adherend becomes weaker. Thus this clearly shows, bonded joints are more advantageous for thin adherends. Alongside this, the overlap length between the adherends must also be considered, it is known that short overlap test coupons are extremely sensitive to failure by creep rapture (which accumulates under both steady and cyclic loads) this is because there is no mechanism for restoring the adhesive back to its original state once the load is removed. Another point of consideration is that the load transfer through adhesive bonds is non-uniform. The analysis carried out by Volkersen [26] established in 1938 showed that the load transfer through the adhesive into uniformly thick adherends is not uniform and in fact peaks at the ends of the overlap. Many improvements have been made to these models by various researchers such as Goland and Reissner [27]. Analysis conducted by Hart-Smith [28] has shown that the original analysis is very close

to perfection. Alongside this, Hart-Smith has built upon these pioneering investigations and added nonlinear adhesive behaviour to the analysis and design of adhesively bonded joints in the form of an elastic-plastic adhesive model [5, 29-31].

Although adhesive bonded joints present several advantages, the use of mechanically fastened joints cannot be avoided. This is because in many cases, disassembly of joints is required for inspection or replacement of components. Alongside this, adhesive joints also lack structural redundancy and are very sensitive to manufacturing deficiencies. Non-destructive techniques such as ultrasonic and X-ray inspection do provide information with regards to gaps in the bonding and other deficiencies, however there are no current non-destructive techniques which can guarantee that a bond is intact and has adequate load transfer capabilities. As a result mechanically fastened joints are preferred over these adhesive bonded joints. The following table summarises some of the key advantages and disadvantages associated with bonded composite joints.

Table 2.2 Advantages and disadvantages of adhesive bonded joints

Advantages	Disadvantages
Reduced stress concentration in adherends	Sudden catastrophic failure
Less weight associated with repair	Limitation on adherend thickness
Less susceptible to corrosion	Cannot be disassembled for inspection
Excellent fatigue properties	Sensitivity to moisture and temperature
Excellent load distribution	High level of preparation for surface treatment
Stiff connection	Sensitive to peel and through-thickness stresses

Various stress relief mechanisms may be implemented to bonded joints such as tapering adherends at the ends of overlap, having adhesive spew fillets as well as changing the bonded step lap joint design from lap joints to scarf joints. Further emphasis on these variables will be made in later sections of the dissertation.

2.3.3 Hybrid Joints

The combination of mechanical fastening and adhesive bonding, commonly known as ‘Hybrid Joints’ present a better solution to composite joints and repairs. A number of

papers [5, 32-38] have investigated the behaviour of hybrid joints in particular the load path within the joints. Initial failure in all types of hybrid joints is predominantly due to debonding.

The effectiveness of mechanical fasteners in an adhesively bonded joint is an important topic, in many cases it has been found that bolts do not take an active role in the load transfer until the initiation of bondline failure [33]; this was also noted by Hart-Smith [34]. As long as the adhesive layer is intact, the fastener cannot be subjected to sufficient relative motion between the adherends to develop any significant load themselves and the most critical location is at the first bolt hole in the composite laminate. Rivets are usually unnecessary in lightly loaded bonded structures because they can never experience any load even after the structure has been damaged. However, bolts can be very valuable for heavily loaded bonded or composite structures in that they can arrest any initial damage that would spread catastrophically otherwise [34]. If the mechanical fastener is stronger than the bond, the joint strength of a hybrid joint improves and vice versa.

The paper written by Kelly [35] investigated the distribution of load in a hybrid joint by using finite element analysis. Determining the load transfer in hybrid joints is quite complicated due to the differences in stiffness and the alternate load paths. Experiments were also conducted using carbon fibre laminates. A parametric study was conducted using Abaqus to see the effects of altering various specimen variables. The following summarise the main factors which influence hybrid joint behaviour [35].

- The load transferred by the bolt increases with increasing adherend thickness
- The load transferred by the bolt increases with increasing adhesive thickness
- The load transferred by the bolt decreases with increasing overlap length
- The load transferred by the bolt decreases with increasing pitch distance
- The load transferred by the bolt decreases with increasing adhesive modulus

Table 2.3 lists the key advantages and disadvantages associated with the use of hybrid composite joints.

Table 2.3 Advantages and disadvantages of hybrid joints

Advantages	Disadvantages
Reduce peel and through-thickness stresses	Highest weight penalty
Suppress bondline defects such as cracks	Sensitivity to hole size tolerance
Added residual strength from fasteners	Sensitivity to moisture and temperature
Excellent fatigue properties	Cannot be fully disassembled for inspection
Good load distribution	High level of preparation for surface treatment
Stiff connection	Machining fastener holes can introduce damage

Overall, hybrid joints may be designed to utilise the advantages of both bonded and fastened joints with the fundamental advantage of improving fatigue life as it can arrest sudden crack propagation which can lead to catastrophic failure. Further details on the fatigue performance of these joints are provided in subsequent sections.

2.4 Types of Composite Structural Joints

Joints play a fundamental role in the design and construction of aircrafts. As such it is vital the strength of these joints are known and in particular the mode of failure. The wing of an Airbus 380 alone is composed of over 30,000 elements, with approximately 750,000 bolted joints [39]. These joints are of key importance since they form a weak point that can contribute to the breakage of the element. Typical structural joints include single lap joints, double lap joints, scarf joints and stepped lap joints. The type of joint used is dependent on the application and the loading it needs to withstand.

2.4.1 Single and Double Lap Joints

One of the simplest joint types is a single lap joint. These are when two adherends/panels are joined together via bonding, bolting or the combination of the two. Single lap joints are not symmetric and hence when pulled outwards there is a bending moment resulting in out of plane bending. This has negative effects on increasing stresses at the ends of bondlines as this is where the greatest strain in the adhesive layer occurs resulting in a

non-uniform shear stress distribution. Figure 2.8 depicts a simplified bonded single lap joint.

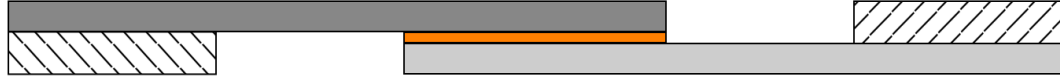


Figure 2.8 Bonded single lap joint

If fasteners are present in a single lap joint, the tilting action causes a non-uniform pressure distribution through the thickness of the adherends which also results in high stress concentrations. A single lap joint is a common test configuration used in civil and military engineering standards [40, 41]. Fu et al. [42] investigated the static and fatigue behaviour of hybrid single lap joints. An experimental study was conducted to see the effects of washer sizing and shapes. Their findings showed that proper washer shape design can improve the mechanical performance of a joint due to the lateral clamping provided. Kelly [35] also used single lap joints in his load transfer study. By using an instrumented bolt with a strain gauge he showed that load transfer to a bolt in a hybrid single lap joint increases with thicker adhesives and adherends. In addition, the load transfer decreases when the overlap length increases and when the elastic modulus of the adhesive increases. Although these tests were conducted on a single lap joint, the same principles may be applied to other joint types such as double and step lap joints.



Figure 2.9 Bonded double lap joint

The double lap joint shown in Figure 2.9 is similar to the single lap joint but comprises of three adherends instead of two. This joint is symmetric about the centre axis (provided the outer adherend thicknesses are the same and the ply layup is symmetric). Hence in terms of numerical modelling, the geometry can be simplified which minimises the computational cost and job run time. Lee et al. [43] compared fastened, bonded and hybrid double lap joint configurations to determine the effects of a single fastener placement. A

number of changes to the geometry were looked at such as varying the width to diameter ratio, edge to diameter ratio and adherend thicknesses. Overall his analysis showed the failure load of hybrid joints were very similar to bonded joints and at least twice as large as the mechanically fastened joints.

Overall single and double lap joints have the advantage of being easily produced. There are minimal geometric complexities which allow easy implementation particularly in the repair of aircraft structures. These joints are also commonly found in thin repair applications. For example, a damage section in aircraft such as cracks or indentations due to impact can be removed by cutting a circular hole in the plate or adherend which is then cleaned. For lightly loaded and secondary structures, a single or double patch can then be easily bonded or bolted onto the existing parent structure. This alters the load path in the damaged region to the neighbouring patch [44].

Generally when designing a bonded joint, it should be stronger than the parts being joined. However, the load carrying capacity of a bonded lap joint is not proportional to the length of the overlap [45]. For example looking at Figure 2.8, an axial load is transferred from one adhered to the other through shear in the adhesive. The shear will only occur over a finite area of the adhesive layer and any increase in overlap length beyond the maximum transfer area will not result in any increase in joint strength; thus requiring a new joint design [45]. Hence, a single lap joint may not produce an optimal joint and thus a double lap joint may be a better alternative. In the case of a damaged panel in an aircraft, if both sides of the panel are accessible then a patch in the form of a double lap joint can be applied. This is a symmetric repair which is one of the most effective reinforcement methods. The issue with single sided repairs is the rise of complicated out of plane displacements, large local rotations and thickness-wise variation of stress intensity factor (SIF) [46]. Hence in this dissertation, stage 1 of the work focuses on using a double lap joint configuration for comparing riveted, bonded and hybrid configurations. Further details are provided in Chapter 3 and 4 of this dissertation.

2.4.2 Tapered Lap Joints

Due to the large peak peel and shear stresses commonly found at the ends of a bonded overlap, premature bond failure may occur due to the initiation of cracking. This overall limits the ultimate mechanical performance of the joint. Several measured can be

implemented into the design of such joints to reduce the severity of such high stresses in these regions. One good measure is to taper the adherends which effectively reduces the cross sectional area of the joint which in turn reduces stress and improves the performance of the joint [5, 47-50].

Bonded composite reinforcements such as boron/epoxy and carbon/epoxy are becoming widely used to repair fatigue or stress corrosion cracks in aluminium alloy aircraft components [51]. Wang et al. [47] investigated how tapering the edges of a patch bonded to an aluminium structure effects the peak peel and shear stresses in order to improve the static and fatigue strength of the repair. Experimental and numerical tests were conducted with different taper angles defined by ' α ' in Figure 2.10.

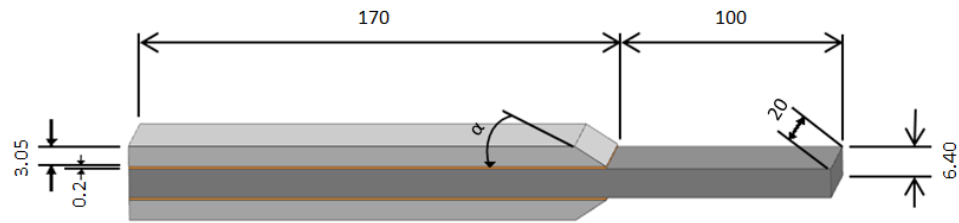


Figure 2.10 Specimen type and dimensions used in taper angle experiment; dimensions in mm [47]

Four different edge angles were used (3° , 6° , 45° and 90°). Results concluded the lowest peak stresses were achieved by the smallest taper angle which also produced the best fatigue performance. An optimisation study was also conducted to further improve the taper design. This study was conducted numerically and was concluded that curved profiles provided the best results [52-54]. Overall when conducting such patch repairs on structures, ideally the same patch material should be used as the parent structure. This is to eliminate residual thermal stresses and other complications which may arise. However, composite patch repairs on aluminium structures have been widely seen in the repair of aircrafts [46, 55-59]. It must be noted to achieve optimum taper design using a composite patch, other factors such as ply orientation need to also be considered [60].

2.4.3 Scarf and Step Lap Joints

The joints discussed thus far quite commonly used in aircraft repair but are suitable for use in thin structures. Scarf and step lap joints are more suitable joints for thicker structures. These joints are considered to be flush repairs and are necessary to restore original stiffness and nearly original strength [61]. Out of all of these joints, scarf joints (Figure 2.11) have been found to exhibit the highest structural efficiency because joint eccentricities which act as stress raisers are minimised in the loading path and a more uniform stress distribution is obtained across joints [62]. This joint only requires a relatively small scarf angle to transfer loads efficiently and hence a favourable option for repair in aircrafts under tensile driven applications.

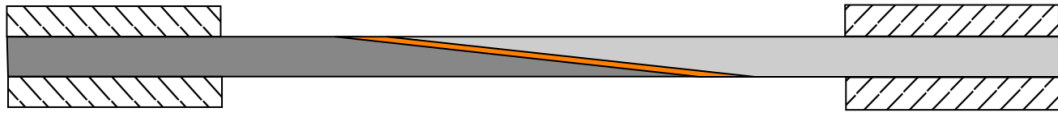


Figure 2.11 Bonded scarf joint

Kumar et al. [62] investigated the effects of changing the scarf angle to determine the effects it has on failure. 2mm thick unidirectional carbon fibre reinforced polymer matrix composites were bonded to each other and loaded in tensile. It was found for scarf angles less than 2° , the joint failed via fibre fracture and pull-out and angles greater than 2° resulted in cohesive shear failure of the adhesive film.

Whittingham et al. [63] looked more into effectively bonding scarf repairs into a damaged structure. There are two methods by which this can be done. The first method is known as the ‘soft-patch’ approach. This involves forming the patch from prepreg and co-bonding it with the adhesive during cure of the patch directly. Advantages such as minimal surface preparation and good adhesion are found in this case. The second method proposed is using the ‘hard-patch’ approach. This involves bonding a pre-formed patch into the scarf cavity. This can be achieved by using either a mould or by machining the patch from a composite panel using surface profiling equipment to capture the scarf cavity surface. A key advantage in this case is that a uniform bondline can be achieved plus there can be a continuity of ply orientation between the patch and the parent structure whilst also maintaining the integrity of the feather edge region.

Step lap joints are another common method of joining/repairing thick structures. They are easier to manufacture than scarf joints which require careful machining to achieve the exact joint area and scarf angle. Figure 2.12 is an example of a bonded step lap joint. There are a number of variables to consider in optimising these joints. Some of the considerations include how many steps to use, the step height and length, flush requirement as well as further complexities introduced when a hybrid step lap joint with fasteners are employed.

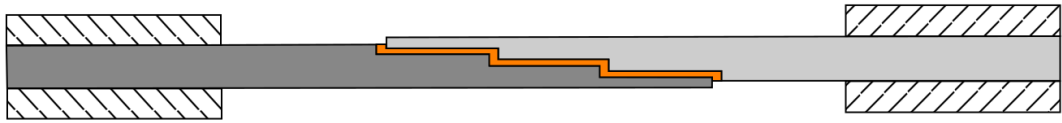


Figure 2.12 Bonded step lap joint with three steps

Hart-Smith [34] mentioned one advantage of a step lap joint over a scarf joint is that the alignment and fit of a step lap joint is far less important when there are joints on more than a single interface. In general, the equations that govern load distribution in single or double lap joints may be applied to step lap joints. However, there are highly non-uniform stress distributions in the adhesive layer due to load transfer associated at the ends of each step [5]. The general criteria to follow when designing a step lap joint includes [5]:

- Outer steps should not have an excessive length to thickness ratio compared to inner steps. This ensures the step does not become overloaded greatly compared to the remaining steps [64]
- A longer step near the middle of the bonded overlap is preferable as it provides creep resistance
- Increasing the bond area for the same number of steps is not as effective as increasing the number of steps

One example of the use of step lap joints in aircraft structures was discussed by Blaricum et al. and Seneviratne et al. [65, 66]. They looked at the performance of step lap joints present in the F/A-18 wing root. Graphite/epoxy laminates were bonded to Titanium 6Al-

4V and assessed for compressive strength subject to impact damage. A total of 18 symmetric steps were used with the graphite/epoxy adherends surrounding the inner Titanium structure. This is a key example of bonded primary structure certified and deployed on air vehicles.

Overall stage 2 of this dissertation focuses on testing thick joint repairs. Step lap joints have been selected as the joint type in this investigation due to the advantages of being easily machinable with more than a single interface. Experimental and numerical work comparing the performance of bonded, bolted and hybrid step lap joints are discussed in later chapters of the dissertation.

2.5 Experimental testing

The widespread use of composite materials has resulted in the need to understand and predict its complicated failure interaction methods and damage mechanisms. To determine the life expectancy of a composite structure requires a clear understanding of the materials response under Mode I, Mode II, Mode III and mixed modes.

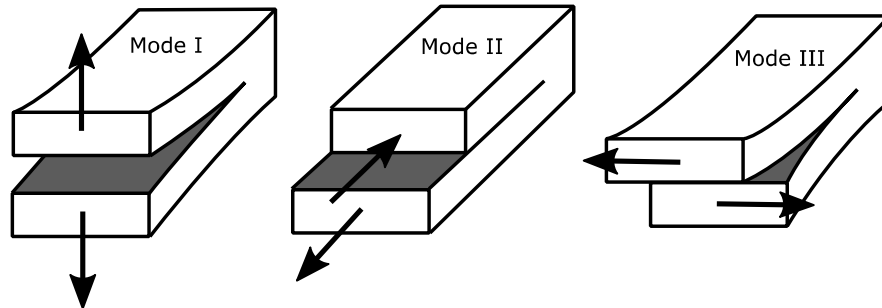


Figure 2.13 Fracture modes

Figure 2.13 defines the three modes of loading. Mode I is an opening mode, Mode II is a shear mode and Mode III is a tearing mode. Although these responses are commonly applied to single material cases, the same terminology is still applicable when multiple materials are used in a joint configuration (e.g. depict a bonded, fastened or hybrid lap joint). In this investigation, predominantly Mode I, II and mixed mode behaviour are looked at in closer detail in later chapters.

The aim of this research is to assist bonded and/or hybrid joint repair certification on composite structures. Figure 2.14 shows a common approach adopted by many aircraft manufacturers for achieving certification. This starts at ‘Level 1’ with simple coupon testing in order to validate and understand material strengths. Following this, there is ‘Level 2’ which looks into testing simple joint structures and eventually ending with full-scale testing in ‘Level 5’. Progressing from Level 1 all the way through to Level 5 is a very lengthy and costly process. A substantial amount of experimental testing in laboratory and service environments, as well as extensive numerical modelling, is needed throughout the entire process.

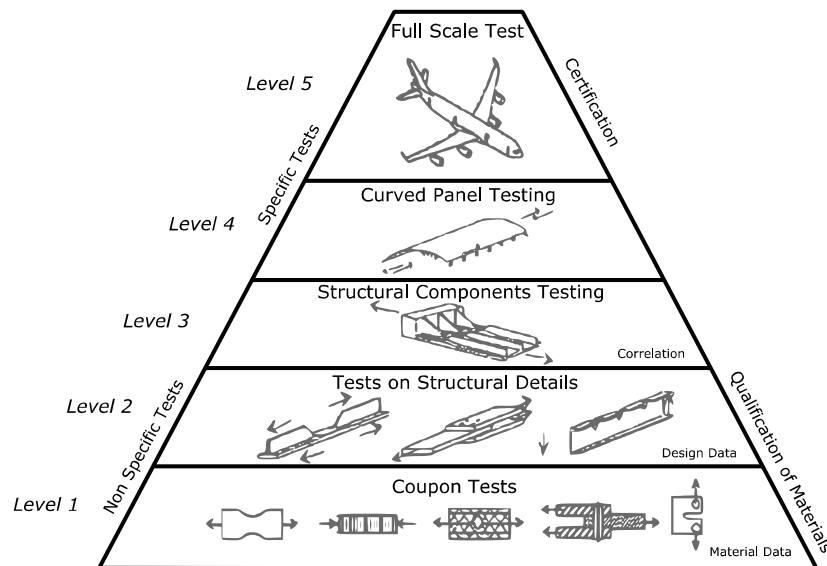


Figure 2.14 Test pyramid approach to achieve certification

This research is focused on ‘Level 2’ structural details. Both experimental testing as well as numerical modelling of thin and thick composite joints/repairs are looked at. The following sections explain some of the experimental and numerical test methods required as part of understanding the joint/repair behaviour.

2.5.1 Static Testing

Mechanical testing of a large scale composite structure is a difficult and complicated task. Often it is vital to test smaller simplified structures to initially gain some basic

understanding of behaviour and thus one of the reasons why the test pyramid approach is utilised.

The data gathered from these tests can be directly related with varying degrees of simplicity and accuracy to very complicated structural shapes. The types of tests conducted can range from static tensile and compression testing right through to dynamic tests such as constant amplitude and variable amplitude loading.

One of the most common forms of testing is the static tensile tests. At a coupon level, this involves using a long strip of material consisting of two regions. The gauge length is the central region of the specimen and is the region where failure is expected to occur. The second region is known as the end region which is where the grip mechanism clamps the test specimen. Typically these regions have bonded tabs to prevent the grips of the testing machine from damaging the actual material of interest. Specimens can be used for longitudinal, transverse, cross-ply and angle-ply testing for composite materials (composite material test specimens are typically uniform in width throughout the length of the specimen). These tests can be conducted according to ASTM D3039 [67].

Compression testing is also conducted for many materials, particularly metals such as aluminium and steel, however these are not as common in composite materials as these materials are mainly used in tension driven applications such as the skin of a fuselage. ASTM D3410 may be used to conduct compression testing [68]. To determine shear properties of the material, there are intra-laminar shear tests and inter-laminar shear test [69]. Most shear tests in existence measure intra-laminar shear properties although both inter-laminar and intra-laminar shear properties should be the same in a perfectly consolidated material. The asymmetric four-point bend test is a popular test used to determine the intra-laminar shear properties. The short beam shear test is commonly used to measure shear delamination where the specimen is placed in three point bending.

In order to measure Mode I fracture toughness, the double cantilever beam (DCB) test method is used to measure delamination in composites. The specimens tested are long thin coupons typically 3mm in thickness. One end of the top and bottom coupon is connected to hinges or T tabs with an indicator on the specimen to determine the length of delamination. The specimen in this case is loaded and unloaded consecutively to measure the small increment of crack growth. Using these results, a load-displacement trace for the double cantilever beam is drawn. This is then used to find the critical Mode I fracture

toughness G_{IC} . Mode II fracture toughness tests are conducted using an end notch flexure (ENF) test.

Overall there are a number of ASTM Standards available for determining constituent properties, interlaminar properties all the way through to determining the bearing response and bond strength of composites. The tests to be conducted are dependent on the application of the material or part. The static experimental work in this dissertation focuses on tensile testing double lap joint specimens and step lap joint specimens. The aim is to obtain the load-displacement behaviour of the respective fastened, bonded and hybrid joint configurations.

2.5.2 Fatigue Testing

Fatigue testing of composite materials play a vital role in helping understand composite failure mechanisms and hence predict the safe life of operation for various aircrafts. Nearly all structures that undergo cyclic loading (in particular, aircrafts) can fail by fatigue. Although composite materials have several advantages, the fatigue behaviour of these materials is vastly different to metallic materials. As a result, the fatigue life modelling and prediction of conventional materials cannot be directly applied to composite materials. The large number of material configurations such as fibres, matrices, manufacturing methods and lamination stacking sequences, makes the development of a commonly accepted method for all of these variances very difficult [25, 70]. A key contrast to be noted is that composites are damaged in fatigue under shear or compression loading much more severely than metals. Additionally, the fatigue resistance of composite materials is much lower in compression-compression loading than in tension-tension loading which is the opposite in metals. The Palmgren-Minor rule is a linear damage model:

$$\sum_{i=1}^N \frac{n_i}{N_i} = 1 \quad (\text{Equation 2.1})$$

This rule has been used in metal fatigue studies and has been carried over to composite fatigue. However, it has also been shown that this model may result in non-conservative results in some cases [71, 72].

Overall fatigue failure in composites is a matrix-dominated event. Microcracks accumulate in the early stage of fatigue life and eventually causes a macroscopic crack which can result

in catastrophic failure. Fatigue failure of unidirectional composites typically fall into one of three categories [73, 74]:

- 1) Matrix cracking parallel to the fibre [75, 76] or by debonding between the fibre and matrix interface
- 2) On-axis failure occurs when a tensile fatigue load is applied in the direction of the fibres. Note that when microcracks occur initially in the matrix, they may be arrested by the fibres which result in increasing the number of stress concentration points in the fibres [77]
- 3) Delamination due to the accumulation of matrix microcracks.

In the case of woven fibres, fatigue failure can be separated into the following five categories [74, 78-80]:

- 1) Transverse cracking in the tows during initial loading
- 2) During the low applied cycle range, matrix pockets begin to microcrack which softens the lamina slightly
- 3) During the larger applied cycles range, the tows perpendicular to the loading direction begin to microcrack, causing further softening of the lamina
- 4) Delamination between fill and warp tows cause further softening to the lamina
- 5) Tows parallel to the loading direction fail and stiffness of the composite lamina is lost

Fatigue analysis can be carried out by various methods experimentally. Constant amplitude loading is one method through which a lot of data is gathered. Constant amplitude fatigue analysis is a quick and simple method to estimate the likely fatigue performance and durability of materials. The residual strength at fatigue failure ($n=N$) equals the applied load [81]. Figure 2.15 shows a typical constant amplitude loading cycle where the stress range is held fixed over time.

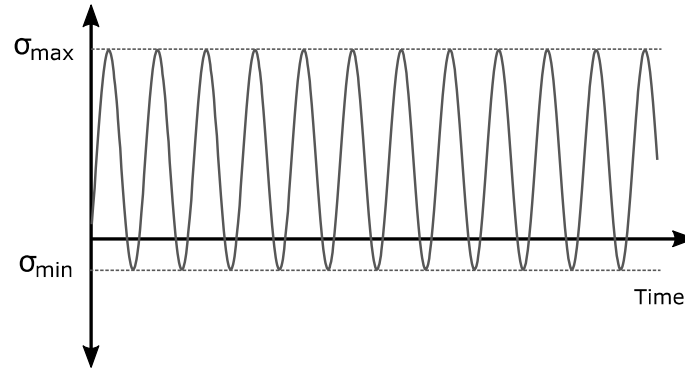


Figure 2.15 Constant amplitude fatigue cycles

Although constant amplitude loading is relatively easy to run and gather data experimentally, variable amplitude loading (spectrum testing) is more representative of the loading experienced by an aircraft as opposed to having a constant stress range.

Variable amplitude fatigue analysis is based on the same concepts as constant amplitude fatigue analysis with the addition of cycle counting and damage summation. The advantage of variable amplitude loading is that real life spectrum data gathered from an aircraft over its service life may be used to get fatigue life estimates on the part being tested. The component can be fatigued at a much faster rate than on field testing. Figure 2.16 is an example of a variable amplitude cycle. It should be noted however that materials tested under variable amplitude loading is only applicable to a specific loading scenario and thus each loading sequence is unique to each aircraft being investigated.

In many cases within the variable amplitude loading spectrum, equivalent constant amplitude loading cycles are identified to try and simplify analysis. This leads to a series of different constant amplitude cycles which make up the variable amplitude cycle (referred to as a form of block loading). This has the advantage of shortening the test time. Typical fatigue loading machines do not cope well with running complicated variable amplitude load cases at a fast speed. The controller setup can often undershoot and overshoot the desired stress limits at high frequencies thus requiring lower frequencies which extend the test duration. By using a block amplitude method, fatigue tests can run faster on servo-hydraulic fatigue machines.

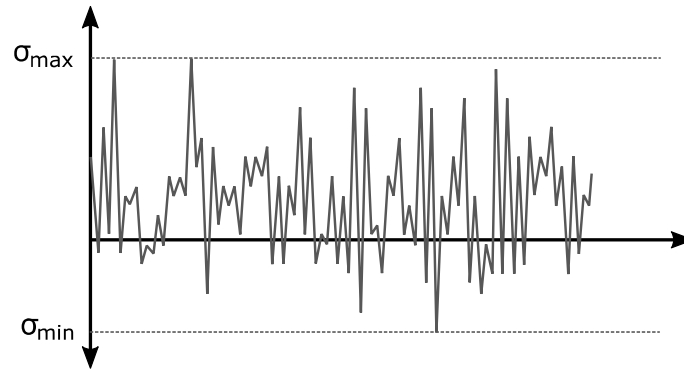


Figure 2.16 Variable amplitude fatigue cycles

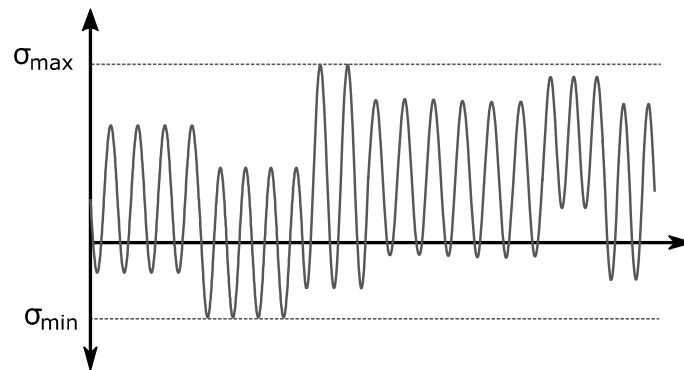


Figure 2.17 Block amplitude fatigue cycles

Due to the wide variety of component materials, manufacturing methods and laminate designs, developing a universal understanding of the performance of variable amplitude loading models for fibre reinforced polymer composite materials is very difficult. Hence, many models are designed for specific material and loading configurations and their applicability to other cases remain somewhat uncertain. When comparing variable amplitude loading with constant amplitude loading, Schön et al. [82, 83] and Hart-Smith [84] suggested based on their tests that variable amplitude loading is more damaging than constant amplitude loading. In the case of metals, a few large amplitude load cycles might increase the fatigue life by introducing compressive stresses from plastic deformation at crack tips but for composites no such effect is thought to be present and the largest load cycles are believed to be the most damaging ones.

Overall, fatigue tests are conducted for all specimen configurations considered in this dissertation. The aim is to compare the fatigue limits of thin and thick fastened, bonded and hybrid configurations. Hence, a constant amplitude fatigue cycle suffices in this case. However as this investigation is focused on testing various joint types rather than at a coupon level, further modifications to the constant amplitude fatigue cycle is made after every 100,000 cycles. This results in a block amplitude fatigue regime. Further insight in this area is presented in Chapter 3 and 4.

2.6 Composite Damage Detection

Composite materials can be used to fabricate complicated internal structures in aircrafts. Damage is likely to occur during manufacture as well as through its operational life. In the case of metallic aircraft structures, corrosion and cracking can be the primary form of damage. Regular inspections carried out during maintenance operations have the ability to detect such damage. However, the primary form of damage in composite materials is due to delamination. This occurs between ply layers and hence, visible inspection is unlikely to detect such forms of damage. Due to these reasons, non-destructive testing (NDT) methods are utilised to detect, localise and determine any forms of damage [85].

Likely forms of damage during manufacture include delamination or foreign object inclusions, whereas during aircraft operation, damage is mainly caused by impacts and high service loads. All of this contributes to decreasing the residual strength and durability of the structures which can result in potential failure [85].

Ultrasonic testing is one of the most commonly used NDT methods to detect different types of damage. An ultrasonic transducer transmits high frequency planar waves through the thickness of the material. A sensor located within the transducer receives the back-reflected wave. As the wave passes through the thickness of the material some are scatter producing different acoustic impedance values. A-Scan is a one-dimensional technique as data is presented for only one point on the surface. B-Scan is a two-dimensional technique as it provides data for a cross section whilst C-Scan is a three-dimensional technique which scans the entire surface of interest. This technique is commonly adopted by aircraft technicians to scan various parts of composite airframes due to its ease of use and portability. Figure 2.18 shows an example of a portable ultrasonic A-scanner.



Figure 2.18 Non-destructive testing using an Olympus Epoch XT ultrasonic A-scanner

Recently, guided wave ultrasonic techniques have gained interest due to their superior accuracy of damage detection and localisation [85]. This technique can be adopted for in-situ NDT also known as structural health monitoring (SHM). SHM is defined as an emerging technology that can offer continuous, autonomous, real-time, in-service monitoring of the physical condition of a structure by means of embedded or attached sensors with minimum manual intervention [86]. This technique uses Lamb waves which have an important property of staying confined inside the walls of thin structures and propagate over large distances along its major axis. Piezoelectric transducers are bonded to the surface of the structure which acts as point sources of the elastic waves as well as wave receivers (pulse-echo). Damage is detected by predicting the expected time of flight for the echo response in a pristine structure and determining the time of flight window for a potentially damaged structure. Numerous studies have been conducted in the use of lamb waves for detecting damage in structures [87-91]. However, a lot of these studies are currently confined to laboratory test conditions.

Thermography is another useful NDT method for damage detection in composite aircraft structures. The initiation and propagation of damage result in a release of energy. This energy is picked up as a temperature change by the thermographic cameras and result in accurate in-situ damage detection. Alternatively, a static component can be excited by an external heating source. By observing the temperature distribution on the surface, various

type of damage can be localised. Papers [92-95] discuss various thermographic techniques which can accurately detect composite damage. Figure 2.19 shows a FLIR A615 camera which may be used to capture thermal data of a component of interest.



Figure 2.19 Non-destructive inspection using a FLIR A615 thermal camera



Figure 2.20 Optical Distributed Sensor Interrogator

A new method which is seeing more promise in NDT is by using a distributed optical fibre sensor (DOFS). DOFS systems contain fibre-based devices which are able to detect, monitor and even measure mechanical strain and/or temperature along a single strand of commercialised telecommunication optical fibre [96]. The device monitors the spectral shifts in the transmitted and reflected light within the core of the fibre. The spectral shift

indicates the intensity of strain or temperature variation along the length of the fibre. Hence by bonding the optical fibre on a structure of interest, localised damage at any point along the fibres length can be detected. The use of this technology is more commonly seen in civil structures such as detecting damage in pipelines. However, it provides an alternative method to using strain gauges commonly used in aircraft structural health monitoring. Figure 2.20 shows an example of distributed fibre sensor interrogator.

Overall there are a number of NDT methods employed to detect damage in composite structures. In addition to the previous methods, there also exists other methods such as digital image correlation [97], vibration methods based on frequency response [98], shearography [99], X-ray computed tomography [100] and others. Parts of the experimental portion of this dissertation utilises ultrasonic A-scanning, thermography as well as the distributed optical fibre sensor technique. These methods are used to help detect damage in the various composite joint configurations during manufacture as well as in static and fatigue tests. Further details are provided in Chapters 4 and 6 of this dissertation.

2.7 Finite Element Analysis

The use of Finite Element (FE) methods to simulate the behaviour of composite joints has increased particularly due to the advancement of many FE packages. The complexity of FE models can vary from a simple two-dimensional analysis of a component made from an isotropic material right through to complex three-dimensional structural analysis of anisotropic components assembled together. Finite Element Analysis is conducted on all joint configurations investigated in this dissertation. This includes thin and thick bonded, fastened and hybrid cases.

Out of the three joint types considered, hybrid joints have the most complex behaviour as it is a combination of bonding and fastening. Most composite hybrid joint models reported so far in literature are restricted to three-dimensional models with a single fastener setup or two-dimensional models [6, 36, 43, 101, 102]. In order for FE to be used as a versatile design tool, the analysis needs to be able to simulate multi fasteners as practically used in a joint, and accurately capture the three-dimensional stress states, material behaviour, bolt clamping, friction, secondary bending effects, load distribution as well as contact interactions between surfaces [103]. In addition, the localised damage in peak stress regions can reduce the laminates sensitivity to discontinuity. This results in highly conservative

strength predictions based on initial failure around hole boundaries [19]. Hence, the modelling must include the capability of progressive failure predictions. From current literature, there is limited work that has included all the above factors.

In this research, Abaqus CAE version 6.13 is used to model all joint configurations experimentally tested. As these joints are manufactured from carbon fibre adherends, the fibre and matrix constituents must be progressively damaged. Various limitations such as which failure theory to use and the extensive computer power required to solve such problems have made the analysis difficult and complicated. In this work the Multicontinuum Theory (MCT) is implemented using a commercial plugin available from Autodesk. The theory offers a number of advantages in modelling composite material behaviour. The background behind this theory is discussed in the following section.

2.7.1 Multicontinuum Theory

The Multicontinuum Theory (MCT) initially introduced by Mayes and Hansen [104] represents an extension of the continuum hypothesis for continuous fibre unidirectional lamina by treating the fibres and matrix as separate but linked continua. In order to gain understanding behind the MCT, the definition of a ‘continuum point’ must be understood. A continuum point is loosely defined as a geometric point in space conceived as occupying no volume but which retains properties associated with a finite volume by taking mathematic limits. Hence the continuum definition of a stress tensor at a point is given by:

$$\tilde{\sigma} = \frac{1}{V} \int_R \tilde{\sigma}(x) dV \quad (\text{Equation 2.2})$$

R represents the continuum point and V is the volume associated with the point in the averaging process [105].

Since a composite material is made up of the fibre embedded in the matrix, both constituents lie within a continuum point. Thus, the stress tensor for the fibre and the matrix may be written as:

$$\tilde{\sigma}_f = \frac{1}{V_f} \int_{R_f} \tilde{\sigma}(x) dV \quad (\text{Equation 2.3})$$

$$\tilde{\sigma}_m = \frac{1}{V_m} \int_{R_m} \tilde{\sigma}(x) dV \quad (\text{Equation 2.4})$$

Where $R = R_m \cup R_f$ and subscripts f and m are the fibre and matrix values respectively.

Based on these three equations the total stress is then written as:

$$\tilde{\sigma} = \varphi_f \tilde{\sigma}_f + \varphi_m \tilde{\sigma}_m \quad (\text{Equation 2.5})$$

Where φ_f and φ_m are the fibre and matrix volume fractions respectively.

Using the same principles, the total strain can be determined using the equation:

$$\tilde{\varepsilon} = \varphi_f \tilde{\varepsilon}_f + \varphi_m \tilde{\varepsilon}_m \quad (\text{Equation 2.6})$$

Hence, Equation 2.5 and 2.6 clearly shows that the MCT is only concerned with the average stress and strain values. Accounting for stress variations throughout every fibre at every material point in even a modest structures is not desirable. By providing constituent average stress and strain fields a more manageable information window on composite materials response to a load is achieved [106].

Based on classical laminate theory the stresses in the composite and constituents are given by:

$$[\sigma] = [C]([\varepsilon] - [\varepsilon_0]) \quad (\text{Equation 2.7})$$

$$[\sigma_f] = [C_f]([\varepsilon_f] - [\varepsilon_{f0}]) \quad (\text{Equation 2.8})$$

$$[\sigma_m] = [C_m]([\varepsilon_m] - [\varepsilon_{m0}]) \quad (\text{Equation 2.9})$$

Where $[C]$ represented the materials stiffness matrix and variables with a subscript 0 are the thermal strain values.

The MCT failure theory follows similarly to Tsai-Wu [107] and Hashin's failure criteria [73]. Five transversely isotropic stress invariants are used in these methods:

$$I_1 = \sigma_{11} \quad (\text{Equation 2.10})$$

$$I_2 = \sigma_{22} + \sigma_{33} \quad (\text{Equation 2.11})$$

$$I_3 = \sigma_{22}^2 + \sigma_{33}^2 + 2\sigma_{23}^2 \quad (\text{Equation 2.12})$$

$$I_4 = \sigma_{12}^2 + \sigma_{13}^2 \quad (\text{Equation 2.13})$$

$$I_5 = \sigma_{22}\sigma_{12}^2 + \sigma_{33}\sigma_{13}^2 + 2\sigma_{12}\sigma_{13}\sigma_{23} \quad (\text{Equation 2.14})$$

Hashin recognised that composites may have different ultimate strengths in tension and compression and hence both fibre and matrix have tensile and compressive sub-forms [73]; this results in a piecewise continuous stress-space failure surface. Hashin's failure criteria focuses on the composite as a whole whereas MCT's failure criteria determines the individual fibre and matrix failure.

All six of the average stress components ($\sigma_{11}^m, \sigma_{22}^m, \sigma_{33}^m, \sigma_{12}^m, \sigma_{13}^m, \sigma_{23}^m$) influence the matrix failure criteria. A unique aspect of the MCT failure criteria is that an anisotropic failure theory is used for an isotropic matrix material. This is because if all the fibres in a unidirectional composite for example was removed, holes in the matrix material will be present. Hence macroscopic failure in the material will be fundamentally different in the longitudinal versus transverse direction resulting in a transversely isotropic failure envelope [108]. Based on all of these assumptions, the matrix failure criterion is expressed as a quadratic function of the matrix average stress components:

$$\pm A_1^m (I_1^m)^2 - \pm A_2^m (I_2^m)^2 + A_3^m I_3^m + A_4^m I_4^m - \pm A_5^m I_1^m I_2^m = 1 \quad (\text{Equation 2.15})$$

Similarly, the fibre constituent failure criteria is expressed as a quadratic function of the fibre average stress components:

$$\pm A_1^f (I_1^f)^2 + A_4^f I_4^f = 1 \quad (\text{Equation 2.16})$$

Where $A_i^{m/f}$ ($i = 1, 2, 3, 4, 5$) are the coefficient of the matrix/fibre failure criteria and the superscript \pm indicates that the numerical value of $A_i^{m/f}$ depends on whether the associated matrix/fibre average stresses are tensile or compressive.

In order to accurately represent the progressive nature of constituent damage leading to ultimate failure, MCT decomposes the ply level stress/strain fields into the constituent level of the fibre and matrix. A variety of non-linear deformation mechanisms introduce inelastic behaviour particularly in the matrix [109]. In order to model non-linear behaviour in the matrix, it needs to be properly degraded once damage is predicted. MCT plugin adopts two approaches, one which is an energy based whilst the second is an instantaneous approach.

The instantaneous approach degrades the matrix to a fraction of its original value once the matrix failure criterion in Equation 2.15 is satisfied. Although this method works well for unidirectional laminates it may provide overly conservative results for multidirectional laminates where matrix failure is largely responsible for ultimate failure [108]. In the energy based approach, matrix properties are gradually degraded with increasing deformation. Note the gradual degradation in matrix behaviour is seen in some laminates because matrix damage is highly localised and load redistribution through complex load paths involving adjacent plies allows the matrix to sustain load a short distance away from the local failure [109].

Although this method is more accurate, due to computational reasons it is more compelling to go with the original approach of instantly degrading the matrix properties. This method is much more computationally efficient and in cases where ultimate failure is fibre dominated, the two approaches often produce very comparable results. In addition, in most cases failure modes in composites are primarily due to delamination and fibre rapture which are largely independent of matrix degradation [109]. Note that failure of the fibre constituents is always treated as instantaneous in MCT. The fibres are assumed to be linear elastic prior to failure.

Overall the use of the MCT plugin in Abaqus CAE presents a number of advantages in optimising model behaviour, improving computational efficiency and minimising convergence issues. Chapters 5, 7 and 8 provide further detail in using MCT in Abaqus. In depth comparisons between experimental static test results with numerical FEA results are provided.

2.7.2 Strain Energy Release Rate

The use of FE methods to simulate the fatigue behaviour of composite joints is not widely seen in literature. The commercial MCT plugin in Abaqus offers progressive fatigue analysis capabilities for unidirectional and woven polymer reinforced composite materials. MCT assumes fatigue failure in composite materials is governed mainly by damage initiation whilst fatigue failure in metals is governed mainly by damage propagation. The initiation of damage in composites is governed by a kinetic process of microcrack accumulation. When the microcracks reach a critical density, a macroscopic crack forms which may result in final failure. This type of fatigue failure can be modelling using the

Kinetic Theory of Fracture (KTF) [110-115]. MCT extracts the stresses in the matrix from the composite stresses (Section 2.7.1). KTF is then used to predict the matrix fatigue life and therefore composite fatigue life. Overall the use of Autodesk's MCT fatigue analysis still requires S-N data for each material of interest. Obtaining such data is a lengthy process and hence one of the main reasons why fatigue analysis of composite materials using FEA is hardly seen in current literature.

As this research is focused on joint/repair analysis a more efficient method is utilised to gain some understanding of fatigue behaviour using FE. When joints are subjected to fatigue, the repeated loading and unloading of the joint eventually results in crack initiation and over time this crack will grow. This results in a constant release of energy.

The strain energy release rate G (SERR) method represents the energy available for crack growth. This can be correlated to crack growth rate according to the following equations:

$$G = \frac{K_I^2(1-\nu^2)}{E} \quad (\text{Equation 2.17})$$

$$\therefore K_I = \sqrt{G * \frac{E}{1-\nu^2}} \quad (\text{Equation 2.18})$$

$$\frac{da}{dN} = C\Delta K^m \quad (\text{Equation 2.19})$$

Where K_I is the stress intensity factor, ν is the Poisson's ratio, E is the Young's modulus, C and m are material constants and da/dN represents the crack growth rate.

From Equation 2.17 and 2.18, the SERR is proportional to the stress intensity factor. Equation 2.19 (Paris's Crack Growth model) shows the crack growth rate is also proportional to the stress intensity factor. Thus the higher the SERR, the higher the rate of crack growth provided the critical G value has been exceeded. This therefore provides an indication of the relative fatigue resistance of different joint structures and thus can provide a method of optimising joint configurations prior to experimental testing.

The individual Mode I, Mode II and Mode III SERR can be derived through post-processing FEA data using the displacement field method based on Figure 2.21 and Equations 2.20 - 2.27 [116].

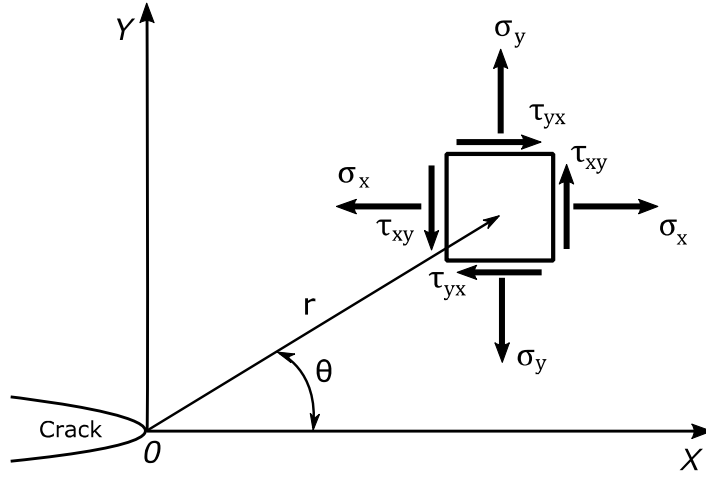


Figure 2.21 Extrapolating stresses at the crack tip

$$\sigma_{ij}^{(Total)} = \sigma_{ij}^{(I)} + \sigma_{ij}^{(II)} + \sigma_{ij}^{(III)} \quad (\text{Equation 2.20})$$

$$\kappa = \frac{3-\nu}{1+\nu} \quad (\text{plane stress}) \quad (\text{Equation 2.21})$$

$$\kappa = 3 - 4\nu \quad (\text{plane strain}) \quad (\text{Equation 2.22})$$

Mode I:

$$u_x = \frac{K_I}{2\mu} \sqrt{\frac{r}{2\pi}} \cos\left(\frac{\theta}{2}\right) \left[\kappa - 1 + 2 \sin^2\left(\frac{\theta}{2}\right) \right] \quad (\text{Equation 2.23})$$

$$u_y = \frac{K_I}{2\mu} \sqrt{\frac{r}{2\pi}} \sin\left(\frac{\theta}{2}\right) \left[\kappa + 1 - 2 \cos^2\left(\frac{\theta}{2}\right) \right] \quad (\text{Equation 2.24})$$

Mode II:

$$u_x = \frac{K_{II}}{2\mu} \sqrt{\frac{r}{2\pi}} \sin\left(\frac{\theta}{2}\right) \left[\kappa + 1 + 2 \cos^2\left(\frac{\theta}{2}\right) \right] \quad (\text{Equation 2.25})$$

$$u_y = -\frac{K_{II}}{2\mu} \sqrt{\frac{r}{2\pi}} \cos\left(\frac{\theta}{2}\right) \left[\kappa - 1 - 2 \sin^2\left(\frac{\theta}{2}\right) \right] \quad (\text{Equation 2.26})$$

Mode III:

$$u_z = \frac{K_{III}}{\mu} \sqrt{\left(\frac{r}{2\pi}\right)} \sin\left(\frac{\theta}{2}\right) \quad (\text{Equation 2.27})$$

Note that r and θ are the cylindrical coordinates for the crack tip fields with the crack tip positioned at the origin and μ represents the shear modulus (not to be confused with ‘ G ’ (SERR)). Note that in Mode I and Mode II, $u_z = 0$ and in Mode III, $u_x = u_y = 0$.

The use of FEA has enhanced the capabilities of determining the SERR associated with particular geometries. A number of factors can affect the results obtained; the common factors include model geometry and element type. Busfield et al. [117] discussed this in more detail. There are three common methods for determining the SERR. This includes the energy balance, J-Integral and the Virtual Crack Closure Technique (VCCT). All three techniques can produce similar SERR results even for complex three-dimensional crack profiles. Hence, the actual technique selected is dependent on ease of implementation and the specific problem being solved. Equations 2.23 - 2.27 represent the displacement field around a crack tip. This approach fits into the J-Integral method. With all FE models based on fracture mechanics principles, a very fine mesh is required around the crack tip to accurately capture the stress fields. Further information on obtaining SERR results using FEA is presented in Chapters 5 and 7 of this dissertation.

2.8 Scope of Further Research

From the literature covered thus far it is clear that in order to understand the behaviour of composite joint repair, it is vital a firm grasp of theoretical models, experimental testing including non-destructive evaluation as well as detailed numerical simulations are conducted. From the work presented thus far, there has been little to no studies focusing on the comparison of similar fastened, bonded and hybrid joint structures. This is more so important when looking into actual aircraft repairs where adhesive spews, fastener array and ply stacking sequences play an important role in the overall joint/repair efficiency.

The lack of static and fatigue test data, followed by finite element modelling has resulted in mixed opinions on the relative comparison of fastened, bonded and hybrid joint repairs. Structures vary in thickness and hence it is also important to compare the respective joint methods for both thin and thick cases.

Numerically modelling these joint types using realistic three-dimensional models is also scarcely seen in the available literature, particularly for hybrid cases. Modern-day computers offer significant processing power to model the behaviour of composites from

the meso-scale right through to large scale structures. These models do require experimental validation and hence it is important to produce realistic simulations which can accurately capture three-dimensional stress states, material behaviour, bolt clamping, friction, secondary bending effects, load distribution as well as contact interaction between surfaces. It is also important to note that modelling must include the capability of progressive failure predictions. From the current literature, there is very little work that has included all the above factors. Hence this dissertation will aim to provide detailed information on mechanically fastened, bonded and hybrid joint repairs for both thin and thick structures to assist composite repair certification.

2.9 Chapter Summary

The replacement of metallic structures with composite materials is now more commonly being seen in the aerospace industry. Understanding the various damage mechanisms and failure modes in these relatively new materials holds substantial importance. The work reviewed in this chapter is mainly concerned with the static and fatigue characteristics of mechanically fastened, bonded and hybrid joint repairs conducted on composite structures.

The break-up of a composite material and commonly used fabric forms have been discussed. As well as the various structural joint types. Single and double lap joints with bonded adherends are more suitable to thin repair applications as the relative strength of the bond decreasing with increasing adherend thickness and thus reducing the overall joint efficiency. Bonded step lap joints and scarf joints are more suitable for thick repair applications as they minimise peak stress at the bondline overlaps. The difficulty associated with detecting weak bonds and their sensitivity to temperature and moisture makes these joint methods difficult to certify even though they are more efficient than mechanically fastened joints. Hence, hybrid joints which are the combination of mechanically fastening and bonding present the opportunity of maintaining the high bondline efficiency whilst still providing added residual strength from the fasteners if bondline failure were to occur. All of these are important factors that need consideration for the certification of a new joint structure.

Static and fatigue tests are a vital part of characterising joint behaviour to achieve certification. Variable amplitude loading will provide more realistic fatigue life predictions of a component/structure in service however its applicability to other general cases is somewhat unknown. Hence, constant amplitude and block amplitude loading are

commonly used to obtain fatigue life estimates. In addition to experimental testing, finite element analysis (FEA) can be used to gather further details on stress and load distribution in different joints. The Autodesk Multicontinuum Theory (MCT) plugin shall be used in Abaqus for modelling the various composite joint behaviour. The later chapters provide detailed information on the manufacture of the various joint configurations considered for testing followed by static and fatigue tests results and FEA comparisons.

End of Chapter 2

Materials and Manufacture

3.1 Introduction

This work is targeted towards the repair of composite aircraft structures. Hence, aerospace grade materials are selected for specimen manufacture. The aim is to experimentally test and validate the various failure mechanisms as well as numerically model each joint configuration.

The research is broken up into two key stages. Stage 1 focuses on thin joint/repair applications and Stage 2 focuses on thick joint/repair applications. This chapter defines the mechanical properties of each material used in the assembly of the various joint configurations. The information is later used during the numerical analysis conducted using Abaqus CAE. Care needs to be taken during the manufacture of composite adherends particularly during the machining and bonding stages of assembly. As discussed in Chapter 2, defects introduced during the manufacturing stage of laminates can influence premature failure. Thus, it is vital proper manufacturing techniques are implemented throughout the specimen production process. The various techniques adopted to produce consistent joint specimens are explained in this chapter.

The influence of various defects is also investigated with explanations on how they were introduced. This provides vital information on how severely a defect influences the static strength and fatigue performance. Non-destructive inspection using Ultrasonic A-Scanning is utilised to ensure proper adhesion occurs in bonded and hybrid joint specimens. Reasons as to why a particular geometry/configuration is selected shall be discussed in more depth in later chapters.

3.2 Material Properties

Both thick and thin joint structures are made up of HexPly M18/1/G939 Carbon Fibre prepreg in a satin weave configuration with 0° and 90° fibres [118]; Figure 3.1. The Tiger Armed Reconnaissance Helicopter (ARH) currently in service with the Australian Defence Force comprises of the same composite material [119, 120]. This material is manufactured by HEXCEL and is a self-extinguishing, has high impact resistance and can operate at a continuous service temperature of 120°C in wet conditions. Table 3.1 summarises the material properties.

Table 3.1 Properties of HexPly M18/1/G939 carbon fibre prepreg; [118]

	E_{11} (GPa)	E_{22} (GPa)	G_{12} (GPa)	G_{13} (GPa)	ν_{12}	Tensile strength			Compressive Strength	
						$+S_{11}$	$+S_{22}$	S_{12}	$-S_{11}$	$-S_{22}$
						(MPa)	(MPa)	(MPa)	(MPa)	(MPa)
M18/G939	65	67	4.0	4.0	0.04	800	800	100	800	800

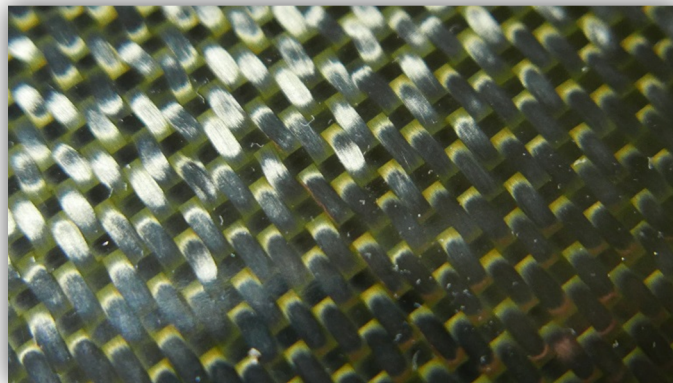


Figure 3.1 HexPly M18/1/G939 satin weave with 0° and 90° fibres

Once the desired ply stacking sequence is arranged, the material is cured in an autoclave based on the manufacturer's recommended curing cycle (2 hours at 177°C).

FM300-2K film adhesive manufactured by Cytec Engineering [121] is used for all specimens containing a bondline. The adhesive has a nominal uncured thickness of 0.41mm and contains a scrim cloth which produces a uniform bondline thickness without significant resin runout. This is an aerospace grade adhesive which provides excellent moisture and corrosion resistance in high humidity environments with minimal reduction in mechanical properties. Figure 3.2 shows an uncured layer of FM300-2K film adhesive and Table 3.2 defines the properties of the adhesive.

Table 3.2 Properties of FM300-2K film adhesive; [121, 122]

	E (MPa)	G (MPa)	ν	X_t (MPa)	S_{xy} (MPa)	ν_e	ν_p	G_{IC} (kJ/m ²)	G_{IIC} (kJ/m ²)
FM300-2K	2400	840	0.4	94.2	54.4	0.055	0.580	1.3	5

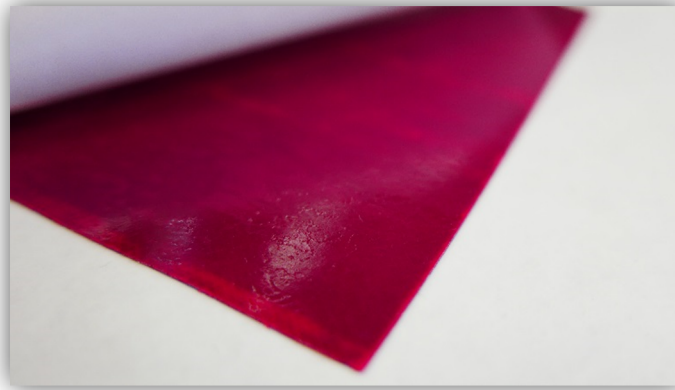


Figure 3.2 FM300-2K film adhesive with nominal uncured thickness of 0.41mm

This adhesive is designed primarily for co-cure and secondary bonding applications. It requires a cure temperature of only 121°C for 90 minutes and is thus significantly lower than the glass transition temperature of most composites. The adhesive is cured in an autoclave. Curing pressure can be varied depending on application; section 3.5.2 discusses how curing pressure effects bondline thickness in this adhesive.

Mechanically fastened joints and hybrid joints require suitable fasteners with the correct grip length and hole diameter. In the case of Stage 1, a double lap joint configuration is selected. These joints have a total thickness between 5mm - 6mm. Thus, Cherry Maxibolt CR7621 rivets are selected. Note that rivets are commonly used in joining parts together as they are quick and easy to install. The rivets are made from A286 CRES alloy comprising of mainly iron, nickel, chromium and titanium. The rivet has excellent temperature and corrosion resistance. The tail section of the rivet is designed to form into a flat section similar to a washer to provide a larger clamping region on the underside of the composite. Alongside this, the tail is designed to prevent swelling of the rivets shank when inside the hole and prevents delamination on the underside of the composite plate caused by many other standard rivets commonly available. Table 3.3 and Figure 3.3 summarises the key specifications.

Table 3.3 Cheri Maxibolt CR7621U-05-04 rivet specification [123]

Rivet	A (mm)	B (mm)	D \pm 0.3 (mm)	Hole Limits	Grip Limits	Installed Strength	
						Single Shear Min (kN)	Tensile Min (kN)
CR7621U-05-04	6.35/	1.575/	4.14	4.166/	5.563/	8.807	5.115
	6.91	1.778		4.242	7.163		

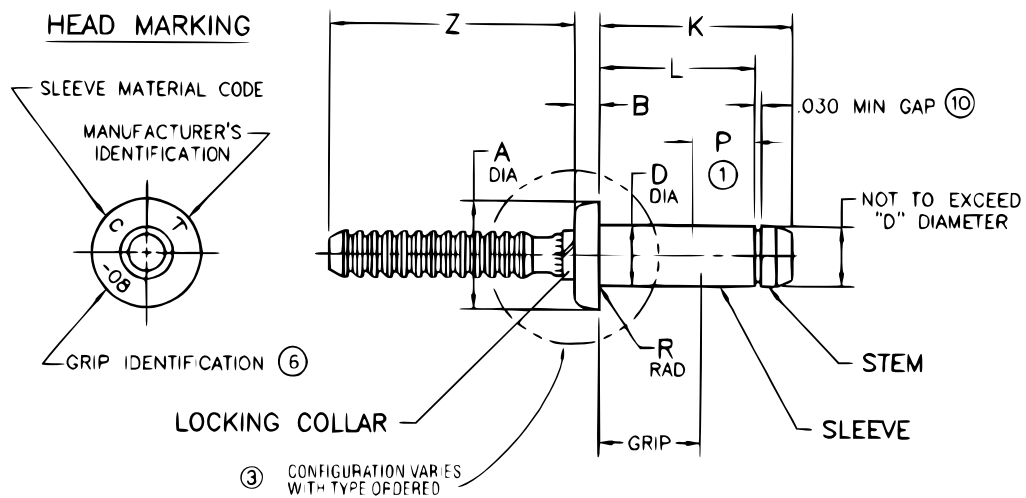


Figure 3.3 Schematic of Cheri Maxibolt CR7621 rivet [123]

An extension to Stage 2 is later conducted in optimising the joint strength by modifying the step lap joint design.

3.3.1 Double Lap Joint

Riveted specimens, bonded specimens and hybrid specimens are selected in Stage 1 of the research. A total of eight specimen configurations are selected and can be broken up into ‘pristine’, ‘defective -2mm crack’ and ‘defective - semi-cured bond’ categories. Table 3.5 summarises the different specimen configurations used.

Table 3.5 Overview of thin double lap joint configurations

Bondline Condition	Specimen	Joint Type	No. Rivets	Curing Pressure (psi)
Pristine	Configuration 1.1	Bonded	n/a	40.0
	Configuration 1.2	Riveted	6	n/a
	Configuration 1.3	Hybrid	6	40.0
	Configuration 1.4	Hybrid	3	14.7
Defective - 2mm Crack	Configuration 1.5	Bonded	n/a	40.0
	Configuration 1.6	Hybrid	6	40.0
*Defective - Semi-cured Bond	Configuration 1.7	Bonded	n/a	40.0
	Configuration 1.8	Hybrid	6	40.0

* Specimens cured at 90°C for 60 minutes in an autoclave; refer to Section 3.6.1

Specimens comprising of rivets (Cherry MaxiBolt CR7621U-05-04) have either a square array (six rivets) or a staggered array (three rivets). Figure 3.5 and Figure 3.6 show the schematic of a fastened/hybrid configuration with the two different rivet array positions. A bonded double lap joint contains the same adherends with the omission of fasteners.

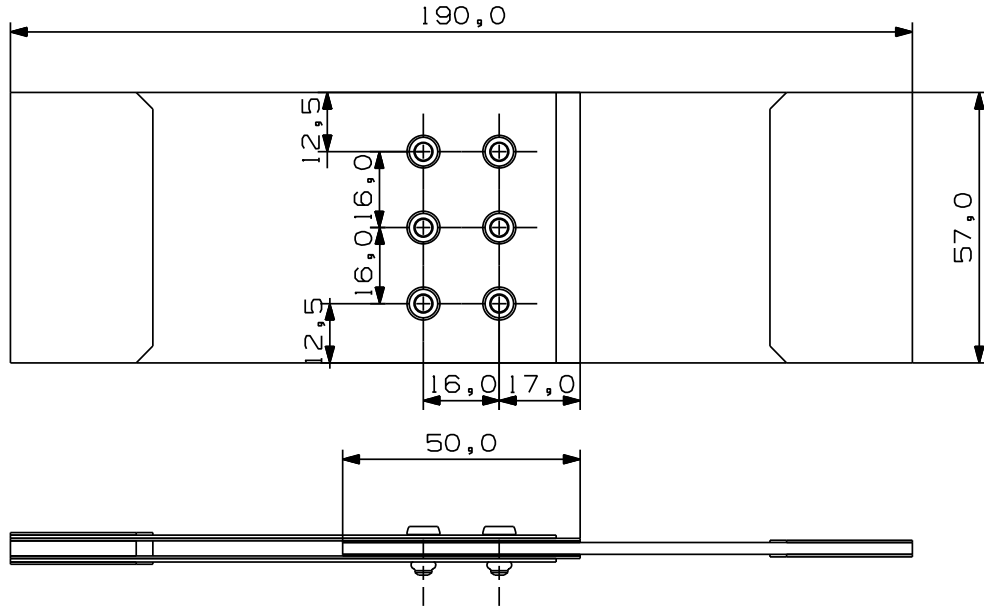


Figure 3.5 Double lap joint containing six fasteners in a square array; dimensions in mm

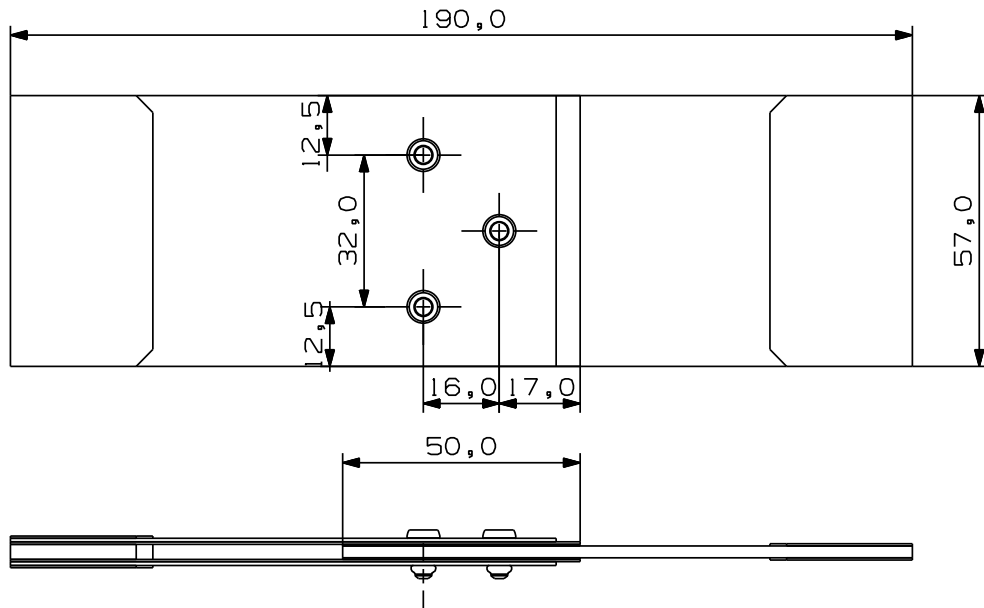


Figure 3.6 Double lap joint containing three fasteners in a staggered array; dimensions in mm

All specimen configurations in this stage have five ply thick outer adherends in a $[(0/90)/(45/-45)/(0/90)/(45/-45)/(0/90)]$ ply orientation. The inner adherend is ten plies thick with a $[(0/90)/(45/-45)/(0/90)/(45/-45)/(0/90)]$ s ply orientation. Hence, this leads to a symmetry line midway through the thickness as well as the width of the specimens. As discussed in Section 2.4.2, bonded lap joints are known to produce severe stress concentrations at the ends of an overlap; to reduce this the outer adherends are

manufactured with a 5mm long taper in the form of a ply drop as shown in Figure 3.5 and Figure 3.6. This is achieved during the layup stage prior to curing the adherend. Excess resin in the prepreg material results in a taper from the bottom adherend to the top adherend.

The rivet array configuration is adopted from a composite airframe currently in service and thus resembles a realistic fastener pattern. A pitch distance of 16mm is selected in the case of the square array.

3.3.2 Step Lap Joint

Bolted specimens, bonded specimens and hybrid specimens are selected in Stage 2 of the research. A total of ten specimen configurations are selected and can be broken up into ‘pristine’, ‘defective -2mm crack’ and ‘defective - semi-cured bond’ categories, similar to Stage 1. Table 3.6 summarises the different specimen configurations used.

Table 3.6 Overview of thick step lap joint configurations containing five steps

Bondline Condition	Specimen	Joint Type	No. Bolts	Curing Pressure (psi)
Pristine	Configuration 2.1	Bonded	n/a	40.0
	Configuration 2.2	Bolted	5	n/a
	Configuration 2.3	Hybrid	5	40.0
	Configuration 2.4	Hybrid	3	40.0
Defective - 2mm Crack	Configuration 2.5	Bonded	n/a	40.0
	Configuration 2.6	Hybrid	5	40.0
	Configuration 2.7	Hybrid	3	40.0
*Defective - Semi-cured Bond	Configuration 2.8	Bonded	n/a	40.0
	Configuration 2.9	Hybrid	5	40.0
	Configuration 2.10	Hybrid	3	40.0

* Specimens cured at 90°C for 60 minutes in an autoclave; refer to Section 3.6.1

Specimens comprising of countersunk bolts (Aviaquip NAS1581C4T4) are aligned in a single column array with either five bolts or three bolts. Bolted and hybrid specimens,

have fasteners placed central of each step, similar to [34]. Specimen configurations with only three bolts are produced to determine whether placing countersunk fasteners close to the ends of the overlap have any effect on the joint performance. Figure 3.7 and Figure 3.8 show the schematic of a fastened/hybrid configuration with five bolts and hybrid configuration with three bolts respectively.

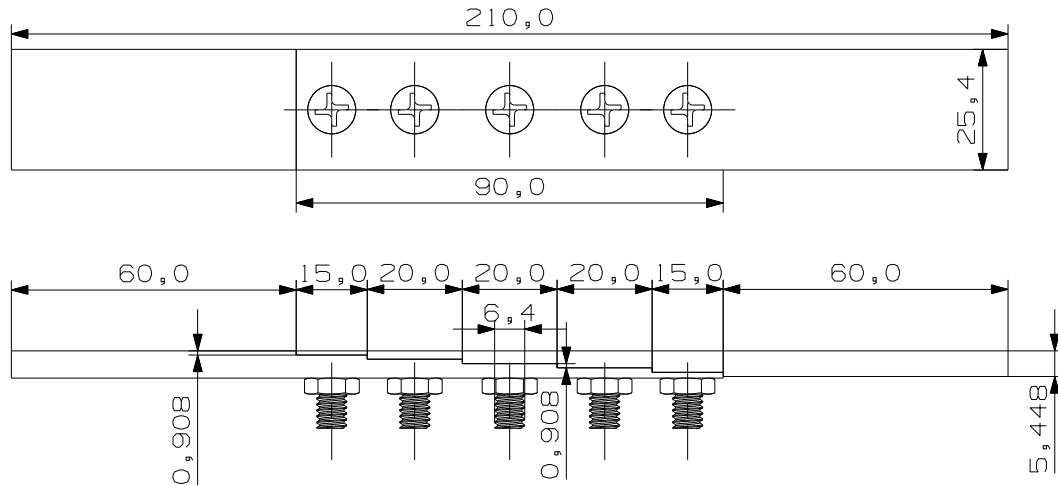


Figure 3.7 Step lap joint containing five bolts in a single column array; dimensions in mm

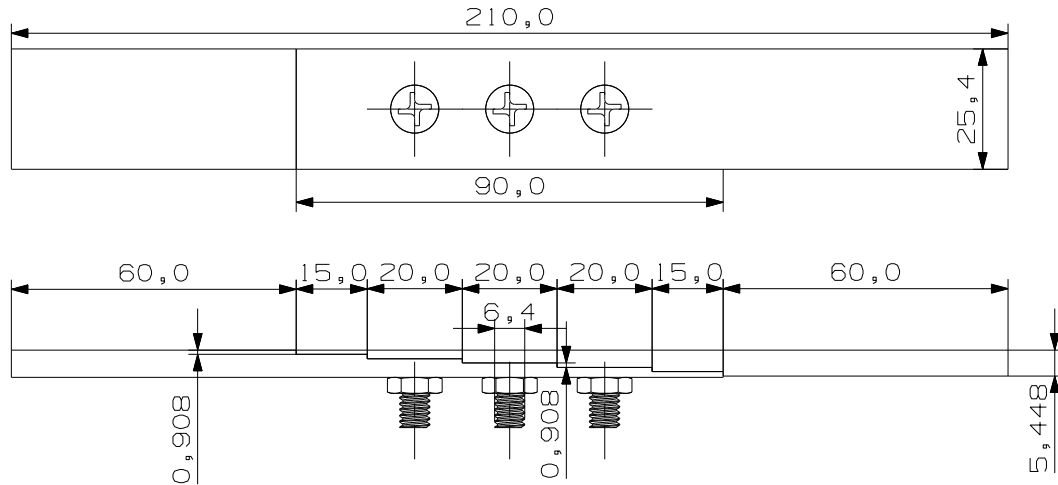


Figure 3.8 Step lap joint containing three bolts in a single column array; dimensions in mm

All specimens are one inch wide with a total of five steps. A parametric study was conducted in optimising the step lengths using Abaqus CAE. Further details are presented in Chapter 6. All adherends manufactured are 24 plies thick with a stacking sequence of

$[(0/90)/(45/-45)/(45/-45)/(0/90)]_6$. Each step is assumed to be of a uniform thickness, resulting in the same ply stacking sequence in each step. Overall due to the step lap joint design, there is symmetry only midway through the width of the specimens.

An additional minor study is conducted in which the previous step lap joint design is further modified to the following configurations shown in Figure 3.9 and Figure 3.10. In this study, the aim is to achieve higher joint strength and fatigue resistance than the previous step lap joint containing five steps (Configuration 2). Further details on these designs are explained in Chapter 8.

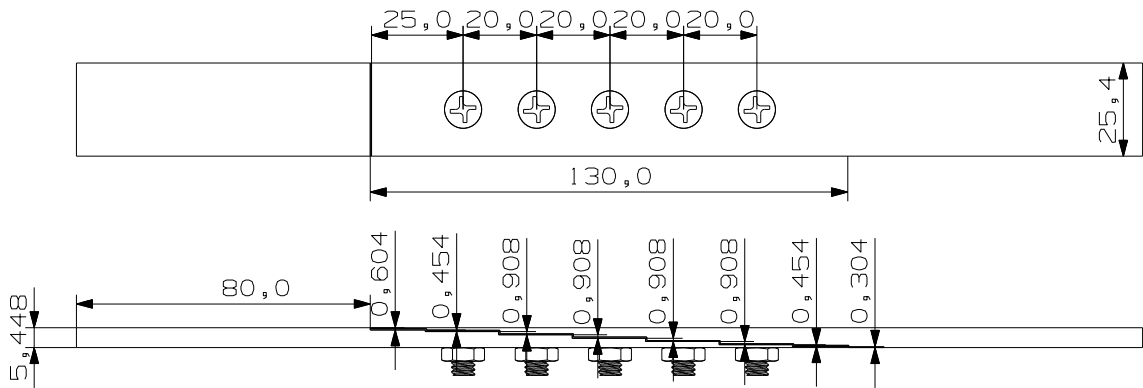


Figure 3.9 Long hybrid step lap joint containing seven steps (Configuration 3.2) with five bolts in a single column array; dimensions in mm

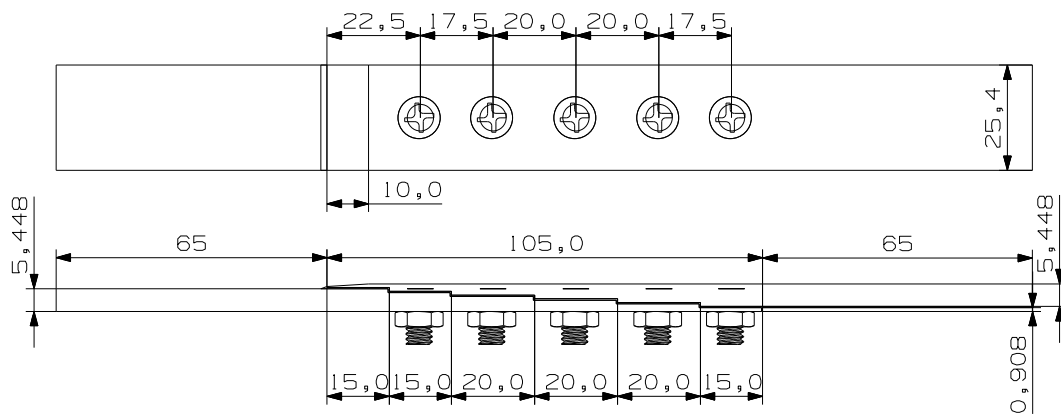


Figure 3.10 Overlap hybrid step lap joint containing six steps with five bolts (Configuration 4.2) in a single column array; dimensions in mm

Note the specimen configuration shown in Figure 3.9 and Figure 3.10 are made using the same material and ply layup orientation $[(0/90)/(45/-45)/(45/-45)/(0/90)]_6$ defined for

Configuration 2. The aim is to optimise performance using the same adherend but with different step lengths/heights and flush requirement. Table 3.7 summarises the different specimen configurations used.

Table 3.7 Overview of the optimised thick step lap joint configurations

Bondline Condition	Specimen	Joint Type	No. Bolts	Curing Pressure (psi)
Pristine	Configuration 3.1	Bonded	n/a	40.0
	Configuration 3.2	Hybrid	5	40.0
Pristine	Configuration 4.1	Bonded	n/a	40.0
	Configuration 4.2	Hybrid	5	40.0

Configuration 3 defined in Table 3.7 is the step lap joint containing seven steps; Figure 3.9. The aim is to improve stress distribution along the bondline without significantly increasing the joint region. Configuration 4 defined in Table 3.7 is the step lap joint containing an overlap; Figure 3.10. The aim is to increase the joint stiffness and reduce high stresses commonly found at the ends of the overlap through the use of a tapered end. Experimental and FEA results are presented in Chapter 8 for these modified step lap joint configurations.

3.4 Machining of Laminates

Machining of composite panels requires a significant amount of care. Drilling of fastener holes may result in fibre pull-out and delamination in composite adherends. The thin carbon fibre adherends in Stage 1, were cut using a water jet. If conventional end mills are used, they will quickly wear out resulting in different roughnesses around the machined edges. Figure 3.11 shows the thin carbon fibre adherends cut from a panel using a water jet. When thick carbon fibre panels (>5mm) are cut, it is beneficial to use diamond coated end mills. This prevents minimum wear on the bit, as well as ensure clean cuts are produced on the edges of the carbon fibre adherends. All specimen configurations in Stage 2 were cut from a 24 ply thick carbon fibre panel using end mills which were regularly monitored for wear; a numerical control (NC) machine is used for this process.

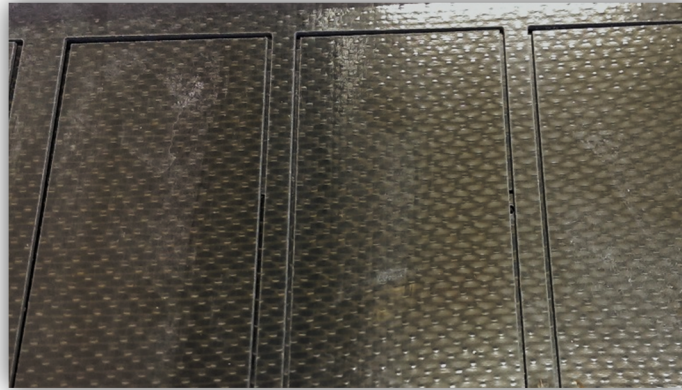


Figure 3.11 Thin HexPly M18/1/G939 carbon fibre adherends cut from a panel using water jet



Figure 3.12 Thick HexPly M18/1/G939 carbon fibre adherends machined using an NC machine

The machining of steps in the 24 ply thick adherends was conducted using a standard milling machine. Figure 3.12 shows an example of two machined stepped adherends. Note that bonded and hybrid step lap joints had slightly thinner outer stepped regions to account for the FM300-2K film adhesive. This ensures a truly flush joint is obtained.

3.4.1 Bolt Hole Clearance

The size of a hole in a composite plate plays an important role in the effectiveness of transferring loads and its stress distribution. The key variable of interest here is the

tolerance between the fasteners hole and the fastener itself. The distribution of loads in multi-fastener joints is given by the established force equilibrium achieved when the applied external loads are balanced by the individual bolt loads and the friction between the associated plates.

Experimentally it has been found that an out-of-tolerance clearance can cause substantial changes in the load distribution of multi-bolted joints [125]. Lawlor et al. [126] experimentally studied the effects of bolt-hole clearance in single-shear and single-bolt arrangements. His results indicated that a tolerance outside the range of the standard fittings used in the aerospace industry (F7/H10) would have a significant effect on joint stiffness and ultimate strain, but less effect on the strength.

60-85% of failures in composite materials occur at fastener joints (bolted configuration) [127]; hence this is a significant problem which must be addressed. As such research in bolted composite joints and the effects of various bolting parameters on the joint strength has been the main area of focus for many researchers. In the past, the conditions between the fasteners and plates are normally ‘clearance fit’, with 0.1mm being the typical clearance in aircraft joints [128, 129]. However, it has been shown by the formerly known McDonnell Douglas Corporation that interference-fit joining improves the fatigue life of carbon epoxy composites [127, 130]. Similar conclusions were made by Kiral and Liu et al. [131, 132].

Based on this information, all joint configurations in Stage 1 were drilled and then reamed to achieve an interference fit. Solid carbide bits were used in the process to minimise wear. Figure 3.13 shows the bits used. In Stage 2, a solid carbide drill bit, reamer and countersink were used to create the appropriate size fastener hole. An NC machine was used for the drilling, reaming and countersinking process. Figure 3.14 shows the three bits used.

Note that proper machining of fastener holes in composite adherends can be achieved by using a top and bottom plate which surrounds the adherends. This ensures back-face delamination and fibre pull-out is prevented. Figure 3.15 shows an example of a poor fastener hole produced when no clamping pressure is applied prior to machining the fastener holes.



Figure 3.13 Solid carbide drill bit and reamer used for rivet holes in Stage 1



Figure 3.14 Solid carbide drill bit, reamer and countersink used for the countersunk bolt holes in Stage 2

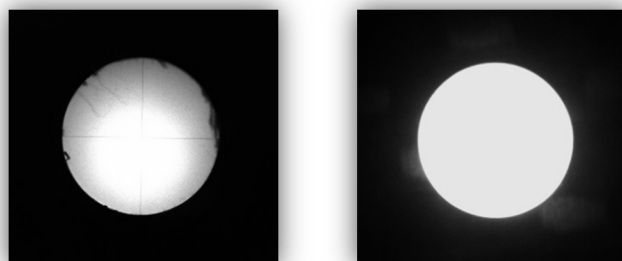


Figure 3.15 Drilled and reamed fastener hole in carbon fibre adherend with no back-face plate (left) and with back-face plate (right)

3.5 Specimen Assembly

Once the adherends are machined to appropriate dimensions, they were assembled into their fastened, bonded and hybrid configurations. The bonded and hybrid configurations required the most amount of time for assembly due to surface preparation and bondline curing. In Stage 1, the rivets and FM300-2K film adhesive were co-cured in an autoclave once vacuum bagged; Figure 3.16. This has the advantage of applying additional clamping pressure in the adhesive during cure as well as ensuring any gaps between rivet and fastener hole are filled with excess adhesive. The effect of installing rivets to apply pressure during cure was testing in Configuration 1.4. This configuration was cured in an oven instead of an autoclave.



Figure 3.16 Vacuum bagging hybrid double lap joint specimens to cure bondline in an autoclave

In Stage 2, all bonded and hybrid specimen configurations were fully cured in an autoclave. Guide plates were used to ensure a uniform bondline thickness was achieved during the vacuum bagging and curing stage. Hybrid specimens had fastener holes machined once the bondline was fully cured.

3.5.1 Surface Preparation

Whenever bonding specimens together, it is vital for the surface in contact with the adhesive is properly abraded and degreased to remove contaminants that may hinder the joint strength. Improper abrasion and degreasing can lead to cohesive failure, hence not fully utilising the full strength of the adherends and adhesive. The amount of time and procedure adopted to prepare a surface depends on the materials being bonded; for instance, bonding aluminium pieces together requires significantly more time and effort compared to composite bonding due to the presence of an oxide layer. As the scope of this research focuses on testing composite materials, the following outlines the procedure adopted for bonding these composite adherends together.

Abrading

In order to ensure a good adhesion between the composite adherend and adhesive is maintained, a rough surface is required to increase the surface area and tension. Scotch Brite hand pads are used to abrade the composite surface. The surface is abraded in a consistent pattern moving from top to bottom and then left to right. Following this, the specimen is rotated 90° and abraded again from top to bottom and then left to right.

Using 400 grit aluminium oxide sandpaper (wet abrade) is an alternative method to using Scotch Brite pads. Most sandpapers available either use aluminium oxide particles or silicon carbide particles. Sandpaper with silicon carbide particles should not be used as these particles are relatively harder and likely to dig deeper into the bonded surface with the risk of exposing fibres in the top layer. Overall the main aim of this initial step is to remove the shine off of the surfaces to be bonded.

Degreasing

Methyl-Ethyl-Ketone (MEK) is a colourless liquid commonly used as an industrial solvent. It is excellent in removing oil and grease off of surfaces and hence creates a very clean surface with minimum contaminants. Once the surface to be bonded has been abraded, tissue paper is lightly damped with MEK. The wiping process should be systematic, moving from top to bottom followed by left to right. Note: the tissue paper should be changed several times when wiping to prevent contaminants being transferred back to the surface. This procedure is repeated until no more discolouration on the tissue paper is seen. If MEK is not available, Acetone can be used as an alternative degreaser.

Grit Blasting

The surface to be bonded is then grit blasted with 50 micron aluminium oxide at 50 psi using dry nitrogen propellant. The surface is checked regularly to ensure all areas have been covered. Care must be taken not to grit blast the surface too much as this can expose fibres on the surface of the composite leading to delamination. This surface roughing procedure is an important step as it creates small pits for the adhesive to bind into. Most film adhesives have excellent properties in shear driven applications and not so much in tension. Grit blasting produces small angular pits on the surface allowing a greater area of the adhesive to act in shear, thus ensuring a stronger bond.

Cleansing

Small particulates of aluminium oxide will be left behind on the surface due to the grit blasting procedure. Excess grit on the surface can be blown away using compressed nitrogen gas. Air should not be used as the propellant since it contains contaminants. Once excess grit is blown off the composite surface, the film adhesive is immediately applied to the surface using gloves. The specimen is then placed in an oven/autoclave ready for curing.

Figure 3.17 shows the grit blasting chamber used to conduct the surface preparation procedure for all bonded and hybrid configurations.



Figure 3.17 Grit blasting machine used to surface prep adherend surfaces for bonding

3.5.2 Adhesive Thickness Determination

The bondline plays an important role in determining the overall specimen thickness. In order to understand how the bondline thickness varies under different pressure conditions in an autoclave, a series of tests were conducted with a bond area of 57mm x 50mm using the FM300-2K film adhesive. As the main interest was to determine the cured bondline thickness, aluminium pieces were used in the initial tests. Carbon fibre adherends were later used to ensure no significant discrepancy in results were obtained.

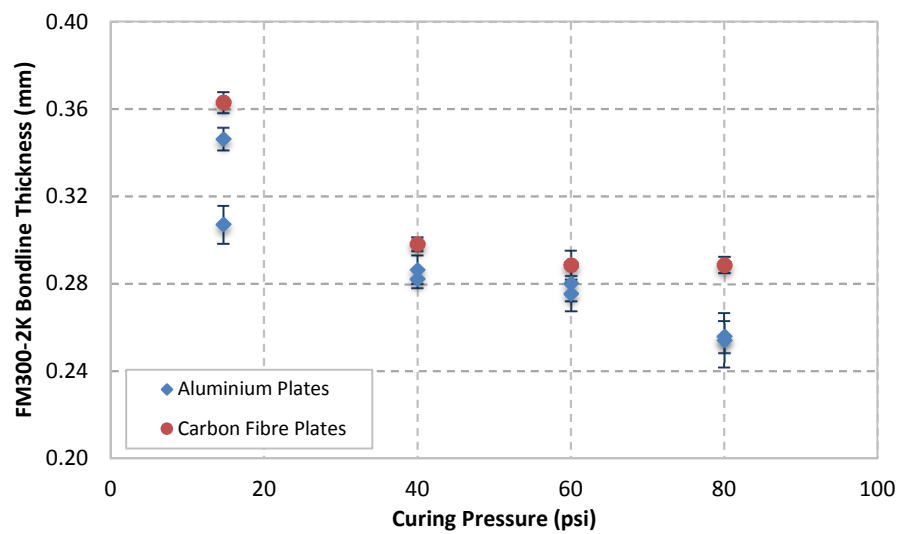


Figure 3.18 FM300-2K bondline thickness determination at different curing pressures (121°C for 90min)

Figure 3.18 shows the final bondline thickness achieved by the FM300-2K film adhesive at different curing pressures. A dial indicator as well as a travelling microscope was used to determine the thicknesses. From Figure 3.18, specimens with carbon fibre plates consistently produced marginally higher bondline thicknesses due to different levels of thermal conductivity. Based on these results, a curing pressure of 40psi was selected due to its lower variance in results. This value also coincides with the recommended curing pressure specified by Cytac [121].

3.5.3 Bolt Clamping Pressure

The fasteners used in this research are either rivets or bolts. The clamping pressure provided by rivets is not easily controllable as they are dependent on the rivet design and the joint thickness. In the case of bolts, the clamping pressure can be controlled by how tightly the nut is torqued onto the bolt. In addition to the tightening torque, the area in which they apply pressure (clamping area) also has an effect on joint performance.

Fu et al. presented a study on the static and fatigue performance of hybrid joints in a structural reaction injection moulded composite. The investigation showed that hybrid joints have a higher static failure load and longer fatigue life than adhesive joints. However, the performance of the hybrid joints depends on the washer design [42]. Both square washers and round washers of various thicknesses were used in the experiment. It was concluded that lateral clamping pressure can significantly decrease the maximum peel stress at the interface and thus improves the overall joint performance.

The effects of clamping pressure on the performance of hybrid joints have also been investigated by a number of other researchers [133-135]. Jadee and Othman [3] investigated the effects of a fibre reinforced composite structure with a bolted joint. They found that preload moment provided clamping pressure to the bolt which resulted in the lateral constraint of the area under the washer; this significantly increased the joint strength. Overall increasing the preload moment could increase the load carrying capacity and hence the bearing strength of the joint [133, 136]. Maajid et al. tested effects of bolt torque in a single-lap composite joint and found that bolts with a higher torque generally have slightly higher maximum failure load [137].

Although improvements in joint strength is seen with increasing clamping pressure, eventually it will reach a limit after which there will be no more increase in bearing strength. Alongside this, significant clamping pressure may result in delamination under the constraint area [138].

In Stage 2 of this research where countersunk bolts have been used, several tests were conducted to determine the most effective torque to apply. From the literature presented previously, the general consensus is the higher the torque, the higher the durability and bearing strength of the joint. However increasing the torque beyond a certain limit can change the viscoelastic effects. Manufacturers of mechanical fasteners typically provide

their own torque recommendations based on fastener material properties and thread pitch. Although these specifications may be given, it is usually assumed they are applied in metal structures. Applying these fasteners to composite adherends will require different specifications as excessive clamping may result in fibre breakage and delamination. The Standard Aircraft Handbook for Mechanics and Technicians [139] states that a torque between 5.65 - 7.91Nm can be applied to a standard ¼" bolt. Several torques were trialled followed by NDI using an Ultrasonic A-Scanner to detect damage. It was found a torque greater than 8.5Nm results in the washer biting into the adherend resulting in fibre and matrix damage. Thus a torque of 8.0Nm is selected for all fasteners in Stage 2. These results still have good agreement to the general specifications provided in [139].

3.5.4 Non-Destructive Inspection

The Olympus Epoch XT Ultrasonic A-Scanner was used to scan the surface of all specimen configurations containing a bondline. This identifies any voids or defects present prior to testing. Figure 3.19 shows one example of Configuration 1.4 used in Stage 1. A total of 12 positions were marked and the corresponding scans recorded against its position number.



Figure 3.19 Ultrasonic scanning positions for Hybrid Configuration 1.4

Ultrasonic A-Scans were also recorded for the simple five ply thick outer adherends as well as the 10 ply thick inner adherends. Figure 3.20 shows the normalised spectrum. Overall a thinner adherend produces more peaks in the spectrum. Hence by monitoring the relative change as well as whether there is an increase or decrease in peaks will provide an indication

of the position of any bondline or interplay delamination's present through the thickness of the carbon fibre adherends.

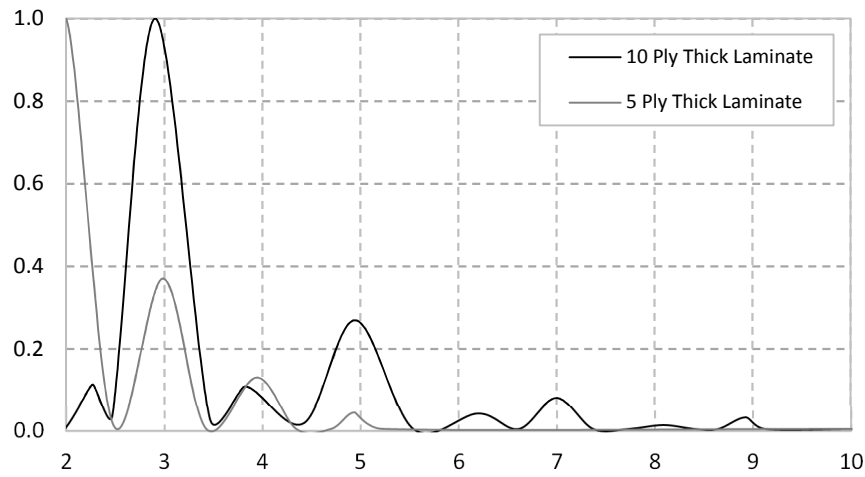


Figure 3.20 Spectrum envelope of a 10 and 5 ply thick adherend used in Stage 1

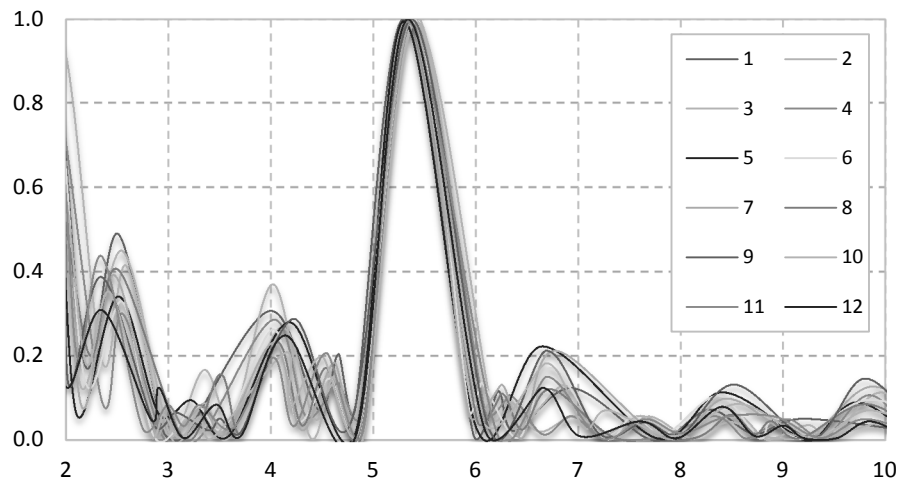


Figure 3.21 Spectrum envelope of Configuration 1.3 - Hybrid double lap joint with six rivets

Figure 3.21 shows the 12 spectrums for Configuration 1.3 defined in Table 3.5 for the 12 respective positions similar to that defined in Figure 3.19. Overall all 12 spectrum peaks are in line with each other with no noticeable difference.

Specimen Configuration 1.4 identified in Figure 3.19 was cured in an oven instead of an autoclave. The lack of even curing pressure results in defects/voids in the bondline. Ultrasonic A-Scans were performed at the 12 respective positions outlined in Figure 3.19.

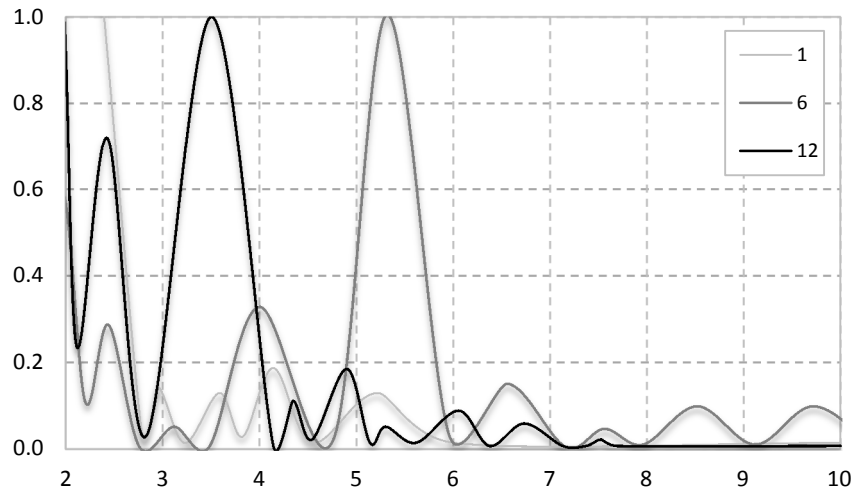


Figure 3.22 Spectrum envelope of Configuration 1.4 - Hybrid double lap joint with three rivets

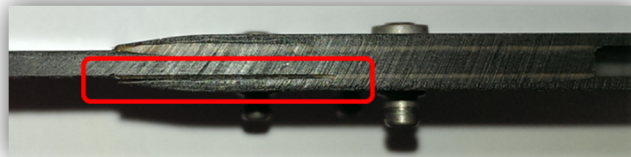


Figure 3.23 Bondline defect in position 1 of Configuration 1.4

Based on the scans, spectrum 1, 6 and 12 shown in Figure 3.22 produced significantly different curves. Spectrum 6 is the most representative profile expected for an intact bondline hence spectrum 1 and 12 contain bondline defects. Upon closer inspection, a void is clearly visible at position 1, Figure 3.23. The lack of even curing pressure and greater clamping provided aft of the overlap by two rivets results in a separation between the bottom adherend and middle adherend. This is not seen if specimens are cured in an autoclave at 40psi. As a result, these defects are expected to negatively affect the joint performance. Chapter 4 provides further details on how severely these defects affect the static and fatigue strength.

The same series of NDI tests using Ultrasonic A-Scanning was conducted on the remaining Stage 1 configurations and Stage 2 configurations. Only specimen Configuration 1.4 contained voids in its bondline with all other bonded and hybrid configurations unaffected. Overall the results here showed that NDI using Ultrasonic A-Scanning was an effective method of detecting and localising defects.

3.6 Initial Bondline Defects

Both double lap joint and step lap joint configurations contained specimens with either a 2mm initial crack or a semi-cured FM300-2K adhesive layer. Specimens containing a 2mm initial crack are tested to determine how much influence they have in reducing the static and fatigue performance of the joint. 2mm is selected as it borders the limit of an undetectable flaw size using Ultrasonic A-Scanning with a 10mm diameter probe.

A semi-cured adhesive layer is selected, as NDI using Ultrasonic A-Scanning cannot detect weak bondlines. Hence, if a joint repair were conducted on an aircraft there may be huge consequences if improper curing conditions were used. The relative severity of such a case is investigated in this research. The following sections outline the methods used to implement the various defects prior to testing.

3.6.1 Semi-Cured Adhesive

The aim of producing a semi-cured bondline is to reduce the peak strength of the joint. FM300-2K film adhesive is a strong yet brittle material. In some cases, the strength of the adhesive is far greater than the bearing strength of composite adherends. This affects the mode of failure and the stress distribution in the joint region. A series of tests were conducted to determine the effects of curing temperature and duration for the FM300-2K film adhesive. Tests were conducted according to the ASTM D5868-01, Standard Test Method for Lap Shear Adhesion for Fibre Reinforced Plastic (FRP) Bonding [140]. Based on this, four specimens were produced and cured at 40psi in an autoclave at different temperatures and curing durations. A 100kN Instron Machine was then used to load the specimens till failure; Figure 3.24.

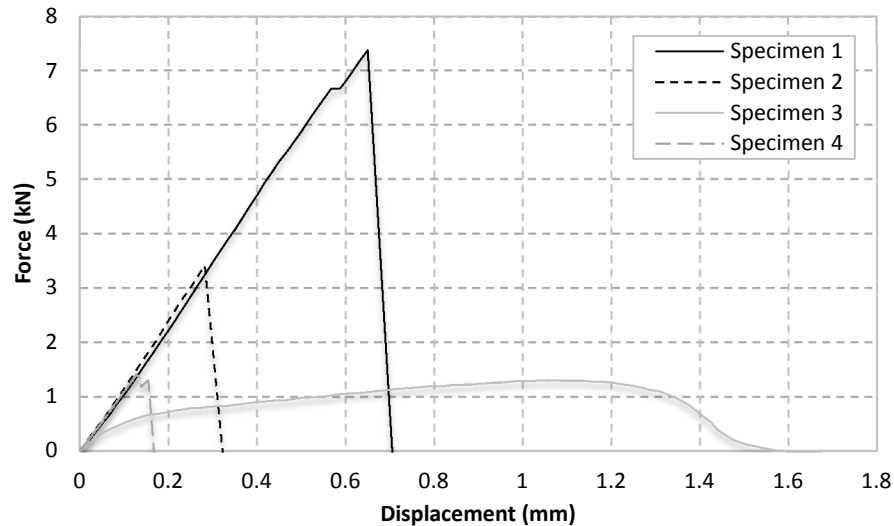


Figure 3.24 Peak strength of FM300-2K cured at different curing temperature and time; Specimen 1 - 121°C for 90min; Specimen 2 - 93°C for 60 min; Specimen 3 - 66°C for 60min; Specimen 4 - 85°C for 60min

Specimen 1

Cured at 121°C (250°F) for 90 minutes. This produced a peak strength of 7.4kN.

Specimen 2

Cured at 93°C (200°F) for 60 minutes. This produces a peak strength of 3.4kN.

Specimen 3

Cured at 66°C (150°F) for 60 minutes. This produced a bond which did not fully cure.

Specimen 4

Cured at 85°C (185°F) for 60 minutes. This produces a peak strength of 1.54kN.

From the results shown in Figure 3.24, Specimens 1, 2 and 4 failed catastrophically due to the brittle nature of the cured adhesive. The joint stiffness in maintained in these three cases however as expected the peak strength reduces with decreasing temperature and duration. A curing temperature of 66°C for 60 minutes results in an un-cured bondline showing a non-linear load-displacement behaviour. A key characteristic of FM300-2K film adhesive is that once cured, the bondline has a deep orange colour. From Figure 3.2, an un-cured layer of FM300-2K film adhesive is violet in colour; Specimen 3 in this case was

also violet in colour, hence indicating the adhesive is in an un-cured state prior to static testing. Based on the four load-displacement results, all specimen configurations containing a defective semi-cured adhesive layer was cured at 90°C for 60 minutes in an autoclave at 40psi.

3.6.2 Initial Bondline Crack

The second defective joint category contained a 2mm long initial crack placed using Polytetrafluoroethylene (PTFE) tape (commonly known as Teflon tape). The adhesive layer in this case was fully cured at 121°C for 90 minutes, similar to the pristine specimen bondline. Teflon has a very low coefficient of friction, this makes it well suited for creating initial bondline defects as the adhesive layer does not adhere well to the material. The Teflon tape used is 0.1mm in thickness and is located at the interface between the adherend and the adhesive prior to cure; Figure 3.25.

In the case of Stage 1 double lap joint configurations, the Teflon tape used spans the entire width of the specimen and located on the top surface of the middle adherend as shown in Figure 3.25. This is expected to be more damaging than placing a crack on both the top and bottom layer of the adhesive as a bending moment is induced. For the step lap joints in Stage 2, the Teflon tape is located in the first step between the adherend and adhesive layer as shown in Figure 3.25 and once again spans the entire width of the specimen.

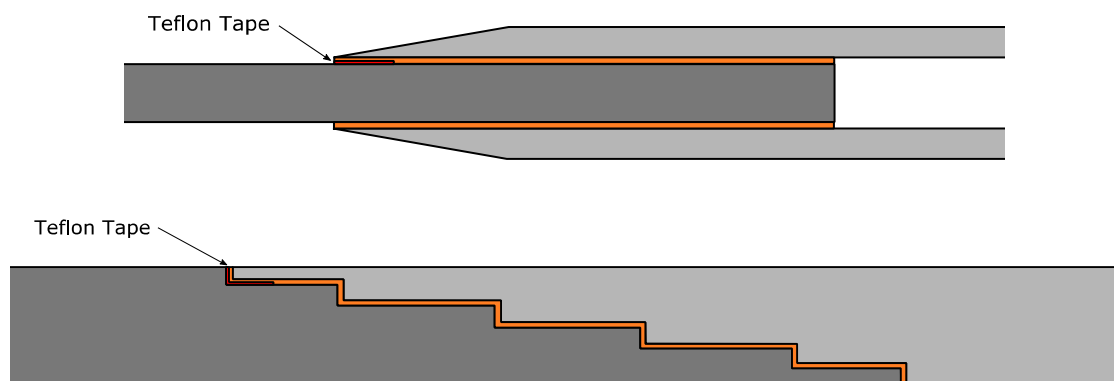


Figure 3.25 Location of Teflon tape to simulate a 2mm long initial crack in a double lap joint (top) and step lap joint (bottom)

3.7 Chapter Summary

Proper manufacturing techniques must be implemented to produce composite joint specimens. Any inconsistency during the manufacturing process will affect the joint performance and lead to large discrepancies in the static and fatigue test results. All specimen configurations used in both Stage 1 and Stage 2 are made from HexPly M18/1/G939 carbon fibre prepreg in a satin weave configuration with 0° and 90° fibres.

Stage 1 focuses on testing thin double lap joint configurations where the outer adherends are five plies thick with a ply stacking sequence of [(0/90)/(45/-45)/(0/90)/(45/-45)/(0/90)] and contains a 5mm tapered end to reduce peak stresses. The inner adherend is ten plies thick with a ply stacking sequence of [(0/90)/(45/-45)/(0/90)/(45/-45)/(0/90)]s. FM300-2K film adhesive cured at 121°C for 90 minutes in an autoclave is used for the pristine specimen configurations. Rivets were selected as the fastener of choice for these thin joint/repair applications as they are easily applied in thin airframes. Rivets were arranged in either a square array or a staggered array, typically found in current airframes.

Stage 2 focused on testing thick step lap joint configurations. The same HexPly M18/1/G939 carbon fibre prepreg and FM300-2K film adhesive are used as Stage 1. Adherends are 24 plies thick with a ply stacking sequence of [(0/90)/(45/-45)/(45/-45)/(0/90)]₆. Countersunk bolts torqued to 8Nm are selected for the fastened and hybrid configurations. Five steps were machined once the adherends were fully cured and arranged into mating pairs. The step lap joint design is then modified to increase joint stiffness as well as include additional stepped surfaces to further improve joint efficiency.

Two additional joint categories were produced in both stages of this research. These categories include either a defective semi-cured bondline (cured at 90°C for 60min) or a 2mm long initial crack. The aim is to determine how severely these effect joint performance under static and fatigue conditions and whether a hybrid configuration can prevent catastrophic failure. Overall this chapter outlined the importance and care required to create consistent joint specimens. Machining, surface preparation and assembly all play a large role in the final joint/repair performance. Static and fatigue tests are then conducted on each specimen configuration.

4

Stage 1-Experimental Testing

4.1 Introduction

The static strength and fatigue resistance of mechanically fastened, bonded and hybrid double lap joints using relatively thin carbon fibre adherends have been experimentally investigated in this chapter. The aim was to compare the static strength and fatigue resistance of a hybrid joint configuration consisting of both bonding and riveting, a purely riveted joint and a purely bonded joint. The effect of changing various parameters such as the mechanical fastener array configuration, rivet clamping pressure, bond strength, initial defects and curing conditions were also investigated.

The combination of mechanical fastening and bonding has been employed to safeguard against defects within the adhesive layer which may cause premature or catastrophic failure [6]. In contrast to the mechanically fastened joint, the stress concentrations around the fastener holes are significantly reduced due to the presence of the adhesive layer which evenly distributes the load within the bond region. It is only after the bond has failed where the fasteners begin to carry the remaining load in the joint. It is this safety factor that has allowed the certification of these joints in some aircraft structures.

A number of papers [5, 32-38] have investigated the behaviour of hybrid joints. Initial failure in all types of hybrid joints is predominantly due to debonding. Sun et al. [33]

showed how the use of ‘attachments’ can allow fasteners to carry more load in a hybrid joint configuration. Hart-Smith [34] provided a non-linear analysis of bonded and bolted joints and concluded that hybrid joint configurations cannot achieve any significant advantage over adhesive bonding in well-designed intact structures, however it may prevent defect/damage propagation. Kelly [35] investigated the load distribution in hybrid joints with a single bolt using finite element analysis. It was concluded that increasing adherend thickness and adhesive thickness increases load transferred by the bolt; whilst increasing overlap length, pitch distance and adhesive modulus has the opposite effect.

Thus far a majority of research has focused on developing numerical models; however there is little published work on experimental investigations, more so fatigue testing in the field of hybrid composite lap joints. The methods in which multiple fasteners interact with each other, how adhesive bond quality affects joint strength and the influence of initial defects are all important questions that need to be answered. Through the series of static and fatigue tests conducted, this chapter aims at answering these questions for thin double lap joint/repair applications.

4.2 Experimental Setup

The eight specimen configurations defined in Table 3.5 and Table 4.1 were manufactured and assembled according to the procedure outlined in Chapter 3. A total of 38 specimens were produced for static and fatigue testing, defined in Table 4.1.

Table 4.1 Number of specimens static and fatigue tested in Stage 1

Bondline Condition	Specimen	Joint Type	No. Rivets	Curing Pressure (psi)	No. Specimens	
					Static	Fatigue
Pristine	Configuration 1.1	Bonded	n/a	40.0	3	3
	Configuration 1.2	Riveted	6	n/a	3	3
	Configuration 1.3	Hybrid	6	40.0	3	3
	Configuration 1.4	Hybrid	3	14.7	3	3
Defective - 2mm	Configuration 1.5	Bonded	n/a	40.0	2	2
Crack	Configuration 1.6	Hybrid	6	40.0	2	2
*Defective -	Configuration 1.7	Bonded	n/a	40.0	2	1
Semi-cured Bond	Configuration 1.8	Hybrid	6	40.0	1	2

* Cured at 90°C for 60 minutes in an autoclave

All ‘pristine’ specimens were static tested followed by fatigue testing. Defective joint specimens were then produced based on the method outlined in Chapter 3. Configuration 1.7 and 1.8 contained semi-cured layers of FM300-2K film adhesive cured at 90°C for 60 minutes in an autoclave at 40psi. Aluminium tabs were bonded to each of the specimens clamping regions to prevent damaging the carbon fibre adherends. Figure 4.1 shows a set of assembled pristine double lap joint specimens.

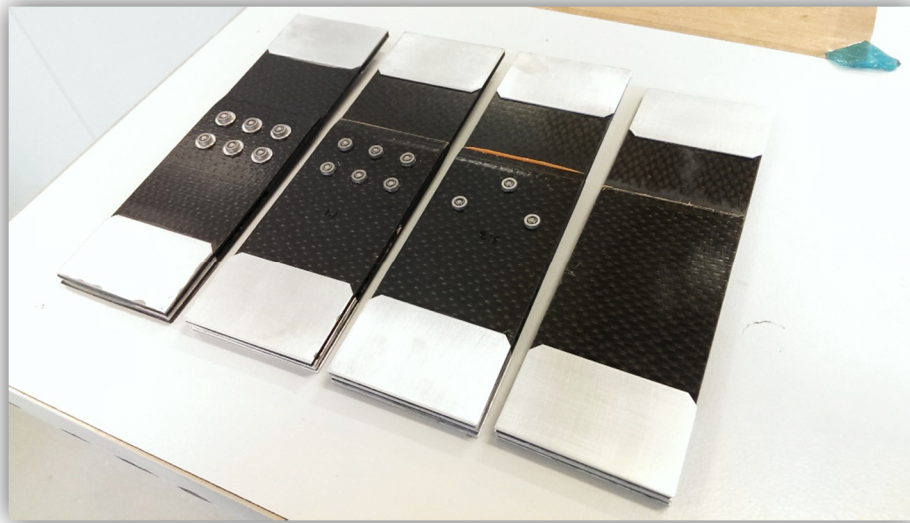


Figure 4.1 Fully assembled pristine double lap joint configurations ready for testing; Configuration 1.2, Configuration 1.3, Configuration 1.4 and Configuration 1.1 (left to right)

4.3 Testing Procedure

Static and fatigue tests were carried out on an Instron 1342 machine with a 100kN load cell; Figure 4.2. The system was controlled by a computer running MTS software. Static tests were conducted under displacement control at a rate of 1mm/min. Cross head displacement and load were recorded for the duration of each test.

Fatigue testing was conducted on all specimen configurations in load control mode at a frequency of 5Hz with a sinusoidal waveform. As these thin double lap joints are only subjected to tension driven applications in aircraft structures a stress ratio ($R = \sigma_{\min}/\sigma_{\max}$) of 0.1 was used; i.e. tension-tension fatigue.



Figure 4.2 100kN Instron 1342 servo-hydraulic machine

A block loading regime was implemented for the fatigue testing. Aircraft components are typically subjected to $3000\mu\epsilon$ [141, 142], an extensometer was used to correlate this strain to load. Initial tests were conducted at a constant amplitude load cycle of $3000\mu\epsilon$ with an r -ratio=0.1, it was found no sign of damage was present even after 10^6 cycles. Thus, the block loading regime shown in Table 4.2 was implemented to assess the fatigue resistance in a relative way. This regime poses a more severe loading condition than an actual component will be subjected to during flight and thus results presented are conservative.

The specimens were inspected visually for the duration of the fatigue tests; a video recorder was set up to monitor large abrupt changes in displacement which were mainly seen towards the end of specimen failure. Both the crosshead displacement and load was recorded on the computer system. In the case of specimen Configurations 1.7 and 1.8 (containing a defective bondline), the same loading regime highlighted in Table 4.2 was used except initial block loading began at $2000\mu\epsilon$ followed by $3000\mu\epsilon$, $4000\mu\epsilon$ and so forth;

this was to ensure the initial load amplitude did not exceed the peak static strength of the defective bonded specimen.

Table 4.2 Block loading regime #1 - strain amplitude increased every 10^5 cycles

Cycles (N)	Strain ($\mu\epsilon$)	R-Ratio	Upper Limit (kN)	Lower Limit (kN)
100,000	3000*	0.1	19.2	1.92
200,000	4000	0.1	25.6	2.56
300,000	4500	0.1	28.8	2.88
400,000	5000	0.1	32.0	3.20
500,000	5500	0.1	35.2	3.52
600,000	6000	0.1	38.4	3.84
700,000	6500	0.1	41.6	4.16
800,000	7000	0.1	44.8	4.48
900,000	7500	0.1	48.0	4.80
1,000,000	8000	0.1	51.2	5.12

* For specimen Configurations 1.7 & 1.8, initial block loading began at 2000 $\mu\epsilon$.

4.4 Experimental Results

4.4.1 Static Test Results

The load-displacement curve for all eight specimen configurations is shown in Figure 4.3 and summarised in Table 4.3.

The mode of failure was dependent on whether the joints were mechanically fastened, bonded or in a hybrid configuration. Configuration 1.3 reached a peak strength of 61.6kN with catastrophic failure occurring at a displacement of 1.89mm. Final failure occurred when the central adherend had cracked through the first row of rivets. Configuration 1.1 contained the second highest peak strength of 60.9kN with a displacement of 1.80mm. In most cases both bonds failed at the same time resulting in an immediate loss in joint strength.

Configuration 1.4 produced similar load displacement behaviour as Configuration 1.3. A peak strength of 60.0kN with a displacement of 1.74mm was achieved. This result shows that curing FM300-2K film adhesive in an autoclave at 40psi or in an oven under standard atmospheric conditions with the addition of rivets prior to curing results in a 2.6% loss in peak strength. A factor to consider during the production of these hybrid specimens cured in an oven is small adhesive voids present around the edge of the overlap region. The rivets provide an uneven clamping pressure compared to curing in an autoclave and thus resulting in a non-uniform bond. Thus, the mode in which the joints failed varied from adhesive failure on one side of the lap joint followed by adherend failure (crack), right through to both bonds failing at the same time and the central 10 ply thick adherend cracking at the first row of rivets.

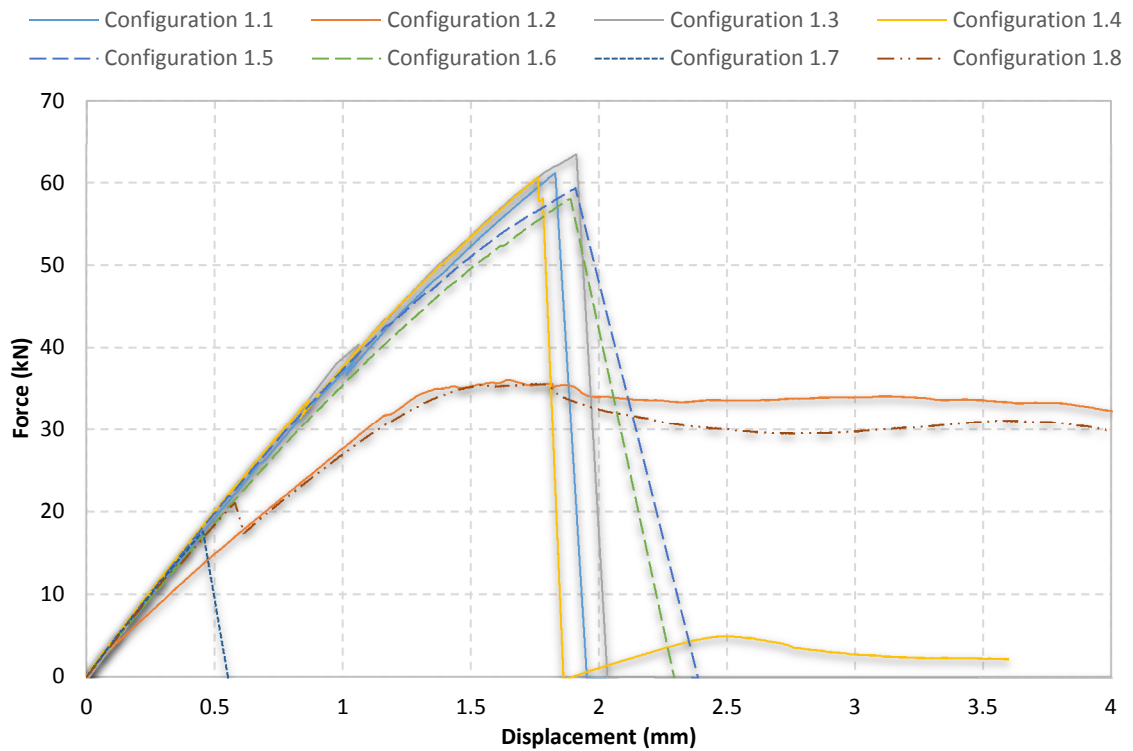


Figure 4.3 Peak strength achieved by fastened, bonded and hybrid configurations; refer to Table 4.1 for the detailed description of the configurations

The average peak load achieved by each of the eight different specimen configurations is summarised in Table 4.3.

Table 4.3 Summary of average peak load achieved by specimen Configuration 1.1-1.8

Specimen	Average Joint Strength	Standard Deviation
	(kN)	(kN)
Configuration 1.1	60.92	2.28
Configuration 1.2	36.80	0.72
Configuration 1.3	61.60	1.59
Configuration 1.4	59.99	2.13
Configuration 1.5	60.10	1.08
Configuration 1.6	58.39	0.68
Configuration 1.7	16.87	1.02
Configuration 1.8	35.29	n/a

Configuration 1.2 failed through bearing failure. The stiffness of the mechanically fastened specimens was 25% less than the stiffness of the purely bonded and hybrid specimens. A peak strength of approximately 35.0kN was achieved in these joints.

The influence of initial bondline cracks is an important test to conduct. This provides an indication as to whether a significant reduction in strength of the joint occurs due to the presence of the defect. Figure 4.3 identifies the load-displacement behaviour of a bonded joint (Configuration 1.5) and a hybrid joint (Configuration 1.6) with six rivets containing a 2mm long initial crack. This is the location of high stress concentrations and is where excessive peeling stresses are present [101]. In both of these joints, a reduction in stiffness is seen after a load of approximately 40kN; this is due to the rapid progression of the initial bondline cracking. Both the bonded specimen and the hybrid specimen failed at approximately 58.5kN with a displacement of 1.86mm. Final failure was identical to each of the respective specimen configurations without the 2mm initial crack.

The results thus far have shown no effect of rivets in the joint strength behaviour in a hybrid joint compared to a bonded joint. This is because the FM300-2K film adhesive has a higher shear strength than the carbon fibre adherends. Thus as soon as the bond fails, the bearing strength of the adherends has already been exceeded and hence the rivets cannot take part in carrying the remaining load in the joint after bond failure. From the

results gathered in Figure 3.24, an FM300-2K film adhesive cured at 90°C for 60 minutes will reduce the strength of the adhesive to below the adherend strength. Based on this information, Figure 4.3 clearly shows that the bond stiffness for Configuration 1.7 is maintained however the peak load achieved by the joint structure is reduced to 16.5kN. More interestingly Configuration 1.8 containing six rivets with a semi-cured adhesive increased the bond strength by 22% just through the addition of fasteners. After Configuration 1.8 reached a load of 20.2kN the bond had cracked all the way through the specimen and hence there was a significant drop in load. As the adherends bearing strength had still not yet been exceeded, the rivets carried the remaining load in the joint. Overall this changed the joint type from a hybrid configuration to a purely mechanically fastened joint. Load carried by the joint continues to increase to a peak value of 35.3kN whereby clear bearing failure around the rivet holes is then present. This joint configuration therefore highlights through careful fastener selection, adherend selection and bond strength the mode in which failure occurs and how it occurs can be controlled.

4.4.2 Fatigue Test Results

All eight specimen configurations were fatigue tested using the same Instron 100kN testing machine. Table 4.4 summarises the fatigue results for each of these configurations.

Note that the fatigue tests were not conducted under constant amplitude loading and hence typical S/N curves cannot be presented in this case. The fatigue tests (refer to Section 4.3) were conducted in a similar manner reported by Chalkley et al. [48] and Wang et al. [47], which is an efficient test method for comparison of fatigue resistance among joints with different configurations.

Results obtained highlight that specimens with a hybrid joint configuration performed better than bonded joints and mechanically fastened joints. Configuration 1.3 had the highest fatigue resistance, failing at approximately 550,000 cycles at the 6000 μE block loading regime. Configuration 1.2 - the mechanically fastened specimen containing six rivets had the lowest fatigue resistance of only 304,000 cycles. Lying in between these two tests was the purely bonded joint. This joint failed at approximately 440,000 cycles at the 5500 μE block loading regime.

Table 4.4 Fatigue resistance of specimen Configuration 1.1-1.8 under block loading, r-ratio = 0.1 frequency = 5Hz.

Type	Specimen No.	Failure Load (kN)/Strain ($\mu\epsilon$)	Cycles to failure (n)	Average (n)	Standard Deviation
Configuration 1.1	1	32.0/5000	377,895	442,175	62,056
	2	38.4/6000	501,739		
	3	35.2/5500	446,890		
Configuration 1.2	1	32.0/5000	302,200	303,768	1,844
	2	32.0/5000	305,799		
	3	32.0/5000	303,304		
Configuration 1.3	1	38.4/6000	527,000	556,699	28,162
	2	38.4/6000	583,019		
	3	38.4/6000	560,077		
Configuration 1.4	1	35.2/5500	476,944	466,652	16,046
	2	35.2/5500	448,163		
	3	35.2/5500	474,849		
Configuration 1.5	1	35.2/5500	417,645	415,097	3,603
	2	35.2/5500	412,549		
Configuration 1.6	1	38.4/6000	513,980	532,282	25,882
	2	38.4/6000	550,583		
*Configuration 1.7	1	12.8/2000	2,096	2,096	n/a
*Configuration 1.8	1	28.8/4500	307,782	321,994	20,098
	2	28.8/4500	336,205		

* Fatigue test started at 2000 $\mu\epsilon$

Specimen Configuration 1.4 performed marginally better (467,000 cycles) than a purely bonded joint. As for the ‘defective’ joint specimens, specimen Configuration 1.5 failed after 415,000 cycles. This is marginally less than a perfectly bonded joint however is expected, as the presence of an initial crack will result in an early failure. The same trend is seen for specimen Configuration 1.6. This joint failed after 532,000 cycles which is a 3.2% reduction in life compared to a ‘defect free/pristine’ hybrid specimen (Configuration 1.3).

Specimen Configurations 1.7 and 1.8 were fatigue tested with a modified block loading cycle. Based on the results shown in Figure 4.3, a bonded joint with a semi-cured adhesive

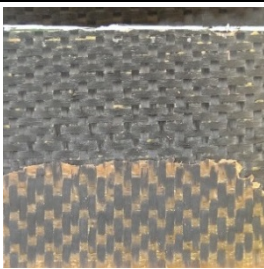
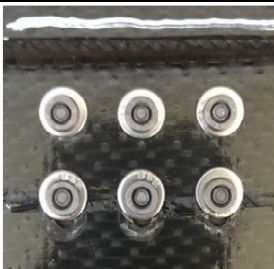
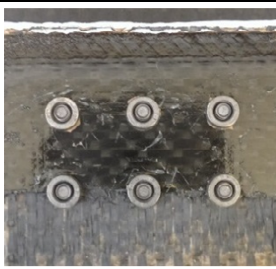

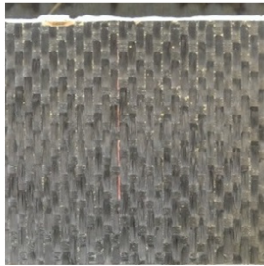

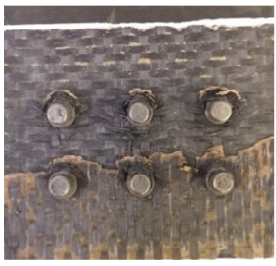
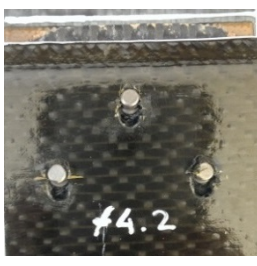
can withstand a peak load of 18kN, (Configuration 1.7). Starting the fatigue cycle at 3000 μ E block regime will cause this joint to fail instantly (19.2kN) which exceeds the static strength of the joint. Thus, the fatigue cycle was started at 2000 μ E (12.8kN) at an r-ratio of 0.1 at 5Hz for 100,000 cycles. The remaining fatigue load cycles followed those in Table 4.2.

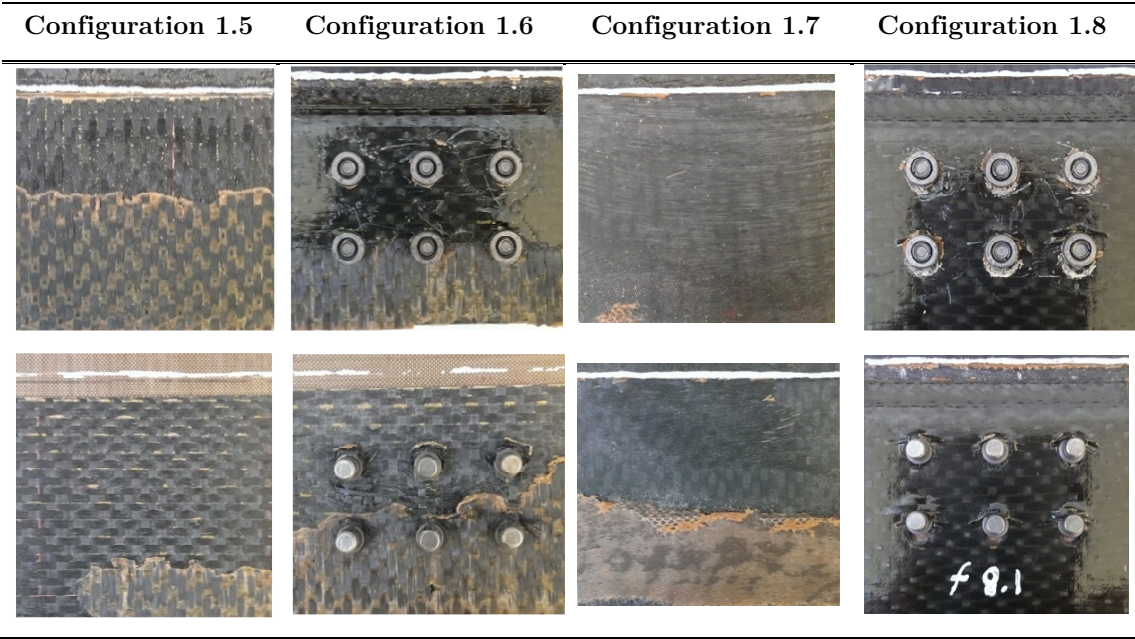
The results obtained through fatigue testing highlights how improperly curing FM300-2K can severely affect the fatigue life. In the case of the purely bonded specimen with a semi-cured adhesive, the specimen failed soon after loading began at 2,100 cycles. For specimen Configuration 1.8, failure occurred after 322,000 cycles at the 4500 μ E regime. This is significantly greater than the semi-cured bonded joint.

4.5 Discussion and Observation

The failure modes in the various joint configurations varied amongst each other and in some case variance between static testing and fatigue testing the same specimen configuration were also seen. Table 4.5 shows the failed gauge region in each of the eight different specimen configurations tested.

Table 4.5 Failure of the eight specimen configurations tested under fatigue loading at an r-ratio = 0.1 at 5Hz; both front and back images of failed gauge region shown

Configuration 1.1	Configuration 1.2	Configuration 1.3	Configuration 1.4
			
			



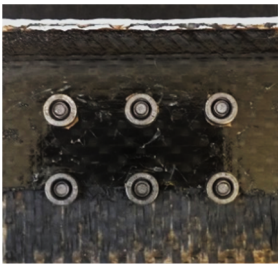


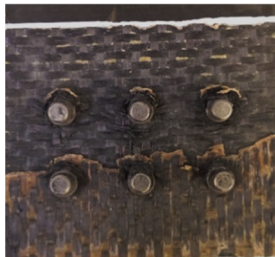

4.5.1 Failure Modes in Pristine Specimen Configurations 1.1-1.4

Final failure of specimen Configuration 1.3 differed between static testing and fatigue testing. Static testing caused the inner ten ply thick adherend to crack across the top row of rivets leaving the outer five ply thick adherends intact, Table 4.6. Cracking of the bond region occurred after a 1mm displacement. The crack continued to propagate through the length of the bond until it reached the first row of rivets. These rivets now began carrying part of the load in the joint and arrested the rapid growth within the bondline. There were no visible signs of bearing failure in the outer five ply thick adherends. However, it is likely that cracking started to initiate from the first row of rivet holes in the middle ten ply thick adherend. Once a load of 61.6kN was reached, the crack propagated across the width of the specimen causing the adherend to detach from the rest of the specimen.

Under fatigue testing, the outer five ply thick adherends cracked across the bottom row of rivets which experienced the most severe stress concentration. The specimen started to show signs of bondline cracking after 250,000 cycles. At the 6000µε block regime, specimen deformation increased and eventually failed at approximately 550,000 cycles. It can be clearly seen in Table 4.5 and Table 4.6 there is a mixture of adhesive and adherend failure above the second row of rivets and then adhesive failure below.

Configuration 1.2 failed in a similar manner under both static and fatigue testing. Substantial bearing failure was present in all six rivet holes. The addition of a washer on the top of the specimens increased the clamping area. The increased surface area provided by the washers prevented the head of the rivets from pulling through the top five ply thick adherend. Final failure occurred by cracking across the bottom row of rivets.

Table 4.6 Specimen Configuration 1.3 failing under a fatigue block loading regime and failing under static testing with a cross-head speed of 1mm/min

Fatigue	Static	
		
		

Configuration 1.1 also produced the same failure mode under both static and fatigue testing. Both the top and bottom bonds failed simultaneously. A crack initiated from the tip of the tapered adherends due to excessive peeling stress. All specimens showed a mixture of adhesive failure and adherend failure. In the case of fatigue testing, after 100,000 cycles a small crack was visible on the bottom bond located on the right hand corner of the tapered region; the crack is approximately 1mm in length. After 250,000 cycles the bond length grew to 3mm in length. Shortly after 400,000 cycles the crack length grew to 15mm whereby final catastrophic failure occurred soon after. It must be noted that a large variance in fatigue limits for this joint was adamant. Failure occurred $\pm 36,000$ cycles and

is primarily due to slight inconsistencies in surface preparation or slight variance in bond area.

Configuration 1.4 was the final ‘pristine’ specimen tested. Final failure under static testing varied from either cracking across the top row of rivets in the central adherend or cracking in the outer 5 ply thick adherends across the bottom row of rivets. The lack of an even clamping pressure across the bond when cured in an oven resulted in different final failures modes. Under fatigue test cases, final failure was consistent across the three specimens tested. After ~150,000 cycles there was a crack length of approximately 5mm in the bottom bond. Cracking was arrested by the single rivet on the first row whereby it continued to propagate along one of the sides of the joint, Figure 4.4.

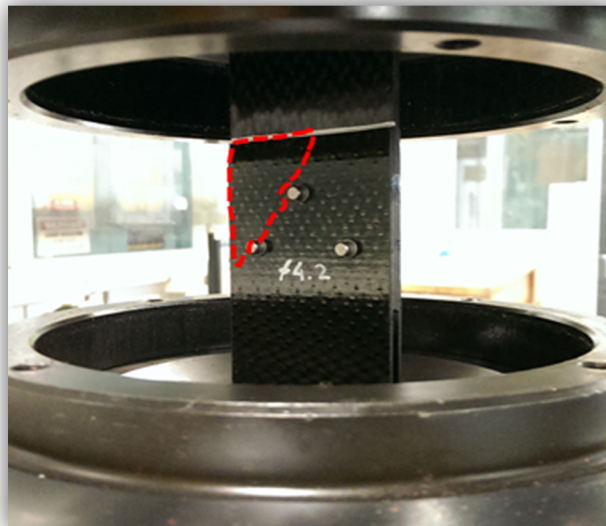


Figure 4.4 Region of disbond (indicated in red) after 400,000 cycles in the hybrid specimen with a staggered rivet array (Configuration 1.4) cured in an oven at 121°C for 90 minutes

4.5.2 Failure Modes in Defective Specimen Configurations 1.5-1.8

Testing defective specimens is vital in carrying out as it provides an indication of the effectiveness of mechanical fasteners in arresting catastrophic failure. In the event a bonded joint was conducted by a technician on field, it is unlikely the repair will be done in proper laboratory environments; this may hinder the quality of the bonded joint. Thus, specimens are likely to contain either initial dis-bonded regions or additional defects as curing

conditions and temperature may be overlooked at some point. Although there are stringent protocols already in place to prevent this from happening, exploring the long-term effects of such a bond is important to understand as it could be the deciding factor of the loss of an aircraft and more importantly its occupants.

Configuration 1.5 showed a mixture of adhesive failure, cohesive failure and adherend failure. Table 4.5 shows the location of the various disbonds. The failure under both static testing and fatigue testing yielded almost the same result. Soon after fatigue testing, it was clear the outer five ply thick adherends had a slight separation at the tip of the tapered region containing the initial crack (crack 1). After approximately 150,000 cycles, the first crack - crack 1 had grown from 2mm to 3mm. Final failure in these specimens occurred at approximately 415,000 cycles at the 5500 μE block loading regime.

Configuration 1.6 failed in a similar manner to Configuration 1.3. After 380,000 cycles it was clear the 2mm initial bondline crack had grown 7-8mm in length. From Table 4.5 it is seen the FM300-2K film adhesive has separated from the central adherend and soon after reaching 450,000 cycles the crack transitioned from the central adherend through the thickness of the bond to the bottom five ply thick adherend. Final failure occurred just over 530,000 cycles which is marginally short of specimen Configuration 1.3.

Final failure in Configuration 1.7 under both static and fatigue once again yielded no significant differences. Comparing this specimen to its 'pristine' counterpart – specimen Configuration 1.1, a significant difference in the failure mode is seen. Alongside this, the scrim cloth present in the FM300-2K film adhesive is visible after the failure of this joint. Under fatigue testing, the joint failed soon after loading began (2000 cycles). This result highlights that inadequately curing FM300-2K film adhesive can have severe consequences on the life of the joint.

Configuration 1.8 failed the same way under both static and fatigue testing. After approximately 230,000 cycles, the bottom tapered region had a crack approximately 10mm long extending through the width of the specimen. In the case of a bonded joint, such a long crack would grow rapidly. This indicates that the rivets are providing additional clamping pressure arresting rapid crack growth. Both bonds are no longer intact after 305,000 cycles and thus the rivets are now carrying the remaining load as a mechanically fastened configuration with reduced stiffness. Final failure in these joints was through

bearing failure due to the presence of micro cracks forming at the front of the rivet holes and hole elongation aft of the rivets.

4.5.3 Double Lap Joint Comparison

Through the experimental tests conducted thus far, it is quite clear that mechanically fastened joints (rivets) do not yield any clear advantage over ‘pristine’ bonded and hybrid joint configurations. The main advantage of mechanically fastened joints for these relatively thin structures lies in bearing failure as it is a slow mode of failure and allows time to be detected in regular inspection intervals. Under static testing, bonded specimens and hybrid specimens with FM300-2K film adhesive cured at 121°C yielded no significant difference in peak loading. Both joints failed catastrophically without much notice prior to failure. Hybrid joints did however perform marginally better than the bonded joints. In the case of specimen Configuration 1.4, there was no significant change in peak loading achieved however there was a slight reduction in displacement. This result indicates that pressure provided by rivets during the curing stage of manufacturing is adequate in achieving the same optimum joint strength as a purely bonded joint. Hence this may present the opportunity to conduct these repairs on field where limited equipment is present to cure adhesive joints under vacuum pressure. However under fatigue testing, this joint does not present a significant advantage over a properly bonded joint as almost the same fatigue life is achieved but with the added weight of the rivets.

Specimen Configuration 1.5 and 1.6 containing the 2mm initial bondline crack showed a marginal loss in peak strength and fatigue life compared to their ‘pristine’ counterparts. The fact that a 2mm initial crack reduces fatigue life by 6.1% and 4.2% for a bonded and hybrid specimen respectively highlights no significant loss (based on the block loading regime used). The presence of rivets does however reduce the severity of initial cracks present in the bond region, thus acting as a failsafe mechanism in the joint.

Although under static test conditions there were no significant differences between bonded and hybrid joints, it is under fatigue test conditions where hybrid joint significantly outperform the riveted joints and the bonded joints. A ‘pristine’ hybrid joint with a bond cured at 121°C for 90 minutes at 40psi (Configuration 1.3) has a final failure life 45% greater than a riveted joint (Configuration 1.2) and 20% greater than a bonded joint (Configuration 1.1). This substantial increase in life shows that hybrid joints using rivets

as the fastening mechanisms clearly outweigh the use of purely bonded joints in these ‘thin’ joint structures found in aircrafts. The presence of rivets also safeguards against defects and inconsistencies present in the bond layer implying easier joint/repair certification. A common failure seen in all joint configurations containing a bond was the faster progression of bondline cracking across the bottom adhesive used in the double lap joint configuration (bond closest to the tail of the rivets). The main contributing factor for this is the lower clamping area provided by the lip of the rivets compared to the head of the rivets. This allows easier opening between the bottom adherends. Maofeng Fu et al. [42] presented a study on the static and fatigue performance of hybrid joints in a structural reaction injection moulded composite. The investigation showed that hybrid joints have a higher static failure load and longer fatigue life than adhesive joints. However, the performance of the hybrid joints depends on the washer design [42]. It was concluded that lateral clamping pressure can significantly decrease the maximum peel stress at the interface and thus improves the overall joint performance. This study suggests increasing the top and bottom clamping area of rivets using washers will also increase the fatigue life further.

In the case of the defective bondline specimens (Configuration 1.7 and 1.8), a vast difference between the bonded specimens and hybrid specimens is seen. Lowering the curing duration and temperature severely affected the life of the joints. The defective bonded specimen failed almost immediately after starting the fatigue test at the 2000 μE (12.8kN) loading regime which is 22% less than the peak strength of the same joint under static testing. Configuration 1.8 performed significantly better than the bonded joint; failing at approximately 322,000 cycles. This test highlights the importance of using mechanical fasteners to act as a failsafe mechanism. One factor to take note is this specimen failed at the 4500 μE loading regime whilst a purely mechanically fastened specimen failed at the 5000 μE loading regime. The difference is due to purely mechanically fastened specimens having a higher rivet clamping pressure applied throughout the test duration. Once the bond failed in a hybrid specimen containing a defective bondline the effective configuration changes to a mechanically fastened specimen. The thickness of the overlap region is also reduced due to bondline cracking which in effect lowers the rivet clamping pressure.

Overall, throughout the operation of an aircraft, the temperature, humidity and moisture conditions will vary and act together to degrade the adhesive over time leading to a loss in strength, not easy to predict [5]. Through the tests conducted it has been clearly demonstrated that bonded joints can fail catastrophically. Through the addition of

fasteners, premature bond failure can be minimised due to additional clamping and overall fatigue resistance can be increased due to the added residual strength.

4.6 Chapter Summary

Static and fatigue tests were conducted on eight thin double lap joint specimen configurations. Tests were run on both ‘pristine’ and ‘defective’ joints. ‘Pristine’ specimens either contained a purely riveted joint or specimens where the FM300-2K film adhesive was cured at 121°C for 90 minutes. ‘Defective’ specimens either contained a 2mm long initial crack or a semi-cured adhesive layer of FM300-2K film adhesive cured at 90°C for 60 minutes. Through the series of experimental tests highlighted in this chapter, the benefits of hybrid joints outweigh those of bonded joints. Under static test conditions, there was relatively no difference between a pristine bonded configuration and a hybrid configuration. However under fatigue cases, a significant improvement in resistance is achieved by hybrid joint configurations.

From a practical point of view, the presence of mechanical fasteners (in this case rivets) not only act in providing improvements in static strength and fatigue resistance, they act in arresting rapid crack growth and prevent sudden catastrophic failure from occurring provided bond strength is less than the bearing strength of the adherends. The experimental observations confirm that a square array of rivets is effective in suppressing rapid crack growth. The clamping pressure is vital in minimising Mode I opening and reduce high peeling stresses in the bondline. This study has shown the effects of varying curing conditions, clamping pressure and initial bondline defects. Current results in the case of relatively thin structures lean towards using hybrid joint configurations, particularly for repair scenarios.

Further work on investigating these effects on relatively thicker composite structures with different configurations such as scarf and stepped lap joints are also areas that need further research. Alongside this, work through finite element analysis will aid in further understanding how load and stresses vary in these different joint configurations. Chapter 5 focuses on the numerical modelling of these double lap joint configurations investigated.

End of Chapter 4

5

Stage 1-Finite Element Analysis

5.1 Introduction

Finite element analysis (FEA) is performed to verify the static and fatigue strength of mechanically fastened, bonded and hybrid double lap joints considered in Chapter 4. These joints are made from thin carbon fibre/epoxy laminates applied in aircraft structures. Several configurations are considered, including variations in rivet array and the addition of bondline defects. Adhesive nonlinear material properties, rivet surface contacts and frictional forces were included in the three-dimensional (3D) Finite Element (FE) models. The Multicontinuum Theory (MCT) is used to simulate the progressive failure process and the stress state for all specimens, whilst the strain energy release rate (SERR) as a function of crack length for bonded and hybrid specimens are also compared.

Joints potentially act as weak links in structures, thus it is important to understand their strengths and the mode in which they fail. The modelling of the various joint configurations discussed in Chapter 4 will aid in further understanding the methods behind failure and provide further insight into improving joint design. These are all important factors to consider in order to achieve composite joint repair certification.

In recent years the use of Finite Element (FE) methods to simulate the behaviour of composite joints has increased particularly due to the advancement of many FE packages.

However, most composite hybrid joint models reported so far are restricted to 3D models with a single fastener or 2D models [6, 36, 43, 101, 102, 143]. In order to be used as a versatile design tool, the analysis needs to be able to simulate multi fasteners as practically used in a joint, and accurately capture the three-dimensional stress states, material behaviour, bolt clamping, friction, secondary bending effects, load distribution as well as contact interactions between surfaces [103]. In addition, the localised damage in peak stress regions can reduce the laminates sensitivity to discontinuity. This results in highly conservative strength predictions based on initial failure around hole boundaries [19]. Hence, the modelling must include the capability of progressive failure predictions. From current literature, there is very little work that has included all the above factors.

This chapter provides details on the 3D FEA conducted to predict the static and fatigue strength of riveted, bonded and hybrid double lap joints made from thin carbon fibre/epoxy laminates. Multiple rivets with different array patterns were used in the riveted and hybrid joints. For the bonded and hybrid joints, the effects of two different types of bondline defects were also assessed (discussed in Chapter 4). Nonlinear adhesive material property, rivet surface contact, friction forces and the Multicontinuum Theory (MCT) to simulate the progressive failure process are all included in the FEA models. The full load-displacement curve and failure mode for each joint configuration are also predicted. In addition, the strain energy release rate (SERR) as a function of crack length for bonded and hybrid specimens are calculated to provide a better understanding of how rivets affect the fatigue resistance of the joints. The FEA predictions are then compared with the experimental test results discussed in Chapter 4 of this dissertation.

5.2 Finite Element Analysis Setup

Abaqus CAE v6.13 is used to model the different thin double lap joint configurations. A quarter of the specimen's geometry is modelled due to symmetry halfway across the width of the specimen and by making the assumption that the fasteners head and tail are the same, the model can be split midway through the thickness. Figure 5.1 depicts the three main geometries used in the FE models and Figure 5.2 shows an example of a meshed hybrid configuration (quarter model).

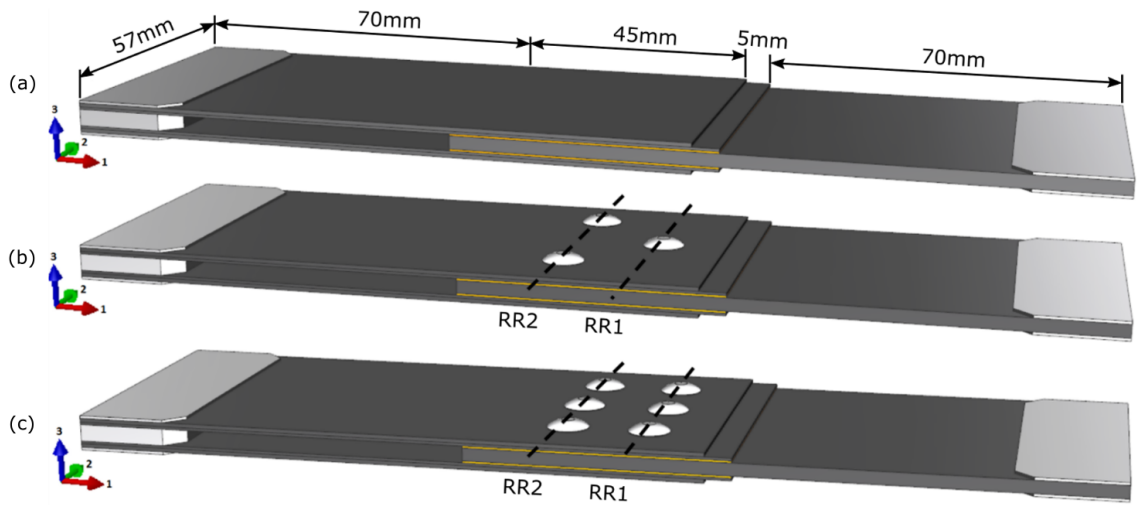


Figure 5.1 Three major geometry configurations (tabs used for clamping shown for representation only); (a) Configuration 1.1 – Bonded Double Lap Joint, (b) Configuration 1.4 – Hybrid Double Lap Joint with three rivets, (c) Configuration 1.3 – Hybrid Double Lap joint with six rivets; RR1 – Rivet Row One (closest fastener row to tapered edge); RR2 – Rivet Row Two (furthest fastener row from tapered edge)

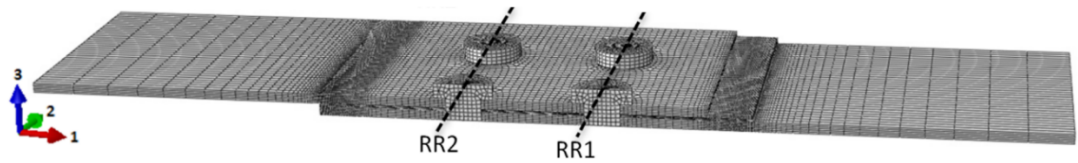


Figure 5.2 Meshed assembly of a hybrid double lap joint (Configuration 1.3); quarter of full geometry

The adherends were modelled using orthotropic material properties defined in Table 3.1. The adhesive was modelled using elastic-perfectly plastic material data specified in Table 3.2. A coefficient of friction of 0.1 was used between the fasteners and composite plate as well as between contacting plate surfaces [144, 145]. This was applied using the master-slave algorithm with small sliding allowed between contacting surfaces and a neat fit between the rivets and the adherends.

Fully integrated linear brick C3D8 elements using a structured mesh is used for the adhesive and composite adherends. Biased seeding was present around the fastener holes and at the ends of the overlap where the element size increased from 0.1 up to 4.0. Coarser meshes were used further afield from the overlap ends. Specimens containing an adhesive layer with no initial cracks had four elements placed through its thickness. Specimen

Configuration 1.1 to 1.6 contained an average element aspect ratio of 6.56, 2.33, 4.54, 5.83, 4.67 and 5.45 respectively. A displacement was applied to the left end of the outer five ply thick adherend in the longitudinal (1) direction, Figure 5.2. The right end of the middle adherend had a clamped boundary condition ($u_1, u_2, u_3 = 0$). A symmetry condition was also applied to the underside of the middle adherend and the plane halfway across the width of the specimen.

In order to accurately simulate the material failure behaviour, the micromechanical analysis method called the Multicontinuum Theory (MCT) provided by Autodesk as a commercial plugin to Abaqus was utilised [7, 8]. As discussed in Chapter 2, micromechanical analysis takes an additional step beyond the conventional laminate theory to separate the stress and strain in the matrix and fibre from a Representative Volume Element (RVE). MCT predicts failure at the fibre and matrix level by obtaining the volume averaged stress states in both the fibre and the matrix. Here, matrix failure is assumed to be influenced by all six of the matrix average stress components in a 3D analysis, whilst a quadratic function is used to find the average stress of the fibre [7, 8].

In contrast, progressive damage models such as Hashin's criteria implemented in Abaqus can be computationally expensive and typically suffer convergence issues due to discrete stiffness reductions whilst not accounting for transverse stress and strain components which are accounted for in MCT. By implementing this method it allows modelling specimen behaviour with far greater accuracy than previously available.

5.2.1 Load-Displacement Correction

Prior to modelling the various double lap joint configurations, the experimental load-displacement data reported in Chapter 4 [146] needed to be corrected. The results presented were the raw force and displacement data provided by the Instron 100kN software interface. The displacement transducer of the Instron machine measured the total displacement that comprises of the deformation of the load train in addition to that of the test specimen. The true specimen deformation can only be determined from the machine displacement transducer once the deformation of the load train is isolated [29]. To do this, a calibrated extensometer was used on a simple coupon specimen made from the same HexPly M18/1/G939 carbon fibre prepreg. An extensometer with a 25mm gauge is then used to record specimen elongation when subjected to increasing load, this is then

correlated to the overall specimen elongation. Figure 5.3 shows the measured load-displacement graph recorded by the Instron machine and the calibrated extensometer. As expected the true specimen displacement is reduced once the deformation of the load train was isolated.

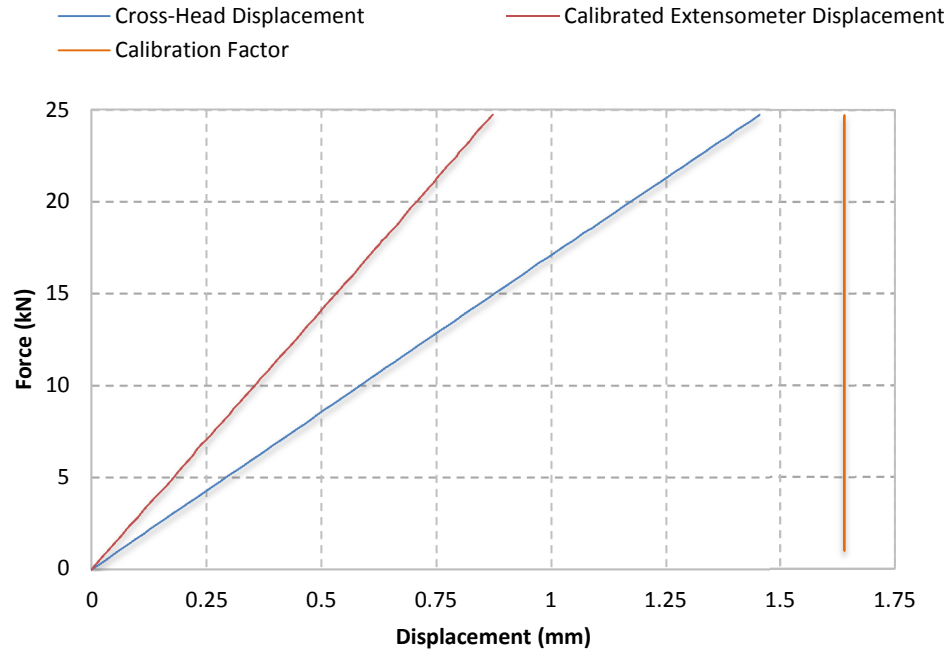


Figure 5.3 Determining calibration factor for specimens true displacement

5.2.2 Fibre and Matrix Degradation

For composite failure simulation, it is quite important to accurately represent the progressive nature of constituent damage leading to failure. MCT decomposes the ply level stress/strain field into the constituent level of the fibre and matrix. The progressive damage of the composite material is non-linear. In order to model non-linear behaviour in the matrix, it is important to degrade the material after damage is predicted. This stiffness degradation drives the stress redistribution that leads to failure propagation in a structure and its ultimate failure. MCT uses a simple approach in which matrix properties are instantaneously degraded (E_{11} , E_{22} , E_{33} , G_{12} , G_{13} and G_{23}) to a fraction of their original value once matrix failure is detected. Likewise, a similar method is used for fibre failure. Fibres are assumed to be linear elastic prior to failure. However once the MCT fibre

damage criterion is met, E_{11} , E_{22} , E_{33} , G_{12} , G_{13} and G_{23} are reduced to near zero values as the damaged fibres are expected to no longer carry any load.

Based on this information, the degradation values are significantly more severe for the fibre constituent compared to the matrix constituent. Determining the specific degradation values for the matrix and fibre are dependent on the material being used. Hence, an iterative approach is used to obtain each of the respective degradation values. Figure 5.4 shows a representation of the instantaneous degradation applied to the matrix and fibre constituents as soon as failure is detected.

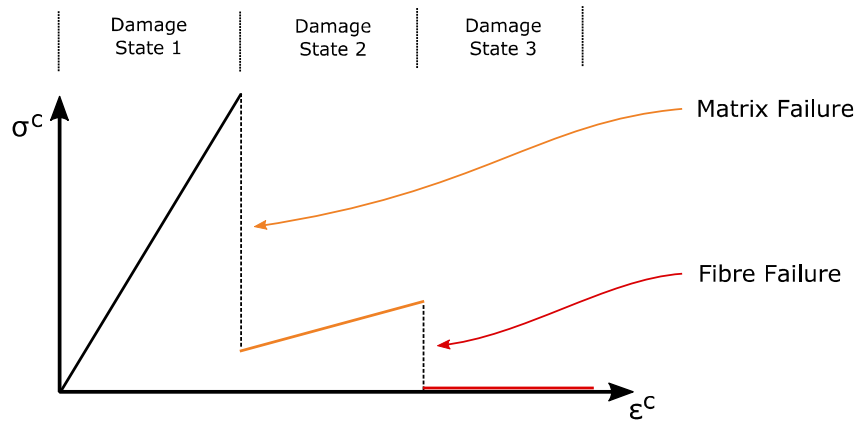


Figure 5.4 Progressive damage states using the Multicontinuum Theory

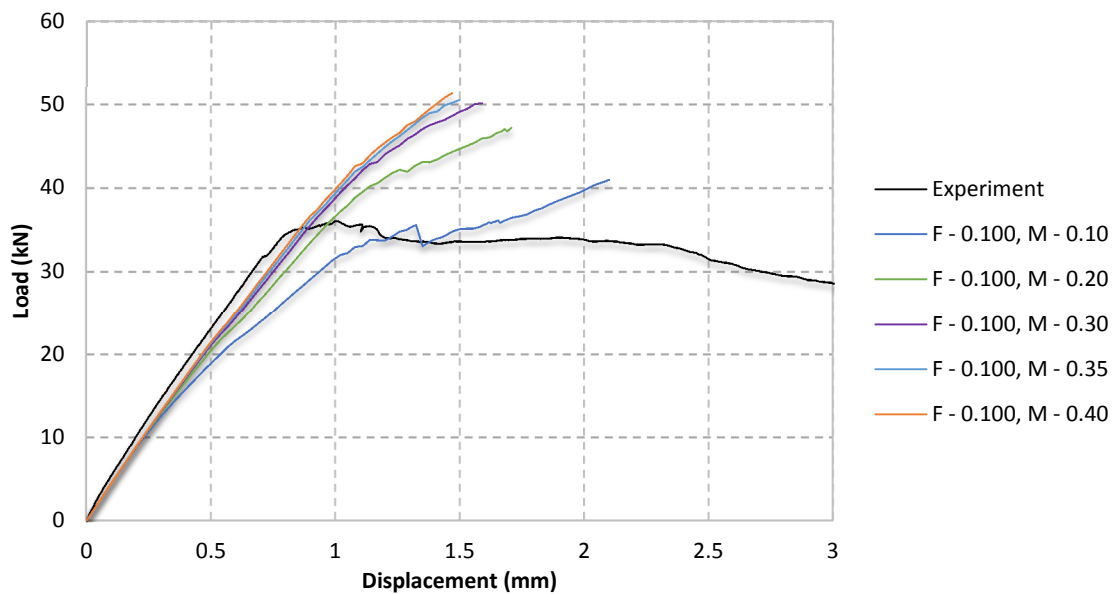


Figure 5.5 Optimising the matrix degradation value for the HexPly M18/1/G939 carbon fibre prepreg; F - (fibre degradation value); M - (matrix degradation value)

The purely riveted joint Configuration 1.2 was used to iteratively determine the degradation values. This joint configuration was selected as no adhesive layer was present. Figure 5.5 shows the experimental load-displacement curve for thin riveted double lap joint. In this case, the fibre degradation value was kept fixed at 0.10 (10%) and the matrix degradation value was varied from 0.10 to 0.40 (10% to 40%). These values represent the percentage at which the material parameters are reduced to. The results show the greater reduction in matrix properties, the greater the softening in the joint. Overall the closest stiffness match between numerical and experimental results occurs when the matrix degradation value is 0.35 (35%), a larger value results in minimal change in the load-displacement curve with the likelihood of overestimating bonded and hybrid joint stiffnesses.

After selecting the matrix degradation value, the fibre degradation value was iteratively determined. Figure 5.6 shows the load-displacement curves for fibre degradation values ranging between 0.005 to 0.100 (0.5% to 10%).

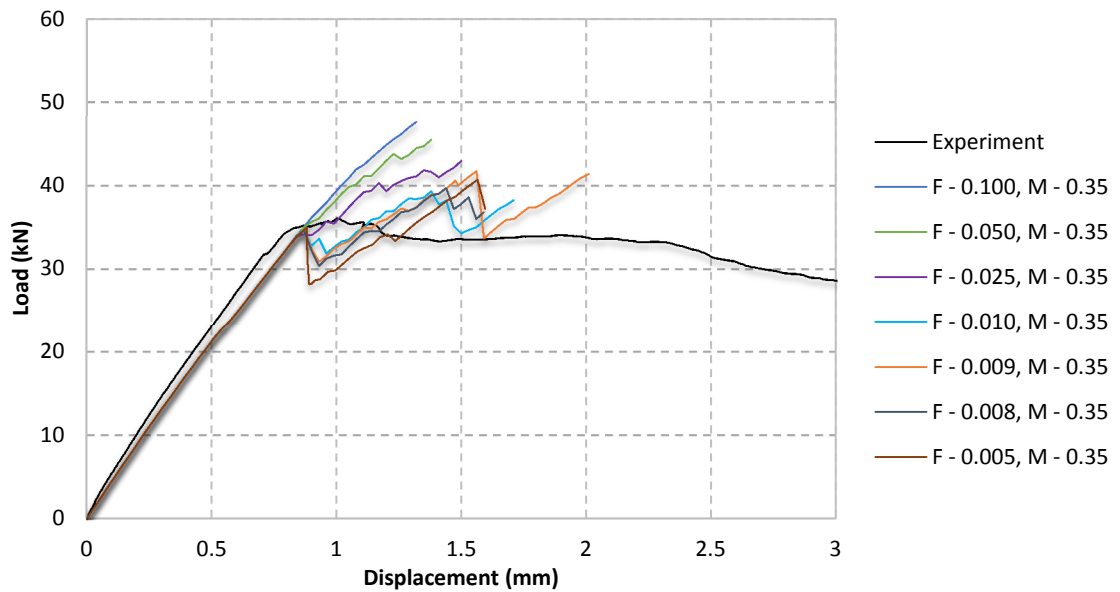


Figure 5.6 Optimising the fibre degradation value for the HexPly M18/1/G939 carbon fibre prepreg; F - (fibre degradation value); M - (matrix degradation value)

Comparing Figure 5.6 to Figure 5.5, it is clearly seen the fibre degradation value is more detrimental to the load-displacement characteristics achieved. A near zero value was required to closely simulate the load-displacement behaviour obtained experimentally.

Based on the various fibre degradation values shown in Figure 5.6, the optimal value was 0.010 (1%). Overall the fibre and matrix degradation values used to progressively damage the HexPly M18/1/G939 carbon fibre adherend in Abaqus CAE was 0.01 and 0.35 respectively. Note these values are slightly higher than the conventional values used in MCT because in a riveted case, bearing failure is a compressive mode of failure, hence requiring slightly higher fibre and matrix degradation values.

5.3 Experimental Comparison with Finite Element

Configurations 1.1 - 1.4 are considered pristine specimens. These specimens are manufactured in a controlled manner with no intentional bondline defects. Specimens containing bondlines have been cured in ideal conditions in an autoclave and for the unique case - Configuration 1.4 was cured in an oven to test whether the clamping pressure provided by the rivets only - are sufficient in obtaining adequate bond strength. Aircraft components are typically subjected to $3000\mu\epsilon$ [141, 142] and hence further analysis is carried out at this strain level as well as its final failure strain (defined by the specimens' maximum elongation in the following load-displacement curves obtained through FEA). Configuration 1.5 - 1.8 are considered to be the defective specimens. These contain either a 2mm long initial crack or a semi-cured adhesive cured at 90°C for 60 minutes. The following sections compare the numerical FEA results with the experimental load-displacement curves discussed in Chapter 4.

5.3.1 Pristine Specimens (Configuration 1.1 - 1.4)

Specimen Configuration 1.1, 1.3 and 1.4 containing an FM300-2K bondline was modelling initially without an adhesive spew fillet and then with an adhesive spew fillet. Figure 5.7 shows an example of a double lap joint containing a spew fillet typically found after the bondline has cured.

Lang et al. [147] and Andreassi et al. [148] investigated the formation and geometry of adhesive spew fillets. A spew is defined as a portion of adhesive that is squeezed out from the lap area and forms a bead at the lap ends as the two substrates are assembled [147]. Although they are minor features in the geometry they play an important role in regards to the joint strength. The type of spew formed dictates its significance in reducing the

shear stress at the end of the overlap. In the case of the double lap joint configurations investigated, the spew formed was triangular in shape due to the contour produced by the vacuum bagging process and through the use of high temperature resistant flash tape. From the manufactured specimens, the spew formed was approximately 1.5mm in length and spanned the entire width of the specimen.

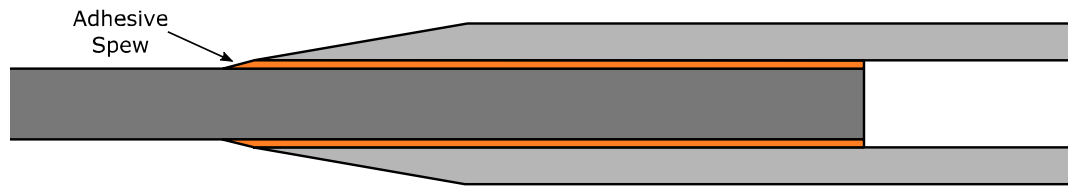


Figure 5.7 Adhesive spew fillet located at the ends of the overlap

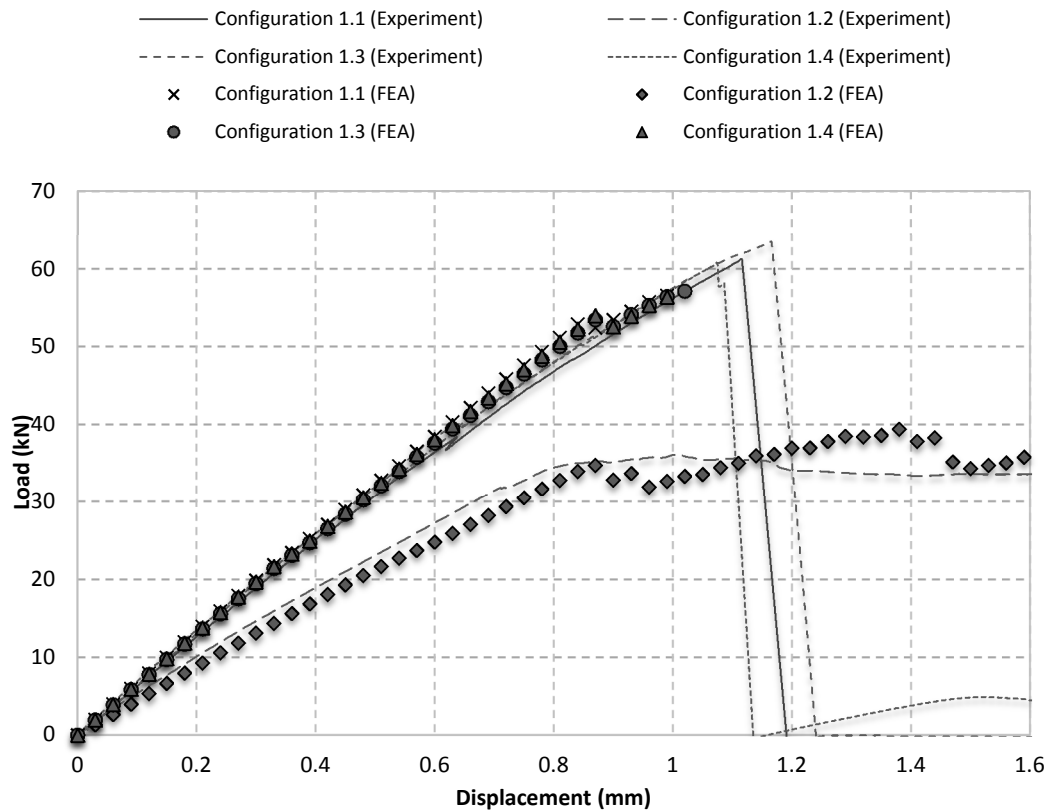


Figure 5.8 Load-displacement comparison between experimental and FEA for Configuration 1.1 - 1.4 with no spew; displacement represents the specimens total elongation for the given load

Initials models in Abaqus CAE did not contain an adhesive spew. Figure 5.8 shows the load-displacement curves for the four pristine specimen configurations. Based on these results, there is a close match between numerical and experimental results although all bonded and hybrid specimens conservatively predict the peak load.

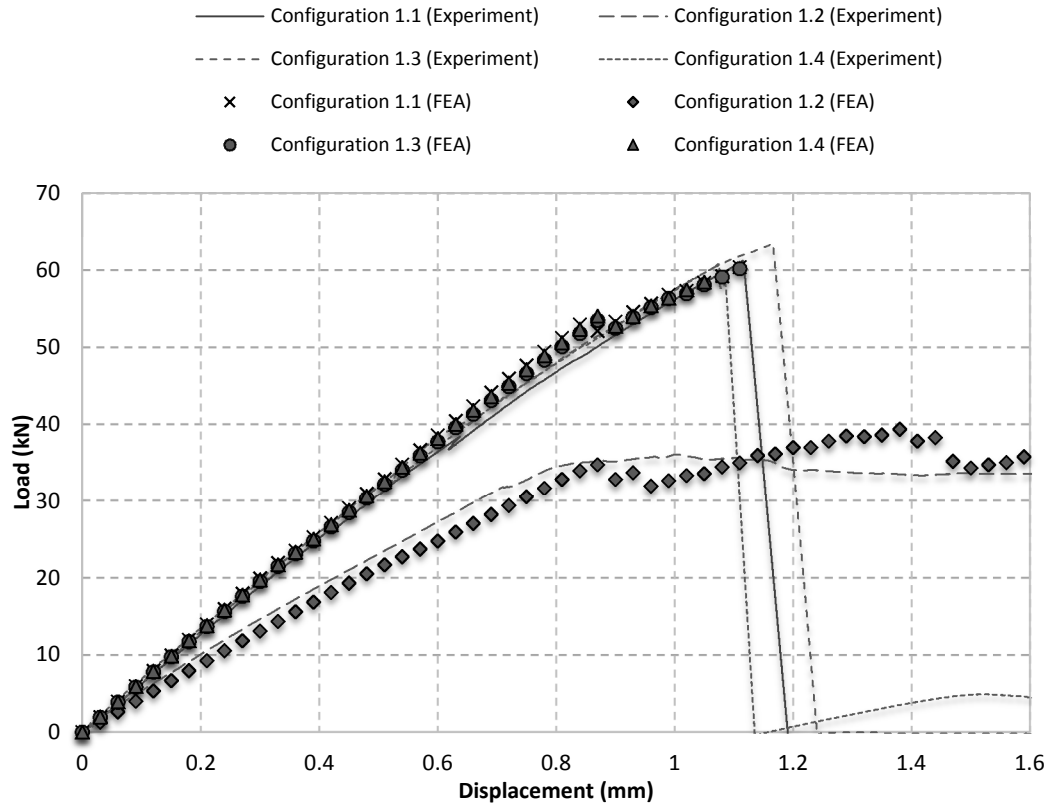


Figure 5.9 Load-displacement comparison between experimental and FEA for Configuration 1.1 - 1.4 with 1.5mm long spew; displacement represents the specimens total elongation for the given load

Modelling the pristine specimens containing a bondline with a 1.5mm long spew produced the load-displacement curves seen in Figure 5.9. Overall by modelling the adhesive spew fillets, more reliable strength predictions are possible.

5.3.1.1 Configuration 1.1

Focusing on Configuration 1.1, failure occurs at a peak load of 60.4kN with a remote strain of $14,500\mu\epsilon$ (1.11mm displacement). The primary mode of failure in this case is due to first ply failure at the tip of the tapered region. Here ‘first ply’ is defined as the initial ply

that is in contact with the bondline in the specimen; hence each bondline can have two respective ‘first plies’. This failure matches the experimental whereby adherend failure occurred near the tapered region. Figure 5.10 shows the shear and normal stress distribution in the bonded Configuration 1.1. The adhesive reached a maximum shear stress of 45.65 MPa located at the interface between the adhesive and adherend. Figure 5.10 peak shear and normal stress values occur at the ends of the bondline overlap. A marginal increase in normal stress occurs 5mm along the length of the overlap. This is where the 5mm long taper in the five ply thick adherends end. Overall by modelling the adhesive spew fillets in this case, a 16.1% reduction in shear stress occurs.

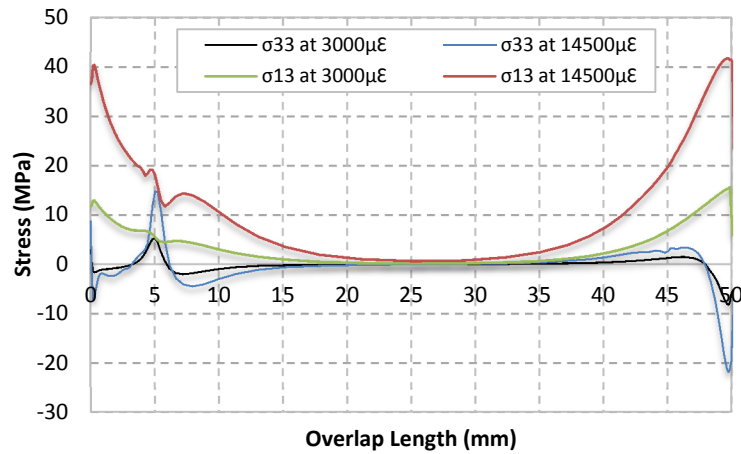


Figure 5.10 Adhesive stress distribution taken midway through the width of the specimen Configuration 1.1;
 σ_{33} - Normal Stress; σ_{13} - Shear Stress

5.3.1.2 Configuration 1.2

Configuration 1.2, containing six rivets failed through bearing failure. This is a slow mode of failure and thus preferable as it allows time for detection upon regular inspection intervals. The disadvantage is its lower load sharing capability. A peak load of approximately 34.1kN is reached followed by hole elongation, Figure 5.9.

From the load-displacement curve, the numerical model is able to accurately predict the load-displacement relationship obtained experimentally. Fibre failure begins to play a larger role in the progressive damage of the joint after a displacement of 0.87mm. This causes a redistribution of stresses and load within the joint region. Figure 5.11 shows the load share of the rivets. From the results it is clear that the outer fasteners (1 and 3, 4

and 6) play a larger role in the load sharing of the joint with the end fasteners (4 and 6) carrying the maximum load.

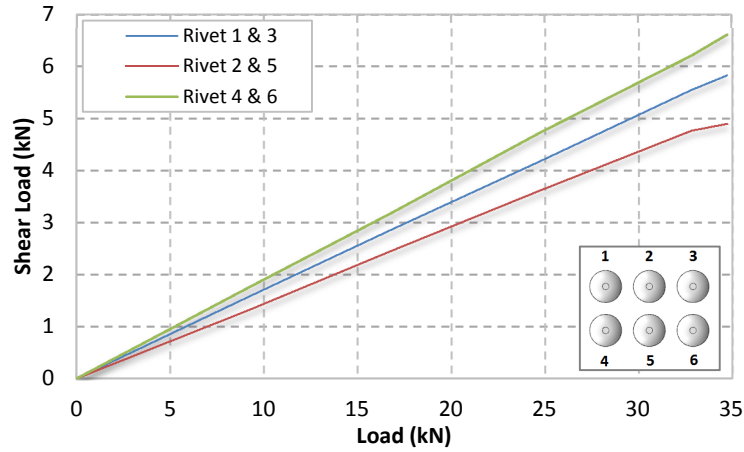


Figure 5.11 Rivet load distribution in Configuration 1.2

5.3.1.3 Configuration 1.3

The hybrid Configuration 1.3 reached a peak load of 57.1kN after displacement of 1.02mm without an adhesive spew, Figure 5.8. This is 10.0% lower than its experimental peak load. The sudden drop in load seen after a displacement of 0.87mm is primarily due to a sudden increase in matrix damage using the MCT progressive damage model [7]. The FEA results indicate a mixed mode failure as both the shear stress in the bond and tensile stress in the first ply exceed their ultimate stress values. Modelling the specimen with a spew fillet significantly reduced the peak shear stress at the end of the adhesive layer by 17.4%. Initial failure now occurs through first ply failure with a remote strain of 13,800 $\mu\epsilon$ (1.11mm displacement) and 60.2kN peak load.

From Figure 5.12, the stress distribution follows closely to Configuration 1.1. Peak stresses occur at the ends of the overlap however are marginally lower than Configuration 1.1 due to the clamping pressure provided by the rivets.

The presence of fasteners in Configuration 1.3 has very little influence on the joint behaviour when the bond is still intact, Figure 5.13. The ‘rivet load’ stands for the total load carried by all rivets in the joint. As expected, the rivets have minimal influence in carrying the load. As the applied load increases, there is a slight increase in the rivet load

share which reaches a peak value of 0.21%. The rivet load increases suddenly beyond a load of 50kN; this is expected to greatly increase as bondline cracks begin to initiate. In addition to this, the amount of load transferred can be controlled by carefully selecting the adherend thickness, adhesive thickness, overlap length, pitch distance and adhesive modulus [6, 35].

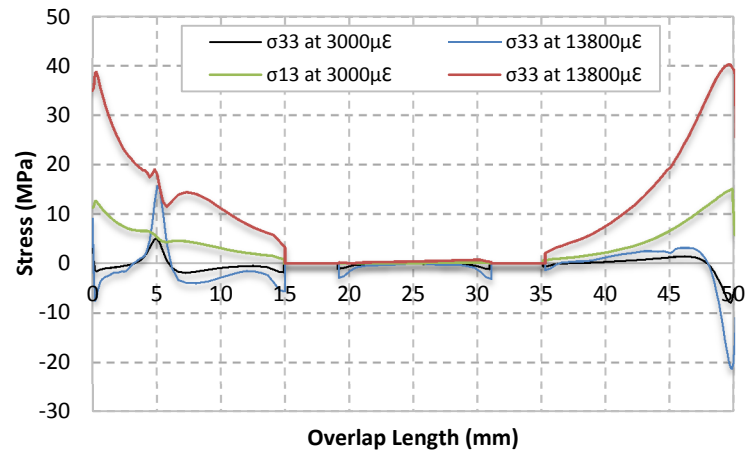


Figure 5.12 Adhesive stress distribution taken midway through the width of the specimen Configuration 1.3;
 σ_{33} - Normal Stress; σ_{13} - Shear Stress

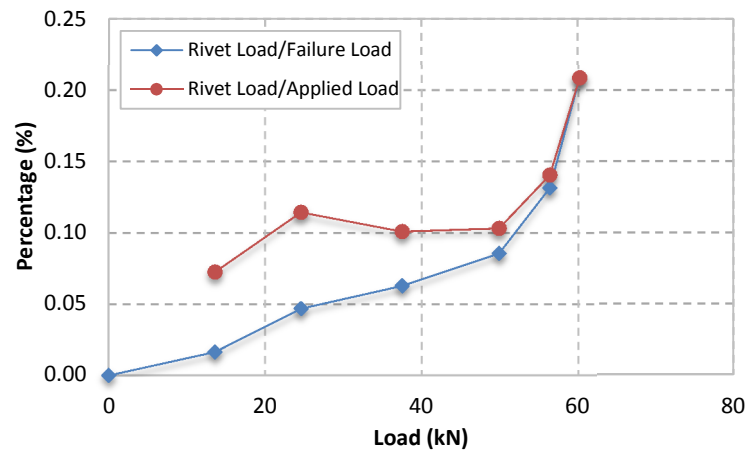


Figure 5.13 Rivet load carrying capability in Configuration 1.3

5.3.1.4 Configuration 1.4

Configuration 1.4 is the hybrid specimen containing three rivets arranged in a staggered array. This is to determine whether the clamping pressure provided by the rivets are adequate in maintaining a properly adhered bond.

It must be noted that since the curing conditions have changed in this case, the adhesive strength of the FM300-2K film adhesive will change due to cross-linking changes in the adhesive layer. The results presented here assume the bond strength of the adhesive is unaffected. Figure 5.9 shows a load-displacement behaviour which slightly under predicts the peak load share of the joint. First ply failure occurs near the tip of the tapered region, halfway across the width of the specimen. This is in very good agreement with the experimental results presented in Chapter 4 [146], which shows adherend failure in the central width area and adhesive failure towards the outer edges of the specimen.

Increasing the applied load in the joint increases the peak shear stress values at the ends of the adherends and maximum stress occurs at the end of the tapered regions. This is where crack initiation occurs. Figure 5.14 shows the stress distribution in the adhesive layer.

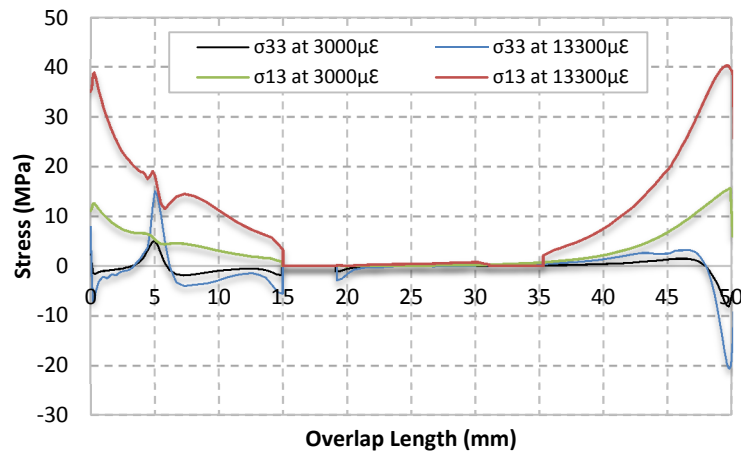


Figure 5.14 Adhesive stress distribution taken midway through the width of the specimen Configuration 1.4;
 σ_{33} - Normal Stress; σ_{13} - Shear Stress

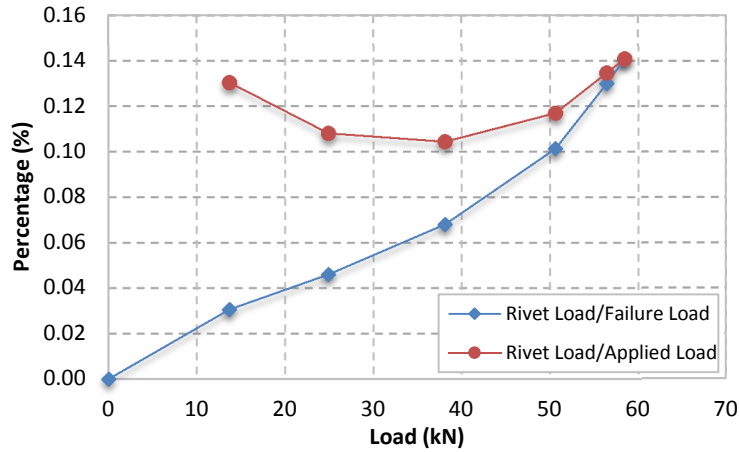


Figure 5.15 Rivet load carrying capability in Configuration 1.4

Similar to Configuration 1.3, the rivets play a minimal role in the joint structure when the bond is intact. Due to the presence of a single fastener in rivet row one (RR1), bondline cracking and defects arise at the corners of the bond region. This results in a corner wise peeling action. Comparing Figure 5.13 with Figure 5.15, Configuration 1.3 applies approximately twice the clamping force than Configuration 1.4. Hence, this shows fasteners play more of a role in the load share of a joint when the ratio between the adhesive area and fastener hole area (AFHR) decreases. i.e. Configuration 1.3 has an AFHR value of 35.3, and Configuration 1.4 has an AFHR of 70.6.

5.3.2 Defective Specimens (Configuration 1.5 - 1.8)

Specimen Configuration 1.5 - 1.8 are considered defective specimens. These specimens contain known defects such as initial bondline cracks or a weak bond achieved by under-curing the FM300-2K film adhesive at a reduced temperature and curing duration. The main role of producing such specimens is to understand whether or not they significantly affect the joint structure, particularly in a hybrid configuration. Such defects can result in various complexities due to altered bondline properties. Thus the main emphasis of such configurations is to understand the joint strength through experimental static and fatigue tests. The numerical and experimental load-displacement curves for specimens containing a 2mm long initial crack are shown in Figure 5.16.

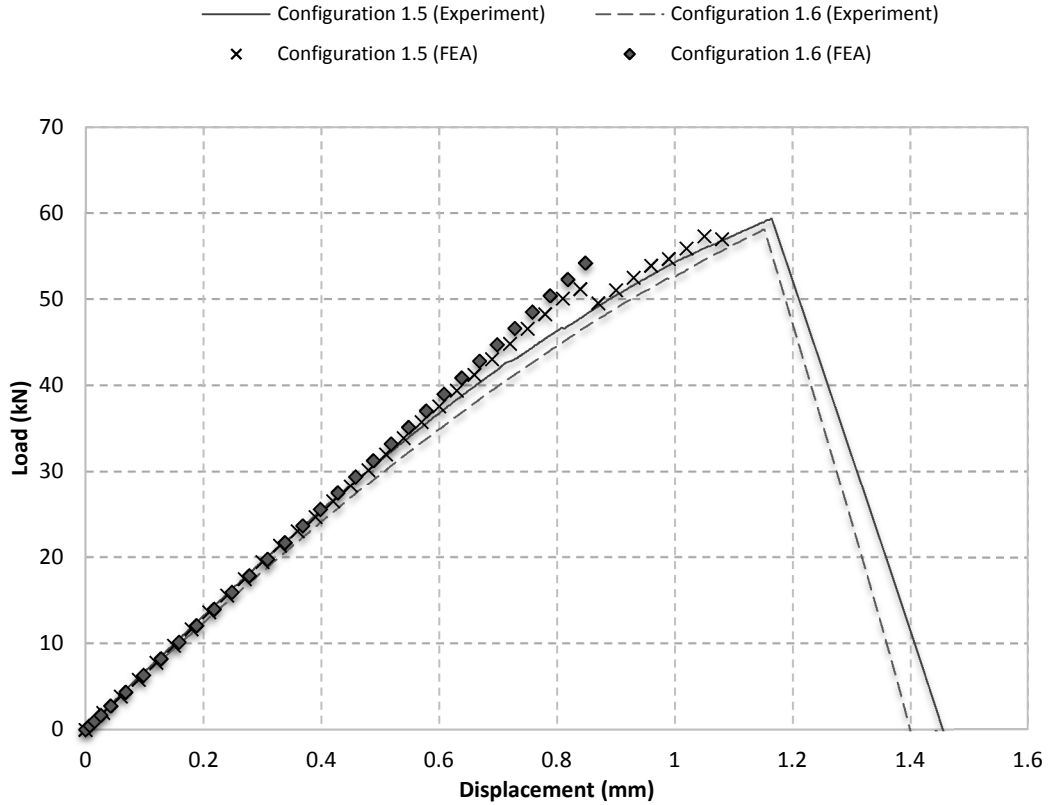


Figure 5.16 Load-displacement comparison between experimental and FEA for Configuration 1.5 & 1.6; displacement represents the specimens total elongation for the given load

5.3.2.1 Configuration 1.5

The initial 2mm long crack in Configuration 1.5 spanned the entire width of the specimen. Due to non-symmetry in both bondlines, only half of the entire specimen is modelled in Abaqus. Compared to the previous models discussed, the finite element model for Configuration 1.5 achieves a peak load of 57.0kN. Initial failure occurs through first ply failure, i.e. first ply of central adherend failed immediately aft of the 2mm crack. The experimental results highlight that beyond a displacement of 0.7mm, the load gradually decreases in contrast to a fairly linear trend in previous configurations containing a bondline.

From Figure 5.17, the shear stress distribution reaches a peak value of approximately 26.3MPa just prior to failure. The normal stress distribution shows a small increase in stress 5mm from the edge of the tapered adherend. This is due to the ply drop off and

hence sudden change in material stiffness. Overall the results presented in this case are conservative in predicting joint failure. Due to plastic deformation in the adhesive layer, joint stiffness reduces at the peak load limits.

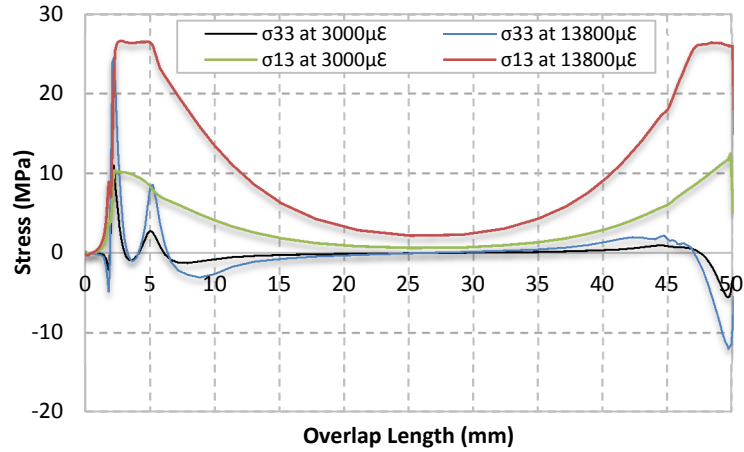


Figure 5.17 Adhesive stress distribution taken midway through the width of the specimen Configuration 1.5;
 σ_{33} - Normal Stress; σ_{13} - Shear Stress

5.3.2.2 Configuration 1.6

Configuration 1.6 contained a 2mm initial crack between the central adherend and adhesive layer. Six rivets are placed in a square array to produce the hybrid configuration. Catastrophic failure occurred through first ply failure. The results once again are conservative compared to the experimental peak load of 58.0kN.

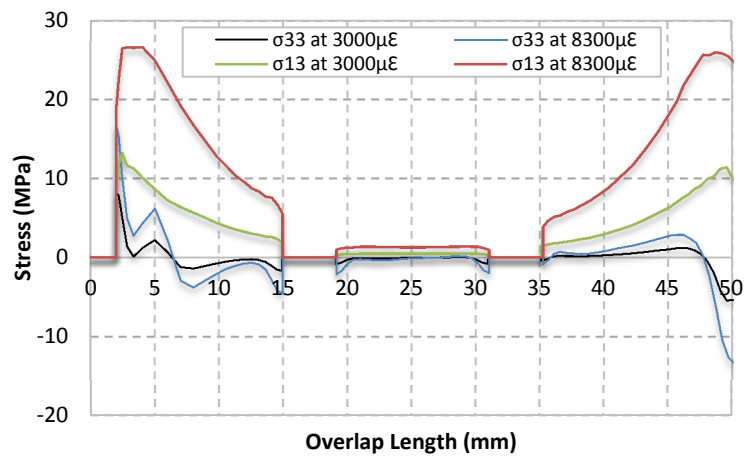


Figure 5.18 Adhesive stress distribution taken midway through the width of the specimen Configuration 1.6;
 σ_{33} - Normal Stress; σ_{13} - Shear Stress

From Figure 5.18, there is a peak shear stress of 26.6MPa following the crack front prior to catastrophic failure. Comparing the numerical load displacement graphs, Configuration 1.5 achieves a higher peak load than Configuration 1.6 which is also reflected in the experimental results discussed in Chapter 4 [146].

5.3.2.3 Configuration 1.7 & 1.8

These configurations contain what is called a ‘defective semi-cured’ adhesive as it is cured at 90°C for 60 minutes as opposed to 121°C for 90 minutes , minimising the peak load share of the joint. From the experimental results conducted in Chapter 4 [146], a peak load of approximately 17.3kN is achieved by a bonded joint due to its reduced fracture energy.

Although a semi-cured adhesive may represent a defective joint, there are numerous other ways to also define a ‘defect’ in a structure. The presence of an initial crack and the use of expired adhesives are just some of many different methods of defining such a ‘defect’. As a result modelling each and every type of joint will be a tedious task with some results already self-evident. Specimen Configuration 1.7 and 1.8 have only been produced and tested to demonstrate one of many examples of a bondline ‘defect’. In this case the ‘defective semi-cured’ adhesive is quite detrimental for a bonded joint configuration [146]. By using a ‘hybrid’ configuration the likelihood of sudden catastrophic failure is minimised through the added residual strength of fasteners.

From Figure 5.19, the combination of FEA results from Configuration 1.2 (rivet only) and Configuration 1.3 (perfect bond) show a type of load-displacement behaviour similar to Configuration 1.8 experimental results [146]. Adhesive failure occurs at a maximum shear stress (σ_{13}) of 19.06MPa with a remote strain of 3300 $\mu\epsilon$ at a load of 21.45kN. Following this, the rivets carry the remaining load in the joint structure resulting in bearing failure.

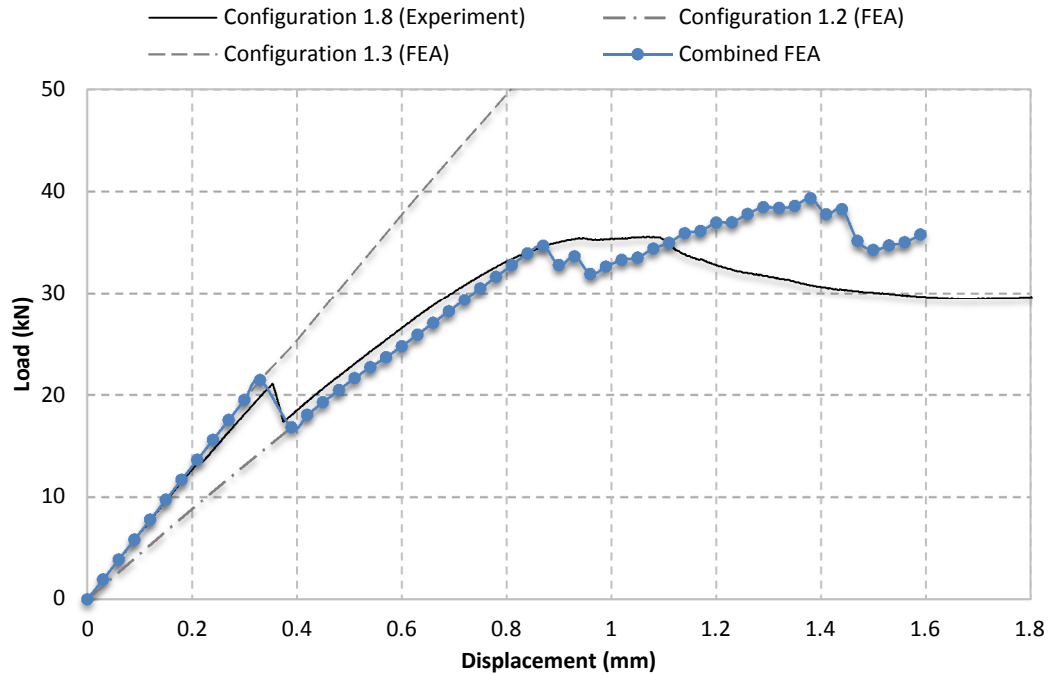


Figure 5.19 Load-displacement comparison between experimental and FEA for Configuration 1.8; a combination of Configuration 1.2 and 1.3 FEA results

5.3.3 Joint Configuration Summary

Overall, from the eight different joint configurations experimentally tested and modelled using Abaqus CAE, the use of the micromechanical MCT progressive failure model and non-linear adhesive properties has resulted in a close agreement between experimental and numerical results. Through this investigation, it has been found that modelling minor details such as the adhesive spew present at the ends of the bondline are critical in achieving reliable results. Stress is reduced around the vicinity of the adhesive spew, therefore marginally increasing the load carried by the bonded and hybrid joint structures. The results are reflected in Figure 5.9 compared to Figure 5.8.

Specimen configurations containing an adhesive has the highest peak normal and shear stress values at the ends of the overlap. This is the region where damage initiates from. Comparing the ‘pristine’ specimens (Configuration 1.1 - 1.4) show that there are no real advantages between bonded and hybrid specimens under static testing. All of which achieve relatively the same stiffness and strength. A purely riveted specimen however has a reduced stiffness which fails over a large period of time due to hole elongation. Overall

the peak loads achieved by Configuration 1.1 - 1.4 using FEA are 60.2kN, 34.1kN, 60.4kN and 58.4kN respectively.

Configuration 1.5 and 1.6 contained the 2mm initial crack. These specimens had a lower stiffness than its pristine counterparts. Configuration 1.7 and 1.8 contained the defective semi-cured adhesive. The numerical results showed that by utilising aspects of the load-displacement graph for Configuration 1.2 and 1.3, an upper and lower bound limit can be set for these defects. This may be used as a quick method of determining the strength limitations of such a joint. Overall the findings here conclude that fasteners play a vital role in preventing catastrophic failure provided the adhesive has a shear strength less than the bearing strength of the adherends. By carefully selecting the adhesive, adherend and fasteners used, the mode in which these joints fail can be controlled.

5.4 Numerical Analysis on the Fatigue of Bonded and Hybrid Joints

Although a number of authors [6, 38, 134, 149-152] have investigated hybrid joint structures, very little insight has been given as to why these joint structures have superior fatigue resistance over their bonded joint counterparts. This is a critical question that needs to be answered in the Aerospace Industry. The drilling of fastener holes in fibrous materials has been a concern as it leads to (1) peeling of higher plies at the entry of the hole, (2) fibre wrenching and resin degradation on the wall of the hole and (3) delamination on the last plies of the laminate [38, 134, 149-152]. This may result in fatigue crack initiation and reduced strength [134]. However the holes for fasteners in a hybrid joint configuration help slow down crack propagation after the initial failure of the adhesive [34] This will result in improved fatigue life compared to bonded joints [6, 35] and ensure structural integrity even after complete adhesive failure [150]. This work is conducted to further validate these points but in addition provide crucial information on the effects of fastener positioning and layout on fatigue performance which is not widely seen in literature. Without fully understanding how positioning fasteners in a bonded joint can improve fatigue resistance, less efficient joints or even weaker joints may emerge.

Results previously discussed in Chapter 4 and published by Chowdhury et al. [146] and Maofeng Fu et al. [34] have shown hybrid joints have a longer fatigue life compared to bonded joints. Although under static cases there may not be any significant advantage

between the two, hybrid joints have shown a 45% and 20% increase in fatigue resistance compared to a purely fastened and a purely bonded joint respectively [146].

Finite element analysis using Abaqus CAE is used to model bonded and hybrid double lap joints. In these joints, significant stresses are present at the ends of the overlap resulting in ‘bondline cracking’. The repeated loading and unloading of the joint eventually results in crack initiation and over time this crack will grow across the length of the overlap. By modelling the bonded and hybrid joints with initial cracks of various lengths, the effects of the fasteners (rivets) are found.

5.4.1 SERR Model Setup

As discussed previously in Chapter 2, the strain energy release rate (SERR) represents the energy available for crack growth. Under fatigue cases due to the constant loading and unloading, there is also a constant release of energy. Hence calculating the SERR for bonded and hybrid joint structures will provide an indication of its fatigue performance. According to Paris’s Crack Growth model, the SERR is proportional to the crack growth rate ‘ da/dN ’. Thus the higher the SERR, the higher the rate of crack growth provided the critical SERR value has been exceeded.

There are three methods by which this can be calculated in Abaqus; the Contour-Integral method, VCCT and XFEM. Several trials of each method were conducted and out of the three methods, the Contour-Integral approach is the easiest to implement in 3D models. An initial crack is position midway through the thickness of the 0.3mm thick FM300-2K film adhesive and is spread the entire width of the specimen. Specimen setup is similar to that mentioned in Section 5.2.

Seven different crack lengths (2mm, 9mm, 14mm, 20mm, 25mm, 30mm, and 36mm) are positioned in the bond region. The nodes positioned aft of the crack tip are tied together using node to node contact. Seeding is implemented in the mesh and refined around the crack tip with a minimum element size of 0.01mm (where bondline thickness is 0.3mm). Average SERR data is taken about the width of the specimens (along the crack front). The individual Mode I and Mode II SERR (assuming Mode III is negligible) are derived through post-processing the data using the displacement field method [116]. Figure 5.20 summarises the SERR results across four specimen geometries.

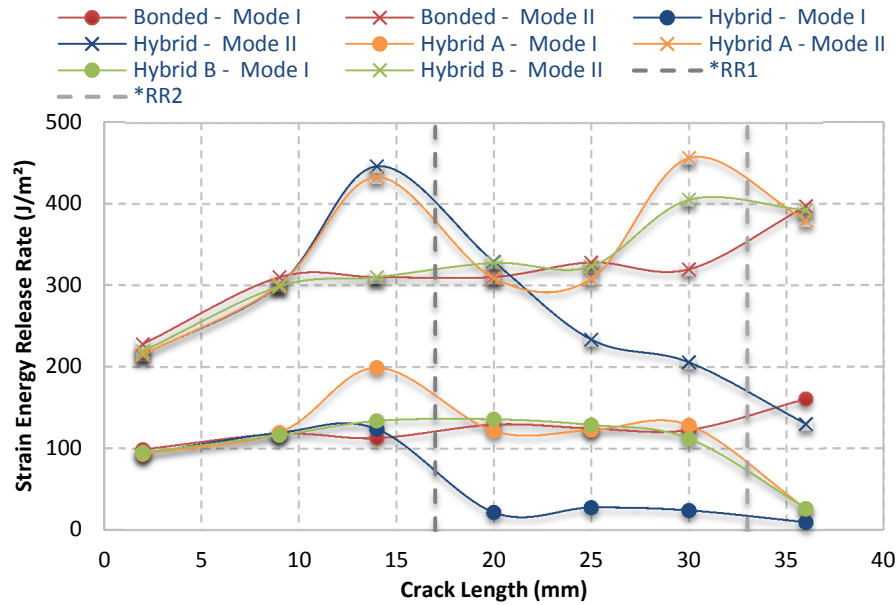


Figure 5.20 Available average energy for crack growth at different crack lengths subjected to a 3000 μ E displacement for a Bonded, Hybrid, Hybrid A (Fasteners in row 1 removed) and Hybrid B (Fasteners and Holes in row 1 removed) Configuration; *Applicable to hybrid joints only; (RR1 – Rivet Row One, RR2 – Rivet Row Two)

5.4.2 Comparison of Bonded and Hybrid Specimens Containing Two Rows of Rivets

From Figure 5.20, a bonded configuration has almost a constant SERR for an increasing crack length. Initially when the crack length is small (<10 mm) there is an increase in SERR, this is due to the higher peeling stresses present at the end of the adherend in addition to the tapering which allows the adherends to separate easily. When the crack length is >30 mm, there is another increase in SERR as a crack can now easily propagate due to the reduced bond area. In all cases the Mode II SERR values are higher than the Mode I SERR values as the joint acts in shear.

For the hybrid configurations, when the crack length is <9 mm the Mode I SERR values are smaller than a bonded joint configuration. Hence, crack initiation occurs at a later point in time for hybrid joints compared to bonded joints. As crack length increases, Mode I and Mode II SERR values decrease sharply as it passes Rivet Row 1 (RR1). This is due to the clamping pressure provided by the head of the rivets and also due to the added bearing strength from the shaft of the rivets. Furthermore, the SERR for every point after

the first row of rivets is much lower than that of a bonded joint. Hence, it is this reduced value which results in a lower crack growth rate and improved durability.

In the hybrid configuration, when the crack length approaches 25mm, the SERR no longer decreases as sharply. Upon closer look at the FEA, the tensile load causes a peeling action between the two rows of rivets, Figure 5.21

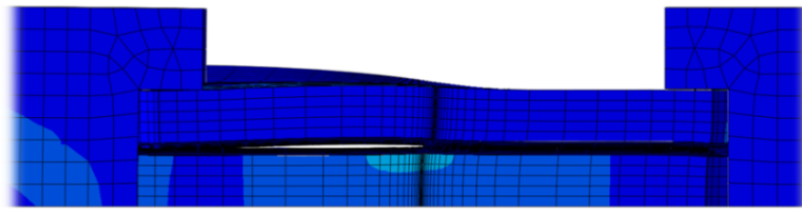


Figure 5.21 Separation of adherends with a 25mm long crack (5x deformation scale)

This ‘opening action’ assists in initially increasing the crack growth immediately aft of a rivet. Further growth moves the crack front towards the second row of rivets which provides additional clamping pressure, reducing the SERR once again.

5.4.3 Hybrid A - Effect on Strain Energy Release Rate by Removing the First Row of Rivets

The first row of rivets in a hybrid joint configuration results in a sudden increase in the SERR prior to reaching RR1. To further understand the cause, the models are modified to contain the following:

- Hybrid A – Hybrid configuration with the first row of rivets (RR1) removed but still containing all six fastener holes, Figure 5.22
- Hybrid B – Hybrid configuration with the first row of rivets (RR1) and fastener holes removed, Figure 5.23

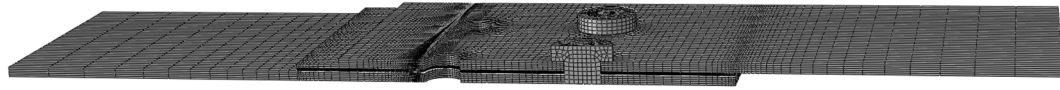


Figure 5.22 Schematic of 'Hybrid A' with the first row of rivets removed and all fastener holes still present

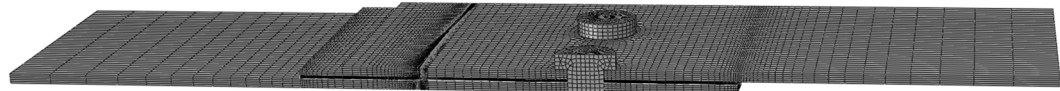


Figure 5.23 Schematic of 'Hybrid B' with the first row of rivets and fastener holes removed

Hybrid A assesses the influence of the fastener holes. Figure 5.24 and Figure 5.25 contains the SERR results taken midway through the width of the specimen as well as averaged across the width of the specimen respectively. The behaviour is quite similar to the standard hybrid joint configuration previously discussed. Both figures show there is a rapid increase in SERR prior to reaching the first row of holes. This indicates that the sudden increase in SERR is not only associated with the presence of rivets but in fact associated with the presence of fastener holes which are known to be regions of high stress concentration [153].

The peak SERR achieved by Hybrid A are slightly higher than the standard hybrid joint configuration previously discussed in this chapter. There is a 38% reduction in the average total SERR if rivets are present in the first row location, Figure 5.25. These are important in reducing the peeling stresses which in turn reduce the crack propagation rate for larger crack lengths. The key underlying difference lies when approaching the second row of rivets.

Figure 5.24, containing SERR values taken midway through the width of the specimen clearly shows that empty fastener holes negatively affect the fatigue performance of a hybrid configuration. This thereby once again highlights the criticality of first row fasteners. In this instance, the Mode II SERR are more critical than the Mode I SERR. The presence of empty fastener holes results in greater localised displacement leading to an increase in Mode I and II SERR.

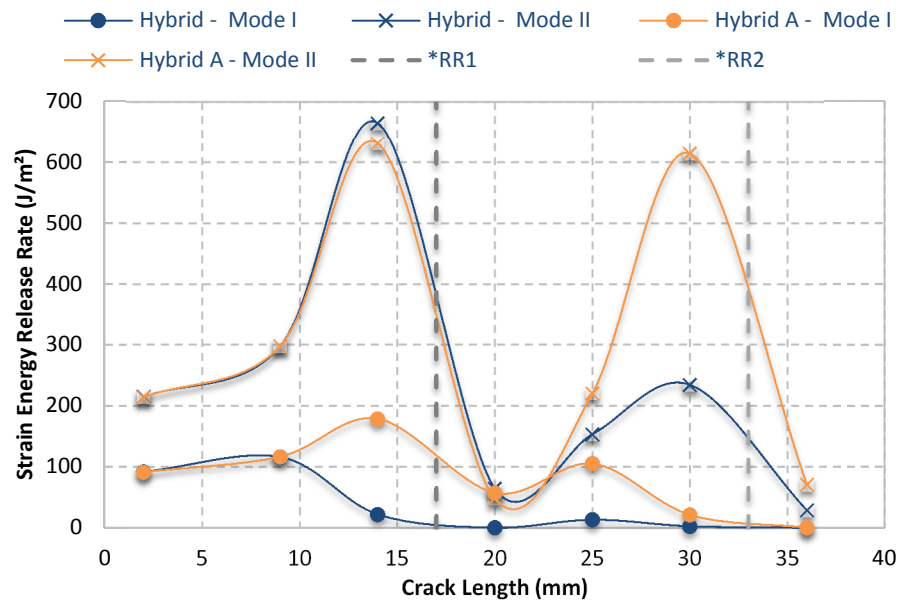


Figure 5.24 Available energy for crack growth taken mid-width for different crack lengths subjected to a 3000 $\mu\epsilon$ displacement for a Hybrid and a Hybrid A Configuration; *Applicable to hybrid joints only (RR1 – Rivet Row One, RR2 – Rivet Row Two)

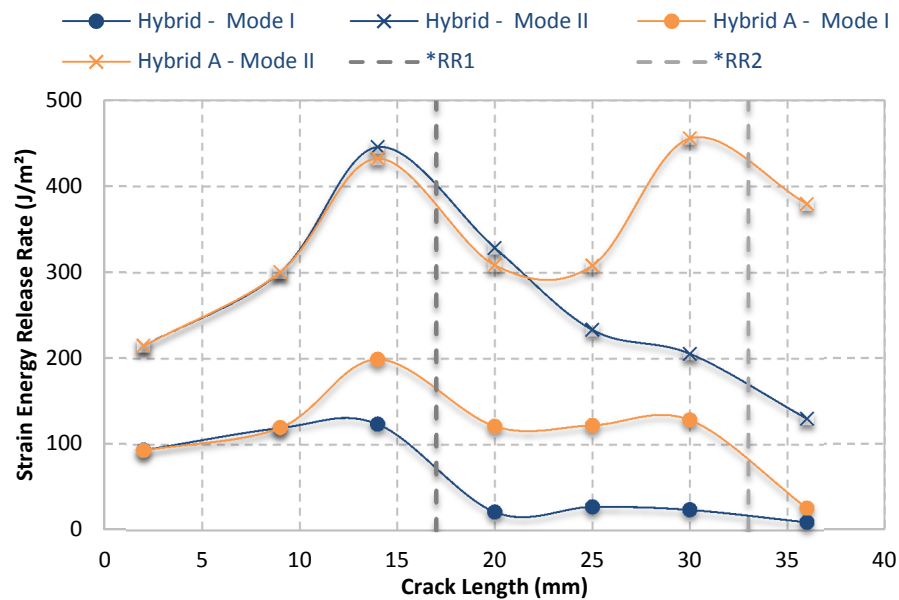


Figure 5.25 Available average energy for crack growth for different crack lengths subjected to a 3000 $\mu\epsilon$ displacement for a Hybrid and a Hybrid A Configuration; *Applicable to hybrid joints only (RR1 – Rivet Row One, RR2 – Rivet Row Two)

5.4.4 Hybrid B - Effect on Strain Energy Release Rate by Removing the First Row of Fasteners Holes and Rivets

Hybrid B is modelled in Abaqus to see the influence of second row rivets only. This is the same as shifting the first row of rivets from 17mm to 33mm along the overlap length. Figure 5.23 shows a schematic of the joint type.

Unlike the previous Hybrid A Configuration, the absence of fastener holes in row one results in a SERR rate behaviour very similar to that of a bonded joint configuration with the advantage of achieving a marginally lower SERR for small cracks as seen in Figure 5.26 and Figure 5.27. This highlights crack lengths less than 25mm are not influenced by the rivets positioned 33mm away from the tapered region. As soon as the crack approaches the second row rivets (RR2), an overall increase in SERR is observed. Under Mode II, a peak value of 588 J/m² and 405 J/m² occurs in Figure 5.26 and Figure 5.27 respectively. These values decline as the crack progresses past each line of rivets; once again highlighting the key advantage of these fasteners in reducing crack growth rate and thereby improving fatigue resistance.

Comparing the two figures also show that crack growth rate is higher around the vicinity of fastener holes. Although there is no significant advantage between a Hybrid B configuration and a purely bonded joint, the results do in fact suggest it is important to have fasteners positioned closer to both ends of the bondline than having fasteners positioned in the central regions.

Overall, the results here clearly show the advantages of using a hybrid joint configuration compared to a bonded joint. It is more advantageous to place fasteners closer to the ends of the overlap to arrest sudden crack propagation and improve fatigue resistance. However there is a limit as to how close the fasteners are placed to the ends, as this is where high stress concentrations are present in the bondline. This will reduce the load carried by the fasteners and will result in shear out failure [34, 154]. Thus the stress behaviour of the joint must first be analysed followed by placing fasteners soon after the high stress concentration regions, (e.g. Figure 5.12).

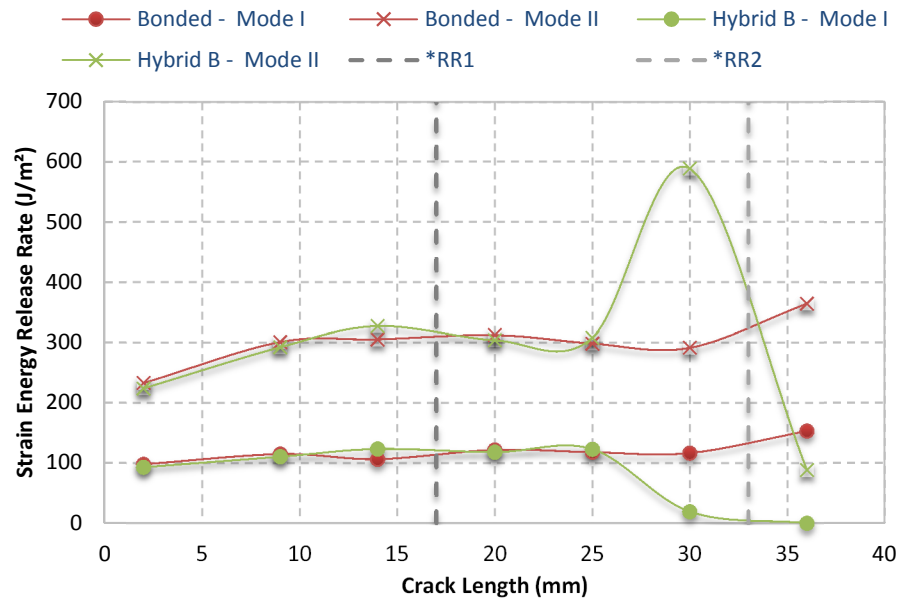


Figure 5.26 Available energy for crack growth taken mid-width for different crack lengths subjected to a 3000 $\mu\epsilon$ displacement for a Bonded and a Hybrid B Configuration; *Applicable to hybrid joints only (RR1 – Rivet Row One, RR2 – Rivet Row Two)

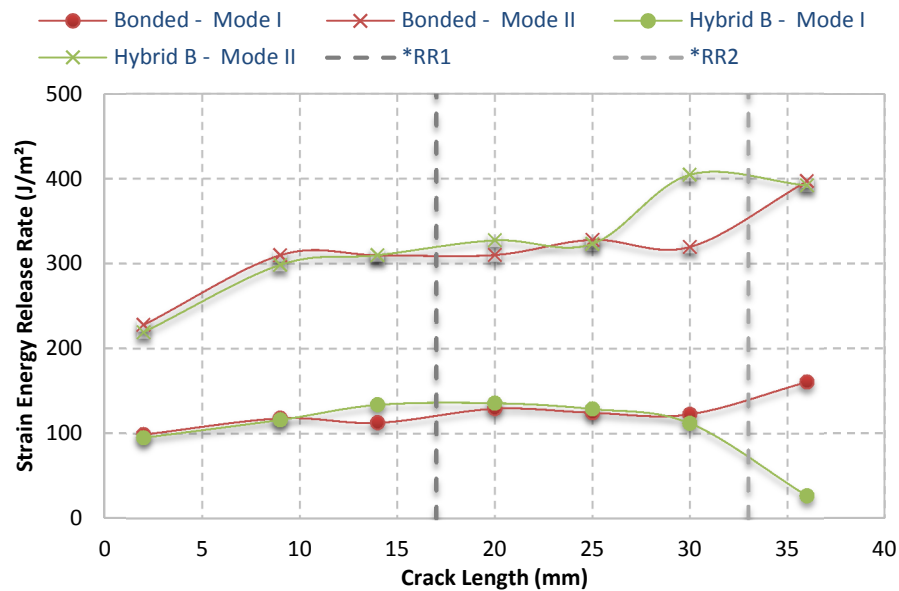


Figure 5.27 Available average energy for crack growth for different crack lengths subjected to a 3000 $\mu\epsilon$ displacement for a Bonded and a Hybrid B Configuration; *Applicable to hybrid joints only (RR1 – Rivet Row One, RR2 – Rivet Row Two)

5.5 Chapter Summary

The use of the micromechanical MCT progressive failure model and the nonlinear adhesive material properties enabled the comparison of fastened, bonded and hybrid joint structures. Both fastened and hybrid configurations utilised detailed three-dimensional multi-rivet arrangements. Overall the numerical models simulated using Abaqus CAE were able to reliably predict joint strength. The greatest accuracy was achieved by modelling the adhesive spew fillets present at the ends of specimens containing a bondline. The results conclude that under static test conditions at room temperature there are no real advantages of hybrid joints over properly manufactured bonded joints. Findings show that the higher the load carried by the joint, the larger the role played by the fasteners in a hybrid configuration; the overall significance of this is however almost negligible.

In addition, previously very little insight using FEA has been given as to why hybrid joint structures have superior resistance over their bonded joint counterparts. However through this work, it has been shown the SERR method using FEA provides an effective way of comparing their fatigue performance and may be used as a tool to optimise fastener placement to enhance hybrid joint durability before manufacture. Results here show the presence of fasteners in a hybrid configuration significantly reduce the average Mode I and II SERR by more than 83% and 27% respectively compared to a purely bonded joint; provided the crack has surpassed the initial row of rivets. The additional clamping pressure provided by the rivets also helps in reducing this value. Further investigating the effects of fastened, bonded and hybrid joint configuration for thicker joint structures such as step lap joints are discussed in the following chapter. Analysing these joints through finite element models will assist in primary composite joint repair certification.

6

Stage 2-Experimental Testing

6.1 Introduction

The emergence of composite materials in the construction of aircrafts has resulted in the need for improved damage growth predictions and effective/ efficient repair techniques for damaged structures. The damage mechanisms in composites differ significantly than those in metals and hence further testing and analysis are required to achieve optimal structural efficiency.

Chapter 4 and 5 investigated the effects of joining thin composite laminates together in a double lap joint configuration [146, 155]. Three fundamental joint structures were looked at – mechanically fastening, bonding and the combination of the two called ‘hybrid’ joints. Results revealed that under static test conditions, there are no significant differences in joint strength between a bonded and hybrid joint; it was during fatigue test cases where hybrid joints showed the greatest durability followed by bonded joints and then fastened joints. This chapter now focuses on the repair of thicker composite structures. In this study it is assumed a flush joint repair is required. Scarf and step lap joints are two common joints used in the repair of thick structures as they are necessary for restoring original stiffness and nearly original strength [61]. Hart-Smith suggested the use of stepped

lap joints or scarf joints for thicker composite adherends as they are more efficient joining methods and reduce adhesive peel stresses induced at the ends of the overlap joint [5].

From the available literature, there is limited experimental data on the static and fatigue performance of flush joints made from composite materials. As previously discussed in Chapter 2, Kim et al. [156] evaluated the fatigue performance of adhesively-bonded composite step lap joints. The number of steps, joint length and edge angle of the adherends were investigated. They concluded that increasing the number of steps and edge angle has the greatest effect in improving bond strength and fatigue. Mollenhauer et al. [61] analysed scarf and step lap joint repairs in composite laminates. They tested one inch wide specimens with a total of eight steps each being two plies thick. However their focus was on comparing experimental strain data to numerical simulations. Blaricum et al. and Seneviratne et al. [9, 65] looked at conducting efficient joints on an F/A-18 wing root using step lap joints. Graphite/Epoxy laminates were bonded to Titanium 6Al-4V and assessed for compressive strength subjected to impact damage. A total of 18 symmetrical steps were used for the repair which surrounded the inner titanium parent structure. This is a key example of a bonded primary structure certified and deployed on air vehicles.

Adhesively bonded joints are generally structurally more efficient than mechanically fastened joints as they perform better in distributing loads, eliminating a majority of high stress concentration problems seen in bolted joints [146, 155]. However, process control during repair applications determines the quality of bonded joints. An improper process can result in weak bonds which may not be detected by non-destructive inspection (NDI). The detrimental effect of some improper surface treatment may not even manifest in a significant reduction of the initial static strength of the bond but in an adverse impact on the durability of the adhesive bond at service temperature and moisture environment and/or under fatigue loading.

The combination of mechanical fasteners and bonding has been employed to safeguard against defects in the adhesive layer which may cause premature or catastrophic failure [5]. Once the bond has failed the fasteners begin to carry the remaining load in the joint. It is this safety factor which shows promise towards the certification of these joints in aircraft structures.

In general, the equations that govern load distribution in double lap joints may be applied to step lap joints however there is a highly non-uniform shear stress distribution in the

adhesive, with load transfer associated at the ends of each step [5]. The general criteria to follow are outlined in [61, 64]:

- End steps should not be too thick or too long in order to ensure the steps do not become overloaded greatly compared to the remaining steps
- Increasing the bond area for the same number of steps is not as effective as increasing the number of steps

Overall a large amount of research has focused on the development of numerical models and parametric studies. However there is very limited work on experimental investigations of hybrid joint repairs in a scarf and/or step lap joint configuration. These repairs are typical when it comes to flush joint requirements and hence understanding the static and fatigue performance of these joints is vital. The work discussed in this chapter aims at qualitatively understanding step lap joint repair for the three fundamental joints (bonded, bolted and hybrid), characterised as ‘thick’ joint structures. Through this work, better understanding in effective and efficient repair techniques for composite structures is gained which highlights an important composite repair design that can meet certification requirements.

6.2 Experimental Setup

For the step lap joint design, a preliminary parametric study was conducted in Abaqus CAE to determine the stress distribution and joint strength in three typical step lap joint geometries. Figure 6.1 shows the three geometries considered.

The number of steps, ply orientation and thickness was varied in all three geometries. The most uniform stress distribution was achieved by the ‘outer symmetric step lap joint’ shown in Figure 6.1(a). Although the geometry presents advantages, it is typically used in the manufacturing stage of a component. In very few cases it may be used in repair which is not ideal as it requires complete disassembly of the part. Likewise, the ‘symmetric flush step lap joint’, Figure 6.1(b) also presents advantages due to symmetry which reduces out of plane bending but once again this is a difficult joint repair to conduct in airframes. Thus

the ‘asymmetric flush step lap joint’ is used in this study, Figure 6.1(c). This stepped geometry allows easy repair as only one side of the component needs to be accessible. This is an important point to consider due to the complex structural configurations found in various airframes.

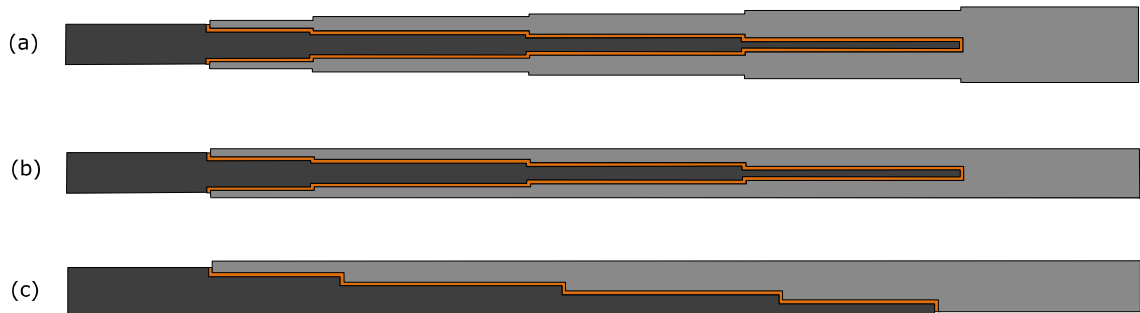


Figure 6.1 Step lap joint geometries considered in parametric study; (a) symmetric outer step lap joint; (b) symmetric flush step lap joint; (c) asymmetric flush step lap joint

The final results showed that increasing the number of steps initially increased the joint strength which eventually reached a limit. Increasing adherend thickness improves peak load carried by the joint/repair but this is dependent on the thickness of the repaired structure. Minimising the step height has the advantage of reducing peak stresses at the ends of each step. Overall, there a number of factors that need consideration, further complexities arise when considering hybrid configurations. Hence, in order to reduce the number of geometric variables, the following parameters were kept fixed:

- Specimens are 24 plies thick (5.5mm thick)
- Specimens have five steps
- Specimens are one inch wide
- Fastened and hybrid specimens have bolts placed central of each step

Based on the parametric study, a step lap joint with four ply thick steps with outer and inner steps 15mm and 20mm long respectively was used, Figure 3.7. Bolted, bonded and hybrid configurations are manufactured based on the optimised step design from the parametric study.

The ten specimen configurations considered in the study is defined in Table 3.6 and Table 6.1. All specimens were machined, surface prepped and assembled according to the procedures outlined in Chapter 3 with a ply orientation of $[(0/90)/(45/-45)/(45/-45)/(0/90)]_6$.

Table 6.1 Number of specimens static and fatigue tested in Stage 2

Bondline Condition	Specimen	Joint Type	No. Bolts	Curing Pressure (psi)	No. Specimens	
					Static	Fatigue
Pristine	Configuration 2.1	Bonded	n/a	40.0	3	2
	Configuration 2.2	Bolted	5	n/a	3	2
	Configuration 2.3	Hybrid	5	40.0	3	1
	Configuration 2.4	Hybrid	3	40.0	3	2
Defective - 2mm Crack	Configuration 2.5	Bonded	n/a	40.0	3	2
	Configuration 2.6	Hybrid	5	40.0	3	2
	Configuration 2.7	Hybrid	3	40.0	3	1
*Defective - Semi-cured Bond	Configuration 2.8	Bonded	n/a	40.0	2	1
	Configuration 2.9	Hybrid	5	40.0	3	1
	Configuration 2.10	Hybrid	3	40.0	2	1

* Cured at 90°C for 60 minutes in an autoclave

All pristine specimens were static tested followed by fatigue testing. Configuration 2.8 - 2.10 contained the same semi-cured FM300-2K film adhesive layer used in the defective double lap joint configurations discussed in Chapter 4 and 5. This was achieved by curing the specimens at 90°C for 60 minutes in an autoclave. Tabs were later bonded to the specimens before testing to prevent the clamps from damaging the composite adherend and prevent slippage at high loads. The bolted and hybrid specimens contained countersunk fasteners torqued to 8.0Nm.

In some cases, non-destructive inspection (NDI) using an Ultrasonic A-Scanner, Thermal Camera as well as using a Distributed Optical Fibre Sensor (DOFS) was employed to detect damage during the testing period. Further details are provided on these results later in the chapter.

Figure 6.2 to Figure 6.5 shows a set of pristine specimen configurations ready for testing.



Figure 6.2 Configuration 2.1 - bonded step lap joint specimen



Figure 6.3 Configuration 2.2 - Bolted step lap joint configuration with five fasteners

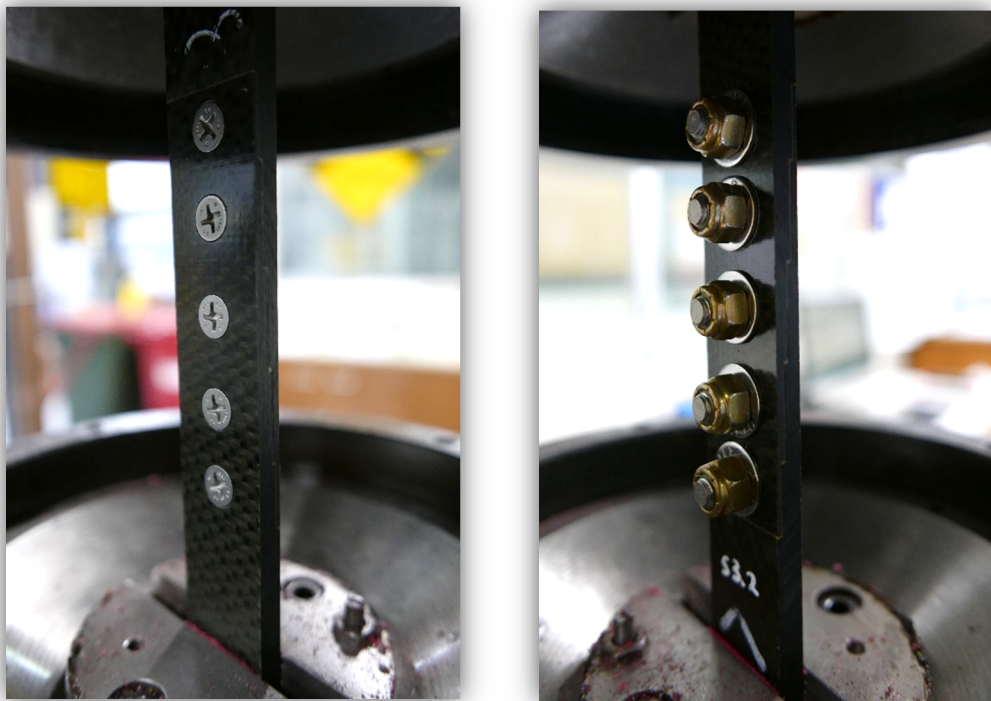


Figure 6.4 Configuration 2.3 - hybrid step lap joint with five fasteners

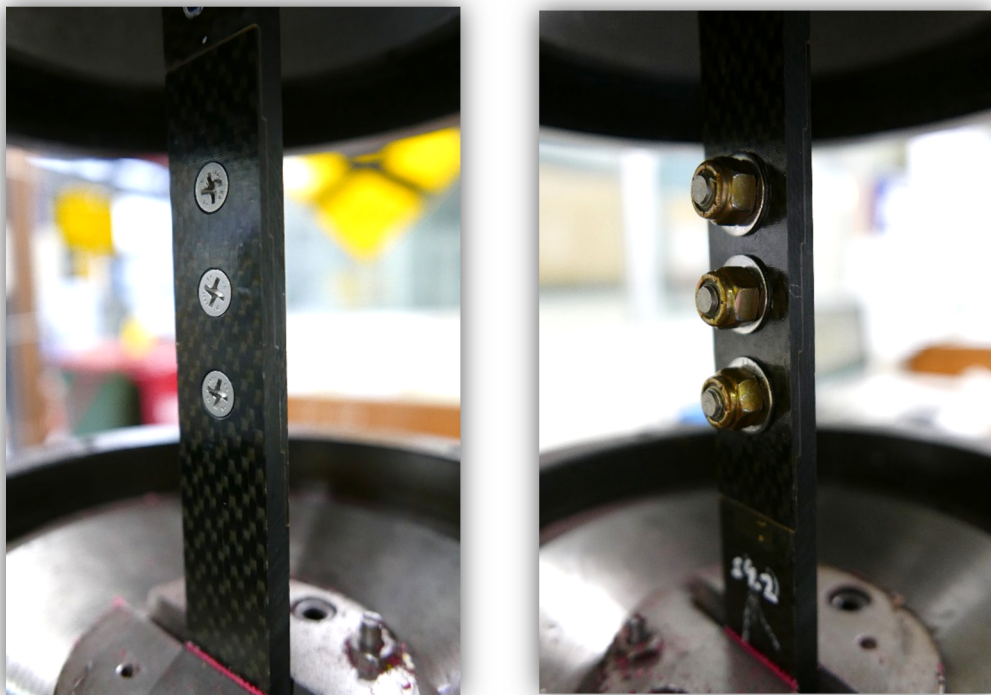


Figure 6.5 Configuration 2.4 - hybrid step lap joint with three fasteners

6.3 Testing Procedure

The same Instron 1342 machine with a 100kN load cell is used for static and fatigue testing all ten specimen configurations similar to the previous double lap joint configurations considered. Static tests were performed on all specimen configurations at a rate of 1mm/min with axial load and displacement measurements recorded until catastrophic failure.

Fatigue tests were carried out on the same machine at a frequency of 5Hz with a sinusoidal waveform. A tension-tension block loading regime similar to tests carried out in Chapter 4 was used in this stage of the project starting at the 1000 $\mu\epsilon$ loading regime. The specimens are subjected to an r-ratio=0.1 with the block loading cycle covering the vicinity of the 3000 $\mu\epsilon$ region which Aircraft components are usually subjected to [141, 142]. An extensometer is used to correlate this strain to load. Table 6.2 identifies the block loading regime used.

Table 6.2 Block loading regime – strain amplitude increased every 10^5 cycles starting at 1000 $\mu\epsilon$

Cycles (N)	Strain ($\mu\epsilon$)	R-Ratio	Upper limit (kN)	Lower limit (kN)
100,000	1000	0.1	6.30	0.63
200,000	2000	0.1	12.60	1.26
300,000	3000	0.1	18.90	1.89
400,000	4000	0.1	25.20	2.52
500,000	4500	0.1	28.35	2.84
600,000	5000	0.1	31.50	3.15
700,000	5500	0.1	34.65	3.47

6.4 Results and Observation

6.4.1 Static Test Results

Several tests were conducted for each specimen configuration which is summarised in Figure 6.6 and Table 6.3 after they had been corrected by isolating the displacement of the load train discussed in Chapter 5. Compared to the results discussed in Chapter 4 [146], the step lap joint specimens failed with similar characteristics. The general trend observed shows bonded specimens have the highest stiffness out of all specimens, followed by hybrid specimens with three fasteners then hybrid specimens with five fasteners and finally a mechanically fastened specimen with five fasteners. Overall as the fastener area to bond area increases, the joint stiffness reduces.

Comparing all ten specimen configurations, there was little change in peak load achieved by the bonded and hybrid step lap joint specimens. This behaviour is once again similar to the bonded and hybrid double lap joint specimens [146].

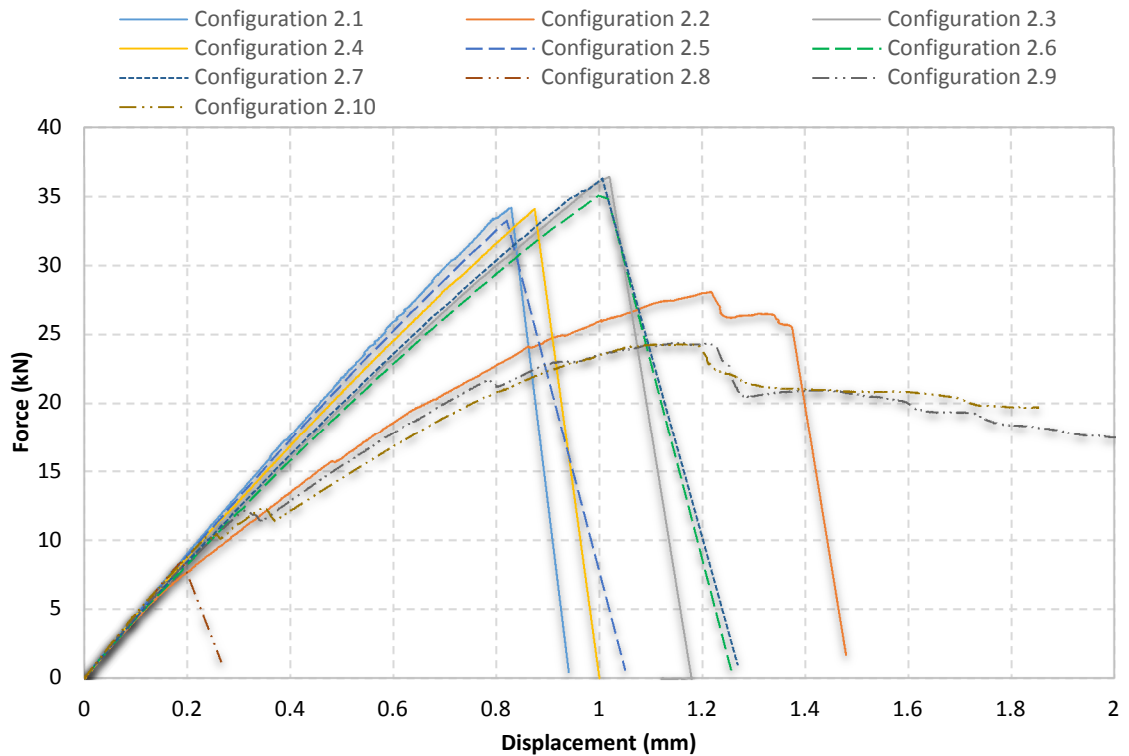


Figure 6.6 Peak strength achieved by fastened, bonded and hybrid configurations; refer to Table 6.1 for the detailed description of the configurations

Table 6.3 Summary of average peak load achieved by specimen Configuration 2.1-2.10

Specimen	Average Joint Strength	Standard Deviation
	(kN)	(kN)
Configuration 2.1	33.58	1.14
Configuration 2.2	27.80	1.03
Configuration 2.3	36.77	0.73
Configuration 2.4	34.01	3.22
Configuration 2.5	33.07	2.11
Configuration 2.6	35.47	0.58
Configuration 2.7	36.51	0.28
Configuration 2.8	9.07	0.75
Configuration 2.9	25.32	1.35
Configuration 2.10	23.18	1.58

From Table 6.3, Configuration 2.1 failed at a peak load of 33.58kN with a displacement of 0.82mm. Upon examining the specimen's surface, initial failure was due to crack initiation at the end of the overlap but catastrophic failure occurred through adherend failure where the first ply separated from the rest of the adherend. A FLIR A615 thermal camera connected to a Texas Data Acquisition (DAQ) device is used to detect damage during the loading process. The camera is angled to face one edge of the specimen's surface. Images were captured at a rate of 6Hz and then by subtracting an initial frame from its previous frame, damage in the specimen is detected based on the thermal data. This allowed correlating bondline cracking with load. Figure 2.19 shows the experimental setup of the Thermal Camera.

An example of critical frames gathered when testing specimen Configuration 2.1 is shown in Figure 6.7. As shown in Figure 6.7(a) the first point of damage occurred at the bottom end of the overlap. This was butt joint failure at a load of 9.64kN. Figure 6.7(b) shows that there is a slight edge crack progressing from the initial butt joint region at a load of 24.9kN. The bottom step of the adherend in Figure 6.7(c) shows damage across its width (which can possibly be due to adherend failure). Catastrophic failure is seen in Figure 6.7(d) at a peak load of 33.58kN due to sudden bondline failure.

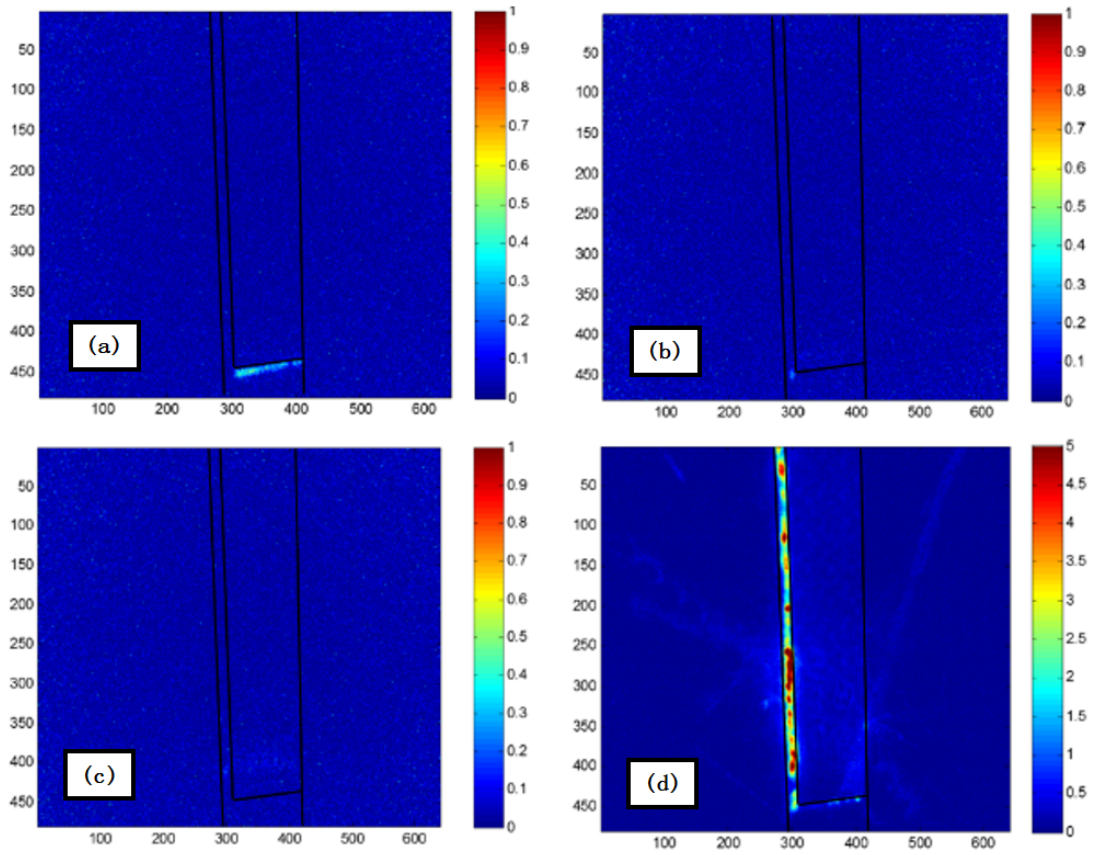


Figure 6.7 Damage detection using a FLIR A615 thermal camera for specimen Configuration 2.1 based on thermal data; (a) Frame 116 captured after 19.3sec; (b) Frame 323 captured after 53.8sec; (c) Frame 440 captured after 73.3sec; (d) Frame 476 captured 79.3sec after commencing the static test

Configuration 2.2 failed through bearing failure. Figure 6.6 shows a reduction of joint stiffness as the load applied increases. This is due to the initiation of fibre damage around the fastener hole locations. Distinct fibre failure started to occur after a load of 27.8kN followed by one of the outer fasteners pulling through the thin outer step. Final failure occurred by net tension failure across the second last fastener hole. Overall out of all ‘pristine’ specimen configurations, this specimen had the highest elongation with the lowest peak load.

Configuration 2.3 failed by net tension failure across the top fastener hole. Based on the thermal imaging results, crack initiation began on the top butt joint region at a load of 9.24kN. Distinct cracking is heard and picked up by the thermal camera at the third butt joint and second butt joint at 10.49kN and 23.56kN respectively. Beyond this point, it is believed fibre and matrix damage occurs whereby a crack suddenly progresses to the first

fastener hole causing a severe stress concentration eventually resulting in net tension failure across this hole at a load of 36.77kN and 1.01mm displacement.

Configuration 2.4 failed in a similar method to Configuration 2.3. Bondline cracking occurred at the bottom butt joint, third butt joint and second butt joint at a load of 11.65kN, 22.80kN and 29.04kN respectively. Note that the second and third butt joint encompass the first fastener hole out of the total of three fasteners used. As a result final failure occurred through net tension failure across the first fastener hole.

Configuration 2.5 was the start of specimens containing 2mm long initial cracks. This bonded specimen with an initial crack has almost the same joint efficiency as its pristine counterpart. From thermal imaging results it has been determined that butt joint failure does not lead to a catastrophic mode of failure. Hence by placing an initial 2mm crack at one end of the overlap, little effect is seen. This is because the 2mm initial crack surpasses the first butt joint but in turn the remaining adhesive across the first step is still largely intact. As a result a peak load 33.07kN is reached (similar to Configuration 2.1).

Configurations 2.6 and 2.7 are the hybrid specimens with five and three bolts respectively. Each has crack progression starting from the 2mm long initial crack. Configuration 2.6 fails by net tension failure across the outer fastener hole closest to the initial crack at a load of 35.47kN and a 1.02mm displacement. Configuration 2.7 also failed by net tension failure across the outer fastener hole closest to the initial 2mm long crack. This occurred at a load of 36.51kN and a 1.01mm displacement. The fact that there is less than a 3% difference in peak load shows how sudden bondline/first ply failure occurs.

Configuration 2.8 represents a defective semi-cured step lap joint specimen. Results for a semi-cured bonded double lap joint discussed in Chapter 4 [146] showed very little load carrying capability. Likewise only a peak load of 9.07kN is achieved by Configuration 2.8 in this investigation. This is desirable as the purpose of semi-curing the adhesive is to determine the effects of the fasteners after bondline failure. Thermal imaging results did not pick up any significant cracking in the joint. Only final failure was detected.

Configurations 2.9 and 2.10 containing the semi-cured adhesive layer with five and three fasteners respectively increased bond strength by more than 250% compared to Configuration 2.8. The additional clamping pressure provided by the countersunk bolts helped arrest early crack initiation. However in both cases, bondline failure occurred at approximately 12.0kN. Immediately a drop in stiffness is seen in Figure 6.6. Configuration

2.10 which contains two less fasteners than Configuration 2.9 had a reduced joint stiffness. Final failure now occurred by bearing failure where either the countersunk fastener eventually pulled through or net tension failure occurred across the middle fastener.

6.4.2 Fatigue Test Results

Fatigue tests were carried out using the Instron 100kN testing machine. Table 6.4, summarises the results. Note that the block loading regime shown in Table 6.2 is used to test each specimen configuration.

Table 6.4 Fatigue resistance of specimen Configuration 2.1-2.10 under block loading, r-ratio = 0.1 frequency = 5Hz.

Type	Specimen No.	Failure Load (kN)/Strain ($\mu\epsilon$)	Cycles to failure (n)	Average (n)	Standard Deviation
Configuration 2.1	1	18.90/3000	212,699	214,973	3,216
	2	18.90/3000	217,247		
Configuration 2.2	1	25.20/4000	318,594	309,604	12,714
	2	25.20/4000	300,614		
Configuration 2.3	1	28.35/4500	400,103	400,103	n/a
Configuration 2.4	1	25.20/4000	300,057	300,108	72
	2	25.20/4000	300,159		
Configuration 2.5	1	18.90/3000	211,383	232,873	30,391
	2	18.90/3000	254,362		
Configuration 2.6	1	28.35/4500	400,088	406,147	8,569
	2	28.35/4500	412,206		
Configuration 2.7	1	25.20/4000	300,070	300,070	n/a
Configuration 2.8	1	6.30/1000	8,139	8,139	n/a
Configuration 2.9	1	18.90/3000	208,849	208,012	1,184
Configuration 2.10	1	18.90/3000	202,933	202,933	n/a

The fatigue test results have been presented in a similar manner to Chalkley et al. [48], Wang et al. [47]. This is an efficient method of comparing fatigue resistance of various

joint configurations. Since fatigue tests in this investigation are not conducted using constant amplitude loading, S/N curves are not applied in this case.

Based on the results gathered in Table 6.4, out of the four ‘pristine’ configurations, Configuration 2.3 has the highest fatigue resistance. This is a hybrid specimen with five fasteners failing in the 4500 μE loading regime. The next highest fatigue resistance occurred from Configuration 2.2; the mechanically fastened step lap joint with five bolts. Configuration 2.3 with three fasteners in a hybrid setup failed with similar fatigue resistance as Configuration 2.2, both failing in the 4000 μE loading regime. Finally Configuration 2.1 which is the purely bonded specimen contained the lowest fatigue resistance out of all specimen configurations; failing at just under 215,000 cycles in the 3000 μE load regime.

The defective joint specimens containing a 2mm long initial crack performed in a similar manner to their ‘pristine’ counterparts. Configuration 2.6 has almost the same fatigue resistance as Configuration 2.3, failing in the 4500 μE loading regime. Configuration 2.7 with three bolts in a hybrid setup had a lower fatigue resistance than Configuration 2.6 with five bolts in a hybrid setup, and once again a bonded joint with a 2mm long initial crack failed at a much lower fatigue loading regime than the hybrid joint cases; 232,873 cycles at the 3000 μE loading regime.

The defective joint specimens with a semi-cured adhesive layer followed the same trend as its ‘pristine’ counterparts. As a purely bonded joint contained a semi-cured adhesive layer, this greatly affected the fatigue performance of the joint; failing after just 8139 cycles in the 1000 μE loading regime. The addition of fasteners improved the fatigue resistance by 26 times. The results overall highlights that fasteners in a hybrid configuration can significantly help static and fatigue performance of a joint and act as a failsafe mechanism if a bondline was not properly cured.

It must be noted that initial test plans consisted of fatigue testing at least three specimens per configuration under fatigue with the aim of identifying a ‘trend’ on whether hybrid specimens have superior fatigue performance than bonded or fastened step lap joints. Test plans were later modified to investigate the effects of out-of-plane bending present in these asymmetric step lap joints (refer to Section 6.4.5). This was done to provide a greater comparison of joint configurations but limited the overall number of repeated tests. Based on the test results, the data is valid due to consistency across the bonded and hybrid

specimens. Tests progressing into the next stage of the block loading regime can be quite detrimental if significant damage has already initiated in the previous block of the fatigue cycle hence resulting in similar failure limits between identical specimens. As a result, a block loading regime helps minimise the scatter range of fatigue tests compared to a constant amplitude fatigue cycle.

From Table 6.4, across all ‘bondline conditions’ hybrid specimens have a greater fatigue performance than bonded specimens. Bonded Configuration 2.1 and 2.5 both fail in the vicinity of 220,000 cycles and are very similar in structure (four specimens tested in this category). Likewise, hybrid Configuration 2.3 and 2.6 fail in the vicinity of 403,000 cycles (three specimens tested in this category). Hybrid Configuration 2.4 and 2.7 fail in the vicinity of 300,000 cycles (three specimens tested in this category). This therefore shows very consistent fatigue data across multiple specimen tests in each respective category and meets the aim of identifying a trend between bonded, bolted and hybrid specimens.

6.4.3 Damage Detection for Specimen Configuration 2.9

Previous studies have shown that bonded composites joints containing a defective semi-cured adhesive layer, fail significantly early under fatigue cases. The presence of fasteners helps in suppressing early crack initiation which typically occurs from the ends of the bondline overlap. The additional clamping pressure provided by fasteners reduce the peeling stresses induced in the joint which in turn improves fatigue performance. As a result of these factors, the fasteners not only enhance fatigue performance significantly but also enhance the overall joint efficiency by up to 12% in static strength for the pristine bondline cases.

The following investigation focuses on detecting and closely monitoring the progression of bondline cracking in a hybrid step lap joint configuration containing five fasteners with a defective semi-cured adhesive layer; Configuration 2.9. The same block loading regime in Table 6.2 is implemented whilst alongside visual inspection, non-destructive inspection (NDI) using an Ultrasonic A-Scanner and thermal imaging are used to detect damage during the fatigue process.

According to the block loading regime used, the strain amplitude is increased after every 100,000 cycles. Based on previous experimental work, bondline cracking/damage occurs in

the initial several thousand cycles of each block. Hence at the start of each block loading cycle, a simple static test is conducted only up to the maximum strain amplitude of that cycle. Following this, Ultrasonic A-Scans are performed in the overlap region whilst the joint is under load and also when the joint is no longer under load (0kN). Ultrasonic A-Scans are also performed after the first 1000 cycles, 3000 cycles 10,000 cycles and 100,000 cycles of each block loading regime with quick tests conducted whilst loaded and unloaded. Thermal imaging data is captured throughout the duration until failure. Table 6.5 summarises the crack growth rate for the hybrid step lap joint specimen containing five fasteners with a defective bondline.

Table 6.5 Monitoring and detecting crack growth rate in specimen Configuration 2.9

Max Strain ($\mu\epsilon$)	Cycles (N)	Crack Length (mm)	Detection Method			Location
			Ultrasonic A-Scanner	Thermal	Visual	
1,000	0.5*	<2	✓	X	X	Bottom right hand corner
	1	<2	✓	X	X	Bottom right hand corner
	1,000	<3-4	✓	✓	✓	End of bottom step
	3,000	<4	✓	X	✓	End of bottom step
	10,000	<4-5	X	X	✓	End of bottom step
	100,000	<5-6	X	X	✓	End of bottom step
2,000	100,000.5*	<5-6	X	✓	X	End of bottom step
	100,001	<7-8	✓	X	X	End of bottom step
	101,000	<7-8	✓	X	✓	End of bottom step
	103,000	<7-8	✓	X	✓	End of bottom step
	110,000	<9-12	✓	X	✓	Past bottom fastener hole
	200,000	<9-12	✓	X	✓	Past bottom fastener hole
3,000	200,000.5*	<12	✓	✓	X	Past bottom fastener hole
	200,001	<13-14	✓	X	X	Past bottom fastener hole
	201,000	<16-20	✓	✓	✓	Second last step
	203,000	<25-28	✓	✓	✓	Second last step
	203,500	90	✓	✓	✓	Entire bondline
	207,175	90	n/a	n/a	n/a	Tension failure across second fastener hole from the top

* 0.5 cycles represents a specimen under load and every integer cycle represents testing with specimen unloaded

✓ and X indicate whether or not the NDI method is able to detect cracking

Initially for small crack lengths $<5\text{mm}$, the crack growth rate is quite small. This is due to the bottom fastener providing clamping pressure which is vital in minimising the crack growth rate. However once the joint is in the $2000\mu\text{E}$ loading regime with over 110,000 cycles the crack progresses past the bottom fastener and thermal imaging shows that the top four fasteners only contributing to the load transfer in the joint, Figure 6.8.

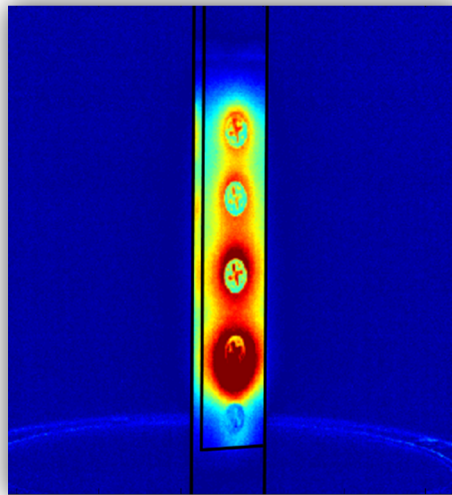


Figure 6.8 Thermal image using a FLIR A615 camera of specimen Configuration 2.9 after 110,000 cycles, $2000\mu\text{E}$

Overall across the three detection methods used - Ultrasonic A-Scanning using a 5MHz probe was able to pick up bondline cracking the most at each interval of the fatigue test. In some cases, cracks were hard to pick up using Ultrasonic A-Scanning whilst the joint was still under load or if a crack was located close to the vicinity of a fastener. The presence of a fastener did not provide a truly flush surface to obtain good contact between the ultrasonic probe and the adherend making it difficult to reliably predict the crack position. It must be noted however that in an actual repair case, the joint region may in fact be larger which eliminates this issue.

The Thermal Camera is able to pick up sudden cracking in the joint region very easily however slow modes of damage cannot easily be picked up due to the gradual release of energy. Cracking in regions of the joint which are not in direct view of the camera also cannot be picked up. However a key advantage of using thermal imaging lies in monitoring damage whilst the aircraft is in flight; performing NDI using an Ultrasonic A-Scanner or

trying to visually detect damage during flight may not be possible. On the other hand, visual detection is still a very useful method for monitoring the cracking. Initially when the cracks are $<2\text{-}3\text{mm}$, they are very hard to see but under fatigue, the repeated opening and closing of the crack front allows easy detection.

In an actual aircraft repair scenario, these flush step lap joints may not have a visible bondline region which is seen in these laboratory tests. Thus when using visual detection methods only the flush butt joint region and any visible adhesive spew in the vicinity of that region (Figure 6.7(a)) can only be seen. As a result, visual detection in an aircraft repair is beneficial up to the point of detecting crack initiation in bondlines. Under the right lighting conditions initial cracking $<2\text{mm}$ in the outer adhesive spew is detectable and confirmed by the experimental results highlighted in Table 6.5 (initial 1000 cycles of the fatigue test). It must be noted that visual detection should still be used to monitor other signs of damage such as adherend cracking and bolt pull through.

Overall based on the experimental tests, Ultrasonic A-Scanning serves as the best method of monitoring internal damage, whether it be bondline cracking or the delamination of plies. The end result presented here clearly shows that a defect present in a bonded joint has a detrimental effect on the life of the repair. A bonded joint with the same defective bondline (Configuration 2.8) catastrophically fails after only 8,139 cycles whilst the same joint with five fasteners in each step (Configuration 2.9) fails after 208,012 cycles which improve the joints resistance by almost 26 times under the given block loading cycle used. In addition to this information, the fasteners were able to sustain the joint even whilst the entire bond failed after approximately 203,000 cycles.

The results presented here overall conclude that for small cracks $<2\text{ mm}$ it is hard to detect damage visually whilst the joint is loaded and unloaded. However, Ultrasonic A-Scanning is able to pick up damage in either of the loaded and unloaded cases. As cracks grow $>5\text{mm}$ in length they are easy to detect using Ultrasonic A-Scanning whilst thermal imaging is useful for detecting the sudden crack propagation. This therefore provides an indication that in-situ health monitoring is possible whilst an aircraft is in flight. Overall, the presence of any crack/defect in an aircraft serves as a purpose to ground the vehicle for repair. There is a very narrow window for detecting such damage in a bonded joint configuration under fatigue but for a hybrid joint the fasteners help in arresting sudden crack propagation. Hence, this will provide significantly more time for damage detection during normal service inspections.

6.4.4 Damage Detection for Specimen Configuration 2.5

A minor extension to non-destructive inspection using the Ultrasonic A-Scanner and the Thermal Camera was conducted using Specimen Configuration 2.5. In this case the Distributed Optical Fibre Sensor (DOFS) technique is adopted to determine whether cracking can be detected whilst being fatigued.

As discussed in Chapter 2, DOFS systems contain fibre-based devices which are able to detect, monitor and even measure mechanical strain and/or temperature along a single strand of commercialised telecommunication optical fibre [96]. The device monitors the spectral shifts in the transmitted and reflected light within the core of the fibre. The spectral shift indicates the intensity of strain or temperature variation along the length of the fibre. Hence by bonding the optical fibre on a structure of interest, localised damage at any point along the fibres length can be detected.



Figure 6.9 Fibre optic cable bonded to one face of Configuration 2.5

Figure 6.9 shows specimen Configuration 2.5 with fibre optic cable bonded to one face of the specimen. In this case, one end of the fibre is connected to the Optical Distributed Sensor Interrogator which then displays real-time data to the user, Figure 6.10. Data is captured along the length of the fibre bonded to the specimen at a rate of 1Hz due to the long fatigue duration.

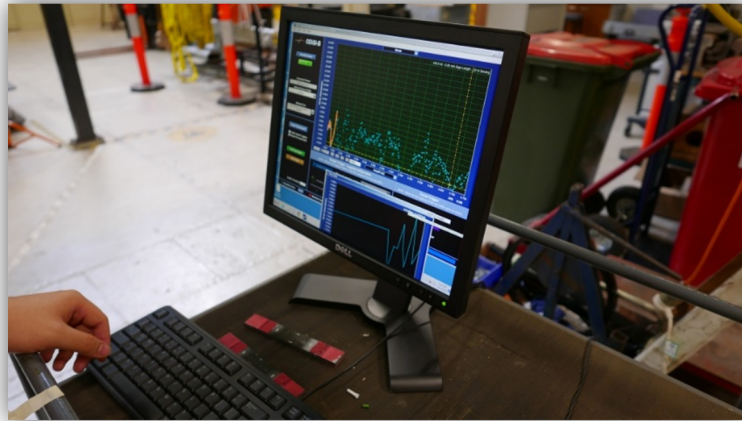


Figure 6.10 Viewing live data from the Optical Distributed Sensor Interrogator

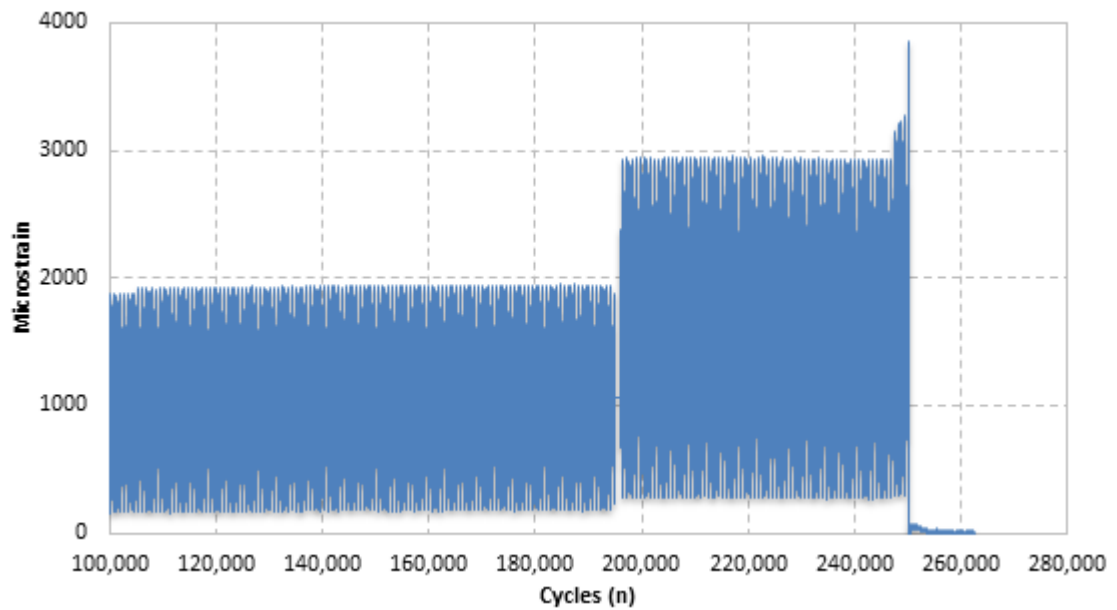


Figure 6.11 Fibre strain measurement at crack location in Configuration 2.5

Localised cracking using the distributed fibre sensor results in an increase in strain measurement. This is because the fibre still remains intact over the dislocated (cracked) area. Hence, a sudden increase in strain picked up by the interrogator can be interpreted as crack initiation and progression. In contrast, a typical strain gauge will detect a sudden drop in strain when crack initiation occurs due to localised stress relief in the given area, provided the strain gauge is not located directly on top of the defect which will damage the gauge.

Figure 6.11 shows the strain readout across the top left butt joint region seen in Figure 6.9. The block loading cycles are clearly broken up into distinct segments, 2000 μE and 3000 μE . After approximately 248,000, a sudden increase in strain is detected by the fibre. This continues to increase for another 5000 cycles until the specimen and fibre catastrophically fail.

Overall, the DOFS Interrogator is not commonly used for monitoring cracking in composite structures. However the work presented here clearly shows promise in its use. The method offers the ability to detect damage real time and may be used as an alternative method for in-situ structural health monitoring in addition to those mentioned in Section 6.4.3.

6.4.5 Suppressing Out of Plane Bending

From experimental tests conducted, out of plane bending was observed in all specimen configurations. Due to the localised increase/decrease in thickness of the steps there are load eccentricities resulting in a shift in the neutral line through the thickness of the specimen causing secondary/out of plane bending. In order to determine whether this is the cause of reducing fatigue performance of the bonded step lap joints, the geometries were now constrained using a guide plate mechanism. Figure 6.12 shows two guide plate system used to constrain the step lap joint specimen. Note under actual aircraft repair, various regions may already be highly constrained due to stiffening of panels through ribs and stringers hence minimising the bending seen in these components. The guide plates are machined from 10mm thick steel plates and teflon coated on the surfaces in contact with the specimen. This is to reduce friction in the system.

Fatigue tests were carried out once again on a select few specimens in order to determine the cause of failure. Figure 6.13 compares specimens fatigue tested with no guide plate (previous results) with specimens constrained using the guide plate.

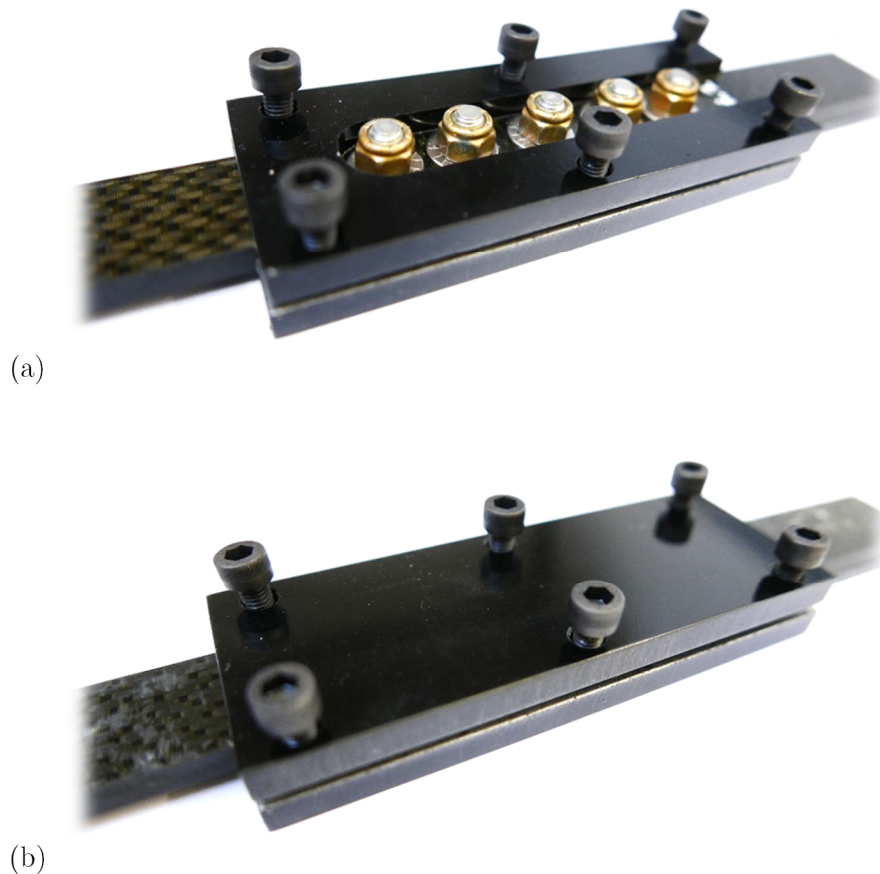


Figure 6.12 Guide plate system used to suppress out of plane bending; (a) hybrid specimen; (b) bonded specimens containing guide without slot for bolts

The use of a guide plate system improved fatigue resistance in all configurations tested. Configuration 2.1 – purely bonded joint and Configuration 2.2 – fastened joints each have a 28% improvement with the guide plate system. Configuration 2.3 – hybrid joint with five bolts shows only a 2% increase in fatigue resistance whilst Configuration 2.4 – hybrid joint with three bolts has a 38% improvement in fatigue resistance. The greatest improvement in fatigue resistance was achieved by the specimen with a semi-cured adhesive layer (Configurations 2.8 - 2.10); therefore highlighting that under-curing FM300-2K film adhesive performs very poorly when out of plane bending is not suppressed. In the case of Configuration 2.3 where minimal improvement is seen in fatigue resistance, the presence of

the outer two bolts located close to either end of the overlap helps in already suppressing early crack initiation. Therefore by placing fasteners close to the ends of bondline overlaps, the joint is able to cope well with out of plane bending.

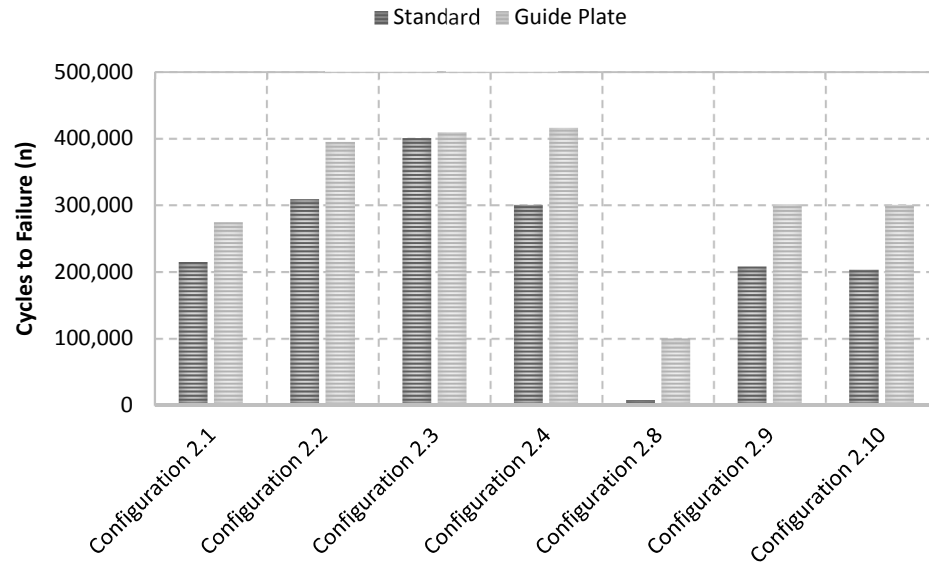


Figure 6.13 Comparison of specimen configurations fatigue tested using the block loading regime; Standard – specimens tested with no guide plate; Guide Plate – specimen constrained using the guide plate system; refer to Table 6.1 for the detailed description of the configurations

Overall although a purely bonded step lap joint has an improved fatigue resistance by constraining the out of plane bending, its performance is still not as high as a purely fastened joint. Overall this suggests early crack initiation is due to the small butt joint regions at the ends of the overlap which under the given loading condition act in tension.

Note that one again, the repair regions on an aircraft may have little to no out-of-plane bending effects due to the constraints provided by the surrounding structures (particularly if near a spar or rib). Thus the test results described in this subsection is useful in repair design.

6.5 Discussion on Failure Patterns

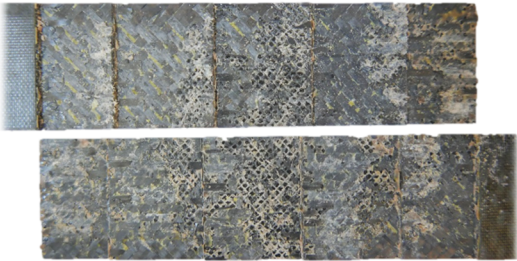


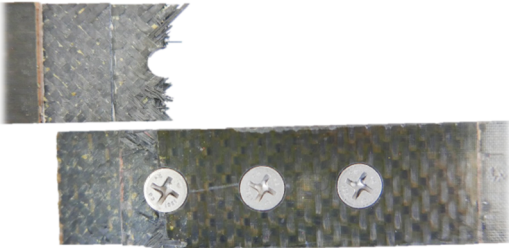
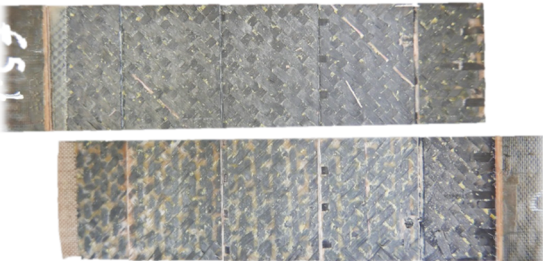
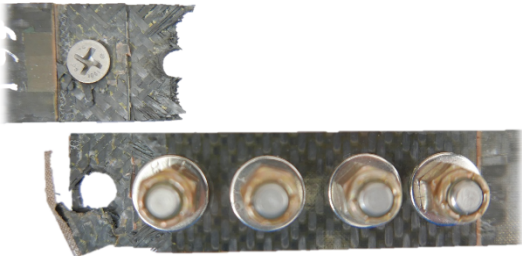




Unlike the riveted, bonded and hybrid thin double lap joint tests discussed in Chapter 4 [146] and 5 [155], the bonded step lap joint specimens had the lowest fatigue resistance followed by bolted specimens and finally hybrid specimens. Static test results have shown that bonded and hybrid specimens yielded almost the same peak load strength with the bolted specimen having the lowest stiffness and peak load failing under bearing failure which is a slow mode of failure. The fact that Configuration 2.1 did not perform as well as Configuration 2.2 shows that an improper geometry may negatively affect fatigue resistance even though static strength behaviour is better. By placing fasteners in a hybrid joint configuration, results show that a far better fatigue resistance is achieved.

Comparing the hybrid configurations with five fasteners and three fasteners (2.3 & 2.4, 2.6 & 2.7, 2.9 & 2.10), fatigue test results show placing five fasteners in the joint area is far more beneficial than just placing three fasteners. Even though the edge distance in the outermost fasteners is quite small, it has the advantage of adding additional clamping which is vital in arresting crack initiation [155]. In addition, the clamping provided by these two outer fasteners allow the joint to cope with out of plane bending as a result of the stepped geometry. For the pristine and 2mm initial crack specimen configurations, specimens with five fasteners had more than a 33% improvement in fatigue resistance than specimens with three fasteners. For the semi-cured adhesive specimens, this advantage is approximately 3%.

Table 6.6 shows the failure surfaces of all ten specimen configurations. As it can be seen from Configuration 2.1, failure occurred across the entire bond overlap. Due to the brittle nature of the FM300-2K film adhesive used, portions of the scrim cloth are visible. Failure in this case was a mixture of first ply failure and adhesive failure. NDI was used to detect damage at various stages of the fatigue cycle. Overall from observations, as soon as bondline cracking initiates, the entire bond fails almost immediately after.

Configuration 2.2 failed due to bearing. Due to the small thickness of the outer steps, a fastener pulled through resulting in the remaining four fasteners carrying the load. Eventually hole elongation reaches a critical level where eventually net tension failure occurs across the second fastener.

Table 6.6 Failure of the ten step lap joint configurations fatigue tested using a block loading regime; r-ratio=0.1

Configuration 2.1	Configuration 2.2
	
Configuration 2.3	Configuration 2.4
	
Configuration 2.5	Configuration 2.6
	
Configuration 2.7	Configuration 2.8
	
Configuration 2.9	Configuration 2.10
	

As soon as the fatigue loading began in Configuration 2.3, slight cracking is heard. This occurs in the outer butt joint regions which acts in tension. Final failure occurred by net tension failure. The crack which initiated in the butt joint region eventually propagated across the first step in the 3000 μE load regime. Failure eventually occurred in the 4500 μE load regime. This is when the crack progressed past the second butt joint region into the second step. This resulted in a significant load transfer in the joint whereby net tension failure occurred across the thin stepped section across the first and second fasteners. Looking at the failed specimen shows there is adherend failure on the bottom bond surface.

Configuration 2.4 with three fasteners failed in a similar manner to Configuration 2.3. The exception in this case is due to the lack of fasteners in the outermost steps. Bondline cracking progressed across the entire first step towards the end of the 3000 μE loading regime. This crack was visible across both 15mm long steps on either end of the overlap. Once the loading entered the 4000 μE loading regime, the bondline crack progressed past the next butt joint region and into the second outermost steps. Once in this region, significant bearing stresses develop across the fasteners hole eventually resulting in net tension failure.

For Configuration 2.5, Table 6.6 shows the 2mm x 25.4mm wide piece of teflon used to simulate an initial crack. Overall there is a mixture of adhesive failure (at the 2mm crack end) and adherend failure further along the overlap region.

Configuration 2.6 and 2.7 failed very similarly to Configuration 2.3 and 2.4. Failure occurred either across the first or second step and in the region closest to the 2mm long initial crack placed on one end of the overlap.

Configuration 2.8, shows a vastly different failure mode compared to previous specimen configurations. In this case, failure is due to adhesive failure.

Configurations 2.9 and 2.10 containing the semi-cured adhesive layer also failed initially due to adhesive failure. The entire bondline had separated once in the 3000 μE loading regime. Following this the fasteners carry the remaining load in the joint. This is when bearing failure occurs eventually resulting in net tension failure.

The findings overall conclude that hybrid joints have the greatest fatigue performance particularly those with five fasteners where the outer most fasteners are critical in providing

additional clamping force. This is important in reducing the peak normal stresses at the ends of the overlap [155].

6.6 Chapter Summary

The step lap joints considered in this study contained a total of five steps with 24 plies arranged in a $[(0/90)/(45/-45)/(45/-45)/(0/90)]_6$ orientation. A total of ten different specimen configurations were considered ranging from purely bonded joints, fastened joints and then hybrid joints containing either three or five fasteners. Defective step lap joint specimens were also considered and these contained either a 2mm long initial crack or a semi-cured FM300-2K film adhesive layer. From the experimental results presented in this chapter, static test results showed that bonded step lap joints have a greater stiffness than hybrid step lap joints. The presence of bolts in a hybrid joint reduces the overall bond area which in turn reduces the overall stiffness. The test results showed that the hybrid joints have the greatest strength under both static and fatigue loading. Hybrid joints with fasteners placed central of each of the step achieved almost two times the fatigue life under higher loading compared to its equivalent bonded joint counterpart.

Detailed damage monitoring in the hybrid joint with defective semi-cured adhesive bond (Configuration 2.9) was also conducted using visual inspection, an Ultrasonic A-Scanner and a Thermal Camera. Results confirmed that damage in these step lap joints can be detected and monitored when an aircraft is grounded (unloaded) as well as during flight, (for in-situ health monitoring) well before the ultimate fatigue failure. The fasteners in a hybrid joint configuration act as failsafe mechanisms which provide residual strength to the joint particularly in the case when the bond strength is lower than the bearing strength of the adherends.

Furthermore, a Distributed Optical Fibre Sensor (DOFS) interrogator was used to monitor damage progression in a bonded step lap joint containing a 2mm long initial crack (Configuration 2.5) when subjected to fatigue loading. The results confirm that the instrument is capable of detecting and localising damage in a structure. The information gathered using this method confirms that as soon as a crack grows in a bondline, catastrophic failure occurs soon after. The presence of fasteners is expected to suppress crack growth and in turn delay final failure. All of this information is vital in assisting composite joint/repair certification.

The step lap joint geometry selected in this instance is prone to out of plane bending when loaded axially in tension. This is due to the localised increase/decrease in thickness of the steps which shifts the neutral line along the length of the specimen. By using a guide plate system to suppress out of plane bending, the fatigue performance is improved in all joint configurations particularly bonded step lap joints and hybrid step lap joints with three inner fasteners. A hybrid step lap joint with five fasteners has minor improvements. This suggests that the outer fasteners provide adequate clamping pressure at the outer ends of the bondline suppressing the peak peeling stresses.

The following chapter focuses on modelling the step lap joint configurations using Finite Element Analysis (FEA). This will aid in further understanding how the load and stresses are distributed in the joint region and determine reasons as to why hybrid joints have outperformed its equivalent fastened and bonded step lap joint configurations.

Stage 2-Finite Element Analysis

7.1 Introduction

Finite element analysis (FEA) is performed using Abaqus CAE to verify the static and fatigue strength of thick mechanically fastened, bonded and hybrid step lap joints considered in Chapter 6. In order to ensure an aircraft is structurally sound depends heavily on how effectively the components are joined together and the method by which they are joined. The wing of an Airbus 380 alone is composed of over 30,000 elements, with approximately 750,000 bolted joints [39]. These joints are of key importance since they form a weak point that can contribute to the breakage of the element.

The three common methods of joining composite laminates together are through mechanical fastening, bonding or the combination of the two, called ‘hybrid’ joints. Mechanical fasteners such as pins, rivets and bolts have commonly been used in the aerospace industry for decades [2-4, 157]. The key problem that arises through the use of mechanical fasteners is the high stress concentrations around the fastener holes which are more severe in composite laminates compared to metal plates [5]. Hence, this Chapter aims at providing further details in the load and stress distribution in the various step lap joint configurations experimentally tested in Chapter 6.

The combination of mechanical fastening and bonding has been employed to safeguard against defects within the adhesive layer which may cause premature or catastrophic failure [6]. It is only after the bond has failed where the fasteners begin to carry the remaining load in the joint. It is this safety factor that has allowed the certification of these joints in some aircraft structures. A number of papers have investigated the use of hybrid joints. Hart-Smith [34] provided a non-linear analysis of bonded and bolted joints and concluded that hybrid joint configurations cannot achieve any significant advantage over adhesive bonding in well-designed intact structures, however it may prevent defect/damage propagation. Furthermore, Kelly [35] investigated the load distribution in hybrid joints with a single bolt using FEA.

In recent years, the use of finite element (FE) methods to simulate the behaviour of composite joints has increased. However, various limitations such as which failure theory to use and the extensive computer power required to solve many problems have made the analysis difficult and complicated. In order for FE methods to be used as a versatile tool on a regular basis, the models need to be able to accurately capture the three-dimensional stress and strain states, material behaviour, bolt tensioning and clamping forces, secondary bending effects, frictional forces as well as the contacts between surfaces. In addition, the localised damage in peak stress regions can reduce the laminates sensitivity to discontinuity. This results in highly conservative strength predictions based on initial failure around hole boundaries [19] and therefore must include the capability of progressive failure predictions. All of this leads to a detailed finite element model (FEM) which has not been widely seen in the available literature.

The work conducted in Chapter 5 showed that it is in fact possible to include all the above factors in FEM for a thin composite double lap joint configuration [155]. The work focused on comparing thin riveted, bonded and hybrid double lap joints. This chapter is an extension of the previous work which now investigates numerically modelling the thick step lap joint repairs discussed in Chapter 6. These joints are more complicated in nature than the thin double lap joints tested in Chapter 4 and 5. A detailed comparison between bonded, bolted and hybrid step lap joint configurations are analysed using Abaqus CAE and compared to experimental results.

Chapter 7 aims at providing vital information to help further understand the behaviour of bolted, bonded and hybrid step lap joint configurations under static and fatigue conditions. For the bonded and hybrid joints, the effects of two different types of bondline defects were

assessed. Nonlinear adhesive material properties, bolt surface contact, friction forces and the Multicontinuum Theory (MCT) to simulate the progressive failure process were all included in the FEA models. Overall this chapter provides clear guidelines on designing effective and efficient joints for composite structures which may aid in hybrid joint certification.

7.2 Finite Element Analysis Setup

Abaqus CAE is used to model the various step lap joint configurations experimentally tested in Chapter 6. The specimens are one inch wide with symmetry midway through the width of the specimen. Hence, only half the specimen is modelled using Abaqus using symmetry constraints. Figure 7.1 shows the three main joint type configurations. In the case of Configuration 2.4 containing only three fasteners, the outer two fasteners (B1 & B5) are removed.

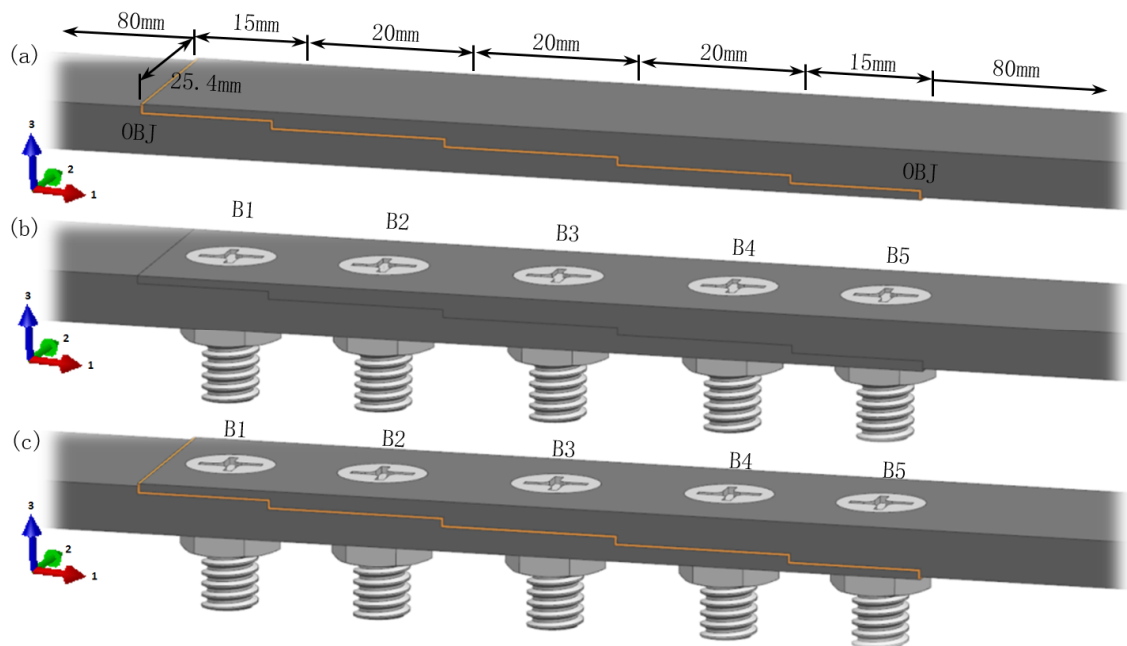


Figure 7.1 Three major geometry configurations; (a) Configuration 2.1 – Bonded Step Lap Joint; (b) Configuration 2.2 – Bolted Step Lap Joint; (c) Configuration 2.3 – Hybrid Step Lap Joint with five Countersunk Bolts; B1-B5 = Bolt 1 – Bolt 5; bolts placed central of each step; OBJ – Outer butt joint where adhesive acts in tension

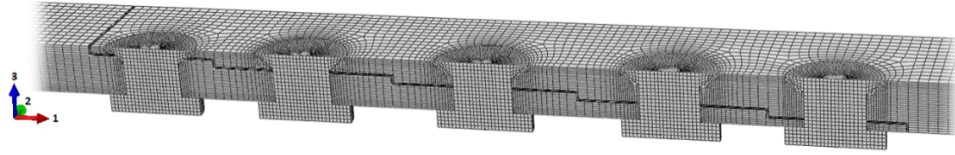


Figure 7.2 Meshed assembly of hybrid joint configuration containing five countersunk fasteners

As previously discussed in Chapter 6, a total of three different materials is used to produce the various joint configurations. The countersunk bolts are modelled using elastic material data with a modulus of 201GPa and a Poisson's ratio of 0.306. The adhesive is modelled using elastic-perfectly plastic material data specified in Table 3.2. The bondline thickness was set at 0.3mm verified using experimental measurements discussed in Chapter 3. A master-slave algorithm with small sliding is allowed between contacting surfaces and a friction coefficient of 0.1 [144, 145]. A neat fit is set between the contacting surfaces and adherends are modelled using orthotropic material properties defined in Table 3.1.

Due to the high localised stresses commonly found around the vicinity of the fastener holes and the ends of the bondline overlap a refined mesh using biased seeding is applied to the relevant configurations similar to Chapter 5. Once again fully integrated linear brick C3D8 elements using a structured mesh is used for both the adherends and adhesive. The seed element size was increased from 0.2 to 1.0. Configuration 2.1 to 2.7 contained an average element aspect ratio of 2.24, 3.95, 4.08, 4.32, 4.97, 4.08 and 4.33 respectively. Specimens containing an adhesive layer had four elements placed through its thickness whilst a longitudinal displacement in the (1) direction defined in Figure 7.1 and Figure 7.2 is placed on the right hand end of each specimen. Displacement in the (3) direction is constrained on the right hand end and a clamped boundary condition is applied on the left hand end. Figure 7.2 shows an example of a meshed hybrid configuration containing five fasteners (Configuration 2.3). Here the adhesive layer contains biased seeding with a refined mesh at the ends of each step. The same principle is applied to the bonded joints and bolted joints respectively.

A commercial plugin for running a micromechanical analysis method called the Multicontinuum Theory (MCT) provided by Autodesk is utilised to accurately simulate the composite material failure behaviour [7, 8]. As discussed in Chapter 3 and 5, micromechanical analysis takes an additional step beyond the conventional laminate theory to separate the stress and strain in the matrix and fibre from a Representative Volume Element (RVE). MCT predicts failure at the fibre and matrix level by obtaining the volume

averaged stress states in both the fibre and the matrix [155]. Here, matrix failure is assumed to be influenced by all six of the matrix average stress components in a 3D analysis, whilst a quadratic function is used to find the average stress of the fibre. In contrast, progressive damage models such as Hashin's criteria provided by Abaqus can be computationally expensive and typically suffer convergence issues due to discrete stiffness reductions whilst not accounting for transverse stress and strain components which are accounted for in MCT. By implementing this method it allows modelling specimen behaviour with far greater accuracy than previously available.

With any progressive damage model, fibre and matrix degradation values need to be found through an iterative process. The previous study discussed in Chapter 5 focused on modelling composite double lap joint configurations. It was found due to bearing failure being a compressive mode of failure, slightly higher fibre and matrix degradation values were needed. Optimal values ended up being 0.01 and 0.35 for the fibre and matrix respectively. This was obtained through iteratively comparing FEA results with Configuration 1.2 experimental results [146, 155]. The same degradation values are used in this study focusing on thick step lap joint configurations.

7.3 Finite Element Analysis Compared to Experimental Results

The experimental load-displacement results presented in Chapter 6 were corrected using a 'calibration factor'. This was because the results gathered from the 100kN Instron software interface are the raw force and displacement data. A similar procedure was used for the thin double lap joint specimens discussed in Chapters 4 and 5.

The displacement transducer of the test measures the total displacement comprising of the load train and the specimen itself. The true specimen deformation can only be determined from the machine displacement transducer once the deformation of the load train is isolated [158]. To do this, a calibrated extensometer was used on a simple coupon specimen made from the same HexPly M18/1/G939 carbon fibre prepreg. An extensometer with a 25mm gauge is used to record specimen elongation when subjected to increasing load. A calibration factor is then easily worked out between the cross head displacement and true displacement. This does not affect the failure load of the specimens tested but corrects for the total specimen elongation; resulting in a closer fit between experimental and numerical stiffness.

The ten specimen configurations defined in Chapter 6 were broken up into three distinct categories:

‘Pristine’ specimens contain adherends, adhesive and fasteners cured and assembled in accordance with the manufacturer’s specifications.

‘Defective – 2mm Crack’ specimens contain a 2mm long initial crack located at the outer end of the first step containing Bolt One (B1), Figure 7.1. This crack length was selected as it borders the limits of being detected by Ultrasonic A-Scanning.

‘Defective – Semi-cured Bond’ specimens contain FM300-2K film adhesive cured at 90°C for 60 minutes as opposed to 121°C for 90 minutes in an autoclave. The same conditions have also been used in [146]. This reduces the shear strength of the adhesive whilst still maintaining the same joint stiffness.

7.3.1 Load-Displacement Behaviour for Pristine Specimens

Figure 7.3 shows the comparison between experimental load-displacement curves with FE load-displacement curves for Configurations 2.1 - 2.4. The FE results are based on the model setup and material properties defined previously.

From Figure 7.3, Configuration 2.1 representing a purely bonded step lap joint has a joint stiffness of 41kN/mm. The stiffness for Configuration 2.4, 2.3 and 2.2 is 3.1%, 9.9% and 42.4% lower than Configuration 2.1 respectively. Hence, this shows that joint stiffness decreases as the bonded area decreases. This trend matches well with the experimental load-displacement results.

Note that final failure was assumed to occur away from the outer butt joint regions (OBJ) defined in Figure 7.1. This is because the experimental observations revealed although damage initiates at the OBJ regions it is not the cause of catastrophic failure [159]. Final failure occurs when damage progresses or is located in the vicinity of the second most outer steps as mentioned in Chapter 6 [159]. This is the point of catastrophic failure as the outer steps are 25% shorter than the three inner steps. This leads to a higher load transfer to the inner steps by preventing significant overloading in the outer steps [160]. Based on this method, a high degree of accuracy is seen in peak failure load predicted by the FE models compared to experimental.

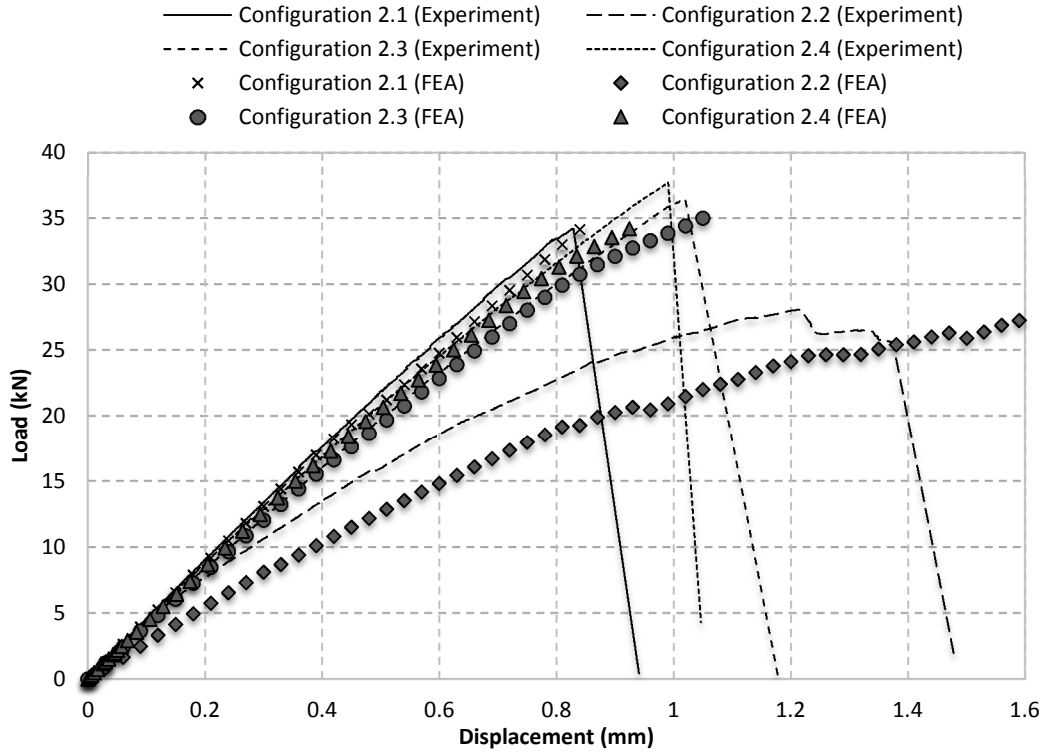


Figure 7.3 Load-displacement comparison between experimental and FEA for Configuration 2.1 - 2.4; displacement represents the specimens total elongation for the given load

Out of all pristine configurations, Configuration 2.4 produces the highest joint strength - reaching a peak load of 35.0kN. The closest match between experimental and FEA results was shown by Configuration 2.1. Failure in this case occurred due to first ply failure at the end of the first step in the top adherend. 'First ply' is defined as the initial ply that is in contact with the bondline in the specimen. Configuration 2.1 reaches a peak load of 34.13kN, displacement of 0.84mm and a remote strain of $6054\mu\epsilon$.

The FEA results for Configuration 2.2 shows a lower joint stiffness compared to its experimental load-displacement curve. This may be due to slight variances in the friction coefficient and by using higher fibre and matrix degradation values. Overall a gradual reduction in joint stiffness is seen as the joint is loaded.

Comparing the peak load predicted by the FEA models for Configuration 2.3 and 2.4 with their respective experimental results show only a 3.8% and 3.5% difference. Failure in both of these cases was due to first ply failure at the start of the second step. Overall the FEA models for these pristine configurations show a high level of accuracy compared to experimental load-displacement data.

7.3.2 Bolt Load Share and Stress Distribution for Pristine Specimens

Configurations 2.2 – 2.4 contained either five bolts or three bolts. In the case of Configuration 2.2, the majority of load carried by the joint was distributed amongst the five bolts. Figure 7.4 shows a uniform increase in bolt loading capability up until a joint load of 19kN, beyond which it is no longer uniform. This is due to increased fibre and matrix damage in the composite adherend. In the case of hybrid Configuration 2.3 and 2.4, the fasteners play a minimal role in load carrying capability, Figure 7.5. Configuration 2.3 containing five bolts carry only 2.5% - 3.3% of the total applied load and Configuration 2.4 containing three bolts only carry 1.5% - 2.1% of the applied load.

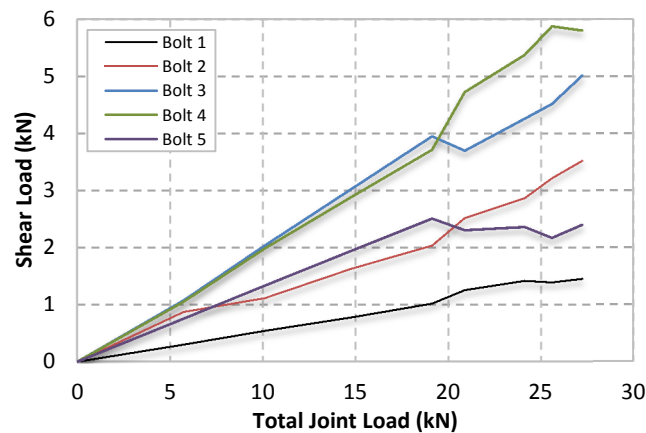


Figure 7.4 Comparison of load distribution between bolts in Configuration 2.2 (fastened step lap joint)

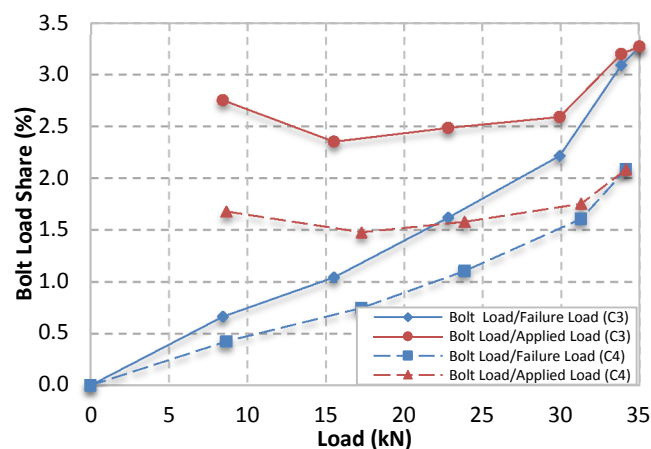


Figure 7.5 Comparison of load distributions in Configuration 2.3 and 2.4; C3 - Configuration 2.3; C4 - Configuration 2.4

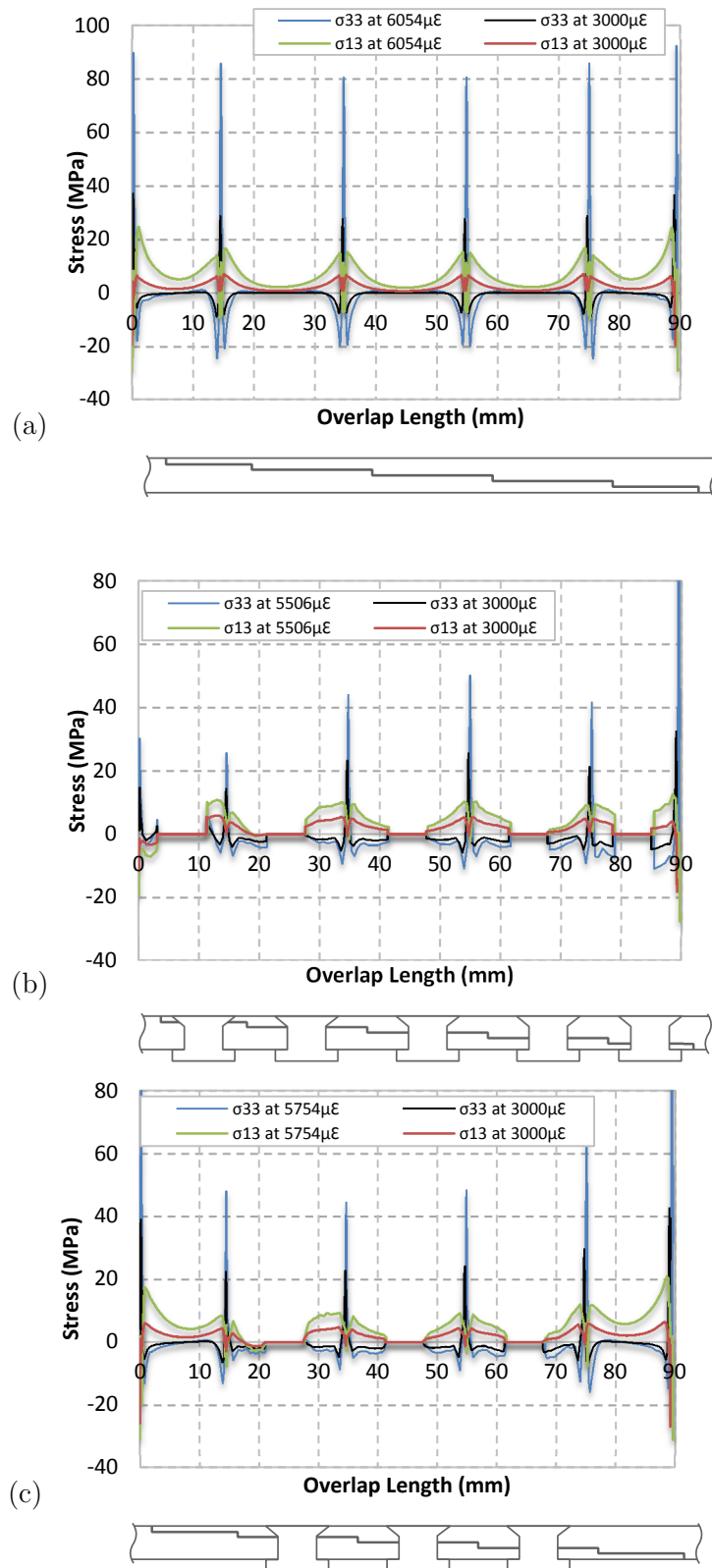


Figure 7.6 Comparison of adhesive stress distribution taken about the middle line; (a) Configuration 2.1; (b) Configuration 2.3; (c) Configuration 2.4; σ_{33} - Normal Stress; σ_{13} - Shear Stress

Figure 7.6 shows the shear (σ_{13}) and normal (σ_{33}) stress distribution for the pristine specimens containing an adhesive layer. Stress values are taken midway through the thickness of the FM300-2K film adhesive layer. Aircraft components are typically subjected to 3000 $\mu\epsilon$ and hence stress distributions are presented at this remote strain value as well as at the point of final failure, similar to Chapter 5.

Catastrophic failure in Configuration 2.1 occurs at a shear stress of -28.9MPa and a normal stress of 92.1MPa. Peak values occur at the end of the overlap. A relatively uniform stress distribution is seen in this case which indicates a good load distribution amongst the five steps. Figure 7.6(b), Configuration 2.3 shows peak shear stress values occur at the ends of the overlap reaching a peak value of -27.63MPa. A more uniform shear and normal stress distribution is seen in Configuration 2.4 which is more representative of a purely bonded joint due to the removal of the outer two fasteners; Figure 7.6(c).

7.3.3 Load-Displacement Behaviour for 2mm Initial Crack Specimens

Figure 7.7 shows the load-displacement comparison between experimental and FEA results for Configurations 2.5 – 2.7 containing a 2mm long initial crack. The cracks span the entire width of the specimen and is located at the outer end of the first step. 2mm is selected as the initial crack length as it borders the limit of crack size detection through Ultrasonic A-scanning. In these three defective configurations, the peak load achieved is marginally lower than their respective pristine counterparts.

Configuration 2.5, 2.6 and 2.7 reach a peak load of 33.25kN, 34.83kN and 36.31kN based on experimental results respectively. FEA predicts a peak load of 31.40kN, 31.92kN and 31.99kN for Configuration 2.5, 2.6 and 2.7 respectively. Overall, a hybrid specimen with three bolts achieves the greatest peak load. The result here agrees with prior knowledge that fasteners should not be placed close to the edge of a bondline overlap, particularly where there may be a high stress gradient [155].

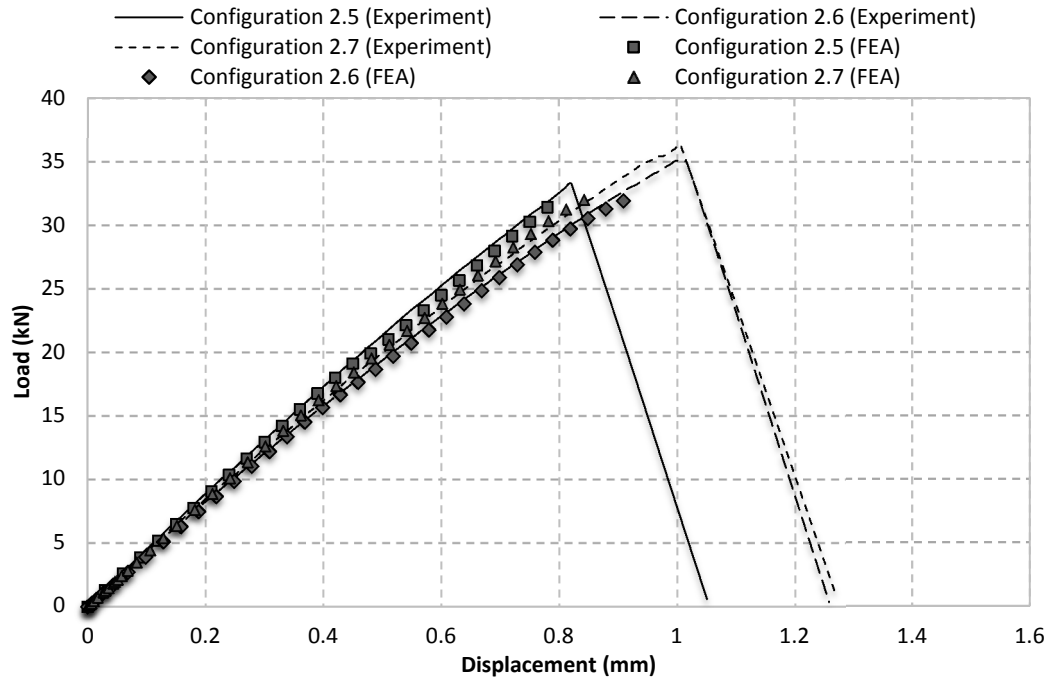


Figure 7.7 Load-displacement comparison between experimental and FEA for Configurations 2.5-2.7; displacement represents the specimens total elongation for the given load

7.3.4 Bolt Load Share and Stress Distribution for 2mm Initial Crack Specimens

Configuration 2.6 and 2.7 containing countersunk fasteners did not achieve as much load as Configuration 2.3 and 2.4. The fastener load carrying capability is shown in Figure 7.8. The results once again show that the greater the number of fasteners, the greater the load carried by the bolts. Hence, the fasteners in Configuration 2.6 is seen to carries a maximum of 2.9% of the joint load whilst the bolts in Configuration 2.7 carries a maximum of 1.8%. The overall trend is identical to Figure 7.5. A slight reduction in load carrying capability in this case is due to the reduction in the effective bond area due to the presence of the 2mm initial crack.

Figure 7.9 compares the shear and normal stress distributions for Configuration 2.5 - 2.7. The presence of the 2mm initial crack in all joint configurations results in varying the stress distribution in the first step. The highest peak stress occurs at the 2mm crack tip. In the case of Configuration 2.6, an abrupt increase in stress is seen immediately after the crack tip to the first fastener hole. A gradual reduction in stress distribution is seen in

Configuration 2.7 due to the absence of the outer fasteners seen in Configuration 2.6. Overall the results here clearly show the presence of a 2mm initial crack alters the stress distribution behaviour compared to an intact bondline (pristine joint configuration).

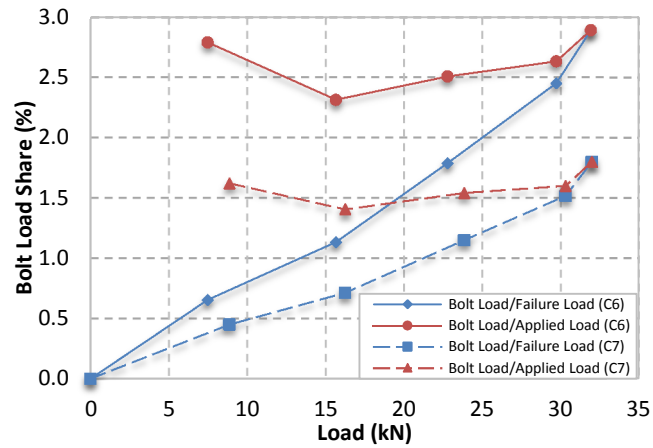


Figure 7.8 Comparison of load distributions in Configuration 2.6 and 2.7; C6 - Configuration 2.6; C7 - Configuration 2.7

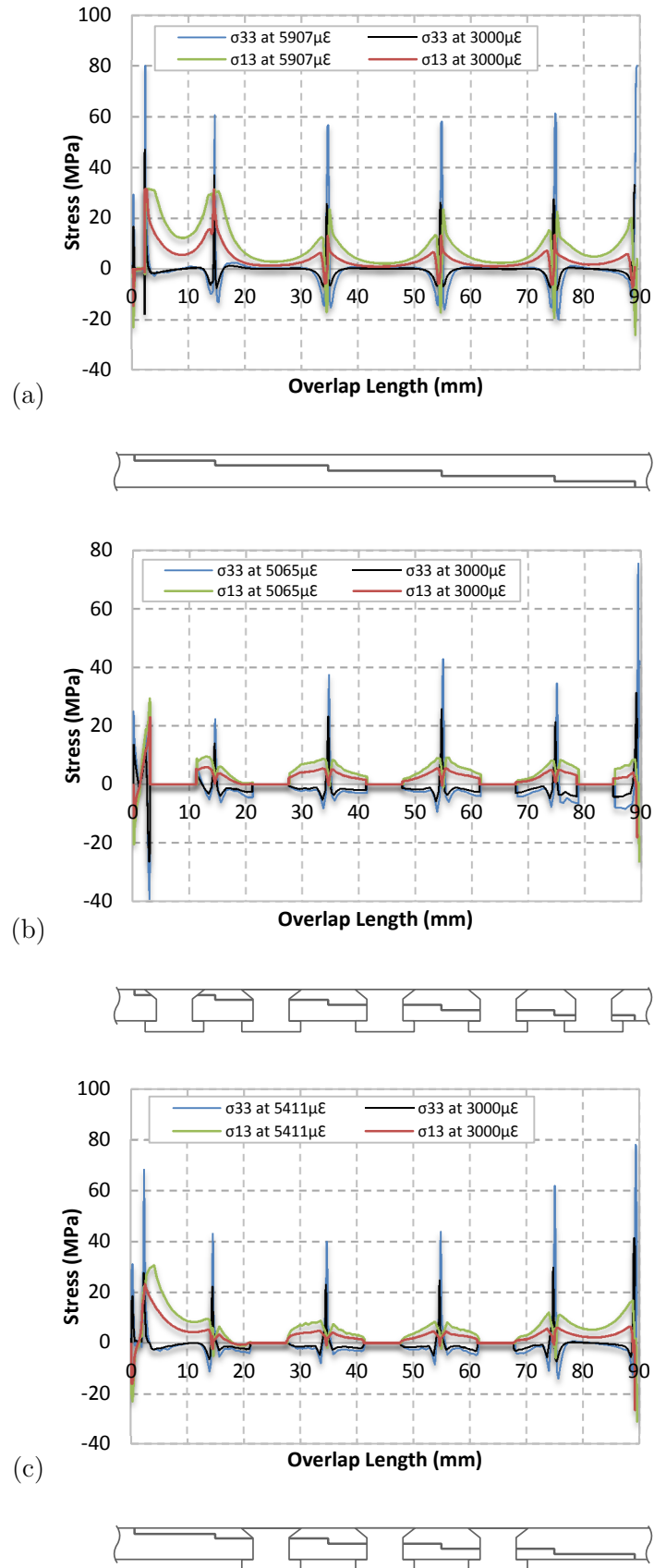


Figure 7.9 Comparison of adhesive stress distributions taken about the middle line; (a) Configuration 2.5; (b) Configuration 2.6; (c) Configuration 2.7; σ_{33} - Normal Stress; σ_{13} - Shear Stress

7.3.5 Defective Semi-Cured Adhesive Specimens

Improper surface treatment and manufacturing techniques can result in weakly bonded joints. This ultimately makes it very complicated to predict final failure. As such Configuration 2.8 - 2.10 have been produced to highlight an extreme case where a weak bondline is present. This is achieved by curing the adhesive at 90°C for 60 minutes as opposed to 121°C for 90 minutes, minimising the peak load share of the joint. This is similar to the method used for the thin double lap joints discussed in Chapter 5 of this dissertation. Figure 7.10, shows the experimental load-displacement curve for a hybrid specimen with five bolts and a semi-cured bond as an example (Configuration 2.9) [159]. The results highlight that by reducing the curing duration and temperature for an adhesive, the defective hybrid step lap joint initially has a high stiffness followed by sudden bondline failure after 12.0kN. This reduces joint stiffness whereby the bolts now carry the remaining load in the joint. A combination of the bonded step lap joint FEA result and bolted step lap joint FEA result resembles a similar relationship as previously shown in Chapter 5 [155].

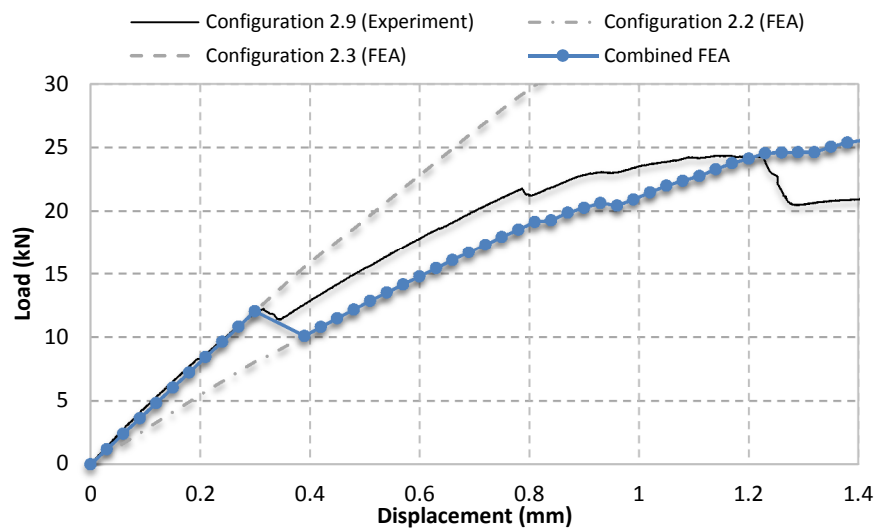


Figure 7.10 Load-displacement comparison between experimental and FEA for Configuration 2.9; a combination of Configuration 2.2 and 2.3 FEA results

Similar to Chapter 5, although a semi-cured adhesive may represent a defective joint, there are numerous other ways to also define a ‘defect’ in a structure. The presence of an initial crack and the use of expired adhesives are just some of many different methods of defining

such a ‘defect’. As a result modelling each and every type of joint will be a lengthy process with some results already self-evident. Specimen Configuration 2.8 - 2.10 have only been experimentally tested to demonstrate one of many examples of a bondline ‘defect’. In this case, the ‘defective semi-cured’ adhesive is quite detrimental for a bonded joint configuration [146, 159]. By using a ‘hybrid’ configuration the likelihood of sudden catastrophic failure is minimised through the added residual strength of the fasteners.

7.4 Fatigue of Bonded and Hybrid Joints

Very little work is currently available in literature which demonstrates the joint performance of step lap joints under both static and fatigue cases both experimentally but especially numerically [38, 134, 149, 151, 152]. Understanding why these hybrid structures have superior fatigue resistance over their bonded joint counterpart is a critical question that needs answers in the Aerospace Industry. Due to the complicated behaviour of step lap joints, very little information is currently found in literature. The work presented here provides answers to these problems and sheds light on how the number of fasteners and the positioning of fasteners can improve joint efficiency and fatigue performance using numerical methods.

Previous investigations conducted in Chapter 5 [155] showed an example of why thin hybrid double lap joints have superior fatigue resistance than their bonded counterparts. The numerical method used is extended to this study focusing on step lap joints which are more complicated in nature. Improper fastener positioning and/or machining of holes may adversely affect the hybrid joint strength and hence it is vital to understand how and where to apply them effectively. Improper drilling of fastener holes in fibrous materials can lead to the peeling of plies, fibre wrenching and resin degradation as well as delamination on the bottom plies [38, 134, 149, 151, 152]. On the other hand, holes for fasteners in a hybrid joint can help slow down crack propagation after initial adhesive failure [34]; this results in improved fatigue performance compared to bonded joints [6, 35]. Overall this section focuses on how multi-fasteners setup in a single column array (Figure 7.1) affect the crack growth rate. This in turn will offer some vital understanding behind the step lap joint fatigue performance.

7.4.1 Model Setup

Due to the repeated loading and unloading of joints in fatigue, there is a constant release of energy. As previously discussed in Chapter 5, the strain energy release rate (SERR) represents the energy available for crack growth and according to Paris's Crack Growth model, the SERR is proportional to the crack growth rate ' da/dN '. As a result, the higher the SERR the higher ' da/dN '. From this information, by modelling step lap joints with artificially placed cracks of various lengths along the bondline, the relative crack growth rate can be determined. This will provide an indication on how fasteners in a hybrid joint configuration affect the fatigue performance.

Initial cracks are placed midway through the thickness of the 0.3mm thick FM300-2K bondline and spread the entire width of the specimen. Experimental test results discussed in Chapter 6 [159] showed that bondline cracks which originate at the end of the overlap can progress to the second and third step before catastrophic failure occurs in a hybrid joint with five bolts. Hence, cracks (at approximately 2.4mm, 11.9mm, 19.0mm, 31.0mm, 39.0mm and 51.0mm) are positioned in the bond region of Configuration 2.1, 2.3 and 2.4. Nodes aft of the crack tip are tied together using node to node contact with average Mode I and II SERR data taken about the width of the specimens (along the crack front) using the displacement field method [116]. Figure 7.11 and Figure 7.12 summarises the SERR results for the three specimen configurations.

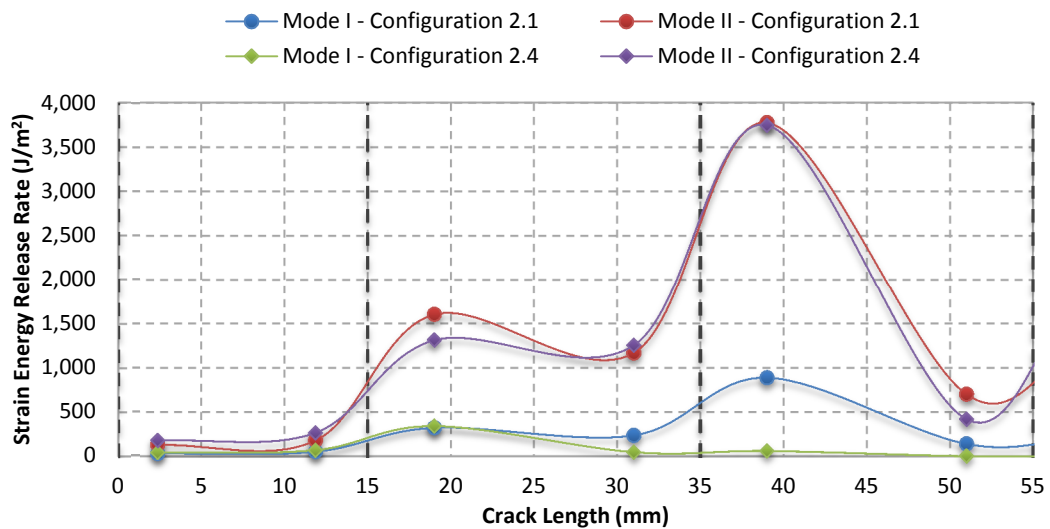


Figure 7.11 Available average energy for crack growth subjected to a remote 1000 μE displacement; Configuration 2.1 - Bonded; Configuration 2.4 - Hybrid with 3 bolts; vertical black dashed lines represent the start/end of each step in the joint

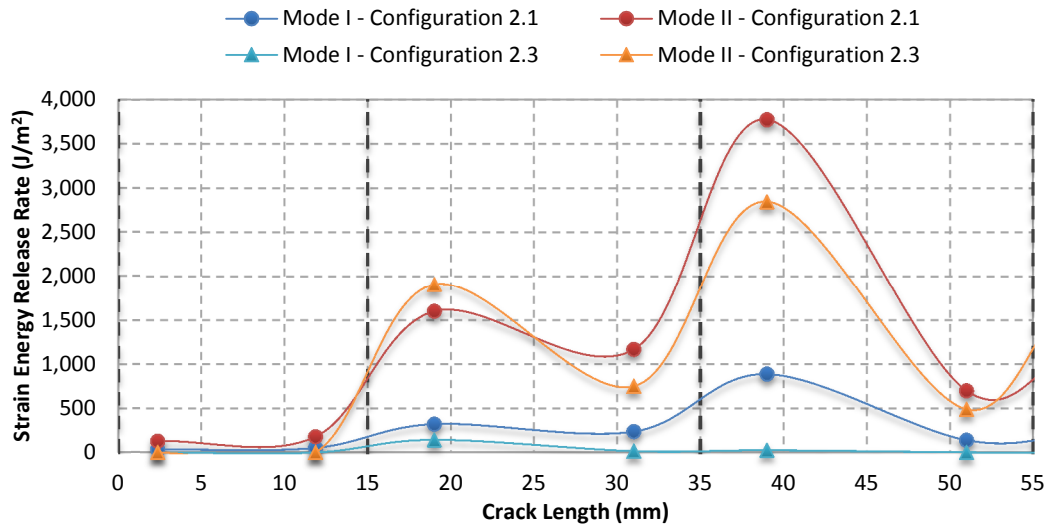


Figure 7.12 Available average energy for crack growth subjected to a remote 1000 μE displacement; Configuration 2.1 - Bonded; Configuration 2.3 - Hybrid with 5 bolts; vertical black dashed lines represent the start/end of each step in the joint

7.4.2 Fatigue Performance Comparison

Experimental fatigue tests were conducted on the bonded and hybrid step lap joint configurations and discussed in detail in Chapter 6 [159]. Based on the average results, Configuration 2.1 failed after 214,973 cycles, Configuration 2.3 failed after 400,103 cycles and Configuration 2.4 failed after 300,108 cycles. Hence, a hybrid step lap joint with five bolts has the greatest fatigue resistance.

A unique aspect of this work is in determining why a hybrid step lap joint with five bolts (Configuration 2.3) has significantly greater fatigue resistance than a hybrid specimen with three bolts (Configuration 2.4). To help understand this, a comparison is made between the bonded Configuration 2.1 and the hybrid Configuration 2.4 SERR results and the bonded Configuration 2.1 and the hybrid Configuration 2.3 SERR results shown in Figure 7.11 and Figure 7.12 respectively.

For crack lengths <12mm, SERR values are quite small across all three joint types. Mode II SERR values are significantly greater than Mode I. This is because the bond acts in shear under the given loading condition. The hybrid Configuration 2.4 with three bolts initially has the highest SERR for these small cracks followed by the bonded Configuration 2.1 and then the hybrid Configuration 2.3 joint with five bolts. Once the crack has entered

the second step (19mm), the Mode I SERR values for the bonded Configuration 2.1 and hybrid Configuration 2.4 with three bolts are relatively the same however the Mode II SERR values are 18% lower in the hybrid Configuration 2.4. Furthermore when the crack length is $>31\text{mm}$ the Mode I SERR are almost negligible in Configuration 2.4, Figure 7.13. A key point to note in this configuration is that cracks 14mm - 28mm in length have lower SERR values compared to the bonded configuration. Hence resulting in a lower crack growth rate. This is the main factor behind improving fatigue resistance in Configuration 2.4 over the bonded Configuration 2.1.

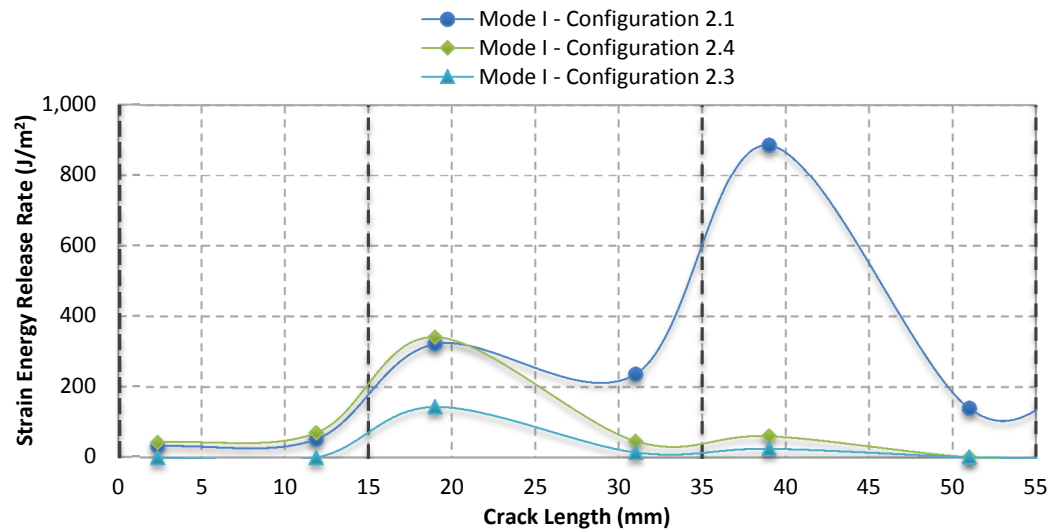


Figure 7.13 Available average energy in Mode I for crack growth subjected to a remote $1000\mu\epsilon$ displacement; Configuration 2.1 - Bonded; Configuration 2.3 - Hybrid with 5 bolts; Configuration 2.4 - Hybrid with 3 bolts; vertical black dashed lines represent the start/end of each step in the joint

Focusing now on the hybrid Configuration 2.3 with five bolts clearly shows a lower Mode I SERR for all crack lengths considered, Figure 7.13. The presence of a fastener in the very first step helps arrest crack opening from the very start which results in the significant reduction in Mode I SERR. Alongside this, the Mode II SERR in the Configuration 2.3 is almost negligible for crack lengths $<14\text{mm}$. This significantly helps improve fatigue resistance in the early stages of crack initiation. Although Figure 7.12 clearly shows a number of advantages for Configuration 2.3 a consequence of placing a fastener close to the edge of the overlap is in increasing SERR values once the crack has surpassed the first bolt. This hinders the overall joint efficiency, however the severity is not significantly

greater than a bonded joint as the total SERR (Mode I + Mode II) must be considered (in this case Mode I values are already quite small).

The real advantage of a hybrid joint occurs in a multi-fastener setup. From Figure 7.12, the position of the second fastener in Configuration 2.3 provided vital clamping pressure which is crucial in lowering the Mode II SERR values below that of the bonded Configuration 2.1 and the hybrid Configuration 2.4 containing five bolts. This would not be possible if only a single fastener is used. Likewise, as the crack length grows past 25mm, the SERR values still remain substantially lower than the other two bonded and hybrid configurations. Thus, the hybrid Configuration 2.3 containing five countersunk bolts has superior fatigue resistance than all the other configurations considered due to the initial low SERR value for small cracks as well as cracks >25mm in length.

A common trend seen in Figure 7.11 and Figure 7.12 is when cracks approach the end of each respective step, the crack growth rate reduces significantly but as soon as the crack has entered the next step, crack growth rate rapidly increases. This can present advantages as well as disadvantages.

The advantage is the butt joint regions may act as crack growth suppressors which may allow some time for detection during inspection

The disadvantage is as soon as the crack has surpassed the butt joint region, rapid crack growth can occur and result in catastrophic failure.

Overall from the numerical analysis discussed in this section, the results show good agreement to those previously discussed in Chapter 5 and 6 [155, 159]. A hybrid configuration with three fasteners (Configuration 2.4) has greater fatigue resistance a bonded step lap joint (Configuration 2.1) as SERR values a lower for cracks >14mm in length. In a hybrid step lap joint containing five fasteners (Configuration 2.3), although its outer fasteners are placed close to the ends of the bondline overlap, results still show that it is vital in suppressing rapid crack growth and in particular minimising the Mode I SERR's.

Overall the numerical analysis shows that by determining the SERR for artificially placed cracks in a bondline, the relative fatigue performance of various joints can be easily found. Once these joints are modelling correctly, it serves as a useful tool in conducting quick comparisons between multi-fastener hybrid joints and bonded joints. Performing further

numerical analysis will also aid in optimising fastener placement without the need for conducting preliminary experimental tests which are a time consuming and costly process.

7.5 Chapter Summary

The use of the micromechanical MCT progressive failure model, nonlinear adhesive material properties, bolt surface contact and friction forces enabled the computational comparison between fastened, bonded and hybrid step lap joint configurations. The load-displacement curves obtained through finite element analysis (FEA) for all configurations matched well with experimental results previously discussed in Chapter 6; these include pristine specimen configurations and defective specimen configurations containing either an initial crack or a semi-cured adhesive layer.

The catastrophic mode of failure in the bonded and hybrid configurations was predicted to be first ply failure located in the vicinity of the second step as observed in the experiment. Experimental and numerical results consistently showed the larger the bond area the greater the joint stiffness. The finite element models highlighted that for an intact bondline, the joint load share of the fasteners is negligible but the fasteners are critical in reducing the peel stress in the bondline of a hybrid configuration. In addition, the fasteners are vital in suppressing crack growth followed by adding residual strength to the joint once the bondline has failed.

The strain energy release rate (SERR) method provides an effective way of comparing the fatigue performance of the joint specimens. The results indicated that hybrid configurations have increased fatigue resistance over bonded configurations due to lower Mode I and II SERR values which in turn reduced the crack growth rate. A Hybrid configuration with five bolts has substantially better fatigue performance than those with three bolts due to the added clamping pressure provided at the ends of the overlap suppressing rapid crack growth. This configuration reduces the peak Mode II SERR by up to 24% (crack length of 39mm).

Overall the SERR method is able to reliably predict the relative fatigue performance of various bonded and hybrid configurations. The results obtained agree well with experimental fatigue test results and hence can be used as a tool to improve various joint configurations. Further optimisation may be achieved by varying the step heights/lengths

along the entire overlap for the same adherend. Analysing these joints through finite element analysis will assist in primary composite joint repair certification.

End of Chapter 7

8

Step Lap Joint Optimisation

8.1 Introduction

As previously discussed in Chapter 6 and 7, scarf and step lap joints exhibit the highest structural efficiency for thick joint structures as predominant load path eccentricities are eliminated when compared to single and double lap joints [5, 61]. Scarf lap joints are structurally more efficient as stress concentrations at the ends of the overlap are minimised. Stepped lap joints on the other hand have the same structural efficiency as a scarf joint when viewed from a strength and fatigue point of view [156, 161]. In addition to this, step lap joints can be manufactured with relative ease and hence selected as part of this investigation [156, 160, 162-164]. A parametric study is initially conducted aiming to optimise the previous step lap joint configurations considered in Chapters 6 and 7. Based on this study a total of four new specimen configurations is produced comprising of a bonded and hybrid joint configuration with a total of seven steps as well as a bonded and hybrid configuration containing six steps.

Previous investigations discussed in Chapters 6 and 7 showed small butt joint regions present at the ends of a flush step lap joint result in early crack initiation [159]. Likewise, other studies have also confirmed similar results [161, 162, 165]. The previous investigation focused on experimentally testing step lap joints containing five steps. The study fixed a

number of parameters such as the total number of steps, the step lengths and the step heights. As a result the maximum possible joint efficiency by this previous step lap joint configuration was 52% compared to an undamaged parent structure made from the same material and ply orientation. In this chapter, a more flexible design approach is utilised to improve the joint efficiency. A parametric study is conducted using Abaqus CAE to individually optimise the step lengths and step heights to achieve greater load recovery and in the case where a truly flush joint requirement was not necessary an overlap step lap joint was employed. Based on the findings, new step lap joint configurations were manufactured for testing. Overall this work presents a greater insight into step lap joint optimisation for use in composite aircrafts; one which has not been widely covered by researchers in the field.

When it comes to numerically modelling composite step lap joints, complications arise due to determining which damage model to use in order to reliably predict joint strength. Orifici et al. [166] reviewed a number of methodologies which incorporate failure of composites. Examples of two-dimensional and three-dimensional analysis of simply bolted composite joints using finite element analysis (FEA) is reported in [167-169] and [170-176] respectively. Further complexities arise when modelling hybrid joints. As previously mentioned, Hart-Smith [34] provided a non-linear analysis of bonded and bolted joints and concluded that hybrid joint configurations cannot achieve any significant advantage over adhesive bonding in well-designed intact structures, however it may prevent defect/damage propagation. The following studies [6, 36, 43, 101, 102, 143] also investigate the behaviour of hybrid joints but these are only limited to single fastener or two-dimensional models with little work focused on multi-fastener hybrid joints which are more complicated in nature.

Overall the work conducted in this chapter investigates whether it is possible to further optimise step lap joint configurations by varying the individual step heights and lengths of the carbon fibre adherends as well as introducing an outer overlap step. Nonlinear adhesive material properties, bolt surface contact, friction forces and the Multicontinuum Theory (MCT) to simulate the progressive failure process are all included in the FEA models. This chapter provides a complete picture in optimising the performance of step lap joints through the parametric study conducted using Abaqus CAE. Following this, details on manufacturing methods, as well as comparisons between numerical and experimental models is discussed. Overall this analysis is vital for composite joint repair certification.

8.2 Step Lap Joint Configurations

The previous step lap joint design containing a total of five steps with a 90mm long overlap showed minimal difference in the static strength of bonded and hybrid joint configurations. The maximum peak load was achieved by a hybrid configuration containing five countersunk fasteners failing after 36.77kN (Configuration 2.3). The bonded step lap joint achieved a peak load of 33.07kN (Configuration 2.1). Comparing these values to a pristine undamaged specimen made from the same HexPly M18/1/G939 carbon fibre prepreg with 24 plies stacked in a $[(0/90)/(45/-45)/(45/-45)/(0/90)]_6$ orientation, a peak load of 70.65kN is achieved. Figure 8.1 shows the relative comparison between the load-displacement results obtained from the 100kN Instron machine for the previous pristine step lap joint specimen configurations discussed in Chapter 6 and 7 with an undamaged parent structure.

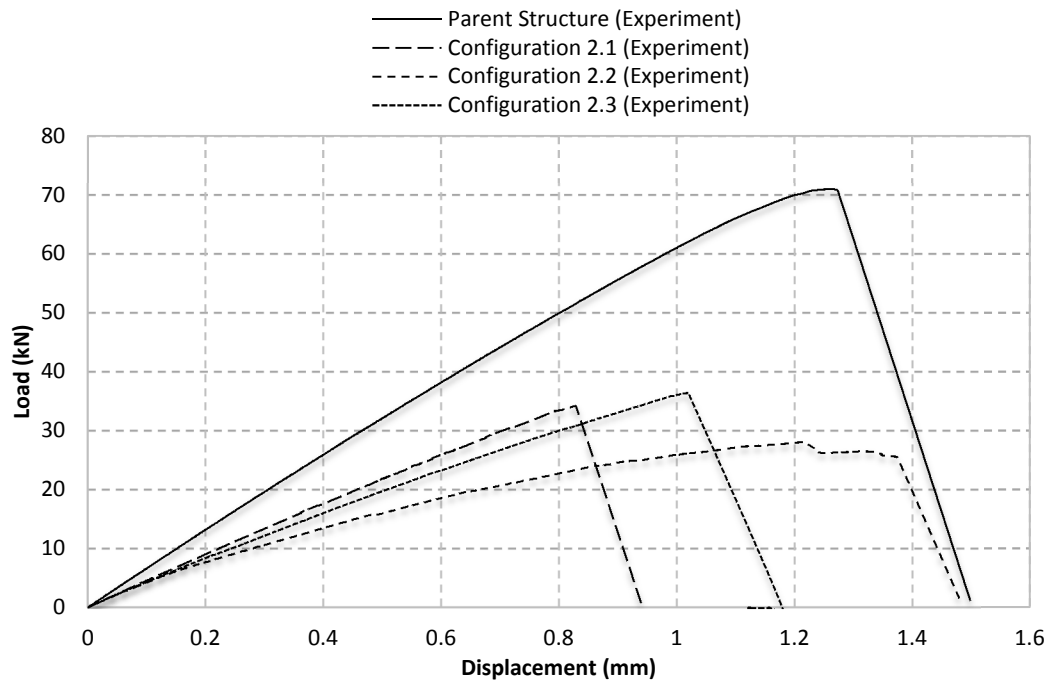


Figure 8.1 Peak strength achieved by an undamaged parent structure and fastened, bonded and hybrid step lap joint configurations; refer to Table 6.1 for the detailed description of the configurations

Overall the step lap joint configurations at best achieved a 52% joint efficiency compared to a uniform 24 ply thick undamaged parent structure. Although for single overlap cases it is unlikely 100% of the load is recoverable, in general a higher joint efficiency than previously reported is possible. Figure 7.1 shows the previous step lap joint design.

As a result a parametric study is conducted in Abaqus CAE to look at improving the step lap joint currently with five steps. Several new configurations were looked at, this includes:

1. Specimens with a double strap placed over the step lap joint overlaps
2. Specimens with a single strap placed over one face of the overlap
3. Specimens with increased number of steps to improve joint efficiency
4. Specimens with an outer overlap region

Further details of the geometry and analysis conducted is presented in the following sections.

8.3 Parametric Study - New Step Lap Joint Designs

A number of parametric studies are conducted using Abaqus CAE to optimise the previous step lap joint design containing five steps with a 90mm long overlap. Three-dimensional models containing orthotropic material properties for the adherends and elastic-perfectly-plastic material data for the adhesive is used (Table 3.1 and Table 3.2). Fastener surface contact, frictional forces and the Multicontinuum Theory (MCT) is used to simulate the progressive damage of the composite material, similar to Chapters 5 and 7.

Overall the numerical models discussed in earlier chapters has successfully been used to accurately simulate the failure of double lap joints [155] as well as step lap joints [159]. The models were able to accurately capture the three-dimensional stress states, material behaviour, bolt clamping, friction, secondary bending effects, load distribution as well as contact interaction between surfaces. Hence, this study adopts the same modelling principles but applies it to new step lap joint designs which are expected to provide the same level of accuracy as before.

The parametric studies determined the effects of adding outer straps, varying step heights, step lengths and the number of steps with the following parameters kept fixed.

- Adherend is 24 plies thick with a ply stacking sequence of $[(0/90)/(45/-45)/(45/-45)/(0/90)]_6$
- Adherends are one inch wide
- A total of five countersunk bolts used as the fasteners in a hybrid joint configuration, $\frac{1}{4}$ inch in diameter

This enabled a closer comparison between the new step lap joint designs with the previous step lap joint design discussed in Chapters 6 and 7. Only bonded step lap joints were modelled in this parametric study as previous findings discussed in earlier chapters revealed although under fatigue cases there may be significant differences between the durability of a bonded and hybrid joint, under static test conditions, there is minimal difference between a bonded and hybrid joint configuration [146, 155, 159].

Furthermore, the residual strength in a hybrid joint repair is determined by the fastener joint pattern. In this case, the fastener pattern is kept the same as the previous step lap joint design (single array of fasteners discussed in Chapters 6 and 7). This results in a similar load-displacement relationship for the numerical modelled bolted joint configurations with a different step geometry, thus providing approximately the same residual strength. Further details are provided in Section 8.4.1.

8.3.1 Double and Single Strap Specimen Configurations

The small butt joint regions present at the very ends of a flush step lap joint result in early crack initiation based on the given loading conditions, Figure 8.2.

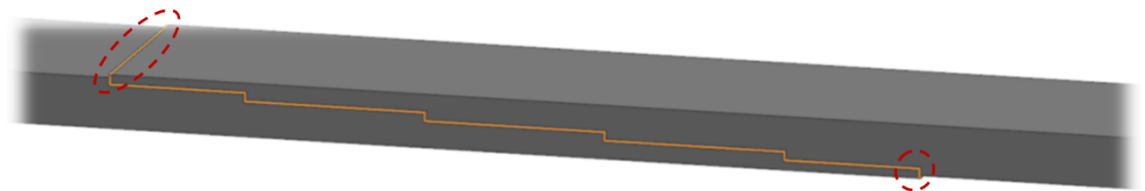


Figure 8.2 Outer butt joint regions (circled in red) result in early crack initiation in a bonded and hybrid step lap joint

Thus two new configurations were initially considered to improve the strength of the joint. In this case, the placement of a strap on either side of the flush surfaces alleviated the exposed butt joint regions and hence suppress the peak stresses which arise in this region.

Figure 8.3 shows an example of the previous bonded step lap joint with five steps (Configuration 2.1) with two straps placed on the outer surfaces. The number of plies used, its orientation and the overall length of the straps were varied. It was found the straps helps minimise the peak shear and normal stresses typically found in the butt joint

regions. The thicker the straps, the higher the joint stiffness but consequently the higher the peak shear and normal stress values present at the ends of the straps. The bonded step lap joint specimen has a 90mm long overlap; when strap lengths were greater than 70mm, out of plane bending increases due to the increase in thickness midway along the lengths of the specimen (as seen by the image at the bottom of Figure 8.3).

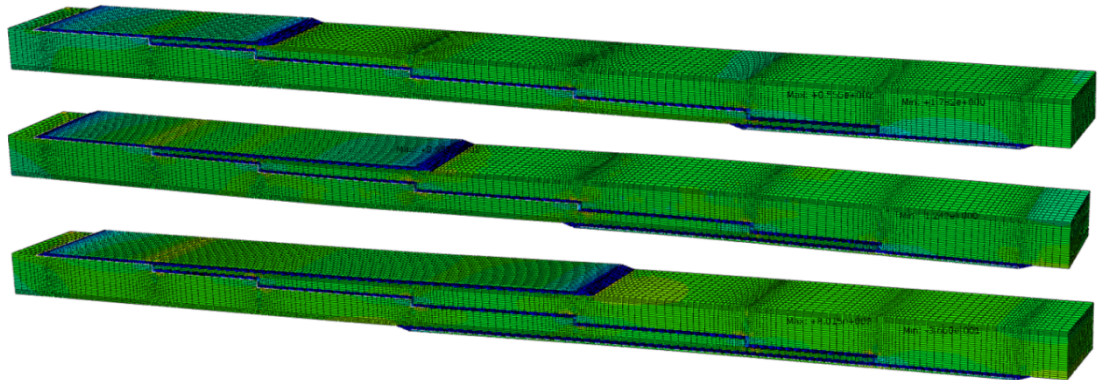


Figure 8.3 Previous bonded step lap joint (Configuration 2.1) with double straps placed on both top and bottom surfaces

One factor that needs consideration in repair is that both sides of a panel may not be accessible and hence two straps cannot be placed on either side. As a result a single strap option was also numerically studied, Figure 8.4.

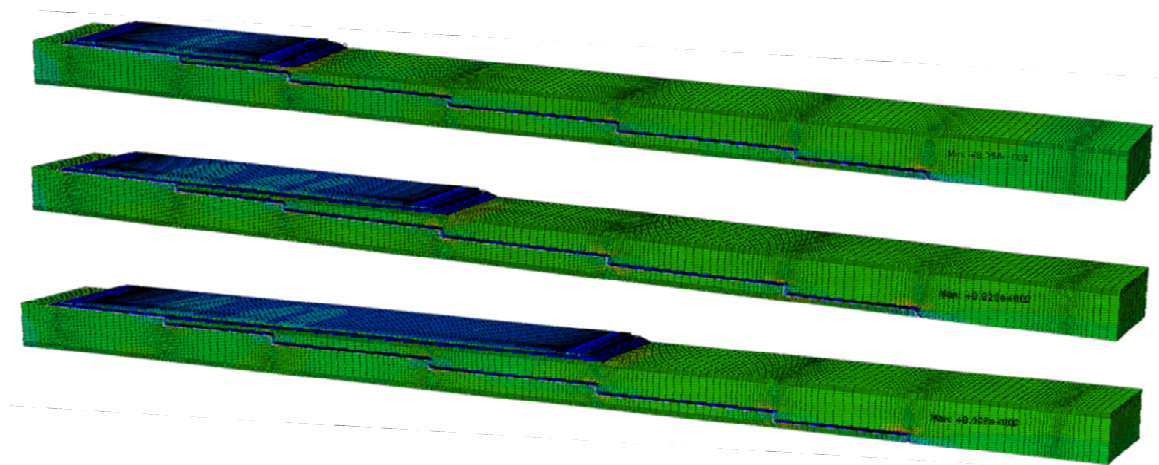


Figure 8.4 Previous bonded step lap joint (Configuration 2.1) with a single strap placed on the top surface

The disadvantage of a single strap placed over one surface of the bonded step lap joint is out of plane bending. Although the strap reduces peak shear and normal stresses present at the top outer butt joint region, in some cases it can negatively affect the bottom outer butt joint region due to out of plane bending. Overall the numerical study conducted using straps showed it may improve joint efficiency, however it lengthens the repair procedure and ultimately conceals visibly detecting cracking in the butt joint regions which may cause premature failure.

8.3.2 Flush Step Lap Joint Configurations

The next parametric study conducted using Abaqus CAE focused on keeping a truly flush step lap joint design similar to the previous step lap joint with five steps. In this new design, the number of steps was increased alongside varying the step heights and step lengths. The models consisted of 5 steps, 7 steps, 9 steps and 11 steps. This enables each step to start and end at a ply interface. The number of plies used in each step is defined in Table 3 and shown in Figure 8.5.

Table 8.1 The number of plies per step placed in a step lap joint made up of 24 plies with a fixed $[(0/90)/(45/-45)/(45/-45)/(0/90)]_6$ orientation

Configuration	Number of Steps	Plies per Step	Total Number of Plies
5	5	4 - 4 - 4 - 4 - 4	24
7	7	2 - 2 - 4 - 4 - 4 - 4 - 2	24
9A	9	4 - 2 - 2 - 2 - 2 - 2 - 2 - 2 - 4	24
9B	9	2 - 2 - 2 - 2 - 4 - 4 - 2 - 2 - 2	24
11	11	2 - 2 - 2 - 2 - 2 - 2 - 2 - 2 - 2 - 2 - 2	24

The main aim in this section is to improve the joint strength using the same parent material and flush requirement, hence the number of plies and its orientation were kept fixed. Figure 8.6 shows the peak load carried by each of the configurations modelled with varying step lengths using Abaqus CAE. Note: in all step lap joint cases the outer steps were kept 25% shorter than all the inner steps. This prevents the outer steps from being overloaded causing premature failure [5, 64].

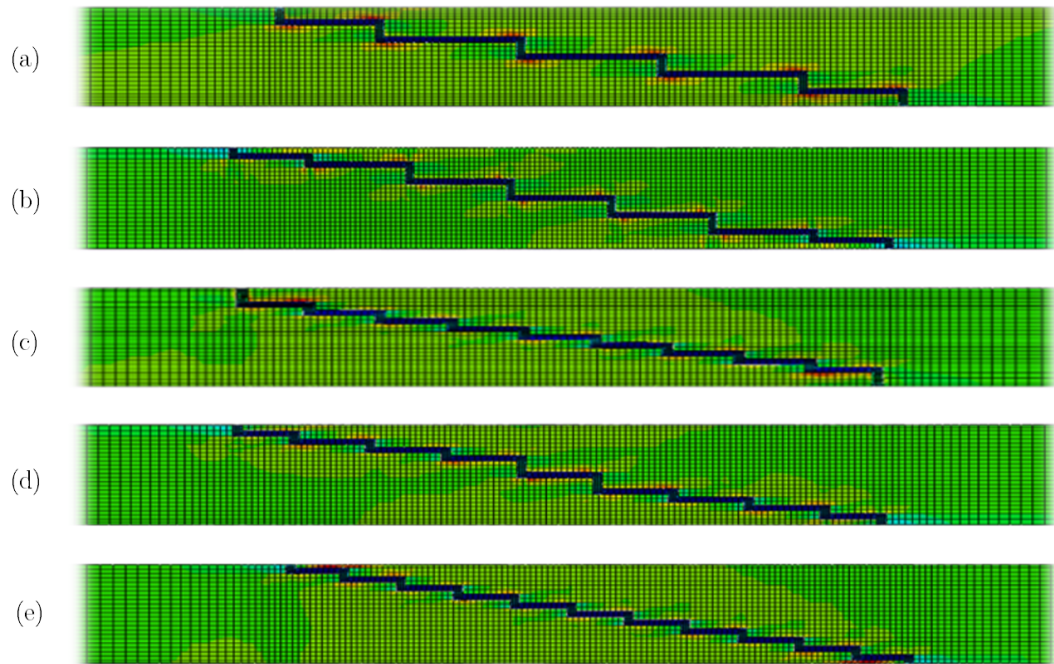


Figure 8.5 Bonded step lap joint specimens (not to scale); a) Configuration 5; b) Configuration 7; c) Configuration 9A; d) Configuration 9B; e) Configuration 11; refer to Table 8.1 for configuration description

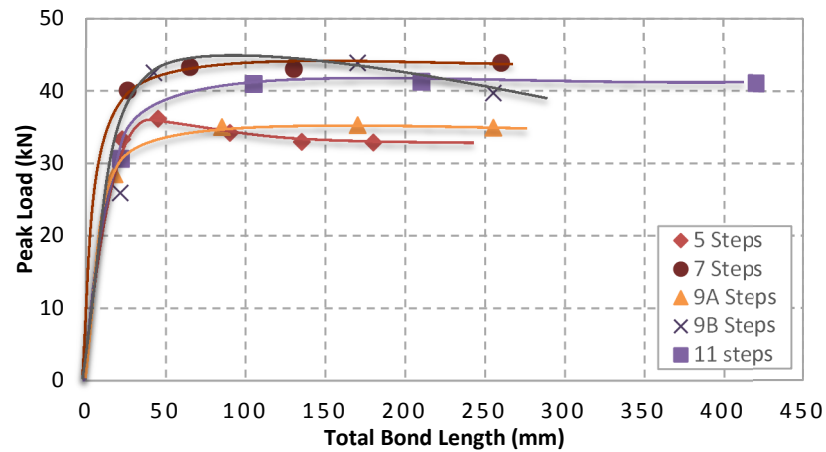


Figure 8.6 Peak load carried by various bonded step lap joint configurations made from 24 plies of HexPly M18/1/G939

From the results shown in Figure 8.6, Configuration 5 and 9A with five and nine steps respectively show very similar strength characteristics due to having the same outer step heights. In general it is clearly seen that increasing the number of steps whilst maintaining the same overlap length is more beneficial for a bonded joint. However, hybrid joints will

also be manufactured using the same step configuration. This poses limitations on the minimum step length as fastener to edge distance need to be considered.

From Table 8.1, Configuration 9A has four ply thick outer steps whilst all the inner steps are two plies thick. In Configuration 9B, the first four outer steps are only two plies thick whilst the inner two steps are four plies thick. Results shown in Figure 8.6 show it is much more beneficial to have thin outer steps which reduce peak shear and normal stress values which contribute to increasing joint strength.

Configuration 11 containing eleven steps also produces one of the highest joint strengths. A disadvantage with selecting this configuration is when considering its hybrid counterpart; this will result in an overlap length greater than 210mm. From a repair point of view, it is ideal to achieve good load recovery whilst still minimising the area required for repair. This ensures further damage is not caused to adjacent pristine regions during the repair procedure. As a result, a specimen with seven steps is selected for further analysis and experimental testing. Only five countersunk fasteners are used in the seven step hybrid configuration as bolt pull through is likely occur in the two ply thin outer steps, Figure 8.7.

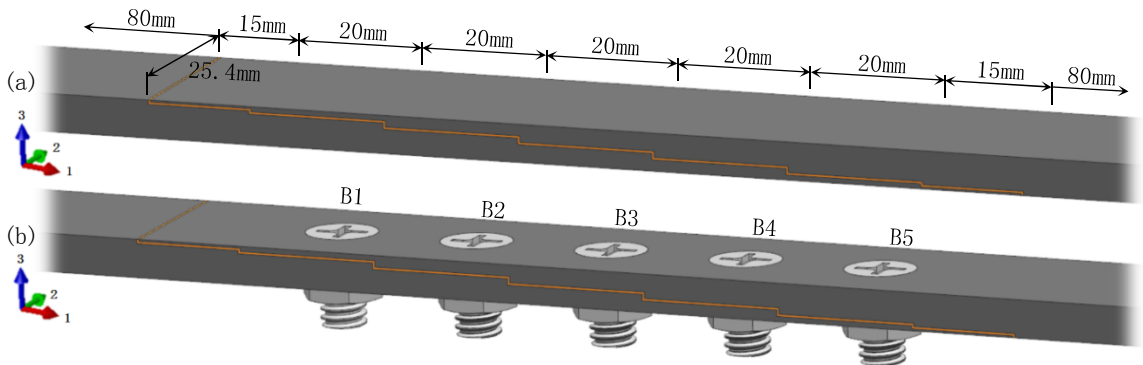


Figure 8.7 Two major geometry configurations; (a) Configuration 3.1 – seven step bonded lap joint; (b) Configuration 3.2 – seven step hybrid lap joint; B1-B5 = Bolt 1 – Bolt 5; bolts placed central of each step

8.3.3 Overlap Step Lap Joint Configurations

Due to the outer butt joint regions present at the very ends of the bondlines in a step lap joint, rather than using composites straps discussed in Section 8.3.1, a new overlap step lap joint is designed. In this parametric study, the same bottom composite adherend discussed in Chapter 6 and 7 is used but now with a newly designed top composite adherend. As a result, a number of parameters are kept fixed such as the individual step lengths and

step heights but with a variable length outer overlap. Figure 8.8(a) shows that previous step lap joint design containing five steps. Figure 8.8(b) shows the removal of the top composite adherend whilst still keeping the bottom adherend. Figure 8.8(c) shows a new top composite adherend placed with an outer overlap step and finally Figure 8.8(d) shows a filler adherend used to maintain flushness on the underside of the joint repair.

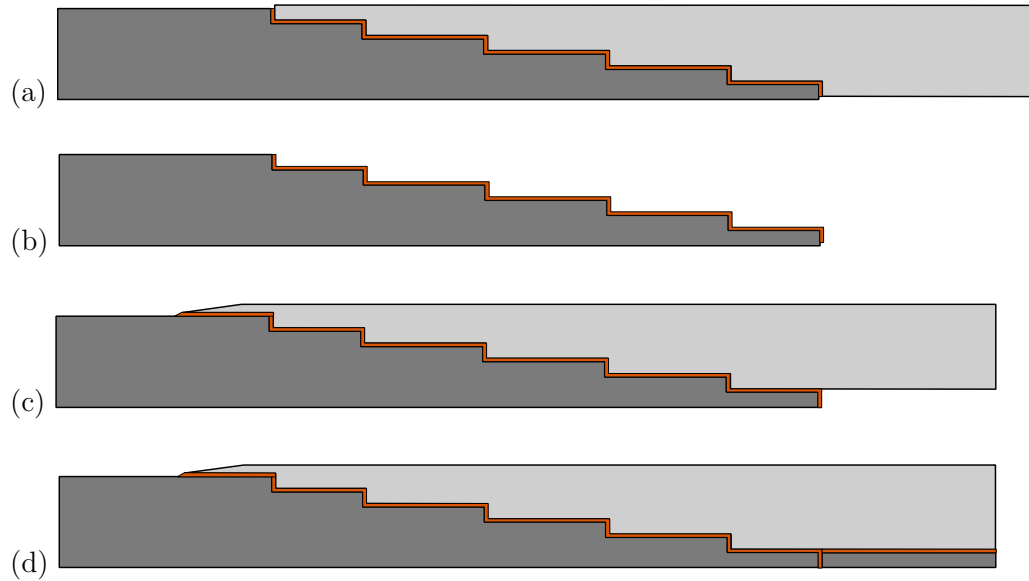


Figure 8.8 Modification of previous step lap joint (Configuration 2) with a new top overlap adherend

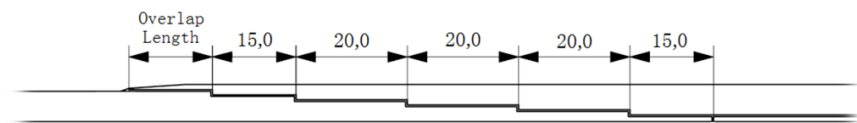


Figure 8.9 Overlap step lap joint optimisation; dimensions in mm and filler adherend placed on bottom right hand end with a 0.3mm thick bondline

The variable length outer overlap is defined in Figure 8.9. Each of the steps consists of four plies with the same orientation as the parent structures. Once again a three-dimensional parametric study is conducted similar to Section 8.3.2 with the aim of optimising the ‘overlap length’ to improve the peak load carrying capability of the joint. Five models were analysed with the overlap length varied between 5mm - 17.5mm. From the results shown in Figure 8.10, an outer overlap length of 15mm provides the highest

failure load for the bonded step lap joint. This results in a total bondline overlap length of 105mm. The preliminary FEA results predict a peak load of 41kN achieved by this bonded overlap configuration. The hybrid specimen in this case consists of five countersunk fasteners placed central of each step aft of the initial overlap length. Due to the increase in thickness caused by the overlap, the filler adherend on the bottom right hand end of Figure 8.8(d) is used to maintain flushness, increase joint stiffness and reduce out of plane bending.

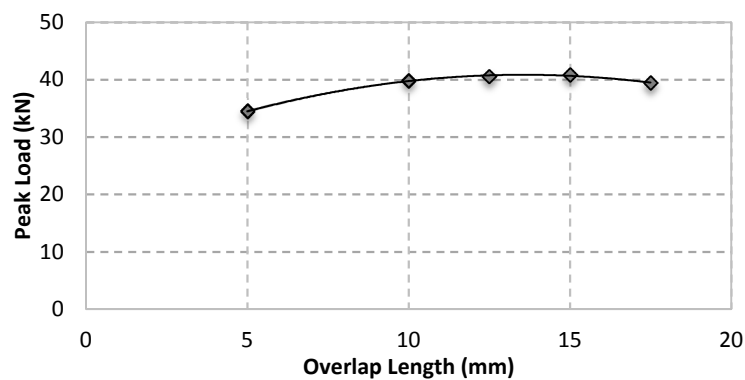


Figure 8.10 Optimising overlap length to improve the peak load carried by a bonded overlap step lap joint specimen

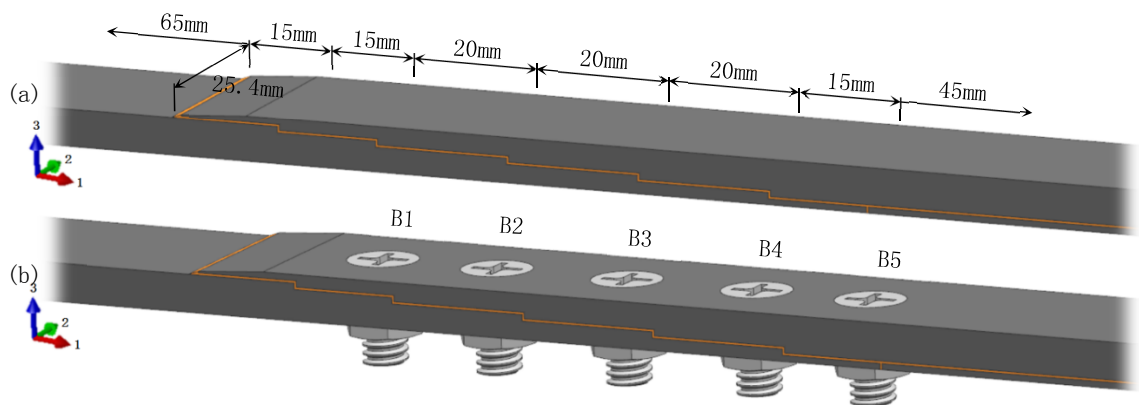


Figure 8.11 Two major geometry configurations; (a) Configuration 4.1 – six step bonded overlap lap joint; (b) Configuration 4.2 – six step hybrid overlap lap joint; B1-B5 = Bolt 1 – Bolt 5; bolts placed central of each step

Based on all of these results a total of four new configurations have been selected for further analysis followed by static and fatigue testing, Figure 8.7 and Figure 8.11:

Configuration 3.1 - Bonded flush step lap joint with 7 steps

Configuration 3.2 - Hybrid flush step lap joint with 7 steps and 5 countersunk fasteners

Configuration 4.1 - Bonded overlap step lap joint with 6 steps

Configuration 4.2 - Hybrid overlap step lap joint with 6 steps and 5 countersunk fasteners

8.4 Computational Results

The following sections numerically compare the new step lap joint designs (Configuration 3 and 4) with the previous bolted, bonded and hybrid step lap joint designs containing five steps (Configuration 2). Model setup follows the same procedure described in Section 8.3. Specimens containing an adhesive layer had four elements placed through its thickness whilst a longitudinal displacement in the (1) direction defined in Figure 8.7 and Figure 8.11 is placed on the right hand end of each specimen. Displacement in the (3) direction is constrained on the right hand end and a clamped boundary condition is applied on the left hand end.

8.4.1 Fastened Step Lap Joint

The fastener array in the new step lap joint designs as well as the previous step lap joint design is the same. A total of five countersunk bolts are used in each of the fastened configurations similar to Figure 7.1, Figure 8.7 and Figure 8.11. The three fastened step lap joint considered are:

Configuration 2.2 - Fastened flush step lap joint with five steps (five bolts)

Configuration 3.0 - Fastened flush step lap joint with seven steps (five bolts)

Configuration 4.0 - Fastened overlap step lap joint with six steps (five bolts)

Figure 8.12 shows the load-displacement relationship for the three fastened configurations. Overall there is no significant difference between the configurations due to the similar fastener array. The highest joint stiffness is achieved by Configuration 4.0 due to the

larger joint thickness. Configuration 2.2 and 3.0 have very similar joint stiffness due to the same joint thickness. Configuration 3.0 does however have a marginally higher joint stiffness than Configuration 2.2 due to the larger overlap lap which results in greater friction between the adherends. The results overall show that the residual strength provided by the fasteners in a hybrid configuration is the relatively the same in all three cases, Figure 8.12.

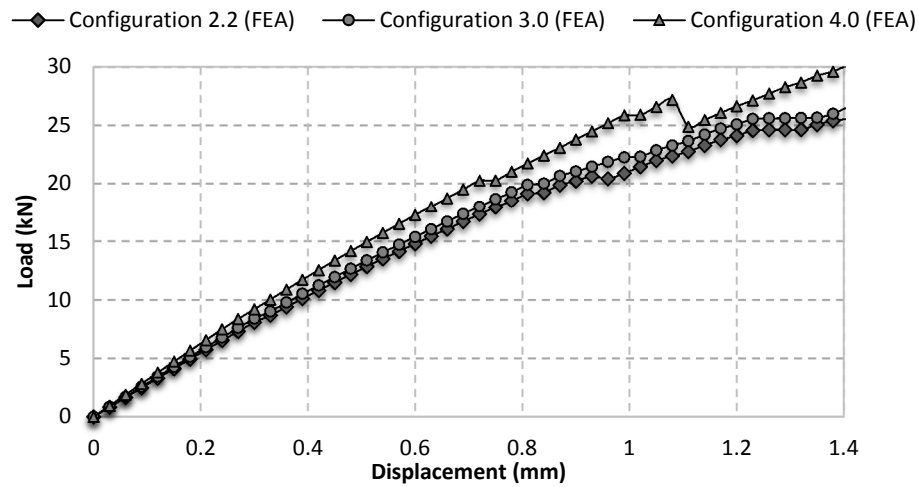


Figure 8.12 Load-displacement comparison of numerically modelled fastened step lap joint configurations for residual strength comparison

8.4.2 Bonded Step Lap Joint

A comparison is made between the three bonded step lap joint configurations in Figure 8.13. The previously tested flush bonded step lap joint with five steps (Configuration 2.1) has the lowest peak load failing after 34.13kN based on the numerical results. The bonded overlap step lap joint specimen containing six steps (Configuration 4.1) has the greatest joint stiffness. Once again this is due to the increase in thickness where a peak load of 40.85kN is achieved. This provides a 20% increase in failure load. The highest joint load was carried by the flush bonded step lap joint with seven steps. A peak load of 43.99kN is predicted from the detailed numerical model. This results in a 29% increase in failure load.

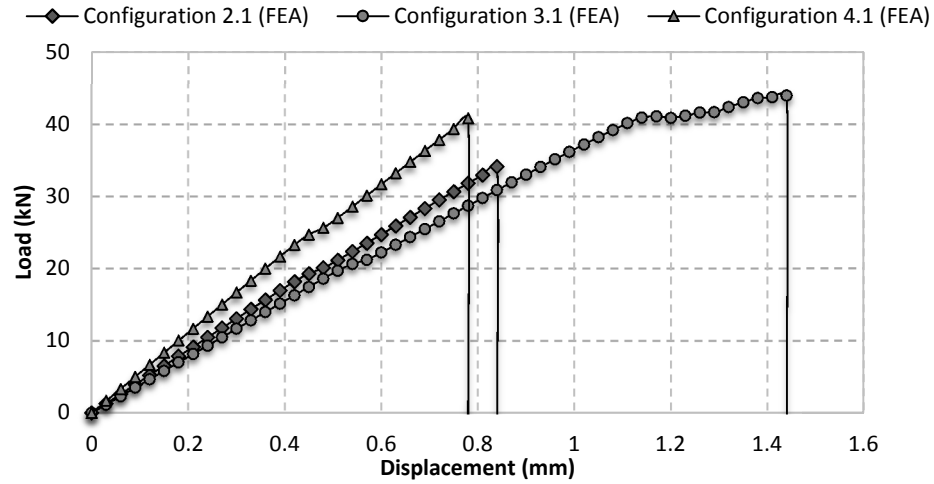


Figure 8.13 Load-displacement comparison of numerically modelled bonded step lap joint configurations

Overall, the new optimised step lap joint containing either six or seven steps have shown improvement over the step lap joint design containing five steps. Based on these results, the shear and normal stress distribution for Configuration 2.1, 3.1 and 4.1 is shown in Figure 8.14. All three stress distributions show peak stresses occurring at the start and end of each step. Configuration 2.1 reached its peak failure load of 34.13kN with a remote strain of 6054 $\mu\epsilon$; peak stresses occurred at the very ends of the overlap.

Configuration 4.1 containing an outer overlap in fact reduced peak stresses found at the outer butt joint region due to the tapered adherend. A peak load of 40.85kN was predicted by the numerical models in this case based on the maximum stress criteria. Peak normal and shear stress values occur at the very end of the overlap where the butt joint regions are present, i.e. adjacent to the filler adherend. This is the location in which failure originates from. Finally Configuration 3.1 failing at a peak load of 43.99kN has the maximum elongation of 1.44mm reaching a remote strain of 7440 $\mu\epsilon$. Based on the new bonded step lap joint designs, experimental tests are conducted to verify the results. Comparisons between the two are made in Section 8.5.2.

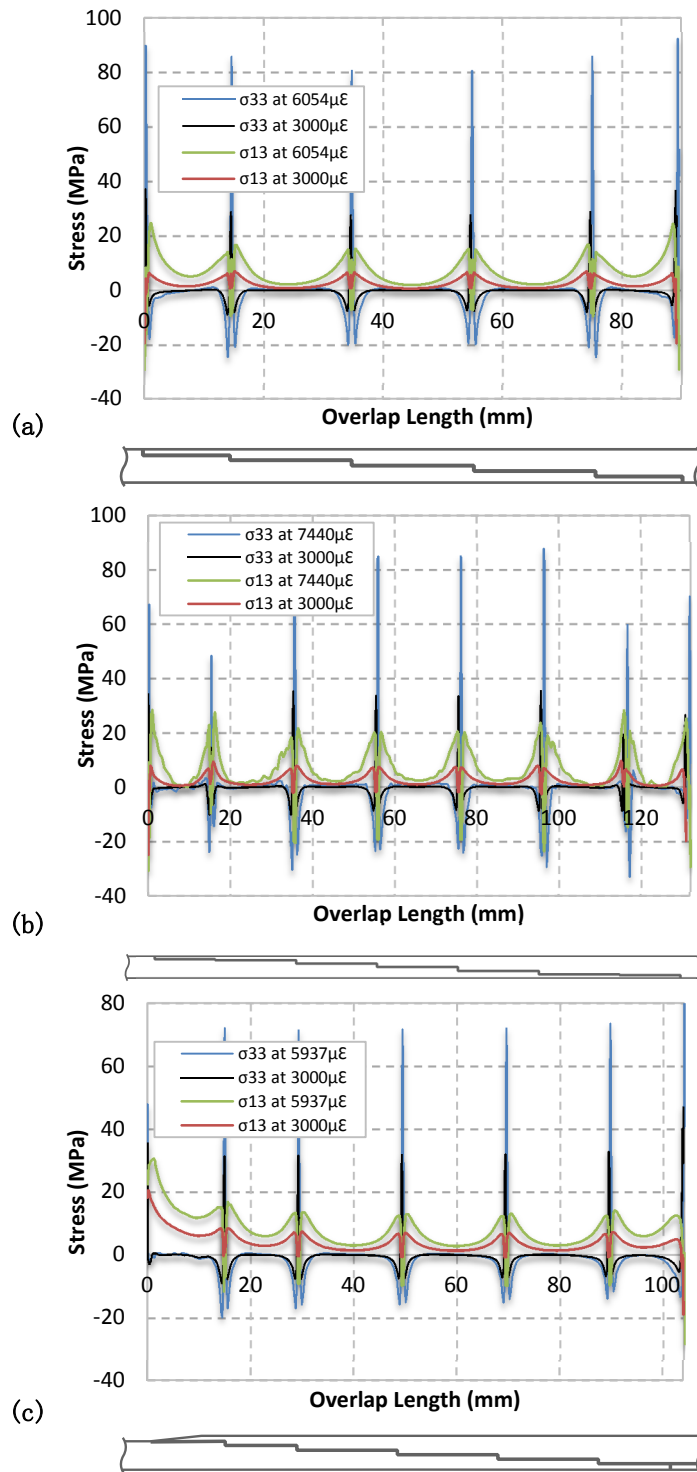


Figure 8.14 Comparison of adhesive stress distribution taken midway through the width of the specimens; (a) Configuration 2.1; (b) Configuration 3.1; (c) Configuration 4.1; σ_{33} - Normal Stress; σ_{13} - Shear Stress

8.4.3 Hybrid Step Lap Joint

The numerical load-displacement curves for the hybrid step lap joint configuration are presented in Figure 8.15. Once again peak stresses occur at the start and end of each step. Figure 8.16(a) shows the highest stress reached at the butt joint region located closest to the end of the overlap (closest to bolt 5). This step lap joint containing five steps had the lowest peak load of 34.99kN with a 1.02mm long displacement. Comparing the two new step lap joint configurations, only a 4% difference in peak load occurs. Configuration 4.2 is predicted to reach the highest peak load of 38.69kN.

Figure 8.16(b) and Figure 8.16(c) shows the stress distribution in each of the new step lap joint configurations. The stress distribution follows similarly to the equivalent bonded step lap joints discussed in Chapter 7. The presence of the five fasteners in each of these configurations significantly reduced the peak normal stresses (σ_{33}) present at the start and end of each step thus highlighting the significance of clamping provided by the fasteners.

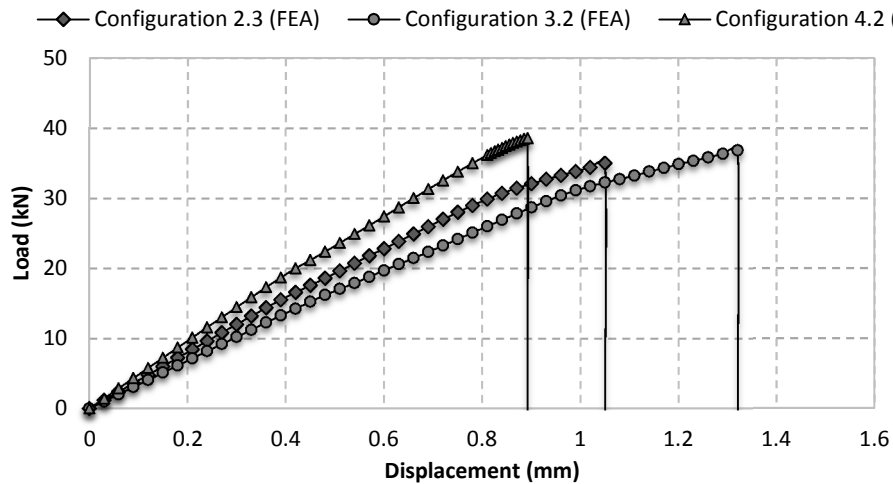


Figure 8.15 Load-displacement comparison of numerically modelled hybrid step lap joint configurations

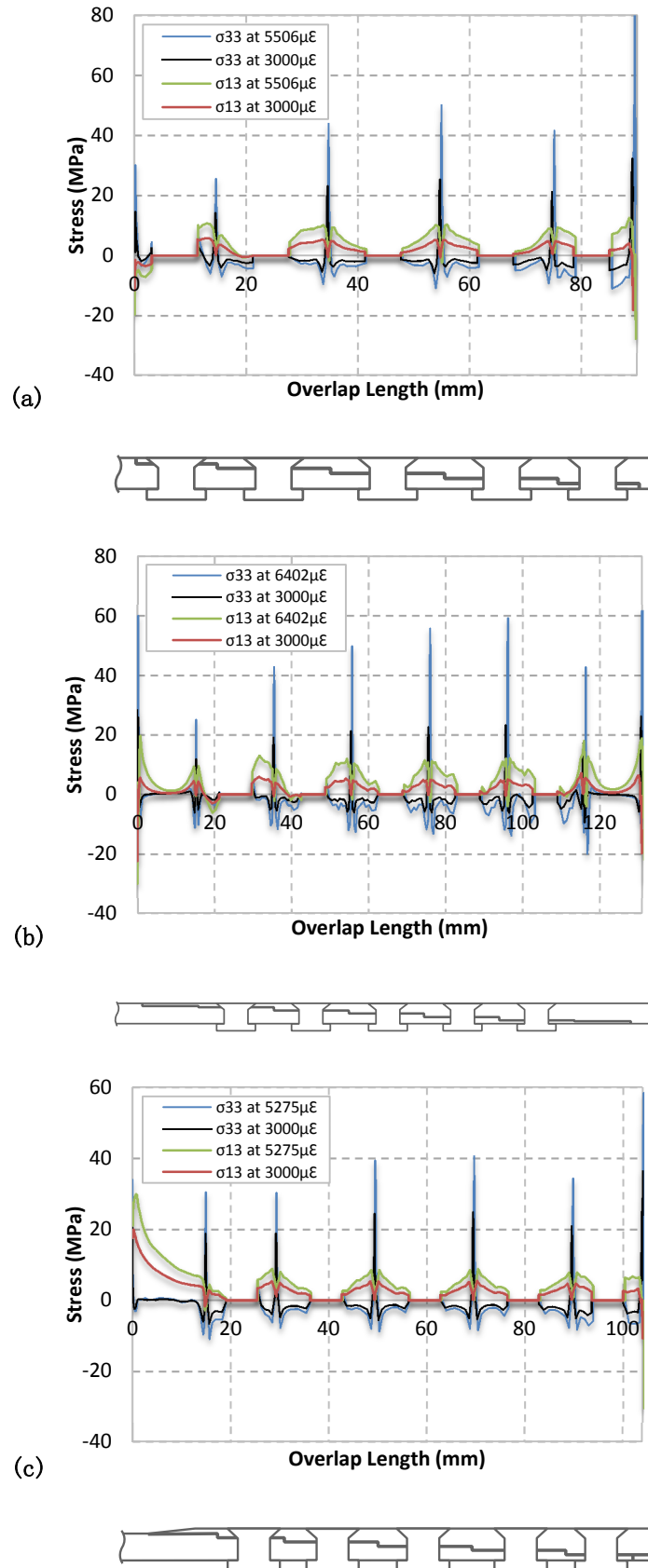


Figure 8.16 Comparison of adhesive stress distribution taken midway through the width of the specimens; (a) Configuration 2.3; (b) Configuration 3.2; (c) Configuration 4.2; σ_{33} - Normal Stress; σ_{13} - Shear Stress

Figure 8.17 shows the bolt load share comparison between the two new hybrid configurations. Fasteners have the highest contribution in Configuration 3.2 but only carry 3.52% of the total load before final failure occurs. Configuration 4.2 reaches a peak load share of 2.55% before final failure. Due to the higher remote strain in Configuration 4.2, a greater portion of the load is distributed amongst these fasteners. Overall it is clearly seen that increasing the applied load results in greater load share in hybrid configurations but the overall contribution is minimal compared to the bonded portion of the joint. The fact that specimens with a higher strain (greater overall elongation) result in increasing bolt load share - agrees with prior findings reported by Kelly [35] which states fasteners play a greater role in the load share of a joint when the modulus of the adhesive is reduced. Comparison between experimental and numerical load-displacement results is provided in the following sections.

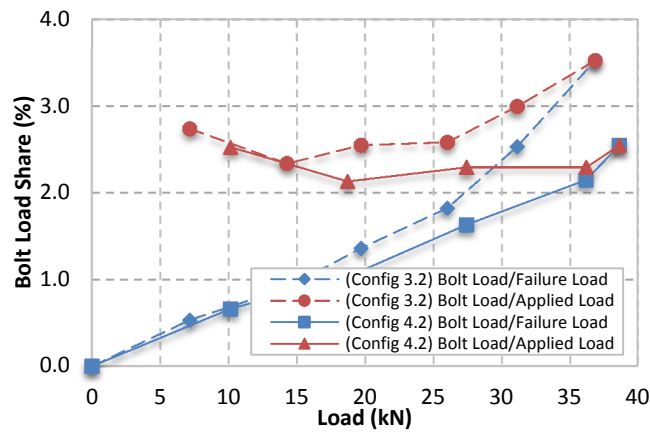


Figure 8.17 Bolt load share comparison between Configuration 3.2 and Configuration 4.2; Failure Load - the peak load carried by the configuration before final failure; Applied Load - total load carried by the configuration for a given point in time

8.5 Experimental Validation

Based on the numerical result previously discussed, it has been demonstrated that the two new step lap joint designs containing either six steps with an overlap or seven steps are predicted to have greater joint strength than the previous step lap joint containing five steps. In addition, the three fastened step lap joints provide approximately the same residual strength and are in fact weaker than their equivalent bonded and hybrid configuration. From a certification point of view, bonded and hybrid joint repairs are not

widely seen in aircraft structures. Hence an experimental test plan is conducted to static test the individual bonded and hybrid joint strengths and compare them with their numerical models. Fatigue tests are also conducted based on the same block loading regime implemented in prior tests discussed in Chapters 4 and 6 [146, 159].

8.5.1 Specimen Manufacture and Methodology

Based on the numerical results discussed in Section 8.4, a 24 ply thick panel made from HexPly M18/1/G939 carbon fibre prepreg was cured in an autoclave. This is the same material previously used to test the step lap joint containing five steps discussed in Chapter 6 [159]. Specimens were machined to size using an NC machine followed by machining the individual steps. The surfaces were then prepped for bonding. This involves abrading the adherends with ScotchBrite 7447 followed by degreasing using Methyl Ethyl Ketone (MEK) then blasted with 50 micron diameter aluminium oxide grit propelled with high purity nitrogen gas which is also used to remove excess grit; the same method discussed in Chapter 3. Figure 8.18 shows some of the bonded configurations after cured in an autoclave. Overall all specimens have a uniform 0.3mm thick bondline whilst Configuration 4.1 contains an adhesive spew fillet at the end of the outer overlap and a filler adherend located on the bottom right hand of the specimen.



Figure 8.18 Bonded step lap joint configurations cured in an autoclave at 121°C for 90min; Configuration 4.1 - top; Configuration 3.1 - bottom

Specimens containing fasteners had holes machined after the bondline was cured. This removes complexities involved in accounting for bondline offsets between adherends and countersunk depths for the thinner steps whilst also allowing for the installation and removal of fasteners at any time.

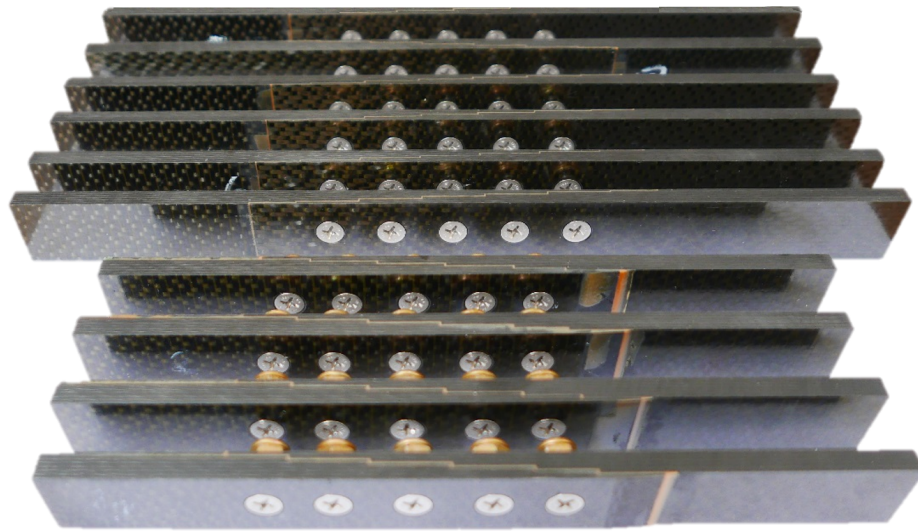


Figure 8.19 Hybrid step lap joint configurations cured in an autoclave at 121°C for 90min; Configuration 3.2 - top; Configuration 4.2 - bottom

After specimen assembly, static and fatigue tests were conducted on an INSTRON 1342 machine with a 100kN load cell controlled by a computer running MTS software. Static tests were conducted on all four specimen configurations at a rate of 1mm/min with axial load and displacement measurements recorded until catastrophic failure. Fatigue tests were conducted based on a block loading regime similar to Chapters 4 and 6 at a frequency of 5Hz and a stress ratio ($R = \sigma_{\min} / \sigma_{\max}$) of 0.1.

8.5.2 Static Test Results

Experimental load-displacement data for the two new bonded and two new hybrid step lap joint configurations are compared to the numerical results in this section. Figure 13 shows the load-displacement comparison. The predicted peak failure load matches closely to the average experimental test data. The trend also shows that an overlap step lap joint with six steps has a greater stiffness than a specimen with seven steps. In addition, hybrid step

lap joints have lower joint stiffness than their bonded joint counterpart due to the reduced bond area.

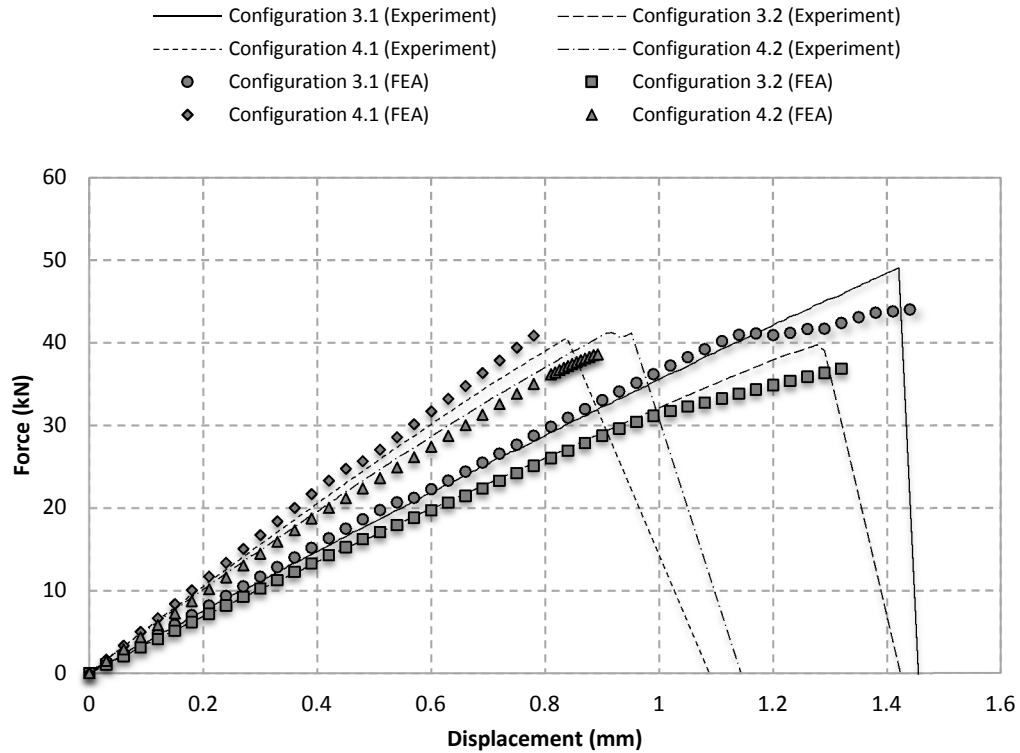


Figure 8.20 Comparison of static load-displacement results for four specimen Configurations 3.1, 3.2, 4.1 and 4.2 numerically analysed and tested experimentally

The numerical results in this case provided conservative estimates for failure load with the exception of Configuration 4.1 which over predicted failure load by 4.5% (40.85kN). Both numerical and experimental data highlighted that a bonded flush step lap joint with seven steps (Configuration 3.1) reaches the highest peak load limit (49.06kN experimentally). The configuration is able to achieve almost a 70% load recovery compared to a pristine undamaged parent structure which is an 18% increase over the previous step lap joint design containing five steps in a hybrid setup (Configuration 2.3). This thereby highlights that it is not only beneficial to increase the number of steps in these thick joint repairs but also important to minimise the outer step heights to reduce peak peeling stresses present at the outer ends of the overlap.

Overall across the four specimen configurations experimentally and numerically tested, a high degree of accuracy is seen using the MCT progressive damage model in predicting

failure. By using orthotropic material properties for the adherends, elastic-perfectly-plastic material data for the adhesive and by carefully modelling the contacts and frictional behaviour, reliable joint predictions are possible using numerical models.

8.5.3 Fatigue Test Results

Fatigue tests are carried out on the same 100kN INSTRON 1342 machine. Note that the block loading regime covers the vicinity of the 3000 $\mu\epsilon$ region which aircraft components are subjected to during flight [141, 142]. An extensometer is used to correlate this strain to load; Table 8.2 identifies the block loading regime used.

A number of fatigue tests were conducted for each of the four new specimen configurations. From the results shown in Table 8.3, the two hybrid joint configurations (Configuration 3.2 and 4.2) have the highest fatigue resistance than their bonded joint counterparts (Configuration 3.1 and 4.1). Compared to the original bonded step lap joint configuration containing five steps (Configuration 2.1), Configuration 3.1 has a 95% improvement in fatigue resistance based on the block loading regime used. This is a significant improvement in durability with only a 40mm increase in bond length. Thus these results clearly show that by carefully designing a bonded joint by minimising peak stresses present at the ends of the overlap, a significant improvement in joint strength and fatigue resistance is achievable.

Table 8.2 Block loading regime – strain amplitude increased every 10^5 cycles; frequency=5Hz, r-ratio=0.1

Cycles (N)	Strain ($\mu\epsilon$)	Upper limit (kN)	Lower limit (kN)
100,000	1000	6.30	0.63
200,000	2000	12.60	1.26
300,000	3000	18.90	1.89
400,000	4000	25.20	2.52
500,000	4500	28.35	2.84
600,000	5000	31.50	3.15
700,000	5500	34.65	3.47

Table 8.3 Fatigue resistance of four specimen configurations subjected to a block loading regime

Type	Failure Load (kN)/strain ($\mu\epsilon$)	Cycles to Failure (n)	Standard Deviation (n)
Configuration 2.1	18.90/3000	214,973	3,216
Configuration 2.3	28.35/4500	400,103	n/a
Configuration 3.1	28.35/4500	419,201	9,784
Configuration 3.2	28.35/4500	475,309	16,491
Configuration 4.1	18.90/3000	266,046	13,563
Configuration 4.2	31.50/5000	527,976	13,568

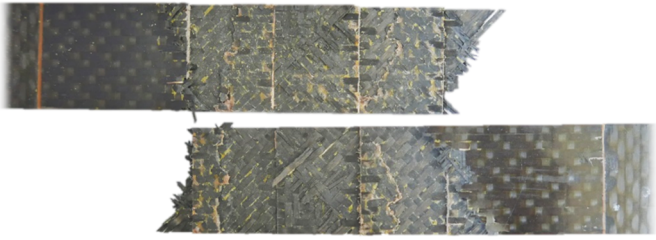

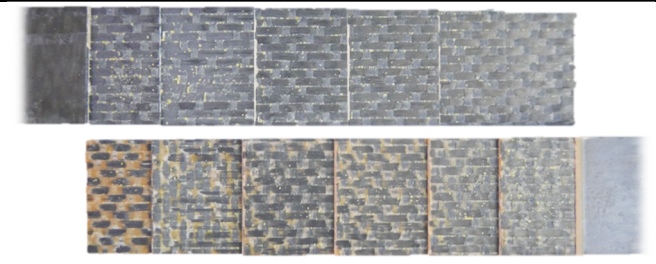
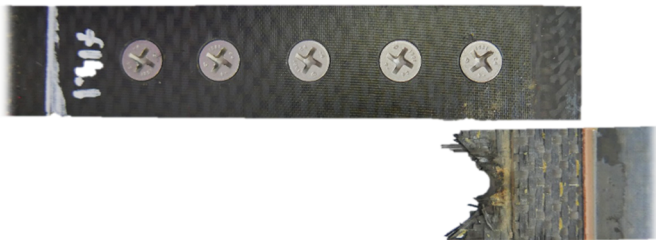
Configuration 4.1 and 4.2, containing the overlap step with a filler adherend also produced a higher fatigue resistance compared to the original bonded and hybrid step lap joint configuration containing five steps (Configuration 2.1 and 2.3). Configuration 4.1 produced a 23.8% improvement in fatigue resistance whilst Configuration 4.2 produced a 32.0% improvement. Overall although a significant increase in fatigue resistance is seen in the new bonded step lap joint configurations, the hybrid step lap joints still have superior fatigue durability over their bonded step lap joint counterparts. This highlights the importance of clamping pressure provided the fasteners which suppress rapid crack growth and add residual strength to the joint repair which is vital for certification.

8.6 Discussion

Experimental results have shown that Configuration 4.1 and 4.2 produce very similar static strength characteristics. Based on the experimental results, the bonded joint Configuration 3.1 catastrophically fails after 49.06kN which is 20.1% higher than its hybrid joint counterpart; Configuration 3.2. This result suggests it may be possible to achieve suitable joint performance from a bonded joint which is comparable to a hybrid joint. However the presence of initial bondline defects will reduce joint efficiency whilst hybrid joints offer the added residual strength. Overall under static test conditions, a specimen with seven steps containing thin outer steps and thicker inner steps is more efficient in a bonded setup. However under fatigue cases, hybrid configurations are still more beneficial due to the added clamping pressure from the fasteners which improve fatigue performance.

Table 8.4 shows the failed joints after fatigue testing the four new configurations. Damage in Configuration 4.1 occurred along the entire bondline overlap. Failure in this case was due to first-ply failure originating from the step closest to the filler adherend where a butt joint region is present. Here ‘first ply’ is defined as the initial ply that is in contact with the bondline in the specimen. Failure in Configuration 4.2 originated from the tapered overlap step. The adhesive spew can clearly be seen on the right hand side in Table 8.4. This is the thinnest section along the entire joint region. Failure initiates by the adhesive spew cracking along its width which then results in first ply failure in the top adherend. Final failure occurs by net tension failure along the right most fastener.

Table 8.4 Failure of four step lap joint configurations fatigue tested using a block loading regime

Configuration 3.1

Configuration 3.2

Configuration 4.1

Configuration 4.2


From Configuration 3.1 in Table 8.4, failure does not occur at the ends of the bondline overlap; instead failure occurs at the start of the four ply thick steps. This is the location of peak normal stresses resulting in fibre pull-out and net tension failure. For Configuration 3.2 the adherend fails at the end of the second step (left hand side). It must also be noted that further improvements may be possible if the ply orientation was not fixed.

Overall the results discussed here clearly demonstrate that joint strength and durability for both bonded and hybrid step lap joints can significantly improve by optimising the individual step heights let alone varying the number of steps and step lengths. In addition to this information, if a flush repair is not required, a simple overlap step can be employed to reduce peak peeling stresses present at the ends of the bondline overlap. This has the advantage of minimising the repair area whilst still achieving high strength and resistance to failure. Through the series of parametric models conducted using Abaqus CAE, four new step lap joint design were analysed and tested. The new bonded Configuration 3.1 achieved the highest peak load of 49.06kN which increased the load recovery to nearly 70% for step lap joint repair as opposed to 52% for the previous hybrid step lap joint with five steps discussed in Chapters 6 and 7. The hybrid configurations did however achieve the greatest durability with Configuration 4.2 failing after 527,976 cycles which is a 32% increase in fatigue resistance than Configuration 2.3.

8.7 Chapter Summary

Through the parametric study conducted in Abaqus, four new step lap joint configurations were experimentally and numerically tested. The aim is to achieve higher joint strength and fatigue durability compared to a bonded and hybrid step lap joints containing five steps. The parametric study confirmed that increasing the number of steps in a joint is more beneficial than increasing step length. Furthermore, optimising the ply orientation for each joint configuration will result in better joint efficiency. The study shows that by varying the individual step heights, similar if not better joint efficiency can be achieved than a joint with more steps and a constant step height. This presents the advantage of minimising the joint region particularly in repair cases by ensuring further damage is not caused to adjacent pristine regions during the repair procedure. The numerical work conducted using the micromechanical MCT progressive failure model and non-linear adhesive properties showed good comparison between FEA with experimental results. The

highest peak load of 49.06kN was achieved by the bonded joint configuration containing seven steps with a 130mm long overlap (Configuration 3.1). This improved the joint efficiency to almost 70% compared to a maximum joint efficiency of 52% achieved by the previous step lap joints containing five steps discussed in Chapters 6 and 7.

The overlap step lap joint specimens (Configuration 4.1 and 4.2) containing a 105mm long overlap were also produced with the aim of minimising early crack initiation commonly originating from the outer butt joint regions. Experimental results found that the hybrid joint Configuration 4.2 produced the highest fatigue performance of 527,976 cycles based on the block loading regime used. The hybrid joint Configuration 3.2 with seven steps failed after 475,309 cycles. All four configurations tested achieved better static and fatigue performance than a bonded and hybrid specimen containing five steps. Although under static test cases Configuration 3.1 had a peak load 25.5% higher than Configuration 3.2, fatigue test results show hybrid joints have superior durability. Hence, the relative static strength characteristics of a joint should not be used as an estimate for joint life. Overall the clamping pressure provided by the countersunk bolts aid in delaying sudden crack propagation and minimising peak peeling stresses which may typically be found in bonded joints. This aids in significantly increasing joint performance and durability and may assist in hybrid joint certification for aircraft structures.

Summary and Conclusions

The primary aim of this dissertation was to compare the relative strengths and durability of mechanically fastened, bonded and hybrid joint configurations for composite aircraft repair. Based on this information, the suitability and efficiency of the three joint types were dependent on the design and application. As a result, this research was broken up into two key stages; Stage 1 focuses on thin joint repair and Stage 2 focuses on thick joint repair.

The move towards light weight high stiffness structures that have good fatigue durability and corrosion resistance has led to the move from metal structures to composite structures. With this brings the added concern of certifying new components as they must meet the same structural integrity and safety requirement of those in metals. Hence, this is where the challenge lies. Bonded joints are currently regarded as structurally efficient repair methods for composite materials however improper process control can result in weak bonds that may not be detected using non-destructive inspection methods (NDI), additionally the failure method is catastrophic making certification quite challenging. This has led to investigating hybrid joint repairs which have gained more attention in recent years. If designed properly, they can provide the structural efficiency of bonded joints with the reliability of mechanically fastened joints.

Studies have shown the mechanical fasteners in a hybrid joint do not take part in the joint, it is only after the bondline is damaged where they begin play an important role. However properly understanding the failure mechanisms, load distributions and efficiency of these joints has seen limited research in current literature. Consequently whether or not these joints present much advantage over bonded joint repairs is not well understood. This has led to the research discussed as part of this dissertation where mechanically fastened, bonded and hybrid joints using similar configurations and repair design are experimentally tested to determine the static and fatigue strength, as well as numerically analysed to gain a better understanding of the repair behaviour.

9.1 Major Findings

In developing the proposed method, many supplementary aspects were investigated and their findings reported. The main conclusions obtained from this investigation and the results obtained from the experimental and numerical studies are presented in the following sections.

Two literature review papers were initially published as part of this work, the details are shown below:

- Nabil. Chowdhury, W. K. Chiu, J. Wang, "Review on the fatigue of composite hybrid joints used in aircraft structures", *Advanced Materials Research*, 2015. Vol 891-892, pp. 1591-1596
- Nabil. Chowdhury, W. K. Chiu, J. Wang, "A review of damage tolerant design, certification and repair in metals compared to composite materials", *Advanced Materials Research*, 2015. Vol 891-892, pp. 1597-1602

9.1.1 Experimentally Testing Thin Double Lap Joint Repairs

Stage 1 of the research focused on static and fatigue testing thin double lap joint repairs in a riveted, bonded and hybrid configuration. The aim was to provide a benchmark comparison between the three joint types in addition to assessing the effects of bondline defects such as initially cracks and weak bonds. HexPly M18/1/G939 carbon fibre prepreg and FM300-2K film adhesive were selected as the primary materials of choice as they are structural aerospace grade materials currently used in a number of aircrafts in service.

Static tests were conducted on a total of eight different specimen configurations using an Instron 100kN servo-hydraulic machine at a rate of 1mm/min until failure. Fatigue tests were also conducted using the same 100kN Instron machine using a block loading regime. The following conclusions were drawn from the experimental tests:

- (i) Under static test conditions, a purely riveted specimen Configuration 1.2 with six rivets arranged in a square array has the lowest joint stiffness compared to a bonded and hybrid joint specimen. Failure in this case is due to bearing failure which is a slow mode of failure.
- (ii) Under static test conditions, there were no significant difference in the peak load achieved by Configuration 1.1 (bonded) and 1.3 (hybrid). The mode of failure in both cases was catastrophic.
- (iii) A hybrid specimen Configuration 1.4 containing three rivets was arranged in a staggered array and cured in an oven. This configuration was produced to determine whether the clamping pressure provided by the rivets is sufficient for curing the bondline. Result found that joint stiffness is maintained however peak load is reduced by 2.6% compared to hybrid Configuration 1.3 cured in an autoclave.
- (iv) Defective joint specimen Configuration 1.5 and 1.6 produced similar load-displacement graphs as their pristine specimen Configuration 1.1 and 1.3 respectively. Peak load achieved was marginally lower than their pristine counterparts due to the presence of the initial 2mm long crack.
- (v) Defective specimen Configurations 1.7 and 1.8 containing a semi-cured adhesive layer of FM300-2K film adhesive cured at 90°C for 60 minutes failed significantly earlier than their pristine counterparts. The semi-cured adhesive layer maintained joint stiffness but produces a weak bond. As a result, the bonded Configuration 1.7 failed after only 16.87kN followed by catastrophic failure. The presence of rivets in a hybrid configuration with the same semi-cured adhesive layer failed after 35.29kN. The rivets improved the bond strength by 20% and was able to carry the remaining joint load after bondline failure. This highlighted a potential failsafe mechanism provided by a hybrid configuration which allows damage detection prior to catastrophic failure.

The work highlighted in this section has been published in the following journal:

- Nabil. Chowdhury, W.K. Chiu, J. Wang, P. Chang, “Static and fatigue testing thin riveted, bonded and hybrid carbon fibre double lap joints used in aircraft structures”, *Composite Structures*, 2015. Vol 121, pp. 315-323

9.1.2 Numerical Analysis of Thin Double Lap Joint Repairs

Numerical analysis was conducted using Abaqus CAE to predict the joint strength of the double lap joint configurations experimentally tested. Three-dimensional models containing orthotropic material properties for the adherends and elastic-perfectly-plastic material data for the adhesive is used. Fastener surface contact and frictional forces are also included in the models while the Multicontinuum Theory (MCT) is used to simulate the progressive damage of the composite material. The results were able to reliably predict the individual joint strengths under static conditions whilst the Strain Energy Release Rate (SERR) method provided further insight into the fatigue behaviour of the bonded and hybrid double lap joint configurations. The following highlights the main conclusions gathered:

- (i) The specimen models were initially calibrated by varying the matrix and fibre degradation parameters as part of MCT. Optimal values were 0.01 and 0.35 for the fibre and matrix respectively.
- (ii) MCT was able to accurately capture the joint stiffness and peak load achieved by the various double lap joint configurations. Slightly conservative results were obtained for the defective bonded Configuration 1.5 and hybrid specimen Configuration 1.6 containing a 2mm long initial crack.
- (iii) Peak stresses occurred at the ends of the overlap in the bonded and hybrid joint configurations. These values were however marginally reduced for hybrid joint cases. In addition, the fasteners in a hybrid joint configuration played a negligible role in the load carrying capability for an intact bondline. The fasteners play a more critical role once the bondline is damaged or a weak bond is present.
- (iv) The SERR provides an effective method of comparing the relative fatigue performance of bonded and hybrid joint specimens by artificially placing cracks of various lengths along the length of the specimen. The SERR can be determined using the displacement field method and according to Paris's Crack growth model,

the higher the SERR the higher the crack growth rate. Using this method, it was found a hybrid joint configuration has a significantly lower crack growth rate than a bonded double lap joint. The fasteners place vital clamping pressure which suppress rapid crack growth thereby increasing fatigue resistance.

- (v) The positions of the fasteners also play an important role in improving the durability of the joint. From the analysis conducted, fasteners placed closer to the ends of the bondline overlap help suppress rapid crack growth.

The work highlighted in this section has been published in the following journal:

- Nabil. Chowdhury, J. Wang, W.K. Chiu, P. Chang, “Experimental and finite element studies of thin bonded and hybrid carbon fibre double lap joints used in aircraft structures”, *Composites Part B: Engineering*, 2016. Vol 85, pp. 233-242

9.1.3 Experimentally Testing Thick Step Lap Joint Repairs

Stage 2 of the research focused on static and fatigue testing thick step lap joint repairs made from the same HexPly M18/1/G939 carbon fibre prepreg and FM300-2K film adhesive. A total of ten different specimen configurations were fabricated for testing. These included purely bonded step lap joints, purely bolted step lap joint with five countersunk bolts and hybrid step lap joints with either five countersunk bolts or three inner countersunk bolts. The specimens had a total of five steps with a 90mm long overlap. The aim was to provide a benchmark comparison between the different joint repair types. The following points summarise the main results:

- (i) The lowest joint stiffness under static test conditions was from the purely bolted step lap joint Configuration 2.2 failing due to hole elongation.
- (ii) Similar to Stage 1, there was no significant difference in peak load achieved by a bonded (Configuration 2.1) and the hybrid step lap joints (Configuration 2.3 and 2.4).
- (iii) Bonded and hybrid joint configurations with a 2mm long initial crack reached a peak load marginally lower than their pristine counterparts.
- (iv) The bonded Configuration 2.8 containing a semi-cured adhesive layer cured at 90°C for 60 minutes catastrophically failed at just 9.07kN. The hybrid Configuration 2.9 with five countersunk bolts and Configuration 2.10 with three

countersunk bolts were able to suppress rapid crack growth with the same semi-cured adhesive layer. Once the bondline failed, the fasteners carried the remaining load reaching a peak of approximately 25.32kN (Configuration 2.9). Failure in this case was now due to bearing.

- (v) Fatigue tests were conducted using a block loading regime similar to Stage 1 where strain amplitude was increased every 100,000 cycles until failure. Out of the ten joint configurations, the two hybrid step lap joints with five counter bolts had the greatest durability failing just over 400,000 cycles (Configuration 2.3 and 2.6).
- (vi) Under the given tension-tension loading regime, there is sufficient out of plane bending in the step lap joint configurations due to the load eccentricities at the end of each step. This increases the Mode I crack opening at the ends of the bondline resulting in early crack initiation. A guide plate system was later designed to suppress the out of plane bending and found to improve durability in a bonded Configuration 2.1 by 28% and a hybrid Configuration 2.4 with three countersunk bolts by 38%. Only a 2% increase in fatigue resistance occurred in hybrid Configuration 2.3. This suggests the outer two fasteners in Configuration 2.3 already help in significantly reducing Mode I crack opening at the ends of the overlap. Thus highlighting the importance of placing fasteners towards the ends of the bondline whilst still maintaining a suitable edge distance.
- (vii) Non-destructive inspection methods (NDI) using an Ultrasonic A-Scanner and a Thermal camera allowed the detection of damage as well as monitoring crack propagation during fatigue cases. Both techniques proved to be useful for detecting damage, especially Ultrasonic A-Scanning. The results concluding that damage detection may be possible whilst an aircraft is in flight as well as in a grounded state.

The work highlighted in this section has been published in the following journals:

- Nabil. Chowdhury, J. Wang, W.K. Chiu, P. Chang, “Static and fatigue testing bolted, bonded and hybrid step lap joints of thick carbon fibre/epoxy laminates used on aircraft structures”, *Composite Structures*, 2016. Vol 142, pp. 96-106

9.1.4 Numerical Analysis of Thick Step Lap Joint Repairs

Similar to Stage 1 of this dissertation, numerical analysis was conducted on the various step lap joint configurations tested in Stage 2. Progressive damage was implemented using the Multicontinuum Theory (MCT) for the three-dimensional finite element models. The following conclusions were drawn from the analysis:

- (i) MCT was once again able to accurately capture the joint stiffness in the various, bolted, bonded and hybrid configurations. The maximum stress based criteria was used to define the point of failure. In all bonded and hybrid step lap joint configurations failure was due to delamination at the first ply nearest to the bonded region.
- (ii) Peak stresses occur at the ends of the bondline overlap which are further reduced by the presence of fasteners in a hybrid configuration. The fasteners in a hybrid Configuration 2.3 with five countersunk bolts and Configuration 2.4 with three countersunk bolts only carry 3.27% and 2.08% of the total load of the joint respectively for an intact bondline.
- (iii) The Strain Energy Release Rate (SERR) was determined for the bonded Configuration 2.1 and hybrid Configuration 2.3 and 2.4. The analysis showed that crack growth increases as soon a crack enters the next step.
- (iv) The clamping pressure provided by the fasteners in a hybrid configuration reduced the Mode I SERR values close to zero. The Mode II SERR values were similar between the bonded Configuration 2.1 and hybrid Configuration 2.4, although the initial SERR in Configuration 2.4 was less for small cracks which result in increasing durability.
- (v) The greatest reduction in SERR occurred in the hybrid Configuration 2.3 which highlighted the importance of once again placing fasteners close to the ends of the overlap to delay rapid crack growth. All of these results agreed with the experimental fatigue test results and hence provides a useful method of optimising fastener placement to further improve the fatigue resistance of hybrid joint configurations.

The work highlighted in this section has been published in the following journal:

- Nabil. Chowdhury, W.K Chiu, J. Wang, P. Chang, “Experimental and finite element studies of bolted, bonded and hybrid step lap joints of thick carbon

fibre/epoxy panels used in aircraft structures”, Composites Part B: Engineering, 2016. Vol 100, pp. 68-77

9.1.5 Thick Step Lap Joint Optimisation

The Stage 2 step lap joint configurations provided a benchmark comparison between bolted, bonded and hybrid configurations. An extension to the study was conducted to now further optimise the load recovery (joint efficiency) which was then compared to an undamaged parent structure made from the same material and ply orientation. Focus was placed on optimising the bonded and hybrid step lap joints by varying the individual step lengths, step heights and the number of steps whilst keeping the same 24 ply thick adherends used in Stage 1. The following points highlight the major findings:

- (i) A parametric study was conducted using Abaqus CAE which varied the individual step heights, lengths and number of steps in a bonded step lap joint configuration. The analysis found it is not only important to increase the number of steps and minimise the outer step lengths but also important in reducing the outer step heights to reduce peak stresses at the ends of the overlap. Based on this analysis a new bonded and hybrid step lap joint configuration containing seven steps and a 130mm long overlap with 2 ply thick outer steps was selected for further analysis and testing.
- (ii) Experimental static and fatigue tests using the same methodology as Stage 1 and 2 found almost 70% of the load is recovered in a bonded Configuration 3.1 as opposed to a maximum load recovery of 52% achieved by the hybrid Configuration 2.3 tested in Stage 2. Under fatigue, the bonded step lap joint Configuration 3.1 failed after 419,201 cycles which is a 95% improvement over Configuration 2.1.
- (iii) A new step lap joint was also modelled containing an outer overlap step with a tapered end. The design had a 105mm long bondline with a total of six steps with the addition of a filler adherend. This design eliminates one of the outer butt joint regions which result in early crack initiation under the given loading condition whilst additionally increasing joint stiffness which reduces the effects of out of plane bending.
- (iv) Experimental static tests showed a 55% and 58% load recovery by the new bonded Configuration 4.1 and hybrid step lap joint Configuration 4.2 containing six steps. Although there was a marginal improvement under static test conditions, when

fatigued the hybrid Configuration 3.2 achieved the greatest durability, failing after 527,976 cycles whilst the bonded Configuration 3.1 failed after 266,046 cycles.

- (v) Based on the numerical and experimental results, in order to improve both static strength and fatigue resistance of a step lap joint, it is not only important to increase the number of steps but also minimise the outer step lengths and steps heights. Increasing joint repair thickness has the advantage of suppressing out of plane bending which in turn improves fatigue resistance, especially for a hybrid joint repair.

The work highlighted in this section is currently under review in the following journal:

- Nabil. Chowdhury, W.K Chiu, J. Wang, P. Chang, “Optimisation of bonded and hybrid step lap joints of thick carbon fibre/epoxy panels used in aircraft structures”, Composite Part B: Engineering, Under Review

9.2 Recommendation for Future Work

Through this study, a thorough comparison between mechanically fastened, bonded and hybrid joint repair structures has been investigated for both thin and thick repair applications. Experimental and numerical analysis has been conducted to determine the joint repair behaviour and assess the effects of fastener placement to further improve repair efficiency. The results thus far conclude that hybrid joint repairs have superior durability over their bonded joint repair counterparts. Furthermore, the fasteners suppress rapid crack growth which enables damage detection prior to catastrophic failure. This is expected to greatly assist composite joint repair certification. The following recommendations for future work should be considered to further aid composite joint repair certification.

- (i) The effects of temperature and moisture conditions during fatigue of all specimen configuration were kept fixed at standard atmospheric conditions as part of this research. Investigating how different environmental conditions affect the durability of bonded and hybrid configurations will provide an important extension to the project.
- (ii) Scarf joint repairs are also commonly used for thick repair applications. Conducting experimental and numerical analysis on bolted, bonded and hybrid

scarf joints with similar geometry and overlap length will provide a useful comparison between the step lap joint configurations.

- (iii) Numerically analysing composite joint repairs under fatigue conditions is an area which has seen very limited research in the past. Developing computational models which work on fatigue failure predictions will provide further insight into the damage mechanisms and failure methods of composite materials.

Bibliography

1. Ogin, S.L., P. Brøndsted, and J. Zangenberg, *1 - Composite materials: constituents, architecture, and generic damage*, in *Modeling Damage, Fatigue and Failure of Composite Materials*, R. Talreja and J. Varna, Editors. 2016, Woodhead Publishing. p. 3-23.
2. Ireman, T., T. Nyman, and K. Hellbom, *On Design Methods for Bolted Joints in Composite Aircraft Structures* Composite Structures, 1993. **25**: p. 567-578.
3. Khudhayer, J.J. and A.R. Othman, *Fiber Reinforced Composite Structure with Bolted Joint - A Review*. Key Engineering Materials, 2011. **471-472**: p. 939-944.
4. Collings, T.A., *The Strength of Bolted Joints in Multi-Directional CFRP Laminates*. Composites, 1977. **8**(1): p. 43-55.
5. Hart-Smith, J., *Bolted and Bonded Joints*, in *ASM Handbook Volume 21*. 1998. p. 167-176.
6. Kelly, G., *Quasi-Static Strength and Fatigue Life of Hybrid (bonded/bolted) Composite Single-Lap Joints*. Composite Structures, 2006. **72**: p. 119-129.
7. Garnich, M.R. and A.C. Hansen, *A Multicontinuum Approach to Structural Analysis of Linear Viscoelastic Composite Materials*. Journal of Applied Mechanics, 1997. **64**(4): p. 795-803.
8. Key, C.T., S.C. Schumacher, and A.C. Hansen, *Progressive failure modeling of woven fabric composite materials using multicontinuum theory*. Composites Part B: Engineering, 2007: p. 247-257.
9. Seneviratne, W.P. and J.S. Tomblin, *Certification of Composite-Metal Hybrid Structures using Load-Enhancement Factors*. 2012, FAA Joint Advanced Materials and Structures (JAMS)/Aircraft Airworthiness and Sustainment (AA&S): Baltimore, MD.
10. Ye, L., *On fatigue damage accumulation and material degradation in composite materials*. Composites science and technology, 1989. **36**(4): p. 339-350.
11. Lee, L., J. Yang, and D. Sheu, *Prediction of fatigue life for matrix-dominated composite laminates*. Composites science and technology, 1993. **46**(1): p. 21-28.
12. Tang, R., Y.-J. Guo, and Y. Weitsman, *An appropriate stiffness degradation parameter to monitor fatigue damage evolution in composites*. International journal of fatigue, 2004. **26**(4): p. 421-427.
13. Hwang, W. and K.S. Han, *Fatigue of composites—fatigue modulus concept and life prediction*. Journal of Composite Materials, 1986. **20**(2): p. 154-165.
14. Rotem, A., *Residual strength after fatigue loading*. International journal of fatigue, 1988. **10**(1): p. 27-31.
15. Chou, P.C. and R. Croman, *Residual strength in fatigue based on the strength-life equal rank assumption*. Journal of Composite Materials, 1978. **12**(2): p. 177-194.

16. Barnard, P., R. Butler, and P. Curtis, *The strength-life equal rank assumption and its application to the fatigue life prediction of composite materials*. International Journal of Fatigue, 1988. **10**(3): p. 171-177.
17. Ben-Amoz, M., *A cumulative damage theory for fatigue life prediction*. Engineering Fracture Mechanics, 1990. **37**(2): p. 341-347.
18. Kliman, V., *Fatigue life estimation under random loading using the energy criterion*. International Journal of Fatigue, 1985. **7**(1): p. 39-44.
19. Wang, J., A. Banbury, and D. Kelly, *Evaluation of Approaches for Determining Design Allowables for Bolted Joints in Laminated Composites*. Composite Structures, 1998. **41**: p. 167-176.
20. Wang, H.-S., C.-L. Hung, and F.-K. Chang, *Bearing failure of bolted composite joints. Part I: experimental characterization*. Journal of Composite Materials, 1996. **30**(12): p. 1284-1313.
21. Valenza, A., V. Fiore, C. Borsellino, L. Calabrese, and G. Di Bella, *Failure map of composite laminate mechanical joint*. Journal of composite materials, 2007. **41**(8): p. 951-964.
22. Cooper, C. and G. Turvey, *Effects of joint geometry and bolt torque on the structural performance of single bolt tension joints in pultruded GRP sheet material*. Composite structures, 1995. **32**(1): p. 217-226.
23. Kinloch, A.J., *Adhesion and Adhesives: Science and Technology*. 1987: Springer.
24. Davis, M.J. and D. Bond, *Principles and Practise of Adhesive Bonded Structural Joints and Repairs*. International Journal of Adhesion and Adhesives, 1999. **19**: p. 91-105.
25. Vassilopoulos, A.P. and K. Thomas, *Fatigue of Fiber-Reinforced Composites*. Engineering Materials and Processes, 2011: p. 1-23.
26. Volkersen, O., *The Rivet-Force Distribution in Tension-Stresses Riveted Joints with Constant Sheet Thickness*. Luftfahrtforschung, 1938. **15**: p. 4-47.
27. Goland, M. and E. Reissner, *The Stresses in Cemented Joints*. Journal of Applied Mechanics 1944. **11**: p. A17-A27.
28. Hart-Smith, L.J., *The Goland and Reissner Bonded Lap Joint Analysis Revisited Yet Again - But This Time Essentially Validated*. Boeing Paper MDC 00K0036, To be published.
29. Hart-Smith, L.J., *Analysis and Design of Advanced Composite Bonded Joints*. 1974: NASA CR-2218, Douglas Aircraft Company.
30. Hart-Smith, L.J. *Design and Analysis of Adhesive-Bonded Joints*. in *First Air Force Conference Fibrous Composites in Flight Vehicle Design*. 1972. Air Force Flight Dynamics Laboratory.

31. Hart-Smith, L.J. *Advances in the Analysis and Design of Adhesive-Bonded Joints in Composite Aerospace Structures*. in *19th National SAMPE Symposium and Exhibition*. April 1974. Society for the Advancement of Material and Process Engineering.
32. Kweon, J.-H., J.-W. Jung, T.-H. Kim, J.-H. Choi, and D.-H. Kim, *Failure of Carbon Composite-to-Aluminium Joints with Combined Mechanical Fastening and Adhesive Bonding*. *Composite Structures*, 2006. **75**: p. 192-198.
33. Sun, C., K. Bhawesh, P. Wang, and R. Sterkenburg, *Development of Improved Hybrid Joints for Composite Structures*. *Composite Structures*, 2005. **35**: p. 1-20.
34. Hart-Smith, L.J., *Bonded-Bolted Composite Joints*. *Journal of Aircraft* 1985. **22.11**: p. 993-1000.
35. Kelly, G., *Load Transfer in Hybrid (Bonded/Bolted) Composite Single-Lap Joints*. *Composite Structures*, 2005. **69**: p. 35-43.
36. Barut, A. and E. Madenci, *Analysis of bolted-bonded composite single-lap joints under combined in-plane and transverse loading*. *Composite Structures*, 2009. **88**: p. 579-594.
37. Paroissien, E., M. Sartor, J. Huet, and F. Lachaud, *Analytical two-dimensional model of a Hybrid (Bolted-Bonded) Single-Lap Joint*. *Journal of Aircraft*, 2007. **44**: p. 573-582.
38. Matsuzaki, R., M. Shibata, and A. Todoroki, *Improving performance of GFRP/aluminium single lap joints using bolted/co-cured hybrid method*. *Composites Part A: Applied Science and Manufacturing*, 2008. **39**: p. 154-163.
39. Zhang, S. and D. Zhao, *Aerospace Materials Handbook*. 2012: CRC Press.
40. D/DM-10, A., *Standard Test Method for Bearing Response of Polymer Matrix Composite Laminates*. 2010, ASTM International West Conshohocken, PA, USA.
41. Handbook, M., *MIL-HDBK-17-2F: Composite Materials Handbook*. Polymer Matrix Composites: Materials Usage, Design, and Analysis, 2002. **17**.
42. Fu, M. and P.K. Mallick, *Fatigue of Hybrid (adhesive/bolted) Joints in SRIM Composites*. *International Journal of Adhesion and Adhesives*, 2001. **21**: p. 145-159.
43. Lee, Y.-H., D.-W. Lim, J.-H. Choi, J.-H. Kweon, and M.-K. Yoon, *Failure load evaluation and prediction of hybrid composite double lap joints*. *Composite Structures*, 2010. **92**: p. 2916-2926.
44. Campilho, R.D.S.G., M.F.S.F. de Moura, and J.J.M.S. Domingues, *Modelling single and double-lap repairs on composite materials*. *Composites Science and Technology*, 2005. **65**(13): p. 1948-1958.
45. da Silva, L.F.M., *Modeling of Adhesively Bonded Joints*. 2008: Springer Berlin Heidelberg.
46. Lee, W.-Y. and J.-J. Lee, *Fatigue behavior of composite patch repaired aluminum plate*. *Journal of composite materials*, 2005. **39**(16): p. 1449-1463.

47. Wang, J., A. Rider, M. Heller , and R. Kaye *Theoretical and Experimental Research into Optimal Edge Taper of Bonded Repair Patches Subject to Fatigue Loadings*. International Journal of Adhesion & Adhesives, 2005. **25**: p. 410-426.
48. Chalkley, P.D., C.H. Wang, and A.A. Baker, *Fatigue Testing of Generic Bonded Joints*. 2002, Defence Science and Technology Organisation: Fishermans Bend, Victoria 3207, Australia. p. 103-126.
49. Liechti, K., W. Johnson, and D. Dillard, *Experimentally determined strength of adhesively bonded joints*. Elsevier Applied Science Publishers Ltd, Joining Fibre-Reinforced Plastics, 1987: p. 105-183.
50. Cheuk, P.T., L. Tong, A.N. Rider , and J. Wang, *Analysis of Energy Release Rate for Fatigue Cracked Metal-to-Metal Double Lap Shear Joints*. International Journal of Adhesion and Adhesives, 2005. **25**: p. 181-191.
51. Baker , A., *Fatigue Life Recovery in Corroded Aluminium Alloys Using Bonded Composite Reinforcements*. Applied Composite Materials, 2006. **13**: p. 127-146.
52. Kaye, R.H. and M. Heller, *Through-thickness Shape Optimisation of Bonded Repair and Lap-Joints*. International Journal of Adhesion & Adhesives 2002. **22**: p. 7-21.
53. Heller, M. and R. Kaye, *Shape Optimisation for Bonded Repairs*, in *Advances in Bonded Composite Repair of Metallic Aircraft Structure*. 2002, Elsevier: UK.
54. Ojalvo, I.U., *Optimisation of Bonded Joints*. AIAA, 1985. **23**: p. 1578-1582.
55. Ratwani, M., *Characterization of fatigue crack growth in bonded structures-crack growth prediction in bonded structures*. Air Force Flight Dynamics Laboratory AFFADL-TR-77-31, 1977. **1**.
56. Baker, A. and R. Jones, *Bonded repair of aircraft structures*. Dordrecht, The Netherlands, 1988.
57. Arendt, C. and C. Sun. *Bending effects of unsymmetric adhesively bonded composite repairs on cracked aluminum panels*. in *NASA CONFERENCE PUBLICATION*. 1994. NASA.
58. Sun, C., J. Klug, and C. Arendt, *Analysis of cracked aluminum plates repaired with bonded composite patches*. AIAA journal, 1996. **34**(2): p. 369-374.
59. Bachir Bouiadjra, B., F. Benyahia, A. Albedah, B.A. Bachir Bouiadjra, and S.M.A. Khan, *Comparison between composite and metallic patches for repairing aircraft structures of aluminum alloy 7075 T6*. International Journal of Fatigue, 2015. **80**: p. 128-135.
60. Chue, C.-H., W.-C. Chou, and T.J.-C. Liu, *The effects of size and stacking sequence of composite laminated patch on bonded repair for cracked hole*. Applied Composite Materials. **3**(6): p. 355-367.
61. Mollenhauer, D.H., B. Fredrickson, G. Schoeppner, E.V. Iarve, and A.N. Palazotto. *Analysis and Measurement of Scarf-Lap and Step-Lap Joint Repair in Composite Laminates*. in *16th International Conference on Composite Materials*. 2007. Kyoto, Japan.

62. Kumar, S.B., I. Sridhar, S. Sivashanker, S.O. Osiyemi, and A. Bag, *Tensile Failure of Adhesively Bonded CFRP Composite Scarf Joint*. Materials Science and Engineering 2006. **132**: p. 113-120.
63. Whittingham, B., A.A. Baker, A. Harman, and D. Bitton, *Micrographic studies on adhesively bonded scarf repairs to thick composite aircraft structure*. Composites Part A: Applied Science and Manufacturing, 2009. **40**(9): p. 1419-1432.
64. Hart-Smith, L.J. *Further Developments in the Design and Analysis of Adhesive-Bonded Structural Joints*. in *American Society for Testing and Materials Symposium on Joining of Composite Materials*. 1980. Minneapolis, Minnesota.
65. Van Blaricum, T.J., P. Bates, and R. Jones, *An Experimental Investigation Into the Effect of Impact Damage on the Compressive Strength of Step Lap Joints*. Engineering Fracture Mechanics, 1989. **32**(5): p. 667-674.
66. Seneviratne, W.P., J.S. Tomblin, and T. Crevens. *Durability and Residual Strength Assessment of F/A-18 A-D Wing-Root Stepped-Lap Joint*. in *AIAA*. 2011. Virginia.
67. Standard, A., *D3039-03, Standard test method for tensile properties of polymer matrix composite materials*. ASTM International, 2003.
68. Standard, A., *D3410/D3410M-03 (2008), Standard test method for compressive properties of polymer matrix composite materials with unsupported gage section by shear loading*. ASTM International, 2008.
69. Standard, A., *D2344/D2344M-13, Standard Test Method for Short-Beam Strength of Polymer Matrix Composite Materials and Their Laminates*. ASTM International, 2013.
70. Bathias, C., *An Engineering Point of View about Fatigue of Polymer Matrix Composite Materials*. International Journal of fatigue, 2006. **28**: p. 1094-1099.
71. Post, N., J. Cain, K. McDonald, S. Case, and J. Lesko, *Residual Strength Prediction of Composite Materials: Random Spectrum Loading*. Engineering Fracture Mechanics, 2008. **75**: p. 2707-2724.
72. Van Paepegem, W. and J. Degrieck, *Effects of Load Sequence and Block Loading on the Fatigue Response of Fiber-Reinforced Composites*. Mechanics of Advanced Material Structures, 2002. **9**: p. 19-35.
73. Hashin, Z., *Failure criteria for unidirectional fiber composites*. Journal of applied mechanics, 1980. **47**(2): p. 329-334.
74. Autodesk. *Phenomenology of Composite Fatigue*. 2015; Available from: <http://help.autodesk.com/view/ACMPAN/2015/ENU/?guid=GUID-71BCDA2E-3011-4C67-821E-5C863BE881AC>.
75. Awerbuch, J. and H. Hahn, *Off-axis fatigue of graphite/epoxy composite*. Fatigue of fibrous composite materials, ASTM STP, 1981. **723**: p. 243-73.

76. Petermann, J. and A. Plumtree, *A unified fatigue failure criterion for unidirectional laminates*. Composites Part A: Applied Science and Manufacturing, 2001. **32**(1): p. 107-118.
77. Talreja, R. *Fatigue of composite materials: damage mechanisms and fatigue-life diagrams*. in *Proceedings of the Royal Society of London A: Mathematical, Physical and Engineering Sciences*. 1981. The Royal Society.
78. Fujii, T. and F. Lin, *Fatigue behavior of a plain-woven glass fabric laminate under tension/torsion biaxial loading*. Journal of composite materials, 1995. **29**(5): p. 573-590.
79. Fujii, T., S. Amijima, and K. Okubo, *Microscopic fatigue processes in a plain-weave glass-fibre composite*. Composites Science and Technology, 1993. **49**(4): p. 327-333.
80. Naik, R.A., S.R. Patel, and S.W. Case, *Fatigue damage mechanism characterization and modeling of a woven graphite/epoxy composite*. Journal of Thermoplastic Composite Materials, 2001. **14**(5): p. 404-420.
81. Passipoularidis, V. and T. Philippidis, *A Study of Factors Affecting Life Prediction of Composites Under Spectrum Loading*. Journal of Fatigue, 2009. **31**: p. 408-417.
82. Schön, J. and T. Nyman *Spectrum Fatigue of Composite Bolted Joints*. International Journal of Fatigue, 2002. **24**: p. 273-279.
83. Starikov, R. and J. Schön, *Quasi-static behaviour of Composite Joints with Protruding-Head Bolts*. Composite Structures, 2001. **51**: p. 411-425.
84. Hart-Smith, L.J. *Analysis Methods for Bolted Composite Joints Subjected to In-plane Shear Loads*. in *Agard 83rd Structures and Materials Panel Bolted/bonded Joints in Polymeric Composites*. 1996. Florence, Italy.
85. Katunin, A., K. Dragan, and M. Dziendzikowski, *Damage identification in aircraft composite structures: A case study using various non-destructive testing techniques*. Composite Structures, 2015. **127**: p. 1-9.
86. Crider, I. and S. Jeffrey, *Damage detection using Lamb waves for structural health monitoring*. 2007, DTIC Document.
87. Polimeno, U. and M. Meo, *Detecting barely visible impact damage detection on aircraft composites structures*. Composite Structures, 2009. **91**(4): p. 398-402.
88. Staszewski, W.J., S. Mahzan, and R. Traynor, *Health monitoring of aerospace composite structures – Active and passive approach*. Composites Science and Technology, 2009. **69**(11-12): p. 1678-1685.
89. Diamanti, K. and C. Soutis, *Structural health monitoring techniques for aircraft composite structures*. Progress in Aerospace Sciences, 2010. **46**(8): p. 342-352.
90. Leckey, C.A.C., M.D. Rogge, and F. Raymond Parker, *Guided waves in anisotropic and quasi-isotropic aerospace composites: Three-dimensional simulation and experiment*. Ultrasonics, 2014. **54**(1): p. 385-394.

91. Giurgiutiu, V. and J. Bao, *Embedded-ultrasonics structural radar for in situ structural health monitoring of thin-wall structures*. Structural Health Monitoring, 2004. **3**(2): p. 121-140.
92. Meola, C. and G.M. Carlomagno, *Impact damage in GFRP: New insights with infrared thermography*. Composites Part A: Applied Science and Manufacturing, 2010. **41**(12): p. 1839-1847.
93. Usamentiaga, R., P. Venegas, J. Guerediaga, L. Vega, and I. López, *Automatic detection of impact damage in carbon fiber composites using active thermography*. Infrared Physics & Technology, 2013. **58**: p. 36-46.
94. Meola, C. and G.M. Carlomagno, *Infrared thermography to evaluate impact damage in glass/epoxy with manufacturing defects*. International Journal of Impact Engineering, 2014. **67**: p. 1-11.
95. Maierhofer, C., P. Myrach, M. Reischel, H. Steinfurth, M. Röllig, and M. Kunert, *Characterizing damage in CFRP structures using flash thermography in reflection and transmission configurations*. Composites Part B: Engineering, 2014. **57**: p. 35-46.
96. López-Higuera, J.M., *Handbook of optical fibre sensing technology*. 2002: Wiley.
97. Caminero, M.A., S. Pavlopoulou, M. Lopez-Pedrosa, B.G. Nicolaisson, C. Pinna, and C. Soutis, *Analysis of adhesively bonded repairs in composites: Damage detection and prognosis*. Composite Structures, 2013. **95**: p. 500-517.
98. Ratcliffe, C., D. Heider, R. Crane, C. Krauthauser, M.K. Yoon, and J.W. Gillespie Jr, *Investigation into the use of low cost MEMS accelerometers for vibration based damage detection*. Composite Structures, 2008. **82**(1): p. 61-70.
99. Růžek, R., R. Lohonka, and J. Jironč, *Ultrasonic C-Scan and shearography NDI techniques evaluation of impact defects identification*. NDT & E International, 2006. **39**(2): p. 132-142.
100. Bull, D.J., S.M. Spearing, I. Sinclair, and L. Helfen, *Three-dimensional assessment of low velocity impact damage in particle toughened composite laminates using micro-focus X-ray computed tomography and synchrotron radiation laminography*. Composites Part A: Applied Science and Manufacturing, 2013. **52**: p. 62-69.
101. Solmaz, M.Y. and T. Topkaya, *Progressive Failure Analysis in Adhesively, Riveted, and Hybrid Bonded Double-Lap Joints*. The Journal of Adhesion, 2013. **89**: p. 822-836.
102. Pirondi, A. and F. Moroni, *Clinch-Bonded and Rivet-Bonded Hybrid Joints: Application of Damage Models for Simulation of Forming and Failure*. Journal of Adhesion Science and Technology, 2009. **23**: p. 1547-1574.
103. Kapidzic, Z., L. Nilsson, and H. Ansell, *Finite element modeling of mechanically fastened composite-aluminum joints in aircraft structures*. Composite Structures, 2014. **109**: p. 198-210.
104. Mayes, J.S., *Multicontinuum failure analysis of composite structural laminates*. 1999, University of Wyoming: ProQuest Dissertations & Theses Global. p. 161.

105. Hansen, A.C. and M.R. Garnich, *A multicontinuum theory for structural analysis of composite material systems*. Composites Engineering, 1995. **5**(9): p. 1091-1103.
106. Mayes, J.S., *Micromechanics Based Failure Analysis of Composite Structural Laminates*, in *Survivability, Structures, and Materials Directorate Technical Report*. 1999, Naval Surface Warfare Center Carderock Division. p. 1-228.
107. Tsai, S.W. and E.M. Wu, *A general theory of strength for anisotropic materials*. Journal of composite materials, 1971. **5**(1): p. 58-80.
108. Mayes, J.S. and A.C. Hansen, *Composite laminate failure analysis using multicontinuum theory*. Composites Science and Technology, 2004. **64**(3-4): p. 379-394.
109. Nelson, E., A. Hansen, T.-E. Tay, D. Kenik, and F. by Institutions. *Delamination and damage progression in a composite laminate subjected to bending using multicontinuum theory*. in *52nd AIAA/ASME/ASCE/AHS/ASC Structures, Structural Dynamics and Materials Conference 19th AIAA/ASME/AHS Adaptive Structures Conference 13t*. 2011.
110. Tamuzh, V., *Fracture and fatigue of polymers and composites (survey)*. Polymer Mechanics, 1977. **13**(3): p. 392-408.
111. Regel', V., A. Leksovskii, A. Slutsker, and V. Tamuzh, *Polymer breakdown and fatigue*. Mechanics of Composite Materials, 1972. **8**(4): p. 516-527.
112. Sauer, J. and G. Richardson, *Fatigue of polymers*. International journal of fracture, 1980. **16**(6): p. 499-532.
113. Coleman, B.D., *Time dependence of mechanical breakdown phenomena*. Journal of Applied Physics, 1956. **27**(8): p. 862-866.
114. Zhurkov, S., *Kinetic concept of the strength of solids*. International Journal of Fracture, 1984. **26**(4): p. 295-307.
115. Tomashevskii, E., V. Zakrevskii, I. Novak, V. Korsukov, V. Regel, O. Pozdnyakov, A. Slutsker, and V. Kuksenko, *Kinetic micromechanics of polymer fracture*. International Journal of Fracture, 1975. **11**(5): p. 803-815.
116. Anderson, T.L., *Mathematical Equations of Linear Elastic Fracture Mechanics*, in *Fracture Mechanics Fundamentals and Applications - Second Edition*. 1995, CRC Press: Texas. p. 101-116.
117. Busfield, J., C. Ratsimba, and A. Thomas, *Crack growth and predicting failure under complex loading in filled elastomers*. Finite element analysis of elastomers, published by IMechE, UK, 1999: p. 235-250.
118. HEXCEL, *HexPly M18/1 180°C Curing Epoxy Matrix Product Data*. 2011.
119. HEXCEL. *Hexcel exhibits at Seoul Airshow 2005*. 2015 [cited 2015; Available from: <http://www.hexcel.com/news/archive/news-20051017>].

120. Charles, A.D., J. Wang, and I. Stoyanovski, *The impact of temperature and humidity on bonded repairs performed in the field*. Journal of Composite Materials, 2015: p. 0021998314567695.
121. Materials, C.E. *FM 300-2 Film Adhesive Technical Data Sheet*. 2011.
122. Donough, M.J., A.J. Gunnion, A.C. Orifici, and C.H. Wang. *Critical Assessment of Failure Criteria for Adhesively Bonded Composite Repair Design*. in *28th International Congress of the Aeronautical Sciences*. 2012. Brisbane.
123. Aerospace, C., *Cherry Maxibolt Blind Bolt*. 2007: California.
124. Standard, N.A., *NAS1581*, A.I. Association, Editor. 2012: Virginia.
125. McCarthy, M.A., C.T. McCarthy, and G.S. Padhi, *A Simple Method for Determining the Effects of Bolt-Hole Clearance on Load Distribution in Single-Column Multi-Bolt Composite Joints*. Composite Structures, 2005.
126. Lawlor, V., W. Stanley, and M. McCarthy, *Characterisation of damage development in single shear bolted composite joints*. Plastics, Rubber and Composites, 2002. **31**(3): p. 126-133.
127. Cao, Z. and M. Cardew-Hall, *Interference-fit riveting technique in fiber composite laminates*. Aerospace Science and Technology, 2006. **10**(4): p. 327-330.
128. Liu, L., J. Zhang, K. Chen, and H. Wang, *Combined and interactive effects of interference fit and preloads on composite joints*. Chinese Journal of Aeronautics, 2014. **27**(3): p. 716-729.
129. Khashaba, U.A., H.E.M. Sallam, A.E. Al-Shorbagy, and M.A. Seif, *Effect of washer size and tightening torque on the performance of bolted joints in composite structures*. Composite Structures, 2006. **73**(3): p. 310-317.
130. Nelson, W.D., B.L. Bunin, and L.J. Hart-Smith, *Critical Joints in Large Composite Aircraft Structure*. 1983, DTIC Document.
131. Kiral, B.G., *Effect of the clearance and interference-fit on failure of the pin-loaded composites*. Materials & Design, 2010. **31**(1): p. 85-93.
132. Liu, P. and K. Zhang, *An experimental study on fatigue life of interference-fit composite joint*. Acta Aeronautica et Astronautica Sinica, 1991. **12**: p. 545.
133. Oh, J.H., Y.G. Kim, and D.G. Lee, *Optimum Bolted Joints for Hybrid Composite Materials*. Composite Structures, 1997. **38**: p. 329-341.
134. Ouellet, M. and A. Vadean. *Design Improvement of Hybrid Composite Joints By Axiomatic Design*. in *The Seventh International Conference on Axiomatic Design*. 2013. Worcester.
135. Caccese, V., K.A. Berube, M. Fernandez, J.D. Melo, and J.P. Kabche, *Influence of Stress Relaxation on Clamp-Up Force in Hybrid Composite-to-Metal Bolted Joints*. Composite Structures, 2009. **89**: p. 285-293.

136. Faruk, S., P. Murat, S. Onur, and B. Semih, *Experimental failure analysis of mechanically fastened joints with clearance in composite laminates under preload*. Materials and Design, 2008. **29**: p. 1159-1169.
137. Chishti, M., C.H. Wang, R.S. Thomson, and A. Orifici. *Progressive damage in single lap countersunk composite joints*. in *IOP conference series: materials science and engineering*. 2010. IOP Publishing.
138. Karakuzu, R., T. Gülem, and B.M. İçten, *Failure analysis of woven laminated glass-vinylester composites with pin-loaded hole*. Composite structures, 2006. **72**(1): p. 27-32.
139. Reithmaier, L., *Standard Aircraft Handbook for Mechanics and Technicians*. 1999: McGraw Hill Professional.
140. Standard, A., *D5868-01 (2008), "Standard Test Method for Lap Shear Adhesion for Fiber Reinforced Plastic (FRP) Bonding," ASTM International, West Conshohocken, PA, 2003, DOI: 10.1520/D5868-01R08*.
141. Johnson, W., G.K. Yamauchi, and M.E. Watts, *NASA Heavy Lift Rotorcraft Systems Investigation*. 2005, Ames Research Center: Hampton, VA.
142. Baker, A., S. Dutton, and K. Donald, *Properties of Composite Systems*, in *Composite Materials For Aircraft Structures*. 2004, American Institute of Aeronautics and Astronautics: Reston, Virginia. p. 275.
143. Fiore, V., F. Alagna, G. Galtieri, C. Borsellino, G. Di Bella, and A. Valenza, *Effect of curing time on the performances of hybrid/mixed joints*. Composites: Part B, 2013: p. 911-918.
144. Herrington, P.D. and M. Sabbaghian, *Factors Affecting the Friction Coefficients between Metallic Washers and Composite Surfaces*. Composites, 1991. **22**(6): p. 418-424.
145. Tong, L., *Bearing Failure of Composite Bolted Joints with Non-uniform Bolt-to-Washer Clearance*. Composites Part A, 2000. **31**(6): p. 609-615.
146. Chowdhury, N.M., W.K. Chiu, J. Wang, and P. Chang, *Static and Fatigue Testing Thin Riveted, Bonded & Hybrid Carbon Fiber Double Lap Joints used in Aircraft Structures*. Composite Structures, 2015. **121**: p. 315-323.
147. Lang, T.P. and P.K. Mallick, *Effect of spew geometry on stresses in single lap adhesive joints*. International Journal of Adhesion and Adhesives, 1998. **18**(3): p. 167-177.
148. Andreassi, L., R. Baudille, and M.E. Biancolini, *Spew formation in a single lap joint*. International Journal of Adhesion and Adhesives, 2007. **27**(6): p. 458-468.
149. Zitoune, R. and F. Collombet, *Numerical prediction of the thrust force responsible of delamination during the drilling of the long-fibre composite structures*. Composites Part A, 2007. **38**: p. 858-866.
150. Davim, J.P., P. Reis, and C.C. Antonio, *Experimental study of drilling glass fiber reinforced plastics (GFRP) manufactured by hand lay-up*. Composite Science and Technology, 2004. **64**: p. 289-297.

151. Singh, A.P., M. Sharma, and I. Singh, *A review of modeling and control during drilling of fiber reinforced plastic composites*. Composites: Part B, 2013: p. 118-125.
152. Sawa, T., T. Kobayashi, and T. Fujii, *Strength of combination joints of an adhesive with bolts (T-flange adherends subjected to an external bending moment)*. JSME International Journal, Series 1: Solid Mechanics, Strength of Materials, 1989. **32**(3): p. 411-419.
153. Kumar, B., C.T. Sun, P.H. Wang, and R. Sterkenburg, *Adding Additional Load Paths in a Bonded/Bolted Hybrid Joint*. Journal of Aircraft, 2010. **47**: p. 1593-1598.
154. Clarke, J.L., *Structural Design of Polymer Composites: EUROCOMP Design Code and Handbook*. E & FN Spon.
155. Chowdhury, N.M., J. Wang, W.K. Chiu, and P. Chang, *Experimental and Finite Element Studies of Thin Bonded and Hybrid Carbon Fibre Double Lap Joints Used in Aircraft Structures*. Composites Part B: Engineering, 2015. **85C**: p. 233-242.
156. Kim, J.H., B.J. Park, and Y.W. Han, *Evaluation of Fatigue Characteristics for Adhesively-Bonded Composite Stepped Lap Joints*. Composite Structures, 2004. **66**: p. 69-75.
157. Wei, J., G. Jiao, P. Jia, and T. Huang, *The effect of interference fit size on the fatigue life of bolted joints in composite laminates*. Composites: Part B, 2013: p. 62-68.
158. Chalkley, P.D. and W.K. Chiu, *An improved method for testing the shear stress/strain behaviour of adhesives*. International Journal of Adhesion and Adhesives, 1993: p. 237-242.
159. Chowdhury, N.M., J. Wang, W.K. Chiu, and P. Chang, *Static and fatigue testing bolted, bonded and hybrid step lap joints of thick carbon fibre/epoxy laminates used on aircraft structures*. Composite Structures, 2016. **142**: p. 96-106.
160. Hart-Smith, L., *Adhesive-bonded scarf and stepped-lap joints*. 1973.
161. Kimiaefar, A., E. Lund, O.T. Thomsen, and J.D. Sørensen, *Asymptotic Sampling for reliability analysis of adhesive bonded stepped lap composite joints*. Engineering Structures, 2013. **49**: p. 655-663.
162. Kim, H.S., S.J. Lee, and D.G. Lee, *Development of a strength model for the cocured stepped lap joints under tensile loading*. Composite Structures, 1995. **32**(1-4): p. 593-600.
163. Matthews, F.L., P.F. Kilty, and E.W. Godwin, *A review of the strength of joints in fibre-reinforced plastics. Part 2. Adhesively bonded joints*. Composites, 1982. **13**(1): p. 29-37.
164. Erdogan, F. and M. Ratwani, *Stress Distribution in Bonded Joints**. Journal of Composite Materials, 1971. **5**(3): p. 378-393.
165. He, D., T. Sawa, T. Iwamoto, and Y. Hirayama, *Stress analysis and strength evaluation of scarf adhesive joints subjected to static tensile loadings*. International Journal of Adhesion and Adhesives, 2010. **30**(6): p. 387-392.
166. Orifici, A.C., I. Herszberg, and R.S. Thomson, *Review of methodologies for composite material modelling incorporating failure*. Composite Structures, 2008. **86**: p. 194-210.

167. Dano, M.L., G. Gendron, and A. Picard, *Stress and failure of mechanically fastened joints in composite laminates*. Composite Structures, 2000. **50**(3): p. 287-296.
168. Dano, M.L., E. Kamal, and G. Gendron, *Analysis of bolted joints in composite laminates: Strains and bearing stiffness predictions*. Composite Structures, 2007. **79**(4): p. 562-570.
169. Xiao, Y. and T. Ishikawa, *Bearing strength and failure behaviour of bolted composite joints (part II: modelling and simulation)*. Composite Science and Technology, 2005. **65**(7-8): p. 1032-1043.
170. Olmedo, A. and C. Santiuste, *On the prediction of bolted single-lap composite joints*. Composite Structures, 2012. **94**: p. 2110-2117.
171. Huhne, C., A.-K. Zerbst, G. Kuhlmann, C. Steenbock, and R. Rolfes, *Progressive damage analysis of composite bolted joints with liquid shim layers using constant and continuous degradation models*. Composite Structures, 2010. **92**: p. 189-200.
172. Camanho, P.P. and F.L. Matthews, *A progressive damage model for mechanically fastened joints in composite laminates*. Journal of Composite Materials, 1999. **33**: p. 2248-2280.
173. McCarthy, C.T., M.A. McCarthy, and V.P. Lawlor, *Progressive damage analysis of multi-bolt composite joints with variable bolt-hole clearances*. Composites: Part B, 2005. **36**: p. 290-305.
174. Ireman, T., *Three-dimensional stress analysis of bolted single-lap composite joints*. Composite Structures, 1998. **43**(3): p. 195-216.
175. Egan, B., C.T. McCarthy, M.A. McCarthy, P.J. Gray, and R.M. Frizzell, *Modelling a single bolt countersunk composite joint using implicit and explicit finite element analysis*. Computational Material Science, 2012. **64**: p. 203-208.
176. Chishty, M., C.H. Wang, R.S. Thomson, and A.C. Orifici, *Numerical analysis of damage progression and strength of countersunk composite joints*. Composite Structures, 2012. **94**: p. 643-653.